# Modeling of Calcium Homeostasis in the Rat and its Perturbations

David Granjon


**Université Pierre et Marie Curie**
**Université de Lausanne**

ED394 Physiologie, Physiopathologie et Thérapeutique
Centre de Recherche des Cordeliers, Equipe 3, Paris
Département de Pharmacologie et Toxicologie, Lausanne

# Modeling of Calcium Homeostasis in the Rat and its Perturbations

**Thèse de doctorat ès sciences de la vie (PhD)**

Présentée le 3 novembre 2016 à Paris

par

**David Granjon**

sous la direction du Dr. Aurélie Edwards[1] et du Prof. Olivier Bonny[2]

[1]Sorbonne Universités, UPMC Univ Paris 06. [2]Département de Pharmacologie et Toxicologie, Université de Lausanne.

**Devant le jury composé de:**

Prof. Jean-Claude Dussaule, Président,
Dr. Aurélie Edwards, Co-directrice de Thèse
Prof. Olivier Bonny, Co-directeur de Thèse
Dr. Fabien Crauste, rapporteur
Dr. Robert Unwin, rapporteur
Prof. Pascal Houillier, examinateur

*à Lucienne,*

# Remerciements

Tout d'abord, j'aimerais commencer par remercier mes deux directeurs de thèse. Aurélie, je suis encore aujourd'hui impressionné par ta patience à toute épreuve et ton calme, qui m'ont permis de pouvoir réaliser cette thèse sans encombres. Ta disponibilité et ton implication dans le suivi de mon travail ont été déterminants. Enfin, j'espère avoir acquis une certaine rigueur à tes côtés, ce qui est indispensable pour continuer dans la recherche.

Olivier, je te remercie pour ton accueil en Suisse et ta sympathie. J'ai pris beaucoup de plaisir à pouvoir discuter avec toi des aspects biologiques de ma thèse, en s'éloignant parfois un peu (voire beaucoup) de la question de départ. Merci de m'avoir fait découvrir d'autres aspects de la recherche, l'expérimentation, dont j'ignorais tout jusque là. Ce fut une belle occasion de travailler avec Suresh avec qui j'ai apprécié faire équipe. Suresh, merci pour ton sérieux et ta motivation, le chapitre 2 de cette thèse n'aurait pas pu être écrit sans tes talents en chirurgie animale ("For Jesus").

Je remercie mon premier Jury de thèse: Pr. Christian Widmann, Pr. Murielle Bochud, Dr. Randy Thomas, Pr. Daniel Fuster pour avoir accepté de "juger" cette thèse. Je n'oublie pas Pr. Carsten Wagner que je remercie pour avoir évalué mon examen de mi-thèse. Un grand merci à Randy Thomas et Olivier Bonny d'avoir accepté d'être mes rapporteurs.

Mes remerciements vont ensuite vers mon deuxième Jury de thèse: Pr. Jean-Claude Dussaule pour avoir accepté de présider ce jury. Je remercie chaleureusement mes deux rapporteurs Fabien Crauste et Robert Unwin. Enfin, merci à Pascal Houillier pour avoir accepté le rôle d'examinateur.

J'aimerais aussi remercier Laurent Pujo Menjouet sans qui je n'aurais pas eu l'opportunité de faire cette thèse.

Un grand merci à Pascal Houillier, Alain Doucet et Kamel Laghmani pour leurs conseils lors des différentes présentations de mes travaux au laboratoire.

Je remercie Michel Daudon avec qui, Aurélie et moi, avons eu une discussion passionnante à propos de la précipitation du calcium et du phosphate.

Je suis très reconnaissant à Luis Almeida pour son accueil et sa sympathie dans le laboratoire LJLL.

Un grand merci à tous les membres de mes deux laboratoires d'accueil: Nicolas, Gabrielle, Marc, Jacques, Stéphane, Nazia, Nadia, Christine, Sylvie, Gilles, Gaëlle, Lydie, Dalila, Luciana, Anne, Mathias, Samuel, Murielle, Gabriel, Dmitri Firsov, Olivier Staub.

Je souhaite une bonne continuation à mes co-thésards: Lucile, Mr Bignon et Elie!

Merci à Natsuko qui m'a supporté comme voisin de bureau pendant presque 3 ans, avec succès. Pour ma part, je l'ai très bien vécu. Encore merci pour tes conseils!

Un merci spécial à Isabelle Rivier Flühmann pour avoir grandement facilité mon intégration à Lausanne.

Cette thèse marque aussi la fin de mon premier quart de siècle, à quelques semaines près. C'est donc la fin "officielle" de mes études, même si on ne s'arrête jamais d'apprendre. A cette occasion, j'aimerais remercier mes parents, mes grands-parents, ma petite soeur et toute ma famille qui ont tant contribué à ma réussite et m'ont soutenu aussi bien dans les bons moments que dans les mauvais moments. Je leur serais éternellement reconnaissant et je m'excuse d'avance si le reste de la thèse est écrit en anglais.

Un grand merci à mes chers amis: Anais et Loic (Félicitations pour votre bébé), Yanou, Anthony, Leo, Pierric, Jessica grâce à qui j'ai pu m'initier à l'équitation, Olivier, Thérèse, Xavière.

Un merci aussi à toutes les salles de sport de Paris qui ont permis de préserver ma santé pendant cette thèse et de prendre du recul pour mieux affronter les difficultés.

Enfin, un pensée toute particulière à ma chérie qui m'accompagne et m'encourage depuis quelques années déjà!

## Résumé

Cette thèse de mathématiques appliquées en physiologie rénale a pour thème principal l'étude de l'homéostasie du calcium à travers le développement d'un modèle mathématique à l'échelle de l'organisme. Ce modèle est construit à partir de données expérimentales récentes ainsi que de travaux théoriques précédents. Nous cherchons à répondre à certaines questions soulevées par les néphrologues dans le cas de pathologies impliquant la formation de calculs rénaux ou de calcifications. Nous examinons notamment les cas de l'hypercalciurie observée durant l'hyperparathyroïdie primaire dont les causes ne sont pas élucidées, l'effet de l'inhibition de la résorption par les bisphosphonates sur le métabolisme du calcium, ainsi que les mécanismes de complexation du calcium et phosphate et notamment les conséquences d'une infusion intraveineuse de phosphate sur l'homéostasie du calcium. Nous commençons par développer un modèle de la synthèse et sécrétion de l'hormone parathyroïdienne (PTH), l'hormone principale régulant la calcémie. Ce modèle prend en compte l'inhibition de la sécrétion de PTH par le calcium qui requiert l'activation du récepteur sensible au calcium (CaSR). Nous simulons l'effet de clamps hypocalcémique et hypercalcémique sur la sécrétion de PTH et comparons les prédictions aux données expérimentales, ce qui nous permet d'ajuster la valeur des paramètres non documentés dans la littérature. Puis, nous construisons un modèle de l'homéostasie du calcium incluant la PTH, la vitamine $D_3$ - deuxième régulateur majeur de la calcémie, ainsi que les compartiments du métabolisme calcique à savoir l'intestin, l'os, les reins et le plasma. Le modèle prend aussi en compte le pool rapidement échangeable de calcium dans l'os, le retard lié à la synthèse de la vitamine D ainsi qu'une description détaillée de la réabsorption rénale du calcium. Ce modèle est validé par rapport à des données expérimentales et nous simulons les cas de l'hyperparathyroïdie primaire, ainsi que l'inhibition de la résorption par les bisphosphonates pour répondre aux questions soulevées. L'effet de l'âge et du sexe sur les paramètres du modèle sont également discutés. Les résultats de ce modèle suggèrent que la présence ou non d'une hypercalciurie lors de l'hyperparathyroïdie primaire peut être expliquée par des mécanismes antagonistes dans la branche ascendante large de Henle, avec d'un côté le CaSR inhibant la réabsorption de calcium et de l'autre la PTH diminuant l'excrétion de calcium. Par ailleurs, lorsque la résorption osseuse est inhibée, notre modèle prédit que des mécanismes complexes se mettent en place afin de limiter les pertes en calcium, en augmentant d'une part l'absorption intestinale et en réduisant d'autre part son excrétion urinaire. Le métabolisme de calcium étant étroitement lié à celui du phosphate, nous construisons ensuite un modèle de l'homéostasie du phosphate, rajoutant une nouvelle hormone, FGF23 synthétisée dans l'os. De plus, nous modélisons les mécanismes de liaison du calcium et du phosphate, prenant en compte la Fetuine A, un inhibiteur des calcifications, ainsi que la formation de particules liées à la précipitation du calcium et du phosphate. Nous comparons les résultats obtenus à ceux du précédent modèle. Ce dernier modèle suggère que l'infusion intraveineuse de phosphate induit une hypocalcémie majeure, due principalement à la précipitation du calcium et du phosphate dans le plasma et dans l'os. Par ailleurs, la divergence entre les prédictions de notre modèle et les observations expérimentales vis-à-vis du comportement dynamique de la PTH plasmatique suggère un retard dans l'activation de la synthèse de PTH par le phosphate.

## Abstract

This thesis of applied mathematics in renal physiology focuses on the study of calcium homeostasis, through the development of a mathematical model at the organism scale. This model is built based upon recent experimental studies as well as previous models in the field. We aim to answer several questions raised by nephrologists regarding diseases involving calcium stone formation or calcifications. In particular, we are interested in the origins of the hypercalciuria observed during primary hyperparathyroidism, the causes of which remain to be elucidated, the effects of bone resorption inhibition by bisphosphonates on calcium metabolism, as well as the consequences of an intravenous infusion of phosphate on calcium homeostasis. We begin by developing a model that describes the synthesis and secretion of parathyroid hormone (PTH), which is the main hormone involved in the regulation of calcemia. This model takes into account the negative feedback loop between calcium and PTH secretion, which is modulated by the calcium sensing receptor (CaSR). Then, we simulate the effects of hypocalcemic and hypercalcemic clamps on PTH secretion and compare the predicted results with experimental observations, which allows us to adjust parameter values that were not available in the literature. The PTH model is then incorporated into a model of calcium homeostasis that considers all the compartments involved in calcium metabolism, that is, the intestine, bone, kidneys and plasma. Vitamin $D_3$, the second major regulator of calcemia is added. We introduce some novel features such as the rapidly exchangeable pool of calcium in bone, the delay in vitamin $D_3$ synthesis, together with a more complete description of the renal reabsorption of calcium. In particular, the effects of CaSR on renal calcium handling in the thick ascending limb are considered for the first time. This model is validated against experimental data; we then simulate scenarios such as primary hyperparathyroidism as well as the inhibition of bone resorption to answer the questions raised above. Additionally, the effects of sex and age on model parameters and predictions are discussed. This model suggests that the variable presence of hypercalciuria during primary hyperparathyroidism can be explained by counteracting mechanisms in the thick ascending limb of Henle, involving on one hand the calcium sensing receptor, which inhibits calcium reabsorption, and on the other hand PTH which decreases calcium excretion. Besides, when bone resorption is impaired, our model predicts that complex feedback mechanisms act to diminish calcium losses, mainly by increasing the intestinal absorption of calcium and reducing its urinary excretion. The metabolism of calcium is tightly bound to that of phosphate. In the next step, we build a mathematical model of phosphate homeostasis, including a new hormone, FGF23 which is synthetized in bone. Furthermore, we represent the binding mechanisms between calcium and phosphate, and account for the effects of Fetuin-A, an inhibitor of calcifications, as well as the formation of calciprotein particles. We compare the results obtained with this combined model and the previous one. The model also explains why, in vivo, the intravenous infusion of phosphate triggers a major hypocalcemia: this is due to the precipitation of calcium and phosphate in both bone and plasma. Moreover, the divergence between our model predictions and experimental observations regarding the dynamic evolution of plasma PTH suggests a delay in the activation of PTH synthesis by phosphate.

# Contents

# List of Figures

# List of Tables

# Chapter 1

# Introduction

## 1.1 General introduction on calcium homeostasis

The introductory material presented below has been summarized in a book chapter that has been submitted for publication (Granjon D, Edwards A. and Bonny O, Calcium Homeostasis, submitted.)

### 1.1.1 Overview of calcium homeostasis

Homeostasis is the capacity of a system to maintain a condition of balance or equilibrium even when external perturbations affect the system. It was defined by Claude Bernard in 1865 and Walter Bradford Cannon in 1926 [43]. Calcium homeostasis specifically refers to the ability of the body to maintain a stable plasma calcium concentration, by controlling the fluxes of calcium between the different organs involved in mineral metabolism. Therefore, calcium homeostasis shouldn't be confused with calcium balance, which corresponds to the net difference between calcium intake and calcium loss in a given organism.

Calcium plays a primary role in many biological processes such as the regulation of cardiac activity, muscle contraction, bone remodeling, and blood clotting. In order to achieve all these functions, the extracellular concentration of calcium has to be kept between tight bounds since any dysregulation may have major consequences on the organism. Indeed, hyper- or hypocalcemia, hypercalciuria, calciphylaxis, vascular calcifications or osteoporosis are caused by abnormalities of calcium homeostasis [224, 40]. The regulation of calcium concentration in the organism takes place at several levels: intracellularly (mitochondria, endo/sarcoplasmic reticulum, cytosolic complexation with intracytoplasmic chelators), within the interstitium, plasma, and tissues, and at the scale of whole organism. Some calcium sensors are involved, which are localized in key organs and also within endocrine glands which secrete hormones to regulate calcium homeostasis. As a result, even modest variations in the plasma or interstitial concentration of calcium can be detected. Hormones whose role is to convey this information are modulated and effectors regulated by these hormones can restore calcemia to normal values (Figure 1.1).

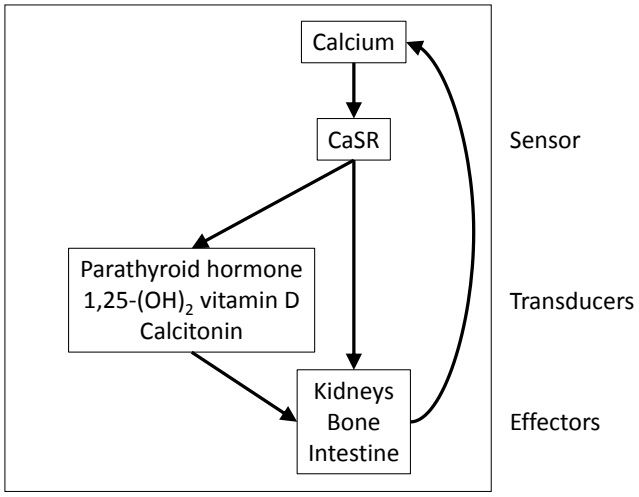


Figure 1.1: The calcium homeostatic system composed of a sensor (the calcium sensing receptor), transducers (hormones such as PTH, vitamin D3 and calcitonin) and effectors (organs). A perturbation activates the sensor which modulates the synthesis of hormones, as required. Theses hormones act on organs so that calcemia returns to its physiological value. Taken from Granjon D, Edwards A, Bonny O, submitted.

Furthermore, in the kidney for instance, these sensors can directly regulate calcemia independently of the most powerful calciotropic hormone, i.e., parathyroid hormone (PTH) [134]. In human, 99.9% of the body calcium is found in the bone and 0.1% in the extracelular compartment and blood (Figure 1.2).

Bone is the major pool of calcium with about 1.25 kg (that is, 31.4 mol) of calcium for a 70 kg person. This calcium is stored as hydroxyapatite, a very stable salt composed of calcium and phosphate whose chemical formula is $Ca_{10}(PO_4)_6(OH)_2$. In plasma, there are three forms of calcium: 55% of total calcium is present as an ionized solute ($Ca^{2+}$), 40% is bound to plasma proteins and 5% complexed to other ions such as bicarbonate, phosphate or citrate [210, 216]. Of note, the percentage of calcium bound to proteins depends on plasma pH; thus in case of acidosis, this fraction decreases and that of ionized calcium is raised. Ionized calcium constitutes the biologically active fraction, and it is the form that is detected by calcium sensing receptors (CaSR) and controlled by a complex regulatory system. The physiological plasma calcium concentration is between 2.2 and 2.5 mM and that of ionized calcium is between 1.1 and 1.4 mM [168, 210].

A part of the plasma calcium is bound to phosphate and Fetuin-A, which is produced by the liver. These complexes are called calciprotein particles [100, 164, 215]. These nanoparticles prevent the precipitation of critical concentrations of calcium and phosphate in the plasma which could ultimately lead to vascular calcifications. When Fetuin-A is missing or in case of excess of calcium or phosphate or lack of magnesium, which destabilize these nanoparticles, calcifications can appear. The stability of these nanoparticles can be tested by nephelometry and is correlated with

cardiovascular mortality in dialyzed patients or those who have received a kidney transplant [155]. Only ionized and complexed calcium is filtered by the kidney, since calcium bound to protein does not cross the glomerular barrier. The filtered fraction, also called ultrafiltrate calcium, represents about 50% of the total plasma calcium, yet it cannot be precisely measured in clinical settings.

Three main organs are involved in calcium homeostasis (Figure 1.2): the intestine where calcium is absorbed across the intestinal mucosa under the influence of hormones and whose calcium flux contributes to approximately one-third of the total calcium influx into plasma; the bone which stores or releases calcium, and which contributes about two- thirds of the total calcium influx into plasma [222, 121]; kidneys which excrete calcium so that calcium balance is preserved. In the following section, we describe in detail each organ.

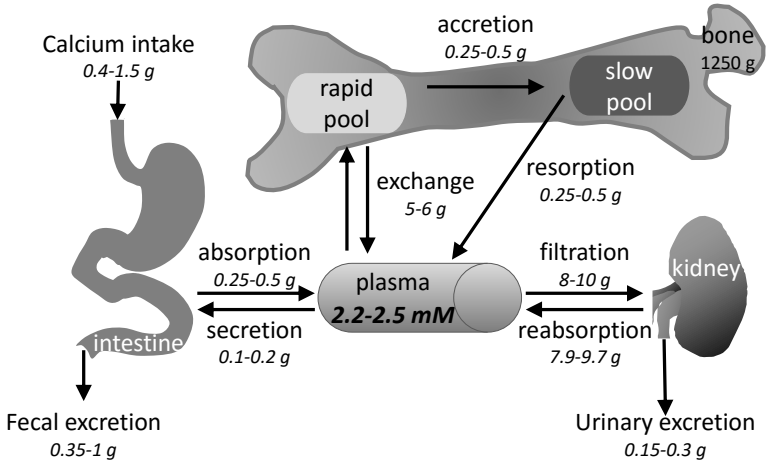


Figure 1.2: Calcium balance in humans. Taken from Granjon D, Edwards A, Bonny O, submitted.

### 1.1.2 Transport mechanisms in organs involved in calcium homeostasis

#### Bone

Bone can be divided in two compartments, namely a rapidly exchangeable pool and a slowly exchangeable pool (Figure 1.2). The rapid pool contains calcium that is immediately available for exchange, probably stored as brushite, a very unstable salt composed of calcium and phosphate (also known as dicalcium dihydrate, $CaHPO_4.2H_2O$). The existence of this pool was evinced by radiolabeled calcium studies, which indicated the presence of a fast calcium deposit in the haversian system of cortical long bones [54, 137, 158]. It contributes to the minute-to-hour regulation of calcemia, for example during the night when calcium intake is reduced. The size and localization of this pool remain to be refined, but it is thought to allow for calcium exchanges with plasma (about 5 to 6g of calcium per day) that are 10-fold higher than those between the deep pool and

plasma. The deep pool is difficult to mobilize and is localized in the calcified matrix of bone. It is composed of hydroxyapatite, as previously described, and it exchanges 0.25 to 0.5 g of calcium per day with plasma.

The bone remodeling process is continuous and involves 2 types of cells:

- Osteoclasts bind to calcified bone matrix and release its components into the bloodstream. Their maturation is complex and highly regulated from monocytes in bone marrow [230].
- Osteoblasts constitute 4 to 6 % of bone cells and their lifespan is about 3 months. They crystallize the bone matrix, regulate osteoclasts maturation, and interact with osteocytes more deeply in the bone [151].

Bone remodeling begins with an activation phase during which pre-osteoclasts are recruited and merge together, leading to large multinucleated cells (Figure 1.3). This step is regulated by PTH, the insulin growth factor I (IGF-I), and the tumor necrosis factor $\alpha$ (TNF-$\alpha$) as well as estrogens. The resorption phase by activated osteoclasts lasts 2 to 4 weeks. The mature osteoclast is a polarized cell that has an integrin crown delimiting a basolateral compartment next to the bone marrow and an apical compartment that has a large ruffled border in contact with the bone matrix, called Howship lacuna. It contains some proteases with an acid pH. The calcium concentration in the lacuna can reach 40 mM. The acidification process participates in dissolving hydroxyapatite crystals, releasing calcium and phosphate, which are then carried into plasma either by crossing osteoclasts or by transcytosis. After a transition period lasting about 9 days, the formation phase or accretion is led by osteoblasts. The building of a new bone matrix takes 4 to 6 months. First, entwined collagen fibers are laid down by osteoblasts and form a non calcified matrix, the osteoid. Then, vesicles containing calcium and phosphate are added to this matrix thereby mineralizing the bone. A quiescent phase ends the cycle: osteoblasts stay and can differentiate into osteocytes or vanish by apoptosis.

Osteocytes are the most abundant bone cells (90-95%), with a life time about 25 years [8, 166]. They are formed from osteoblast differentiation, but unlike osteoblasts, they are located in the bone matrix, also called the osteoplast. Cellular processes called canaliculi of 250-300 nm diameter constitute a network connecting osteocytes to each other as well as to other bone cells such as osteoblasts and osteoclasts. Osteocytes are the major producer of RANKL, responsible for the maturation of osteoclats (Figure 1.3). Conversely, they are capable of mineralizing the osteoid laid down by osteoblasts. Additionally, they are the major source of FGF23, which is involved in the regulation of phosphate homeostasis (Section 1.2.3) [8]. The role of osteocytes in calcium homeostasis was uncertain for a long time but is now established, through the concept of osteolytic osteolysis [8, 166]. The mecanism is thought to be similar to that of osteoclasts since proton pumps are expressed by osteocytes [8]. However, the relative contribution of osteoblasts and osteocytes remains to be elucidated. Moreover, comparing the quantity of osteocytes to that of osteoclasts, they could be a good candidate for the rapid regulation of calcium homeostasis [8].

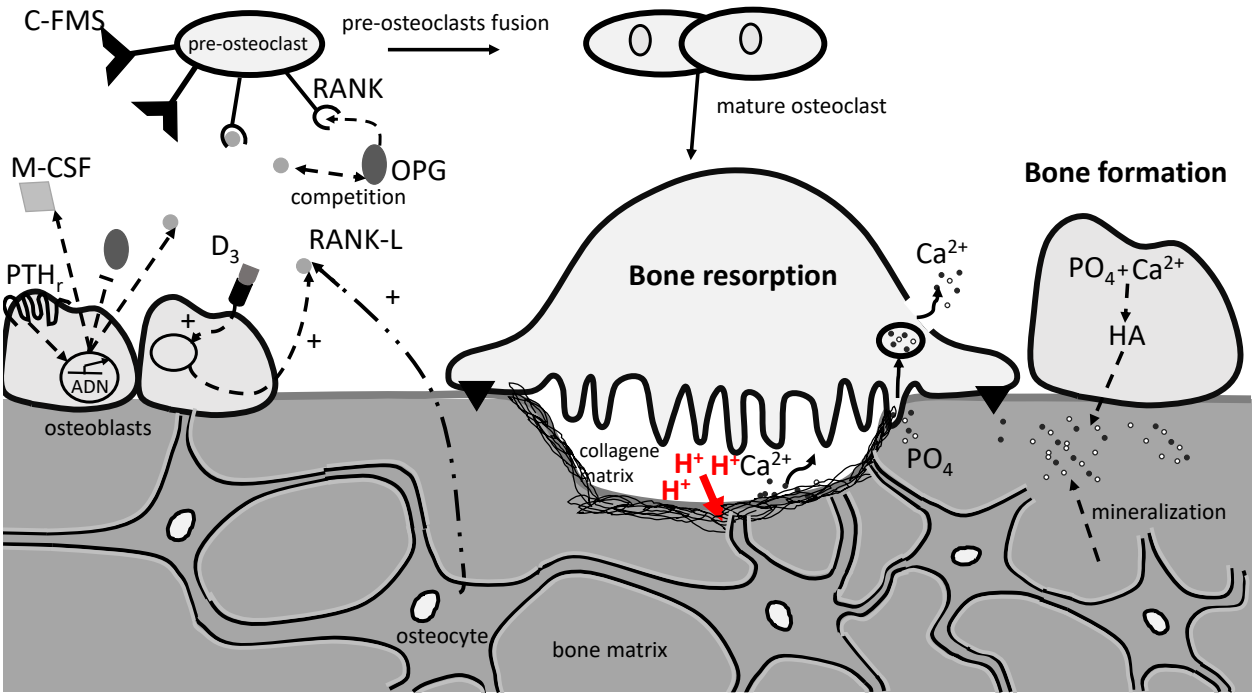


Figure 1.3: The bone remodeling process.

### The intestine

Intestinal absorption mainly occurs in the duodenum and to a lesser extent in the ileum and jejunum [117]. Calcium transport across the intestinal epithelium can be decomposed into paracellular and transcellular pathways (Figure 1.4). The relative contribution of each pathway depends on calcium intake: in case of high calcium intake, 90% of the absorption is achieved via the non-saturable paracellular pathway. Conversely, in case of calcium deprivation, the transcellular pathway prevails and accounts for 80% of total absorption. Paracellular calcium transport consists of passive diffusion between cells, across tight junctions under the control of a concentration gradient: the luminal concentration of calcium in the intestine, which varies according to food intake, is about 10-20 mM; thus it is higher than its interstitial concentration, which is 2 mM. This paracellular flux is mediated by specialized proteins, claudins, and is also regulated by cytokines (which increase the permeability of cells for calcium [5]), hormones and kinases.

In contrast, the transcellular transport of calcium is an active process that requires energy and proceeds through channels, pumps, and transporters that carry calcium from the intestinal lumen to the interstitial compartment. At the apical side, calcium enters the cell by transient receptor potential cation channels type 6 (TRPV6). Once in the cytosol, calcium binds to calbindin $D_{9k}$ which plays a buffering role, preventing intracellular calcium concentrations from reaching toxic levels [117]. Finally, calcium extrusion occurs at the basolateral side via plasma membrane calcium pumps (PMCA) in conjunction with type 1 exchangers $Na^+/Ca^{2+}$ (NCX1) [218]. PMCA has a

high affinity for calcium ($k_M$ = 0.3 mM) and requires ATP consumption. This pump is the main basolateral transporter of calcium in the intestine, whereas NCX1 exchangers only play a minor role in that organ. The active form of vitamin D (calcitriol) is a major regulator of intestinal calcium transport, where it acts by modulating the expression of TRPV6, PMCA, as well as calbindin $D_{9k}$ [189]. Indeed, vitamin D response elements have been discovered on the promoters of these genes [142] and it has been shown that mice invalidated for the vitamin D receptor (VDR) exhibit a substantial drop in the intestinal absorption of calcium (-40%) together with a decrease in TRPV6 and calbindin $D_{9k}$ expression [212]. Additionally, the intestinal absorption of phosphate appears to be reduced in VDR-KO mice [177]. The intestinal response to a stimulation by vitamin D occurs with a delay of several hours. TRPV6 expression at the surface of enterocytes is also directly regulated by dietary calcium, with an increase in TRPV6 expression in case of low calcium intake. Other regulating factors have been highlighted, such as estrogen and pH.

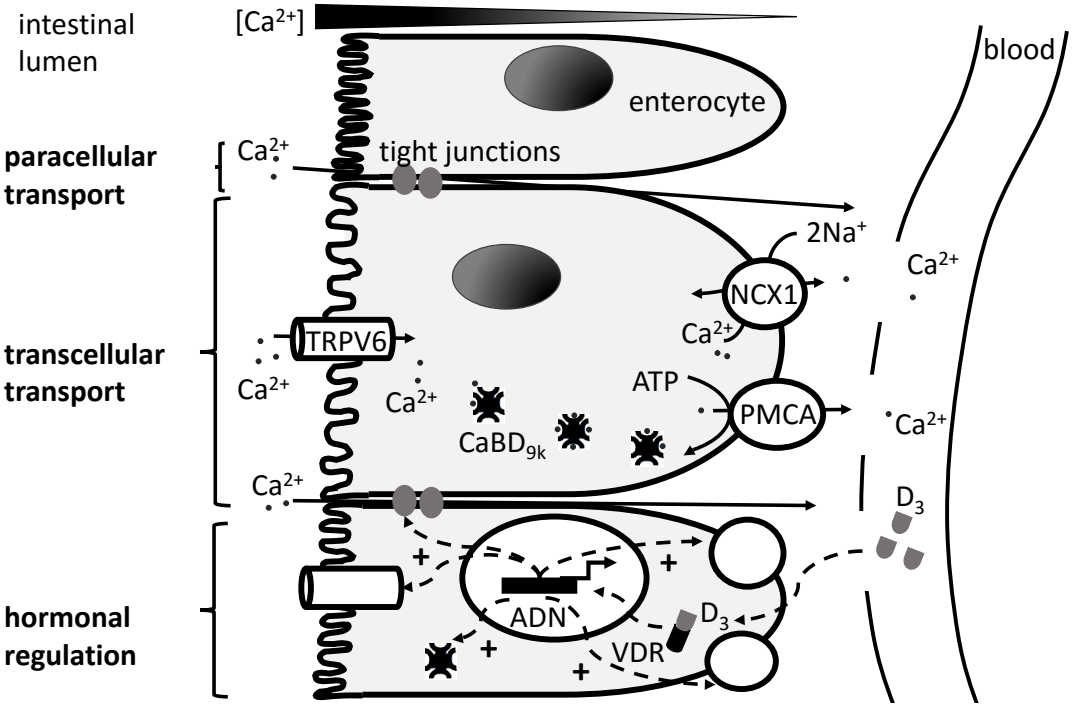


Figure 1.4: Intestinal calcium absorption.

### The kidney

Under normal conditions, kidneys excrete about 1-2% of the calcium filtered by the glomerular capillaries. Along the nephron, calcium is first reabsorbed passively, via the paracellular pathway, in the proximal tubule (60-65%) and the thick ascending limb of Henle (20-25%) [20, 32]. The regulation of calcium transport in the proximal tubule is not fully understood. It is known that PTH inhibits $Ca^{2+}$ reabsorption in that segment indirectly: it inhibits the activity of the sodium/proton

exchanger NHE3, thereby reducing the transmembrane electric potential difference that drives the paracellular reabsorption of $Ca^{2+}$ (Figure 1.5). In the thick ascending limb, the paracellular permeability to calcium is regulated by claudins 16 and 19 [66].

Downstream, the remaining part of the filtered load of calcium (10-15%) is actively reabsorbed across cells constituting the tight epithelium of the distal convoluted tubule (DCT) and the connecting tubule (CNT). This transcellular transport occurs by means of TRPV5 calcium channels at the apical side, and via $Na^+/Ca^{2+}$ exchangers (NCX1) and plasma membrane calcium pumps (PMCA4) at the basolateral side. In contrast with the intestine, the contribution of NCX1 to basolateral calcium extrusion predominates compared to that of PMCA. Inside the cell, calbindin $D_{28k}$ enhances calcium transport from the apical side to the basolateral side by unknown mechanisms. PTH stimulates calcium reabsorption in the distal nephron. In the thick ascending limb (TAL), it increases the paracellular permeability to $Ca^{2+}$ [134] (Figure 1.6). In the DCT and CNT, it induces a rise in the expression of TRPV5, NCX1, as well as calbindin $D_{28k}$ [211] (Figure 1.7). Calcitriol also increases the expression of proteins involved in transepithelial calcium transport in the DCT [103].

Some studies have suggested that $Ca^{2+}$ is transported across the inner medullary collecting duct (CD) epithelium [16, 136, 47], and the CD has been estimated to reabsorb up to 3% of the filtered load of calcium [104]. However, other studies have found no evidence of $Ca^{2+}$ transport in that segment [94, 3]. The issue remains controversial in part because the medullary CD is not easily accessible to micropuncture [94]. A recent, epithelial-cell based model of $Ca^{2+}$ transport along the nephron indicates that passive transport favors $Ca^{2+}$ secretion along the CD [69], which means that if it occurs, calcium reabsorption in CD must be an active process, against the electrochemical potential gradient.

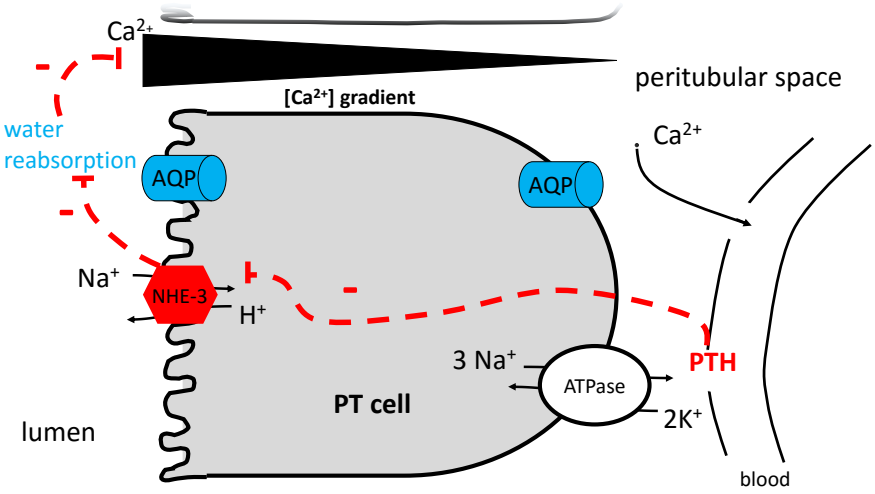


Figure 1.5: Renal calcium handling in the proximal tubule. PTH inhibits the activity of NHE-3 [56]. The entry of $Na^+$ is then reduced, thereby lowering water reabsorption through cells via aquaporins. This decreases the lumen-to-basolateral side calcium concentration gradient, thus blunting calcium reabsorption across the paracellular pathway [56].

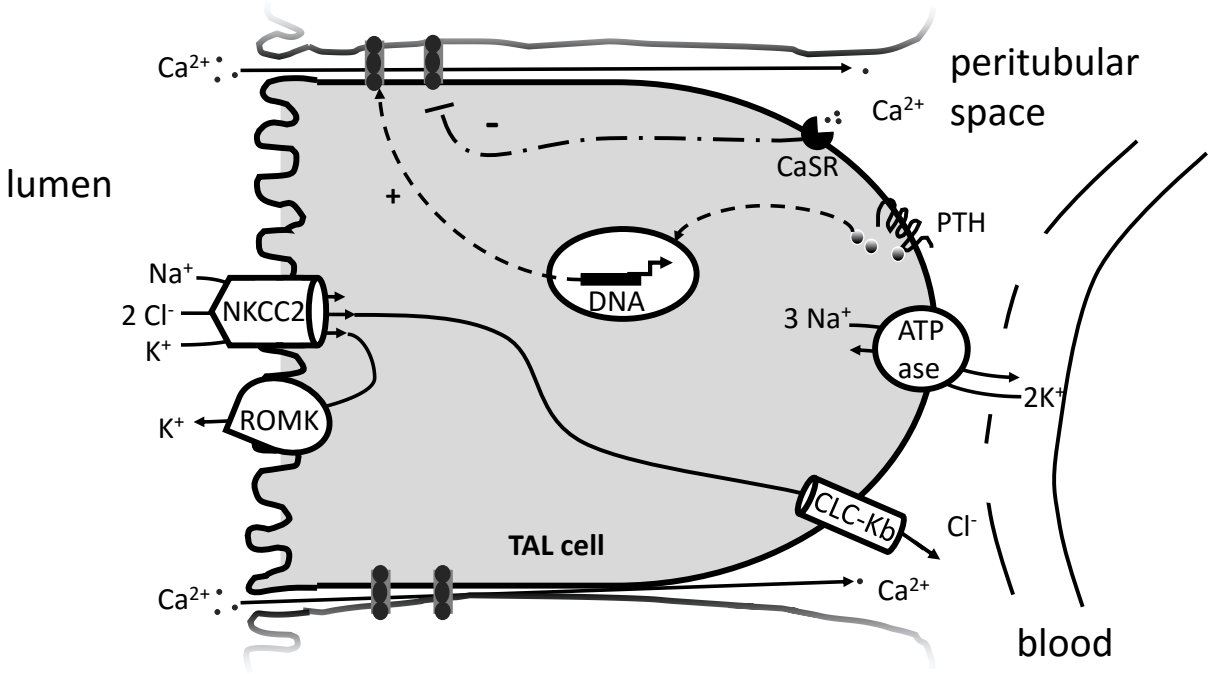


Figure 1.6: Renal calcium handling in the thick ascending limb.

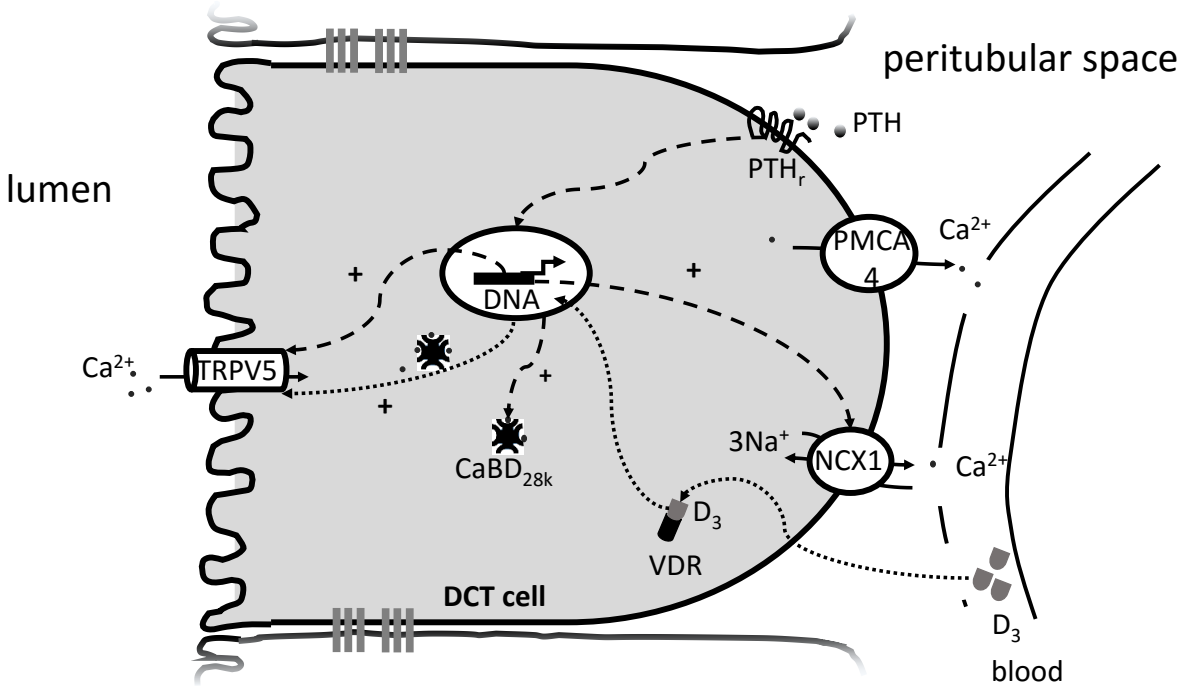


Figure 1.7: Renal calcium handling in the distal convoluted tubule.

### 1.1.3 Regulation of calcium homeostasis

Calcemia is regulated by various feedback systems, which involves the calcium sensing receptors (CaSR) and calcitropiques hormones, primarily parathyroid hormone (PTH), calcitriol ($1,25(OH)_2$ vitamin D, the active form of vitamin D), and calcitonin. Other determinants are known but their exact role remains to be determinded (estrogens, klotho, FGF23, etc.).

#### Parathyroid hormone

Parathyroid hormone (PTH) is synthesized in the chief cells of parathyroid glands, where it is stored in vesicles ready to be carried out of the cells. As a result, PTH acts on the scale of minutes. Its half-life in plasma is about 7 minutes and its plasma concentration is between 1.6 and 6.8 pM [49, 81]. PTH can be rapidly cleaved into a multitude of fragments by plasma proteases. The intact form of PTH contains the 1 to 84 amino acids, whose N-terminal fragment binds to the PTHR1 receptor leading to the specific action of the hormone [87]. It has been recently suggested that the active form of PTH is non oxidized, but the physiological relevance of this observation remains to be proved [204]. PTH secretion is pulsatile, with a complex rhythm, including a pulse every 7-10 minutes and a circadian rhythm. The maximum PTH secretion occurs during the night and its nadir is reached in the morning. The significance of this circadian rhythm is illustrated by its opposite effect on bone: in case of continuous secretion at a high dose, PTH has a catabolic effect, whereas given once a day (teriparatide), it is used to treat osteoporosis for its anabolic action.

The determination of PTH concentration is tricky and a lot of tests have been developed; the most recent tests measure the concentration of intact PTH instead of its fragments. The value of plasma PTH must always be interpreted in light of calcemia (ionized calcium concentrations if possible), phosphatemia, and the concentration of vitamin D. Indeed, $Ca^{2+}$ directly regulates PTH secretion with a reverse sigmoidal function whose slope is steep and with an affinity coefficient $K_i$ of about 1.24 mM. This means that above this value, PTH secretion is substantially inhibited. Conversely, in response to a drop in plasma calcium, PTH is secreted and binds to its receptor, PTHR1, at the surface of osteoblasts in bone and some renal cells [60]. There, it stimulates bone resorption indirectly by increasing the maturation of osteoclasts via osteoblasts. It also stimulates renal calcium reabsorption by two mechanisms: (a) by acting on tight junctions in the TAL, thereby increasing the permeability to calcium; and (b) by enhancing the expression of genes involved in calcium transport such as TRPV5 and NCX1 in the DCT, restoring calcemia to its basal value [81]. Besides, it enhances the synthesis of calcitriol ($1,25(OH)_2D_3$). Calcitriol increases the intestinal absorption of calcium [4, 46, 68, 77] and its renal reabsorption, leading to plasma calcium normalization in the long term [4, 35, 68, 145, 168, 210]. Conversely, when plasma calcium concentration is too high, PTH secretion is blunted (Figure 1.8); as a result, calcium reabsorption decreases and calcium urinary excretion increases, which favors a return to equilibrium [60, 210].

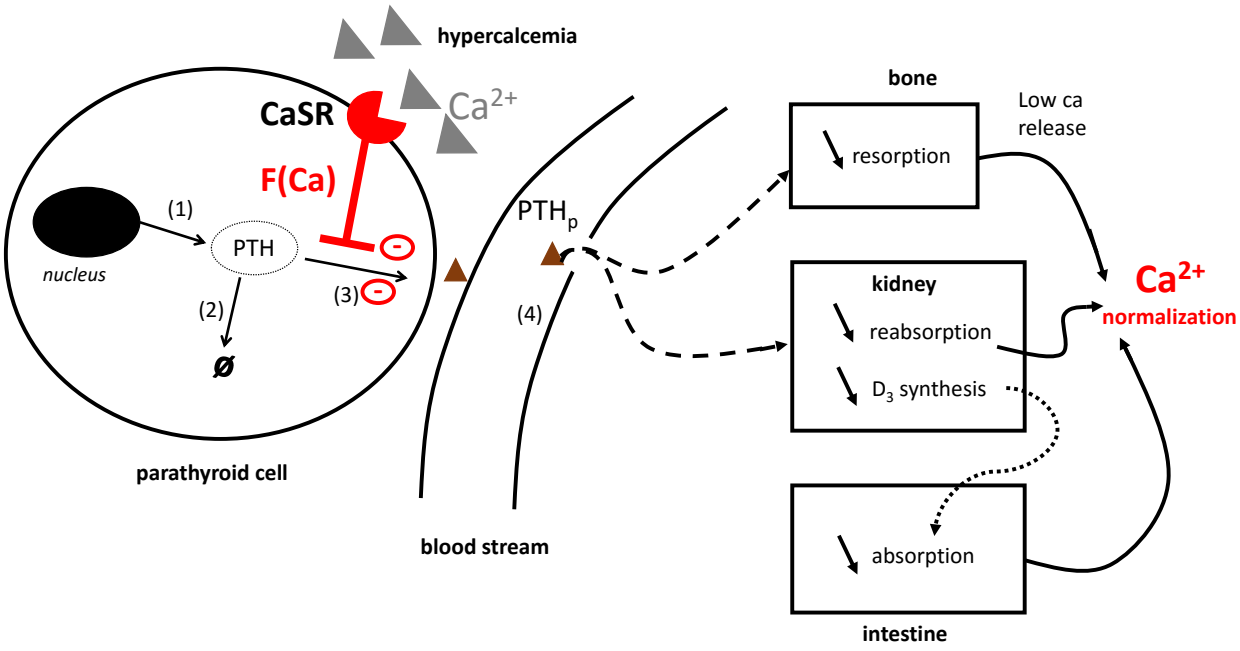


Figure 1.8: Consequences of an hypercalcemia on PTH secretion. (1) PTH synthesis; (2) vesicles degradation; (3) PTH secretion; (4) low concentration of PTH in plasma. During hypercalcemia, PTH secretion is repressed by the calcium sensing receptor. As a result, less PTH is active in plasma, thereby lowering the bone resorption of calcium, its renal reabsorption, and its intestinal absorption (via vitamin D3). Ultimately, this contributes to normalizing calcemia.

### The calcium sensing receptor (CaSR)

PTH secretion is directly regulated by ionized calcium concentration, via the calcium sensing receptor (CaSR). The CaSR can detect very small variations in the concentration of calcium, that is, 0.1 mM or 4% of its equilibrium value [210], and its sensitivity is maximal when the concentration of ionized calcium is between 1.0 and 1.5 mM. CaSR belongs to the protein G coupled receptor C family (GPRCs). There are several calcium binding sites at its surface but they are specific not only to calcium but also to magnesium ($Mg^{2+}$), aluminium ($Al^{3+}$), as well as other cations. CaSR is mainly expressed at the surface of parathyroid glands but also in kidney, bone and intestine [71]. When the plasma calcium concentration increases, more calcium binds to the CaSR, which triggers an intracellular signaling pathway involving G proteins. The subsequent activation of phospholipase C (PLC) stimulates inositol triphosphate production ($IP_3$), which in turn releases calcium from the endoplasmic reticulum. The subsequent increase in intracellular calcium activates proteases which then cleave and inactivate PTH contained in vesicles. This signaling cascade characterizes the rapid regulation of PTH by calcium (in a few minutes). In addition, CaSR has another role: it enhances the rise and proliferation of chief cells in parathyroid glands in case of sustained hypocalcemia, leading to the long term regulation of the parathyroid gland size, on the scale of days or even

weeks.

CaSR is also present in kidneys, where it acts to decrease calcium reabsorption in the TAL by reducing the paracellular permeability for calcium in this segment [134]. Its specific localization and its function in other segments of the kidney are controversial [44, 134, 170]. In bone, studies with mice lacking CaSR in osteoblasts show a decreased bone mass together with an excess of RANKL expression, thereby increasing bone resorption [38]. Besides, CaSR plays an anabolic role in case of high calcium concentration by stimulating osteoblasts maturation and the synthesis of alkaline phosphatase, but its precise impact on calcium homeostasis, that is on the rapidly exchangeable pool in the bone and also deep pool remains unknown [38]. In the intestine, CaSR expression was found in both humans and rats [86]. CaSR is localized on the apical and basolateral sides in the colon and small intestine [89]. Garg and Mahalle suggested the presence of an "intestinal calcistat" which would control intestinal calcium absorption, in addition to the vitamin D system [88]. CaSR could be the sensor of such mechanism since it is widely expressed in the intestine. It would be able to adjust vitamin D synthesis as a function of the calcium concentration in the gastrointestinal tract. For example, in case of high calcium intake, CaSR would be saturated leading to the inhibition of 1-$\alpha$-(OH)-ase in the intestine to reduce vitamin $D_3$ levels [70]. Besides the number of vitamin $D_3$ receptors could be decreased. This would lead to a reduction in intestinal calcium absorption, and inversely in case of low calcium diet. Yet, the precise mechanisms by which CaSR acts are still to be elucidated.

### Vitamin D

The synthesis of vitamin D is intricate and tightly regulated (Figure 1.9). Many nutrients contain the precursor of vitamin D, cholecalciferol. However, sunlight is the main provider of cholecalciferol, through a reaction between cholesterol in skin and ultraviolet (UV) light: 7-dehydrocholesterol is converted to pre-vitamin $D_3$, then to cholecalciferol. Cholecalciferol is carried in the plasma bound to the vitamin D binding protein (VDBP) and is hydroxylated in position 25 in the liver by several enzymes of the P450 cytochrome, particularly CYP2R1. 25(OH)-vitamin D (or calcidiol) is the storage form of vitamin D. Its plasma concentration is about 20-100 nM and its half-life is several days. It is converted to 1,25$(OH)_2$ vitamin D (calcitriol) by hydroxylation in position 1 by 1-$\alpha$-hydroxylase (CYP27B1) [106] mainly in proximal tubule cells.

Calcitriol is the active form of vitamin D. Its plasma concentration is tightly regulated, at the synthesis level by CYP27B1 and at the degradation level by CYP24A1. Its concentration is between 50 and 150 pM, that is, about 1000 times less than that of 25(OH)-vitamin D [92]. Besides, its half-life is several hours. CYP27B1 activity is increased by PTH and repressed by plasma calcium and phosphate, together with the FGF23/klotho axis (see below) [68]. Calcitriol inhibits its own synthesis and activates its degradation by respectively repressing CYP27B1 and raising CYP24A1. In case of inactivating mutations of CYP27B1, vitamin D-dependent rickets is observed (OMIM 264700). Inactivating mutations of CYP24A1 lead to infantile hypercalcemia (OMIM 143880) and hypersensitivity to low doses of vitamin D, resulting in hypercalcemia [181].

Calcitriol is a calcitropic hormone that mobilizes calcium by acting on the kidney, specifically by increasing calcium reabsorption in the distal tubule. In addition, it enhances calcium absorption in the intestine, and it stimulates resorption in bone. Furthermore, calcitriol inhibits PTH synthesis, thereby contributing to the maintenance of calcium homeostasis [189] (Figure 1.10).

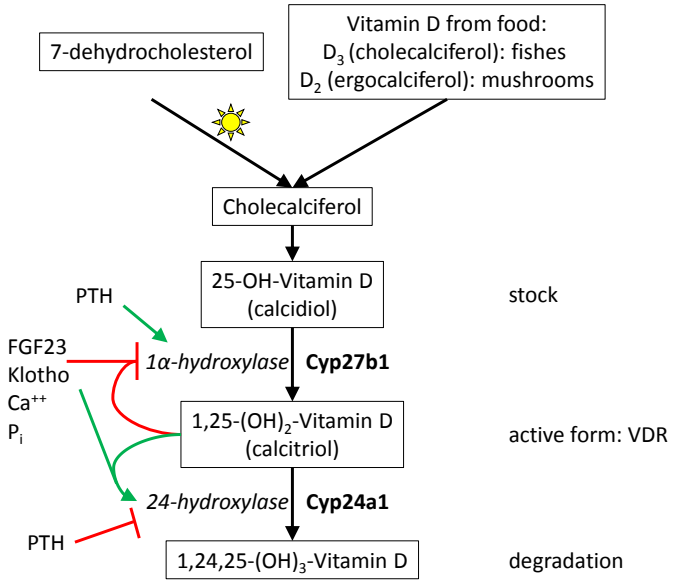


Figure 1.9: The vitamin D synthesis pathway. Taken from Granjon D, Edwards A, Bonny O, submitted.

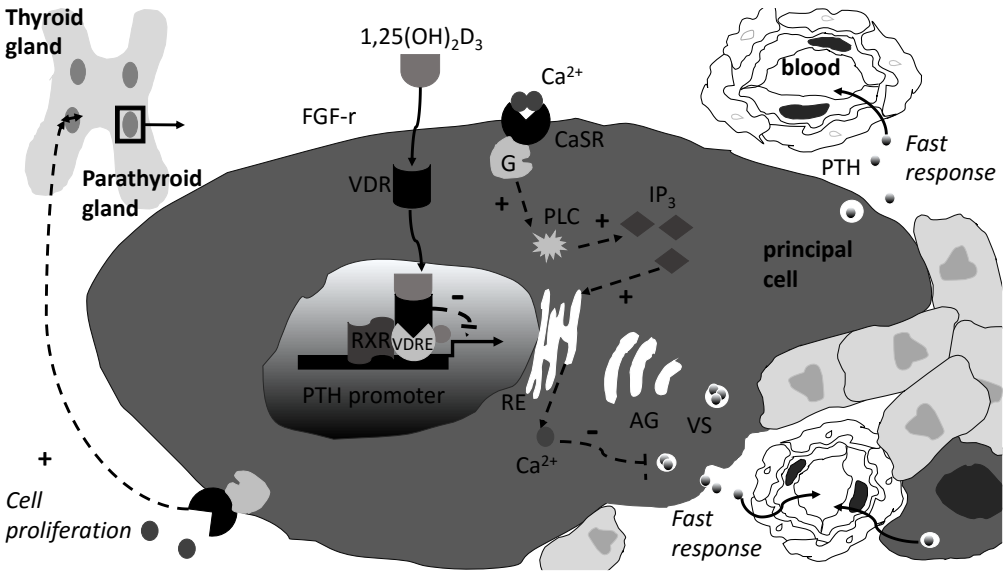


Figure 1.10: CaSR inhibits PTH secretion through a complex mecanism. Additionally vitamin $D_3$ represses PTH synthesis.

### Calcitonin

Calcitonin is another hormone that regulates calcium homeostasis. It is composed of 32 amino acids and secreted by parafollicular cells in the thyroid gland [59]. Its secretion is regulated by the calcium sensing receptor. Calcitonin receptors (CTR) are coupled to G-proteins and are found in osteoclasts and kidneys. Calcitonin is an antagonist of PTH, that is, it decreases plasma calcium concentration thus preventing acute hypercalcemia. Calcitonin decreases bone resorption by inhibiting the maturation osteoclasts [74]. Furthermore, it has been shown in humans that it increases renal calcium excretion, even if the mechanisms remains to be clarified. Its role in bone and in kidney is limited and a desensitization is quickly observed when calcitonin is used to treat hypercalcemia.

In conclusion, calcium homeostasis is the result of an extremely complex regulation system composed of sensors, hormones (transducers) and effectors (organs), as shown in Figure 1.11.

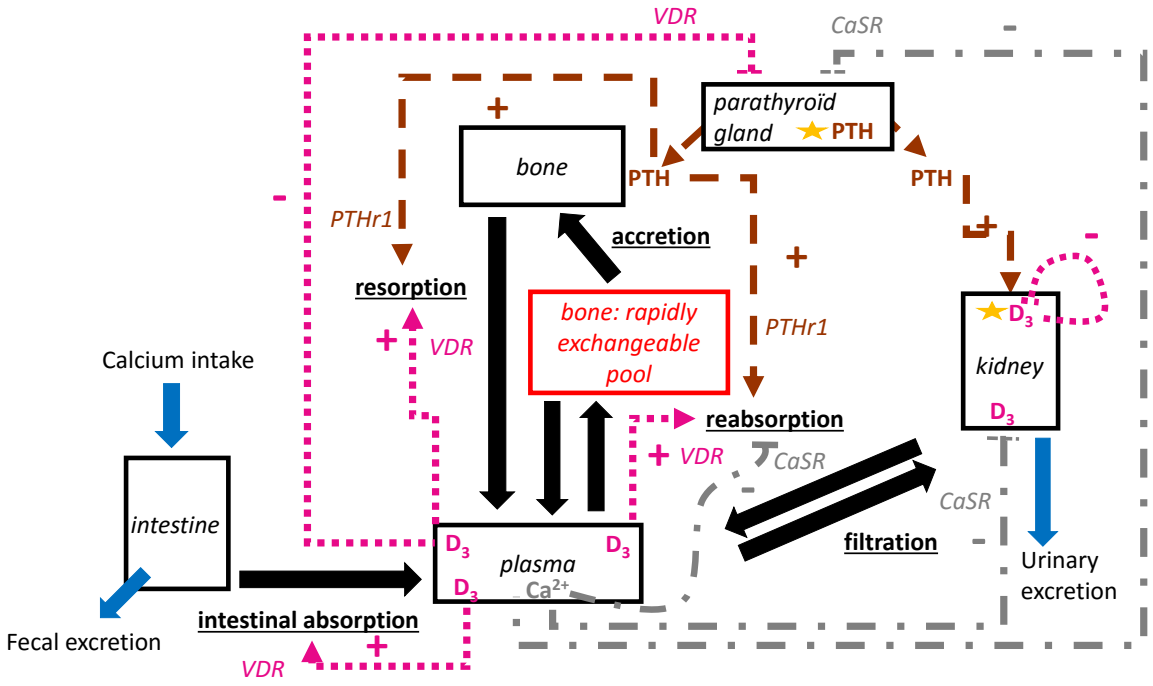


Figure 1.11: A global overview of calcium homeostasis and its regulation by PTH, vitamin $D_3$ and CaSR. PTH, vitamin $D_3$, calcium regulation pathways are respectively shown in brown, pink and grey.

## 1.2 Overview of phosphate homeostasis

The homeostasis of calcium cannot be studied without considering that of phosphate, owing to the tight relationship between these two species. In the following section, we briefly described the determinants of phosphate homeostasis and its interaction with calcium.

### 1.2.1 Phosphate distribution in the organism

In the organism phosphate is the skeleton of DNA, and the second major element of bone after calcium. It plays a key role in metabolic pathways, such as ATP hydrolysis, and in transduction signals (MAPK,MAPKK). It is present in two forms in the body, as inorganic phosphate and as a component of organic compounds. Phosphate is distributed as follows: 85% is found in bone and teeth (as hydroxyapatite), 14% in tissues and cells (as phospholipids, phosphoproteins), and 1% in the extracellular compartment. In plasma, 50% of phosphate species is present as $H_2PO_4^-$ /$HPO_4^{2-}$ , 40% forms complexes with other ions such as $Ca^{2+}$, $Na^+$ and $Mg^{2+}$, and the last 10% is bound to proteins [131, 72]. Sodium-phosphate complexes account for 30% of total plasma phosphate. All but the protein-bound forms, that is, 90% of plasma phosphate, are freely filtered by the kidney.

### 1.2.2 Phosphate transport in organs

#### Intestinal absorption of phosphate

Phosphate crosses the intestinal barrier via paracellular and transcellular pathways [138, 85]. About 70% of the ingested phosphate is absorbed mainly in the duodenum and jejunum [203]. On a low phosphate diet, the transcellular route predominates, whereas on a high phosphate diet, paracellular transport prevails. There are several phosphate transporters in intestinal cells, namely Pit1, Pit2, NaPi-IIb (apical side); Pit transporters belong to the Type III sodium-phosphate co-transporters also known as SLC20, whereas NaPi-IIb is part of Type II sodium-phosphate co-transporters or SLC34. NaPi-IIb mediates 90 % of total absorption. The regulation of phosphate absorption by vitamin D is controversial; in the jejunum, the effects of vitamin D appear to be small [219, 45, 138, 172]. Moreover, it has been shown that aging could reduce the stimulatory effect of vitamin $D_3$ together with NaPi-IIb expression [226].

#### Renal phosphate handling

The ionized and ion-bound forms of phosphate are freely filtered by the kidney, representing about 90% of the total plasma phosphate, but this fraction can decrease in case of hypercalcemia through calcium-phosphate fetuin complexes [162]. Approximately 70 to 80 % of the filtered load is reabsorbed in the proximal tubule [203], mostly via the cotransporter NaPi-IIa (or SLC34A1), which accounts for 80% of phosphate reabsorption in that segment, but also by NaPi-IIc. About 10% is reabsorbed in the distal tubule but the nature of the transporter(s) involved has yet to be discovered [23]. In the proximal tubule, phosphate reabsorption is negatively regulated by PTH, FGF23

[184, 114], and high phosphate intake. However, the role of 1,25$(OH)_2$D in the regulation of renal phosphate reabsorption remains unclear [85].

### 1.2.3 Hormonal control of phosphate homeostasis

#### FGF23, a regulator of phosphate homeostasis

FGF23 is a 32 kDa protein that belongs to the family of fibroblast growth factors; FGFs are involved in diverse functions such as development, repair, and metabolism [133]. FGF23 exists under 2 different shapes: $^{25}$(FGF23)$^{251}$ which is biologically active, and $^{25}$(FGF23)$^{179}$ which lacks the binding domain to klotho, resulting in an inactive pattern [139]. FGF23 is synthetized in bone by osteocytes and osteoblasts [28].

FGF23 is an important regulator of phosphate homeostasis. It inhibits phosphate reabsorption in the kidney by reducing the expression of NaPi-IIa [18]. It may also indirectly affect serum calcium by acting on vitamin $D_3$, as further described below. FGF23-null mice have hyperphosphatemia and increased vitamin D levels. In addition, their bone turnover is unexpectedly decreased, for reasons that remain unclear [95].

Vitamin $D_3$ is the most important systemic regulator of FGF23 production. Indeed, VDR-null mice have undetectable levels of FGF23 [139]. Several other regulators are known: DMP1 and PHEX inhibit the synthesis of FGF23 through mechanisms that remain to be elucidated [139]. Conversely, CYP27B1 (1-$\alpha$-(OH)ase) and phosphate enhance the production of FGF23 [186]. It has also been shown that PTH activates the orphan receptor Nurr1 to induce FGF23 transcription [141]. Moreover, FGF23 synthesis is blunted in PTX rats and conversely enhanced in primary hyperparathyroidism. However, the effects of PTH could be indirect, that is, mediated by vitamin $D_3$ [15, 139].

FGF23 is known to protect cells against the toxicity of vitamin $D_3$ (Figure 1.12). The overexpression of FGF23 triggers the suppression of vitamin $D_3$ synthesis. On the other hand, the plasma levels of vitamin $D_3$ are 3-fold higher in FGF23-null mice than in control mice [139, 48, 15]. FGF23 regulates the metabolism of vitamin $D_3$ by inhibiting the expression of CYP27B1 and increasing that of CYP24A1 [48, 184].

Several studies suggest that FGF23 affects the synthesis and secretion of PTH, in part via the MAPK signaling pathways [15]. Intravenous injections of FGF23 decrease the gene expression and secretion of PTH in a dose-dependent manner [124]. On the other hand, other studies suggest a stimulatory effect of FGF23 on PTH secretion, as summarized in reference [139]. In parathyroid glands, FGF23 increases the expression of CaSR and VDR, and thereby plays a hypocalcemic role [42]. In case of hypocalcemia, PTH mRNA is doubled and if FGF23 is added, PTH mRNA is drastically reduced. Interestingly, in hypercalcemia, PTH mRNA is reduced but the addition of FGF23 does not change anything. Besides, the expression of VDR and CaSR is stimulated by FGF23 in case of low calcium concentration, whereas FGF23 has no effect in hypercalcemia even if the expression of VDR snd CaSR is doubled. Uremic patients may develop a resistance to FGF23 since PTH levels are not decreased despite the presence of FGF23. Note that recently, Martin *et*

*al.* observed CKD patients with secondary hyperparathyroidism in spite of elevated FGF23 levels [139]. This is not in line with an inhibitory action of FGF23. There may exist confounding factors to explain this contradiction, especially the reduction in klotho and FGFr1 levels in CKD patients. To date, the interactions between PTH and FGF23 remain to be fully elucidated, as depicted in Figure 1.12.

### Phosphate, a regulator of PTH and vitamin D

Phosphate itself is known to be a regulator of PTH gene expression as shown in Figure 1.12 [188, 119]. On a low (0.02%) phosphate diet, PTH mRNA levels are more than halved; conversely they increase by 25% on a high (1.2%) phosphate diet [119]. The effects of phosphate are direct (i.e., independent of those of vitamin $D_3$ and $Ca^{2+}$) and post-transcriptional, even if the sensing mechanism remains to be identified [140]. Phosphate may also regulate parathyroid cell proliferation in the long term [146]. In addition, phosphate is an independent inhibitor of CYP27B1 (Figure 1.12); however, the underlying mechanisms are not well established [85].

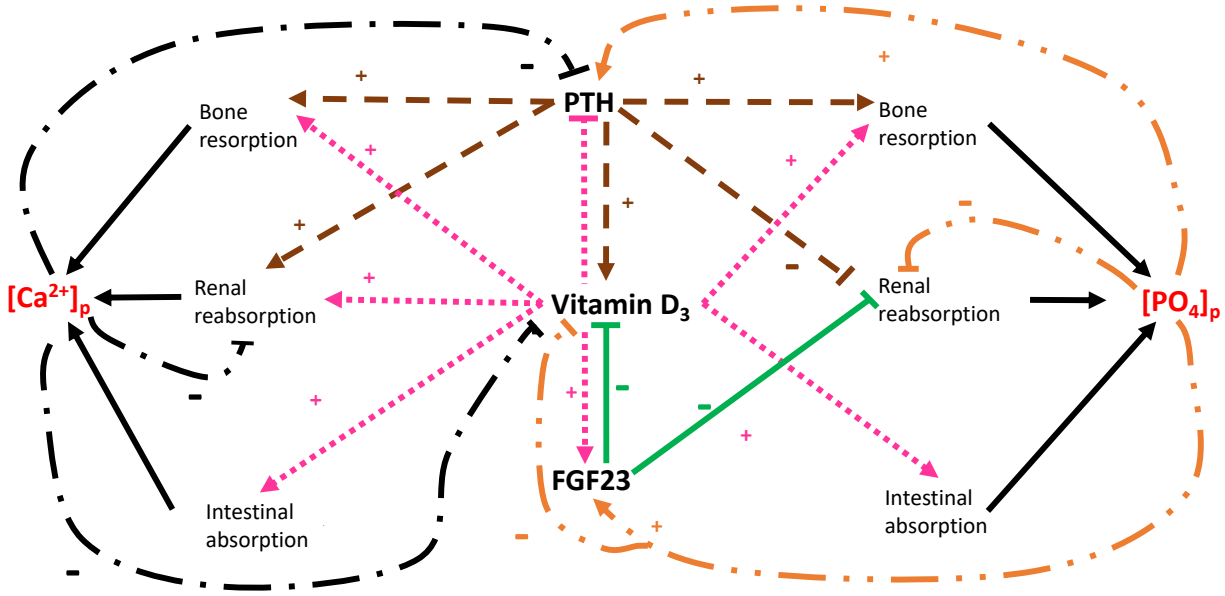


Figure 1.12: Hormonal regulation of calcium and phosphate homeostasis. Shown on the left is the regulation of calcium homeostasis by PTH and vitamin D3. Shown on the right is the regulation of phosphate homeostasis by PTH, vitamin D3, and FGF23.

### 1.2.4 Precipitation of calcium-phosphate

Precipitation and crystallization are often erroneously mingled, yet there are substantial differences. Whereas precipitation is a fast irreversible process, crystallization is relatively slow. Moreover, during crystallization, elements are organised according to a specific lattice while in precipitation, amorphous precipitates are formed. However, they are both dependant on the solubility of the solution, particularly when the concentration of some components exceed their solubility in this solution, they can precipitate or crystallize. In this section, we introduce some aspects of calcium phosphate precipitation, in plasma as well as in the urine.

#### Acid base equilibria between phosphate components

At physiological pH (7.4), the major components of phosphate in plasma are $H_2PO_4^-$ and $HPO_4^{2-}$, whose ratio varies with pH [203]. Phosphate can also be found in the form of $PO_4^{3-}$, but as shown below, the plasma concentration of $PO_4^{3-}$ is negligible. The acid-base reaction between these species can be written as

$$H^+ + HPO_4^{2-} \rightleftharpoons H_2PO_4^-$$

The equilibrium constant of this reaction is defined as

$$K_A = \frac{[H^+][HPO_4^{2-}]}{[H_2PO_4^-]}.$$

In other words,

$$pH = pK_A + \log_{10}\Big(\frac{[HPO_4^{2-}]}{[H_2PO_4^-]}\Big). \tag{1.1}$$

The p$K_A$ of the pair $H_2PO_4^-/HPO_4^{2-}$ is 6.8. Thus, at pH = 7.4

$$\frac{[HPO_4^{2-}]}{[H_2PO_4^-]} = 10^{(pH-pK_A)} = 10^{0.6} = 3.98$$

Note that since the p$K_A$ of the pair $HPO_4^-/PO_4^{3-}$ is 12.3, at pH = 7.4

$$\frac{[PO_4^{3-}]}{[HPO_4^{2-}]} = 10^{-3.9}$$

Hence, the amount of $PO_4^{3-}$ in plasma is negligible, and if $[PO_4]_p$ denotes the total concentration of phosphate species in plasma, we have

$$[HPO_4^{2-}]_p = 0.80[PO_4]_p, \tag{1.2}$$

$$[H_2PO_4^-]_p = 0.20[PO_4]_p. \tag{1.3}$$

### Binding of calcium and phosphate

In plasma, $Ca^{2+}$ reacts with $HPO_4^{2-}$ and $H_2PO_4^-$ as follows:

$$Ca^{2+} + HPO_4^{2-} \underset{k_d^{\mathrm{CaHPO_4}}}{\overset{k_f^{\mathrm{CaHPO_4}}}{\rightleftharpoons}} CaHPO_4.$$

$$Ca^{2+} + H_2PO_4^- \underset{k_d^{\mathrm{CaH_2PO_4^+}}}{\overset{k_f^{\mathrm{CaH_2PO_4^+}}}{\rightleftharpoons}} CaH_2PO_4^+,$$

If the concentration of $CaHPO_4$ and $CaH_2PO_4^+$ reaches a certain threshold, these salts precipitate and form insoluble crystals. The different species that can be formed are listed in Table1.1:

Table 1.1: Calcium Phosphate species

| Name | Abbreviation | Chemical formula | $K_{sp}$ at 37°C |
|---|---|---|---|
| Dicalcium phosphate dihydrate | DCPD | $CaHPO_4.2H_2O$ | $1.87 \times 10^{-7}$ $M^2$ |
| Octacalcium phosphate | OCP | $Ca_8H(PO_4)_6.5H_2O$ | $5.1 \times 10^{-50}$ $M^8$ |
| Hydroxyapatite | HAP | $Ca_{10}(PO_4)_6(OH)_2$ | $2.35 \times 10^{-59}$ $M^9$ |

### Mechanisms of calcium-phosphate precipitation

Whether precipitation occurs depends on the supersaturation S of the system:

$$S = \frac{IP}{K_{sp}}, \tag{1.4}$$

where $IP$ is the ionic product and $K_{sp}$ is the constant of solubility. If $S < 1$, the solution remains below saturation and no insoluble crystals are formed. Conversely, if $S > 1$, the solution is saturated, and the complex forms a solid precipitate. The ionic product is given by:

$$IP = \prod^{n_T} ([x_i] f_{z_i})^{n_i}. \tag{1.5}$$

where $n_T$ is the total number of ions that form the complex, $[x_i]$ is the concentration of ion $i$ and $n_i$ is the stoichiometric coefficient of $i$. The activity coefficient (denoted $f_{zi}$ below) depends on the valence $z_i$ of $i$ as well as the ionic strength $I$ of the solution, which is determined using the Davies formula [213]:

$$-\log_{10}(f_{zi}) = A \times z_i^2 \Big( \frac{I^{1/2}}{1 + I^{1/2}} - 0.3 \times I \Big). \tag{1.6}$$

$$I = \frac{1}{2}\sum_{1}^{n}[x_i]z_i^2. \tag{1.7}$$

where $A$ is estimated as 0.52 at 37°C. Note that Eq. (1.6) can be used only if $I \leq 0.5$ M; in human and rat plasma, $I$ is approximately equal to 0.16 M [80]. Substituting this value of $I$ into Eq. (1.6), we obtain

$$f_{zi} = 10^{0.12\times z_i^2}, \tag{1.8}$$

which yields $f_1 = 0.76$, $f_2 = 0.33$ and $f_3 = 0.08$, respectively, for monovalent, divalent, and trivalent ions. In practice, the renal threshold for saturation is not 1 but about 10 [101] even if there exist a individual variability, depending on plasma pH and other individual-specific factors..

Thus, the supersaturation index for DCPD is given by:

$$S_{DCPD} = \frac{IP_{DCPD}}{K_{sp,DCPD}} = \frac{[Ca^{2+}][HPO_4^{2-}]f_2^2}{K_{sp,DCPD}} = 0.9. \tag{1.9}$$

Since $S_{DCPD}$ is less than 10, DCPD does not precipitate in plasma under normal conditions. However, it is important to note that changes in the concentration of calcium and/or phosphate could raise $S_{DCPD}$ above 10. As the amount of $PO_4^{3-}$ in plasma is negligible (see 1.2.4), we assume that OCP and HAP never form.

However, some mechanisms are known to prevent the formation of crystals outside of bone.

### Regulation of bone mineralization by fetuin-A

Fetuin-A is a glycoprotein synthetized in the liver which accounts for 25% of the noncollagenous proteins in the bone. It is known to play a major role in mineralization, owing to its high affinity for calcium-phosphate salts such as brushite (DCPD) and hydroxyapatite (HAP). By binding to calcium-phosphate complexes , it forms calciprotein particles (CPPs) in a multistep process, thereby preventing the formation of larger aggregates. However fetuin-A cannot dissolve already formed minerals [110, 164, 126, 123, 163, 155, 215]. Fetuin-A has a major role in preventing the formation of vascular calcifications. It has been shown that patients with chronic kidney disease or with inflammation have reduced levels of Fetuin-A, thereby increasing the risk of mortality [192, 198].

### Precipitation of calcium and phosphate in the urine

The formation of small crystals or precipitate does not necessary lead to kidney stones. Indeed, early crystals can be filtered and are ultimately eliminated in the urine, the latter called crystalluria [116]. Thus the formation of urinary stones involves not only a crystallization step, but also a retention process as well as growth of the initial crystal. Most of the kidney stones are composed of calcium-oxalate, altough some are made of calcium phosphate (brushite, hydroxyapatite) or magnesium phosphate (struvite). There exist several inhibitors of hydroxyapatite formation such as citrate [91], or more recently, hydroxycitrate [53]. Several methods have been designed to estimate the risk of CaP precipitation in urine. In the eighties, Tiselius developed an index based on the

concentrations of calcium, phosphate, citrate and pH [206]. It is defined as follows:

$$\text{Risk}_{CaP} = \frac{1}{pH_{CaP} - 5.8}. \tag{1.10}$$

$\text{pH}_{Cap}$ is the pH corresponding to the formation of 500 particles which is interpolated and 5.8 is the starting pH (in urine pH may vary from 4 to 8). As a result, if $\text{pH}_{Cap}$ is near 5.8, the risk is high and conversely. Tiselius also considered the ion activity product of CaP in human which is:

$$AP_{CaP} = \frac{0.0027 \times Ca^{1.07} \times PO_4^{0.70} \times (pH_u - 4.5)^{6.8}}{Cit^{0.20} \times V_u^{1.31}}. \tag{1.11}$$

He concludes that if $AP_{CaP}$ is higher than 60, there is a great risk of precipitation. According to this formula, calcium, phosphate and $\text{pH}_u$ are activators of precipitation, whereas citrate and urine volume $\text{V}_u$ are inhibitors. Equation (1.11) was refined in 2012 by the addition of magnesium [207] and extended to the mouse. Furthermore, several programs exist to calculate the supersaturation of ions such as SUPERSAT, EQUIL2 and JESS [173].

## 1.3 Historical perspectives on Mathematical Models of Calcium Homeostasis

In this part, we review the evolution of calcium homeostasis modeling and their increasing complexity over time.

### 1.3.1 The first calcium kinetic studies

The first models designed to understand calcium homeostasis were developped in the early sixties [11, 9]. $^{45}$Ca was used to investigate the dynamic aspects of calcium exchanges in the rat. Aubert and Milhaud [11] proposed a new method to quantify the contribution of each compartment after an intravenous injection $^{45}$Ca. Their model is composed of a central compartment and a bone calcium pool. They considered calcium absorption by the intestine and calcium excretion by kidneys together with fecal excretion and bone turnover (Figure 1.13). They showed that $^{45}$Ca disappearance can be modeled by a 4 exponential decreasing curve corresponding to several exchangeable pools of calcium. Yet, it is not obvious that each of these pools corresponds to an existing, physiological pool. They mentionned the existence of two mechanisms for bone calcium exchanges: a fast phenomenon at the surface of bone and a slow process in the deep bone. However, they did not incorporated these features in their model. Furthermore, the hormonal regulation of calcium homeostasis was not studied at all, even though the impact of PTH on calcium homeostasis had been known for several years. PTH was discovered in 1925 by Collip [57], and its resorptive effects were observed by Barnicot in 1948 [13]. Jahan and Pilts highlighted its anti-calciuric effect the same year [109]. Calcitonin was discovered later in 1962 [59].

The model of Aubert and Milhaud aimed to determine calcium exchanges between plasma and

bone such as accretion and resorption. Finally in 1969, Besançon and Gueguen suggested that bone resorption can be regulated by parathyroid hormone and calcitonin [21].

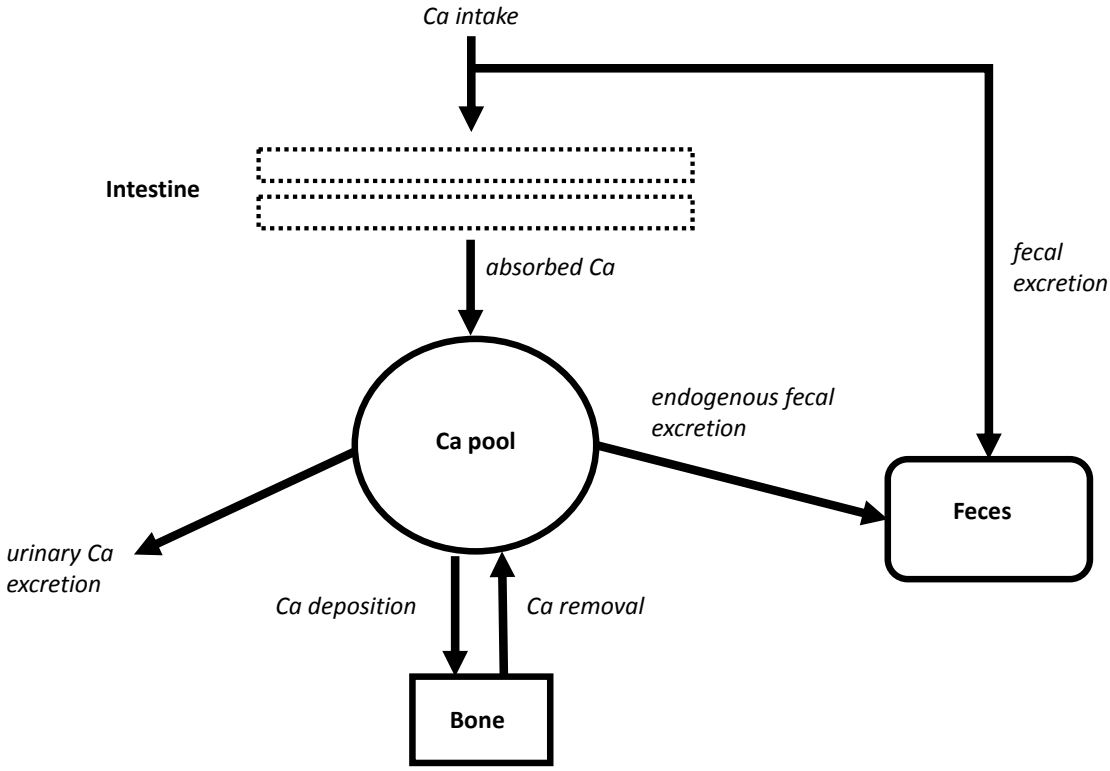


Figure 1.13: Schematic diagram of calcium exchanges between plasma, bone, intestine, and kidney in the model of Aubert and Milhaud [11].

### 1.3.2 A global model of calcium Homeostasis

Later, Powell developed a more complex model including hormonal regulation by parathyroid hormone and calcitonin [160]. This model was inspired by the one that of Aubert and Bronner developed 5 years later after their original study [10]. Even though the author mentioned the existence of a rapid bone pool and a fast bone pool, only one bone compartment was taken into consideration. The model did account for the opposite effects of PTH and calcitonin on bone metabolism; as depicted in Figure 1.14, whereas PTH increases bone resorption and inhibited bone accretion, calcitonin enhances calcium storage in bone and decreases calcium release from bone. However, the role of PTH and calcitonin on the intestinal absorption of calcium were not integrated as they are controversial. Finally, the model took into account the feedback mechanisms between PTH and calcium and those between calcitonin and calcium [160] whereas Aubert and Bronner in 1965 had only considered the effect of PTH [10].

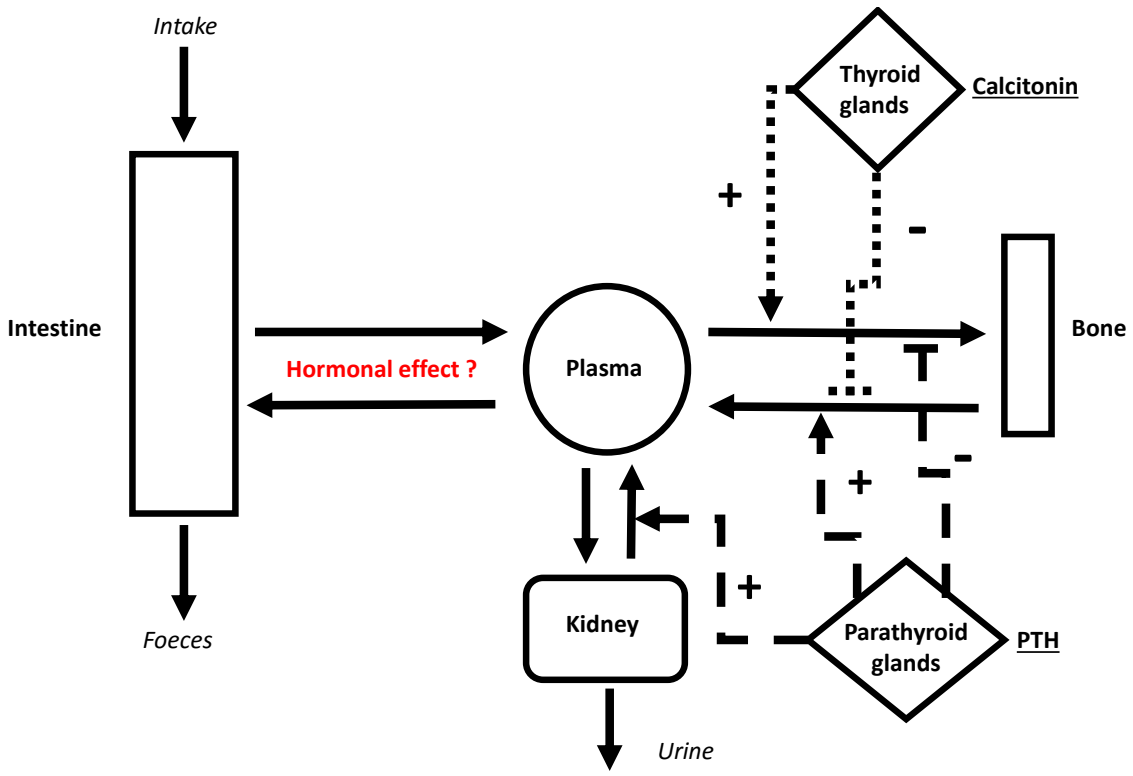


Figure 1.14: Schematic diagram of the model proposed by Powell in 1972.

The rate of calcium intake is denoted $\nu_i$, $\alpha$ is the fraction of ingested calcium absorbed in the intestine, therefore the rate of calcium absorption is $\nu_a = \alpha\nu_i$. The rate of endogenous fecal excretion $\nu_f$ is defined as $\nu_f = \nu_d(1-\beta)$, where $\nu_d$ is the rate of calcium excretion from plasma into the the intestine and $\beta$ is the fraction reabsorbed into plasma. Thus, the net flux $J_c(t)$ from intestine to plasma is:

$$J_c(t) = \alpha\nu_i - \nu_f \tag{1.12}$$

Bone metabolism is modeled as follows:

$$\Delta(t) = \nu_{o+} - \nu_{o-}, \tag{1.13}$$

where the first and second terms on the right-hand-side respectively characterize the rates of bone accretion and bone resorption. As a result, the dynamic evolution of the plasma calcium concentration is given by:

$$\frac{d[C]}{dt} = \frac{1}{V_p}\Big(S_i(t) - \Delta(t)\Big). \tag{1.14}$$

$S_i(t)$ is defined as $J_c(t) - \nu_u$, where $\nu_u$ is calcium urinary excretion and $V_p$ the plasma volume. Then to take into consideration hormonal regulation, Powell decomposed each flux into two components,

a non regulated part and a regulated part; for example:

$$\nu_{o+} = \nu'_{o+} + l_i[H]. \tag{1.15}$$

The first term on the right-hand-side represents the part of bone accretion that is not regulated and the second part incorporates its regulation by hormones (H) such as PTH and calcitonin (respectively denoted [P] and [T]).

The dynamics of each hormone are described by the following equations:

$$\frac{d[P]}{dt} = \frac{R'\Big(C_{ZP} - [C]\Big)}{V_p} - m(P)[P]. \tag{1.16}$$

$$\frac{d[T]}{dt} = \frac{M'\Big([C] - C_{ZT}\Big)}{V_p} - m(T)[T]. \tag{1.17}$$

$J_P(t) = R'\Big(C_{ZP} - C\Big)$ is the secretion rate of PTH from parathyroid gland. Dilution into plasma is taken into account. m(P) represents PTH degradation from plasma. The terms for calcitonin are similar. The control of PTH and calcitonin secretion by calcium is expressed by the constants $C_{ZP}$ and $C_{ZT}$ at which secretion rates are null; beyond these values, secretion is fixed to 0 so that it cannot be negative, for physiological consistency.

Powell mentionned that techniques to determine hormonal concentration were not available for his model. Thereby, this model enables to investigate their contribution on calcium homeostasis. Furthermore, plasma concentration of calcium is known to be very stable allowing only small variation ($\pm$ 10%) and this model has some problems to corresponds to this criteria.

### 1.3.3 Dividing the bone compartment into two exchangeable pools

One of the first models to included the rapidly exchangeable pool of calcium in the bone was that of Cohn and coworkers [55]. The model is shown in Figure 1.15. This study is noteworthy since it compares model predictions to a balance study and tries to quantify the size of each pool. However, they assumed that the rate of exchange between the rapidly exchangeable pool of calcium in the bone and plasma are equal, a hypothesis that has since been refuted. Moreover, the fast bone pool in their model is decoupled from the deep bone pool, which has not been demonstrated experimentally. Besides, the investigators described difficulties in determining the resorption rate: since the method is indirect and based on balance studies, they found negative resorption rates for high calcium intake, which is not physiological. Finally, the hormonal regulation was not incorporated in this model even though the authors highlighted it in the discussion.

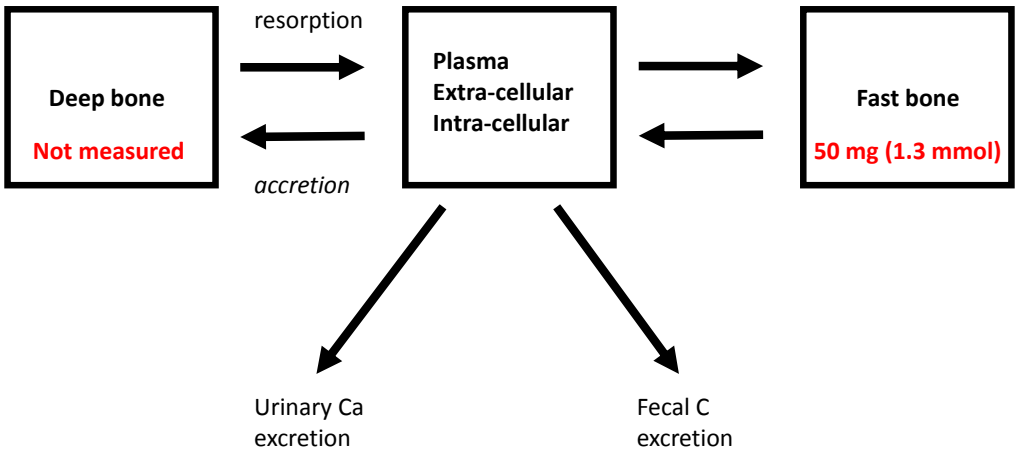


Figure 1.15: Simplified model of calcium homeostasis including the two calcium bone pools from [55]. Parameters have been measured using radiolabelled $^{45}$Ca.

Later in 1977, Knop *et al.* developed a more elaborate model of calcium homeostasis in human [122]. It is a multi-compartmental model including the two bone compartments which are coupled. Contrary to previous models (Figure 1.15), they considered accretion as the flow from the rapidly exchangeable pool to the deep bone pool of calcium, not the direct flow from blood to the rapidly exchangeable pool.

The model consists in 4 linear first-order differential equations that result from Figure 1.16. Their model predicts that in a healthy subject, the flux from the rapidly exchangeable pool to soft tissue (i.e., the extracellular and intracellular pools) represents 70% of the exchangeable bone calcium while accretion is only 13%. The mineralization turnover (that is, the percentage of calcium incorporated into bone compared to the total skeletal mass of calcium) is predicted to be 15% per year . Several cases, in addition to the "normal" condition, were examined, including pseudohypoparathyroidism and primary hyperparathyroidism. In conclusion, this study supports the hypothesis that calcium homeostasis is mainly regulated by the turnover of the rapidly exchangeable pool.

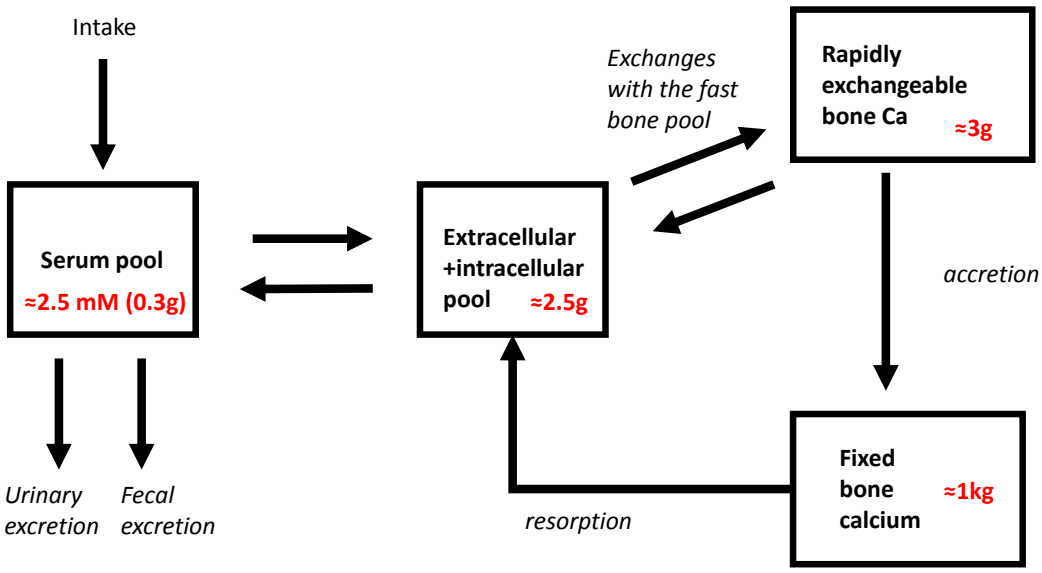


Figure 1.16: A model of $^{47}$Ca kinetics in humans according to Knop and coworkers [122].

### 1.3.4 Toward more elaborate models

The main weakness of the previous models is that they do not consider the impact of hormones on calcium homeostasis, except that of Powell [160]. None of them included the effects of vitamin D effects on calcium metabolism. In this part, we review the first models that included such regulation.

#### The model of Hurwitz

In 1983, Hurwitz *et al.* developed a global model of calcium homeostasis in the bird using experimental work on vitamin D and parathyroid hormone metabolism [106]. Calcitonin was not included because its role in calcium homeostasis was not clear. The model is composed of the main calcium compartments, that is, the intestine, bones, and kidneys, together with parathyroid glands. The equation describing plasma calcium dynamics is:

$$\frac{dC}{dt} = \frac{1}{V_b}\Big(F_i - F_k - F_b\Big). \tag{1.18}$$

$F_i$, $F_k$ and $F_b$ respectively denote net intestinal, kidney and bone calcium fluxes; $V_b$ is the blood volume. $F_i$ is the difference between calcium intake and calcium fecal excretion. It is increased by

vitamin $D_3$.

Hurwitz *et al.* computed $F_i$ as:

$$F_i = \alpha F_{in} = 0.13F_{in} + 0.70LF_{in}, \tag{1.19}$$

where $F_{in}$ is calcium intake. The coefficient 0.13 corresponds to the fraction of intestinal absorption that is independent of vitamin D, 0.70 is the fraction that is regulated by vitamin D and $L$ is the calcium absorption capacity. $F_k$ is the difference between filtered plus secreted calcium and reabsorbed calcium. $F_b$ is the difference between calcium utilized for bone formation and calcium released by bone resorption. Bone resorption is enhanced by PTH such that $F_b$ can be rewritten as:

$$F_b = A - P_b P, \tag{1.20}$$

where $A$ is the PTH-independent calcium flux into bone and $P_b$ characterizes the linear effect of PTH. Thus, if $A < P_b P$ there is negative net flux and vice versa.

Furthemore, Hurwitz *et al.* added the extracellular calcium compartment ($C_e$) of volume $V_e$ which can exchange calcium with the plasma:

$$\frac{dC_e}{dt} = \frac{K\Delta C}{V_e}. \tag{1.21}$$

$K$ is a kinetic distribution constant and $\Delta C$ is the calcium concentration difference between plasma and the extracellular compartment. Eq 1.18 becomes:

$$\frac{dC}{dt} = \frac{1}{V_b}\Big(F_i - F_k - F_b - K\Delta C\Big). \tag{1.22}$$

Parathyroid hormone dynamics was modeled as follows:

$$\frac{dP}{dt} = G_p - B_p P. \tag{1.23}$$

The first term on the right-hand-side represents PTH secretion. This function was tabulated according to the data of Brown [37] so that it is a decreasing sigmoidal function of calcium. The second term is a first order degradation rate. Regarding vitamin $D_3$ synthesis, Hurwitz *et al.* assumed an infinite supply of vitamin D precursor (25(OH)D). They took the effect of PTH on CYP27B1 into consideration but not that of calcium. The activity of 1-$\alpha$(OH)-ase (E) was then defined as:

$$\frac{dE}{dt} = G_E - B_E E. \tag{1.24}$$

$G_E$ corresponds to a sigmoidal increasing function of PTH (P). Two pools of vitamin $D_3$ were considered: one in plasma ($D_B$) and the other in the intestine ($D_I$) such that:

$$\frac{dD_B}{dt} = -R_2 D_B + R_1 D_I + \frac{E}{V_T} - B D_B. \tag{1.25}$$

The first two terms characterizes vitamin $D_3$ exchanges between intestine and plasma whereas the third one represents vitamin $D_3$ production by CYP27B1 divided by the total volume $V_T$ (i.e., the sum of $V_e$ and $V_b$); lastly, the fourth term is the inactivation of vitamin $D_3$. It is obvious that:

$$\frac{dD_I}{dt} = -R_1 D_I + R_2 D_B. \tag{1.26}$$

This simple model allowed the authors to perform simulations such as investigating the effects of a calcium load, an EDTA infusion and also a vitamin $D_3$ defficiency. They concluded that bones handle hypocalcemia whereas kidneys handle hypercalcemia. Bones and kidneys react within minutes whereas intestine reacts with a lag of several hours, due to the delay in vitamin $D_3$ production and diffusion. Besides, intestinal absorption can adapt to a large range of calcium intake so as to maintain plasma calcium concentration within tolerated bounds with an exception for very low intake where it is not enough to allow for normal bone formation. In spite of the effort made to include hormonal regulation, this model lacks a lot of feedback loops partly because some discoveries were made after the model was developed. For instance, the net flux of calcium towards the kidney was modeled as a third degree polynomial function without taking the effect of PTH nor vitamin D and calcium sensing receptor into consideration. The different sites of calcium along the nephron, namely the proximal tubule, the thick ascending limb, and the distal tubule, were not distinguished. In addition, vitamin $D_3$ regulation was incomplete since the inhibition of PTH synthesis was missing together with its effect on bone metabolism.

This model was improved in 1987 [107]. Remarkably, the authors included the effets of growth process which had never been done before. They modeled the body weight by a Gompertz function:

$$W_B = W_1[\exp -W_2(\exp -W_3 t)]. \tag{1.27}$$

Consequently, they linked plasma volume and extra-cellular space with body weight as follow:

$$V_b = V_1 W_B, \tag{1.28}$$

and

$$V_e = V_2 W_B. \tag{1.29}$$

Additionally, Hurwitz and coworkers modified their bone and kidney functions according to body weight [107]. They limited the calcium absorption capactity to 90%, which seems too high based on actual observations. They predicted oscillations probably as a result of the dual effect of PTH, but did not provide experimental support.

### The latest models of calcium homeostasis

To date, the most complete models of calcium homeostasis are those of Raposo and Peterson [168, 157]. They gather all improvements of previous models. Among the most noticeable changes, they include phosphate which had never been done before. The model proposed by Raposo *et al.* is composed of 11 compartments relative to calcium and phosphate homeostasis. Figure 1.17 only depicts the calcium homeostasis model developped by Raposo *et al.* in 2002.

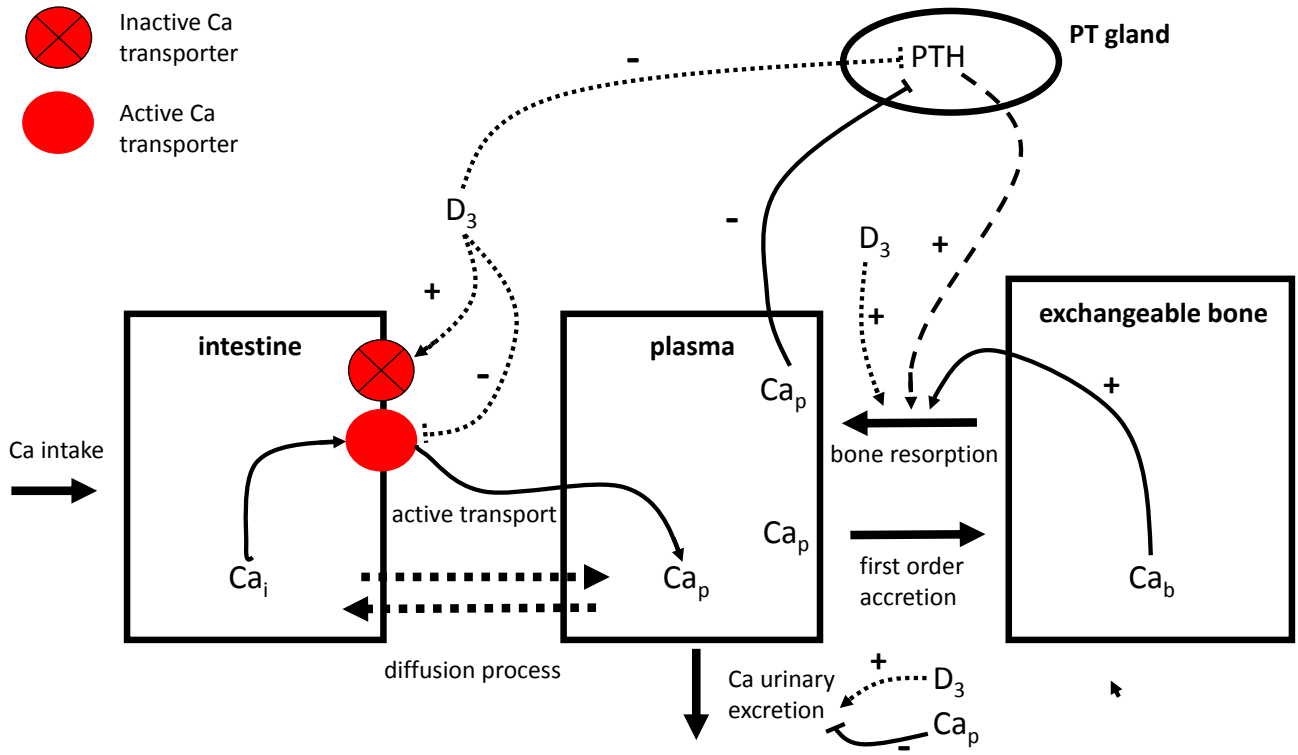


Figure 1.17: A model of calcium homeostasis according to Raposo and coworkers.

In contrast to previous models [107], Raposo *et al.* considered the effect of vitamin D on bone resorption. Moreover, the intestinal transport of calcium was modeled as follows: calcium diffuses from the intestine into plasma and conversely; active transport is regulated by vitamin D such that inactive translocators are activated and active translocators are inactivated. This pathway is saturable and modeled by a Michaelis-Menten function. However, Raposo and coworkers did not consider the regulation of the intestinal paracellular pathway, specifically the vitamin $D_3$-mediated modulation of calcium transport across claudins. PTH synthesis and secretion are inhibited by plasma calcium and vitamin $D_3$. Yet, the vitamin $D_3$ synthesis pathway was not represented in that study. One of the most regulated flux is bone resorption which is increased by PTH, vitamin $D_3$ and bone calcium. The model representation of the renal compartment is the most questionable. The authors erroneously assumed that urinary excretion is increased by vitamin D3 and inhibited

by calcium, whereas the opposite holds. As mentionned above, this model also includes phosphate metabolism for which regulation mechanisms are not described as well as for calcium. Furthemore, the coupling between calcium and phosphate, that is to say calcium phosphate salt formation, is not explicitly represented. Finally, some aspects of bone metabolism, such as the role of interactions between osteoblasts and osteoclasts in bone remodeling processes, are not taken into account.

In 2010, Peterson and Riggs compiled almost all existing models about calcium homeostasis, including that of Raposo *et al.*, and improved the description of the bone compartment [157]. They added bone morphogenenic units such as RANK, RANK-L and OPG based on models of Lemaire and Bellido [129, 14]. Their main goal was to predict the two different effects of PTH on bone namely an anabolic effect in case of daily ponctual administration and catabolic effect if the administration is continuous. The model is composed of 28 highly coupled non-linear differential equations. Stimulation effects are modeled with a sigmoidal increasing function:

$$H_x^+ = \frac{\alpha x^\gamma}{x^\gamma + \delta^\gamma}, \tag{1.30}$$

where $\alpha$ is the maximum response, $\gamma$ is the slope, $\delta$ is the value for which the response half maximal. This function is equal to 0 in the absence of the activator which is not always the case. For example, the enzyme 1-$\alpha$(OH)-ase is activated by PTH but has a basal, PTH-independent production rate. As a result authors defined a threshold sigmoidal function:

$$H_x^\pm = \alpha \pm \frac{(\alpha - \rho)x^\gamma}{x^\gamma + \delta^\gamma}, \tag{1.31}$$

with $\rho$ the minimum response. These functions are frequently employed to model activating-inhibiting processes. They replace functions tanh previously defined by Raposo *et al.* which are more difficult to interpret from a biological point of view.

The model is depicted in Figure 1.18. The authors considered two bone pools assuming that 90% of bone exchange occurs passively whereas 10% is under the control of osteoblasts and osteoclasts. Compared to the model of Raposo, they did not considered the effects of vitamin $D_3$ on calcium release from the exchangeable bone pool. They only modeled the contribution of PTH in the RANK/RANK-L/OPG system. Yet vitamin $D_3$ is known to enchance the production of RANK-L by oseoblasts. Intestinal absorption follows the same scheme as in the model of Raposo and coworkers. Kidney reabsorption of calcium is stimulated by both PTH and vitamin $D_3$ in agreement with experimental observations. The inhibition of calcium reabsorption by the calcium sensing receptor is missing. Finally, 1-$\alpha$(OH)-ase activity is enhanced by PTH and repressed by phosphate. In this model, the authors include phosphate but do not include important aspects of the coupling between phosphate and calcium. For example, it has been known for a long time that calcium and phosphate exist in different forms in plasma such as $CaHPO_4$ and $CaH_2PO_4^+$. Besides, in the bone a lot of calcium-phosphate salt can be found and mainly hydroxyapatite which results from

a cascade of chemical reactions. However, none of these chemical processes has been included in the model. Furthermore, several hormonal regulation mechanisms of phosphate homeostasis are missing, of note the effect of vitamin $D_3$ on phosphate absorption, the inhibition of phosphate reabsorption in the kidney by PTH. FGF23 which is a major regulator of phosphate metabolism, is not included either in the model.

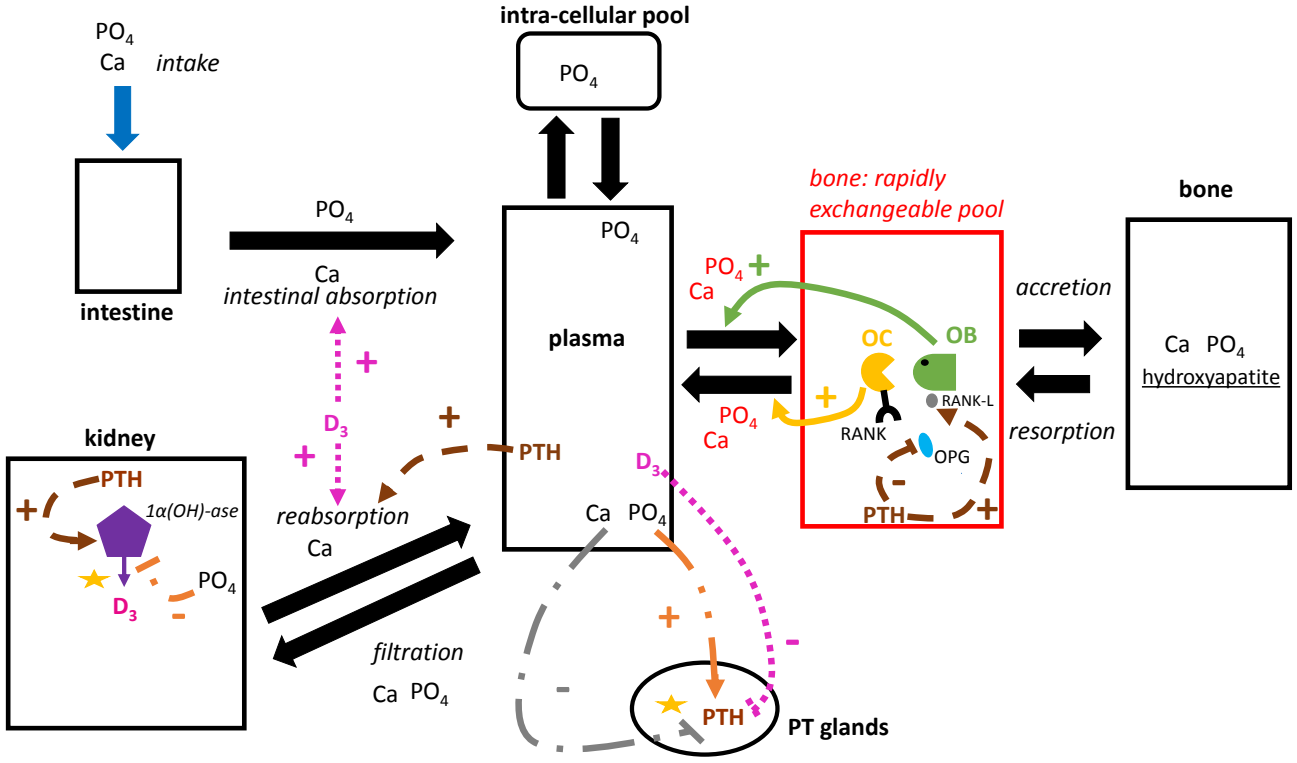


Figure 1.18: A model of calcium and phosphate homeostasis according to Peterson and Riggs.

Recently, Christie and coworkers developed a mathematical model of calcium homeostasis based on that of Peterson and Riggs [51]. They simulated several diseases such as primary hyperparathyroidism (PHP1), vitamin D deficiency. However they found some issues in PHP1 since their model was predicting an hypocalciuria, while in the major cases PHP1 is characterized by hypercalciuria. This is likely a problem in their way to model calcium reabsorption in the kidney since they did not incorporated the effect of calcium sensing receptor in the thick ascending limb.

### 1.3.5 PTH modeling review

In this part, we describe models of PTH synthesis which is the main hormone involved in the regulation of calcium homeostasis.

#### A sigmoidal relationship between PTH and calcium

In 1983, Brown determined the mathematical relationship between PTH secretion and ionized calcium plasma concentration using isolated human and bovine parathyroid cells [37]. He used the following equation to describe PTH secretion

$$Y = D + \frac{(A - D)}{1 + \left(\frac{Ca}{C}\right)^B}, \tag{1.32}$$

where $D$ is the minimal PTH secretion rate, $A$ is the maximal secretion rate, $Ca$ is the ionized calcium concentration, $C$ is the set point and B the slope of the curve. This is a sigmoidal decreasing curve. The set point is about 1.2 mM in humans, versus 1.1 mM in rats. Brown examined the influence of all parameters on PTH secretion. For example, the greater the slope is, the more substantial PTH secretion is for small calcium variations. Increasing the set point shifts the curve to the right and conversely. Figure 1.19 depicts some parameter changes that can be made and their effects.

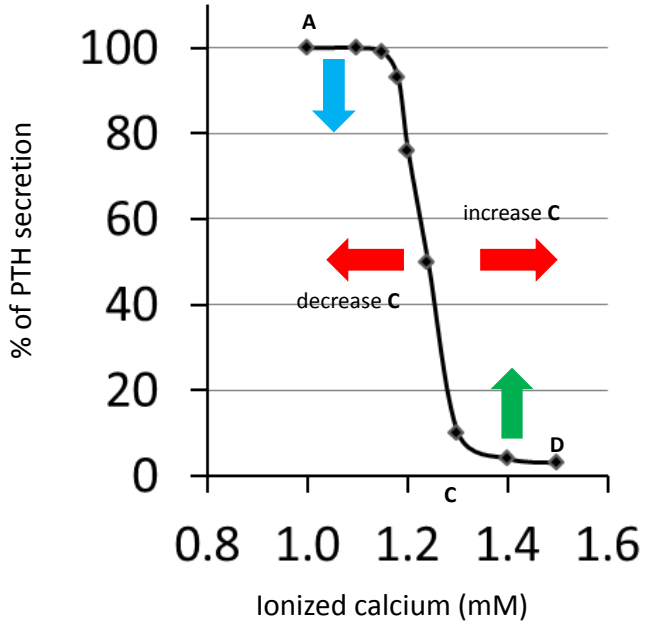


Figure 1.19: Sigmoidal curve representing the percentage of PTH secretion as a function of ionized plasma calcium concentration.

### The first model of PTH synthesis and secretion

Momsen and Shwarz developped the first mathematical model of PTH synthesis and secretion based on the work of Brown [144]. As depicted in Figure 1.20, PTH is synthetized in the parathyroid cells and stored in vesicles. Vesicles can degrade at a constant rate or be carried out the cell. PTH exocytosis is regulated by calcium concentration through the calcium sensing receptor present at the surface of parathyroid cells. Ultimately, PTH is cleared by the liver and kidneys at a constant rate.

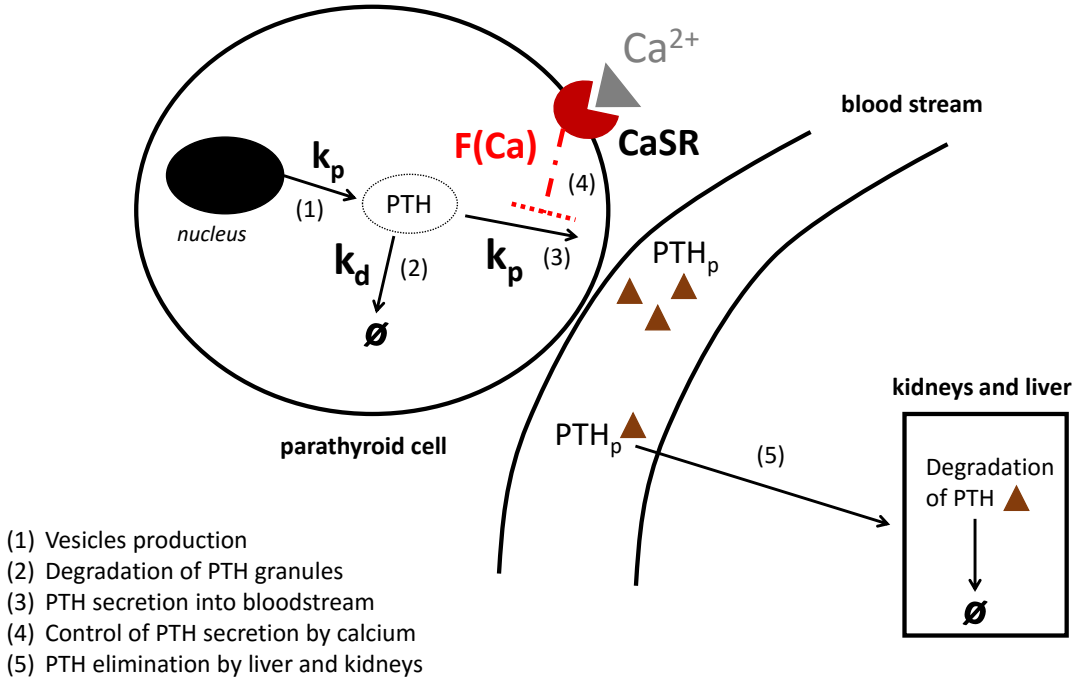


Figure 1.20: The model built by Momsen and Shwarz in 1997.

PTH in the parathyroid gland is denoted $m_c$ and PTH in the plasma is denoted $m_b$ (in mass unit). The corresponding equations are

$$\begin{cases} \dfrac{dm_c}{dt} = k_p - (k_t(Ca) + k_d)m_c, \\ \dfrac{dm_b}{dt} = k_t(Ca)m_c - k_u m_b. \end{cases} \tag{1.33}$$

$k_p$ represents the rate of PTH production within parathyroid cells, $k_d$ is the degradation rate, and $k_t(Ca)$ is the exocytosis function:

$$k_t(Ca) = D + \frac{(A-D)}{1+\left(\frac{Ca}{Ca_s}\right)^C}, \tag{1.34}$$

defined according to Brown (1983). The above system has one steady state ($m_c^*$,$m_b^*$) that satisfies:

$$m_c^* = \frac{k_p}{k_t + k_d}, \tag{1.35}$$

and

$$m_b^* = \frac{k_t k_p}{k_u(k_t + k_d)}, \tag{1.36}$$

Momsen and Scharz assume that Ca can reach a steady state such that $k_t(\text{Ca}) = k_t^{ss}$. Linearizing the system around ($m_c^*$,$m_b^*$) yields:

$$J^* = \begin{pmatrix} -k_t^{ss} - k_d & 0 \\ k_t & -k_u \end{pmatrix} \tag{1.37}$$

Given that Tr(J)$<0$, det(J)$>0$ and $\Delta > 0$, the equilibrium point is a stable node.

The authors performed some experiments such as citrate injection to study the impact of the calcium sensing receptor on PTH response. Ca concentration was reduced by about 0.3 mM during 2 hours. This resulted in a transient PTH release up to 2-10 times the baseline within the first 5-10 minutes. Then plasma PTH decreased until it reached a new steady state value above the previous one. It would have been interesting to also analyze the impact of an hypercalcemic clamp on PTH secretion.

### A more elaborate model of PTH synthesis and secretion

In 2009, Abraham *et al.*, proposed a revised model of PTH synthesis and secretion in both humans and rats [1]. They explicitly modeled the dynamics of plasma calcium by using the following differential equation:

$$\frac{dCa^{2+}}{dt} = k_{in-Ca^{2+}} - k_{out-Ca^{2+}}\Big(1 + H(C_{chel})\Big)Ca^{2+}. \tag{1.38}$$

The first term on the right-hand-side describes the calcium production rate. $k_{out-Ca^{2+}}$ is the first order degradation rate of calcium. The function $H(C_{chel})$ which models the effect of the calcium chelating agents (such as EGTA, EDTA) is a mathematical function often used in pharmacology called precursor-dependent indirect response [183]:

$$H(C_{chel}) = \frac{S_{max}C_{chel}}{C_{chel} + EC_{50}}. \tag{1.39}$$

This description of calcium homeostasis is very simple compared to that found in the model of Peterson and Riggs [157], but coupled to a model of PTH, it is a better way of investigating the

effect of a chelating agent such as EGTA on PTH secretion than the model that Momsen and Shwarz developed several years before [144]. Equations for PTH in parathyroid gland and PTH in plasma are similar to those of Momsen and Shwarz except the function of exocytosis which has been modified:

$$k_{exo} = k_p(1 + mPTH(0)\rho'(Ca^{2+})), \tag{1.40}$$

with

$$\rho'(Ca^{2+}) = \frac{K_D(Ca_0^{2+} - Ca^{2+})}{Ca_0^{2+}(Ca^{2+} + K_D)}, \tag{1.41}$$

$\rho'$ represents the change in CaSR occupancy between time $t = 0$ and any time $t > 0$. The sign of $\rho'$ is directly determined by that of $\Delta_{Ca} = Ca_0^{2+}$ - $Ca^{2+}$. If $Ca^{2+} < Ca_0^{2+}$, $\rho' > 0$ meaning that $k_{exo}$ increases, thereby leading to more exocytosis and conversely. Curiously, authors did not choose a sigmoidal curve. This model adequately reproduces situations of hypocalcemic clamp together with transient calcium drop. Abraham *et al.* mentioned that their model could be improved by adding a plasticity for parathyroid cells to investigate more long-term effects.

**An asymmetric exocytosis function for PTH secretion**

Two years later, Shrestha *et al.* introduced a new function for PTH exocytosis [187]. In their paper, they showed that when they chose a symmetric sigmoidal function as earlier defined by Brown [37], they could predict the bi-exponential behaviour of PTH during an hypocalcemic clamp by sodium citrate. However, in the case of a hypercalcemic clamp, the predicted time profile of PTH did not fit at all the experimental data. Consequently, they modified the sigmoidal function of Brown as follows:

$$\lambda_{Ca(t)} = B + \frac{(A - B)}{1 + \left(\frac{Ca(t)}{S}\right)^{m(Ca(t))}}, \tag{1.42}$$

where the slope $m(Ca(t))$ is given by:

$$m(Ca(t)) = \frac{m_1}{1 + \exp^{-\beta(R - Ca(t))}} + m_2. \tag{1.43}$$

The slope mainly depends on the difference between $R$ and $Ca(t)$. $\beta$ is an amplification coefficient which can produce a shift between the highest value of the slope (that is, $m_1 + m_2$) to a lower value ($m_2$) following variations in the plasma calcium concentration. However, the authors did not manage to interpret this function from a physiological point of view.

### A subpopulation of PT cells to model PTH dynamics

Recently, Pruett and Hester introduced a novel approach to model PTH synthesis and secretion [165]. Their reasoning is based on a study in bovine parathyroid cells published by Sun *et al.* in 1993 [199] suggesting that these cells respond heterogeneously to a perturbation in $[Ca^{2+}]_p$. Indeed, only 50% of them secrete PTH in case of severe hypocalcemia, whereas only 25% release PTH during hypercalcemia. Sun *et al.* proposed the existence of a secretory cell cycle, which explains why some cells are unable to release PTH since they are at the early stage of the cycle while others are capable of releasing PTH. This mecanism would be useful during several perturbations that take place at different time points and could explain the circadian rythm observed for PTH secretion. Thus, Pruett and Hester [165] considered parathyroid cells as a mass of responsive and unresponsive cells to external stimuli such as hypocalcemia. The two types of cells have the same secretion mechanisms but their parameters can change. Moreover, the authors took into consideration the extra-cellular compartment as depicted in Figure 1.21. The secretion function is:

$$PTH_{secreted} = \beta - \frac{\gamma[Ca^{2+}]^m}{[Ca^{2+}]^m + K_d^m}. \tag{1.44}$$

Sensitive cells have high values of $K_d$, $\gamma$, and $m$, whereas unsensitive cells have low values for these parameters. Whereas each cell is considered to have its own rate of PTH synthesis, the rate of granule degradation is the same for all cells. The authors considered 20 parathyroid cells subpopulations for simulations.

Their model was adjusted to previous experimental data obtained by Shwarz *et al.* [182] who performed two successive hypocalcemic clamps. Pruett and Hester compared their predictions to those of Brown [37] and found a better agreement with the data of Shwarz *et al.*. The authors mentioned that this model makes some simplifications. Indeed, they did not explicitly consider plasma calcium concentration dynamics in order to avoid including PTH effects on calcium metabolism. It would have been also interesting to model the kinetic switch between inactive cells and active cells. Finally, PTH production inside parathyroid cells was chosen to be constant; this could be improved by adding the effect of vitamin $D_3$ on PTH transcription or some time delays. Overall, this model is laudable for its innovative approach to characterize PTH secretion.

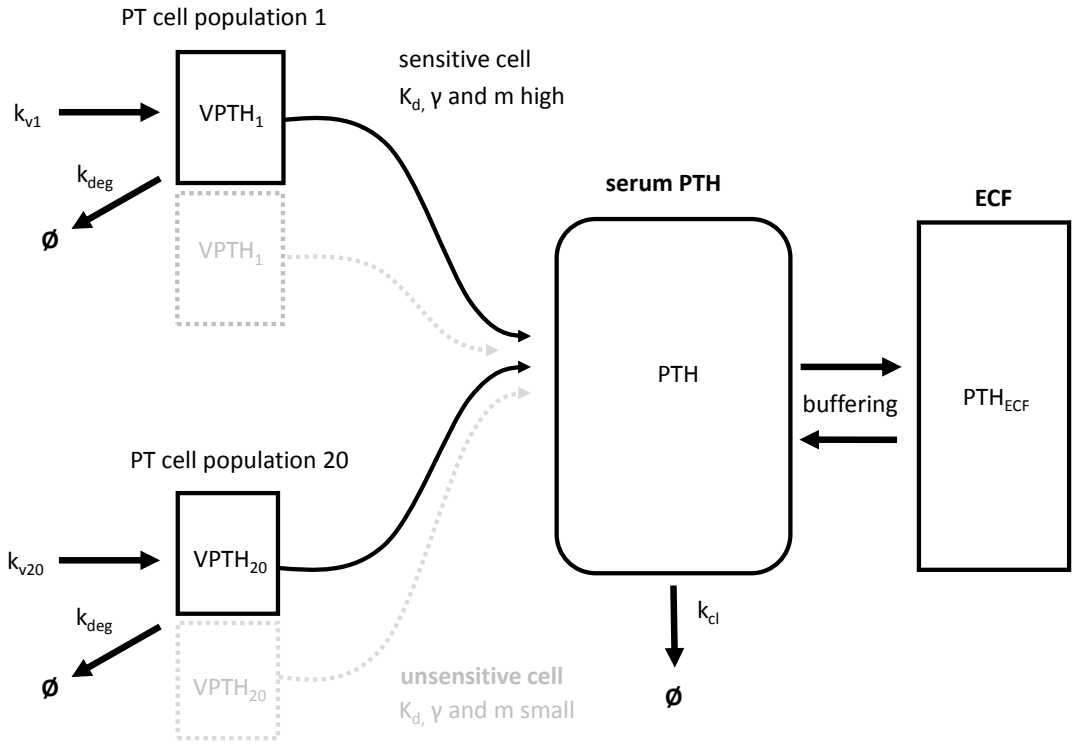


Figure 1.21: The parathyroid cell subpopulation model of Pruett and Hester.

### 1.3.6 About Vitamin D and FGF23

#### Modeling the vitamin D3 synthesis pathway

As mentioned previously, the vitamin $D_3$ synthesis pathway is quite complex since it involves a lot of compounds and several organs, in contrast with PTH which is only synthetized by parathyroid glands. As a result, few models have been built to represent its absorption, metabolism, and distribution. A rather complex pharmacokinetic-pharmacodynamic model was recently developed by Ramakrishnan *et al.* [167]. Briefly, this model takes into consideration the presence of plasma, liver, kidney, brain, ileum and other compartments. It models the kinetic behavior of CYP24A1 and CYP27B1.

#### Modeling the effects of FGF23

Similarly, very few models account for FGF23 dynamics, mainly because it was discovered later than vitamin D and PTH [228]. In 2009, Yokota *et al.* [229] proposed a mathematical model of calcium and phosphate homeostasis based on the previous model of Raposo *et al.*. This new model described the dynamic evolution of FGF23 as:

$$\frac{dQ_{FGF23}}{dt} = J_{FGF23} - \delta Q_{FGF23}. \tag{1.45}$$

$Q_{FGF23}$ is the quantity of FGF23 in plasma. The first term on the right-hand-side characterizes the rate of FGF23 synthesis, which is given by:

$$J_{FGF23} = \frac{V_P X_P}{X_P + K_P} \frac{V_{D_3} X_{D_3}}{X_{D_3} + K_{D_3}}. \tag{1.46}$$

$X_P$ and $X_{D_3}$ are the concentrations of phosphate and vitamin $D_3$, respectively; $V_P$ and $V_{D_3}$ are the maximal rates of activation by phosphate and vitamin $D_3$, respectively; $K_P$ and $K_{D_3}$ are the concentrations of phosphate and vitamin $D_3$, respectively, that yield half the maximal response.

FGF23 synthesis is activated by both phosphate (P) and vitamin $D_3$. The term $\delta$ denotes the first-order rate constant for the degradation of FGF23. Yokota *et al.* simulated the effect of transient increase of FGF23 on PTH, vitamin $D_3$, phosphate and calcium as well as steady state increase in FGF23 concentration [229]. They mentioned that their model parameters have to be validated.

## 1.4 Aim of this thesis

### 1.4.1 Building of model of calcium homeostasis

The overall goal of this thesis work was to build a new mathematical model of calcium and phosphate homeostasis that takes into account recent findings on calcium and phosphate metabolism, in order to investigate their dysregulations. In particular, we wanted to investigate the following questions:

- what could explain hypercalciuria during primary hyperparathyrodism?
- what is the effect of inhibition of bone resorption on calcium metabolism?
- Is it better to treat secondary hyperparathyroidism by giving small amounts of vitamin D once daily or giving one dose every 3 months?
- In case of intestinal hyper-absorption of calcium (triggering hypercalciuria), do vitamin D injections allow reabsorption of enough calcium in the kidney, without stimulating too much intestinal absorption?
- what are the effects of a large intravenous infusion of phosphate on calcium and phosphate homeostasis? Are the effects of a large intestinal absorption of phosphate similar?

The mathematical models developed until now do not allow us to answer these questions. Indeed, these models do not include the effects of PTH on renal calcium handling, which is a significant shortcoming when examining the consequences of primary-hyperparathyroidim on calcium homeostasis, particularly on the renal component. Our model considers separately the effects of PTH in

the thick ascending limb, the distal convoluted tubule, together with the proximal tubule so as to model more accurately its role on renal calcium reabsorption.

Besides, even the most recent models (Raposo *et al.* and Peterson and Riggs) do not take into account the action of the CaSR on calcium reabsorption in kidney [157, 168]. The model of Christie *et al* erroneously predicted hypocalciuria in the case of primary-hyperparathyroidism, and this could be due to the absence of CaSR-induced regulation in their model [51]. The counteracting mechanisms between PTH and CaSR could explain why calciuria is inconstant during primary-hyperparathyroidism. We incorporated these counterbalancing effects in our model.

Our model is also unique in that it represents the regulation of vitamin $D_3$ synthesis by PTH and FGF23, by including feedback mechanisms involving CYP27B1 as well as CYP24A1. It also incorporates the regulation by vitamin $D_3$ of paracellular intestinal calcium absorption, via modulation of transport across claudins, and of calcium reabsorption in the distal convoluted tubule, both of which were missing in other models. Considering these specific effects of vitamin $D_3$ makes it possible to examine the impact of vitamin $D_3$ supplementation in the case of vitamin D defiency (low levels of 25(OH)D). Indeed, the issue is to avoid triggering hypercalciuria after (uncontrolled) vitamin D supplementation.

The last difference between our model and the ones described previously concerns the link between calcium and phosphate. Only Raposo *et al.* together with Peterson and Riggs examined the contribution of phosphate to calcium homeostasis [157, 168]. However, as described above, their modeling approach had some shortcomings; in particular, they omitted the binding between phosphate and calcium, as well as the effects of FGF23, which we added to our model in order to predict accurately the consequences of hyper/hypo-phosphatemia, acidosis, alkalosis and FGF23-related dysregulations.

The thesis is divided into 6 parts. The first part describes our experimental studies, whereas the latter parts focus on model development.

More specifically, in the second chapter, we describe the experiments we designed so as to (a) determine the total content in bone of calcium and phosphate, which had not been measured previously, and (b) understand the kinetics of calcium fluxes between plasma and the rapidly exchangeable pool in bone.

In chapter 3, we present a model of PTH synthesis and secretion regulated by calcium through the calcium sensing receptor. We explain our modeling approach considering what has been done in section 1.3.5. This model is then qualitatively and quantitatively analyzed using usual phase plane analysis and integration methods. For this analysis, we consider that calcium is at steady state. We then conduct simulations to probe the effects of hypocalcemia and hypercalcemia on PTH secretion. We then add vitamin $D_3$ to this model so as to understand the interactions between PTH and calcitriol. We finally consider the time delay necessary for vitamin $D_3$ synthesis and explore the consequences of adding such a lag. This hormonal model is eventually included in a preliminary model of calcium homeostasis.

In chapter 4, we introduce our mathematical model of calcium homeostasis in the rat which has been accepted for publication in the American Journal of Physiology. The novel characteristics of this model are the following: (a) it considers the presence of two bone pools, a rapidly exchangeable pool and a slow exchangeable pool; (b) it distinguishes between calcium reabsorption mechanisms in the different nephron segments, from the proximal tubule to the distal convoluted tubule; (c) it accounts for the inhibitory effects of CaSR on calcium reabsorption in the thick ascending limb; (d) it is the first which includes the delay needed for vitamin D to be synthetized. We used the model to simulate the effects of perturbations related to calcium homeostasis such as primary-hyperparathyroidism, hypoparathyroidism, vitamin $D_3$ deficiency, and the full inhibition of Cyp24a1. We also simulated treatments such as inhibition of bone resorption by bisphosphonates, or the administration of cinacalcet to treat patients with primary-hyperparathyroidism who cannot be treated by surgery. Finally, we discussed the effects of age and sex on model results.

In chapter 5, we improve upon the previous model by including the binding mechanisms of calcium and phosphate in both plasma and bone so as to potentially consider the effect of external factors such as an intravenous infusion of phosphate or calcium, a hypocalcemic clamp, pH variations (acidosis, alcalosis) as well as Fetuin-A deficiency. At the hormonal level, we consider the threesome PTH, vitamin $D_3$, and FGF23; to our knowledge, the latter has thus far rarely been included in homeostatic models. The regulation of vitamin $D_3$ synthesis is also represented more accurately, as we take into account the regulation of CYP27B1 and CYP24A1 by phosphate and FGF23, in light of recent observations.

Chapter 6 summarizes the results obtained in the model we have built and lists the remaining task to complete.

# Chapter 2

# Experimental measurements of some bone parameters

## 2.1 Aim of these experiments

In section 1.3.3, we show that some modeling studies have tried to determine the quantity of calcium in the different pools of bone. Cohn *et al* [55] quantified the size of the rapidly exchangeable calcium pool in the bone of 15 male Sprague-Dwaley rats of 81 days and found 50 mg (or 1.3 mmol) of calcium. In a later study, Blanusa *et al.* [27] obtained values of 15 mg and 30 mg of calcium, respectively, in the rapidly and slowly exchangeable pools in 4 months old female albino rats. The corresponding values in male albino rats of the same age were 23 and 43 mg of calcium, respectively. These results differ significantly from those of Cohn *et al* [55]. Besides, the latter investigators did not measure the total quantity of calcium in bone. Finally, the amount of phosphate was not assessed. These discrepancies led us to conduct our own experiments to evaluate the calcium and phosphate content in bone. In this chapter, we aimed to address basic aspects of the rapidly exchangeable pool, and to measure the size of the deep bone calcium pool in mice. We also sought to quantify fluxes between plasma and the rapid bone pool (2.1). These data were then included in the mathematical model of calcium homeostasis introduced in Chapter 4.

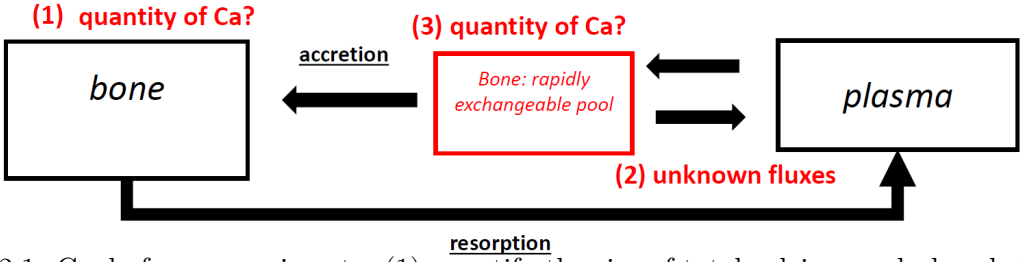


Figure 2.1: Goal of our experiments: (1) quantify the size of total calcium and phosphate pools in bone; (2) clarify the kinetics of calcium exchanges between plasma and the rapidly exchangeable pool in bone; (3) estimate the quantity of calcium in this rapid pool.

## 2.2 Method

All experiments were conducted in accordance with the regulations of the Veterinarian office of the Canton de Vaud.

### 2.2.1 Determination of the total calcium and phosphate bone content in mice

We performed experiments to determine the total quantity of calcium in bone of normal mice. Five male and five female C57Bl/6J mice aged 55 days and weighing about 20g were sacrificed, and their skeleton was prepared according to the method of Pramod *et al.* [161]. Skin was removed, as well as viscera and muscles. The uncleaned skeletons were washed with water, immersed in a 95% ethanol solution during 2-4 days, and then in a 2% KOH solution. KOH bathing was repeated during 3 extra days (to remove remaining parts of skin, gristles). The skeletons were then cleaned with hot water in a mesh strainer to prevent small bones from being lost, and then weighed. Two samples of final KOH solutions from each mouse were examined to ensure that no calcium was dissolved in the bath. Skeletons were dried in a stove during 1 day at 37°C. Finally, they were reduced to ashes in ceramic cups in an oven at 800°C during 4 days (60h heating + cooling time). Ashes were collected, weighed and ultimately dissolved in a 6 mol/L HCl solution (4mL). Calcium content, was assessed by the NM-BAPTA method on a Cobas analyzer.

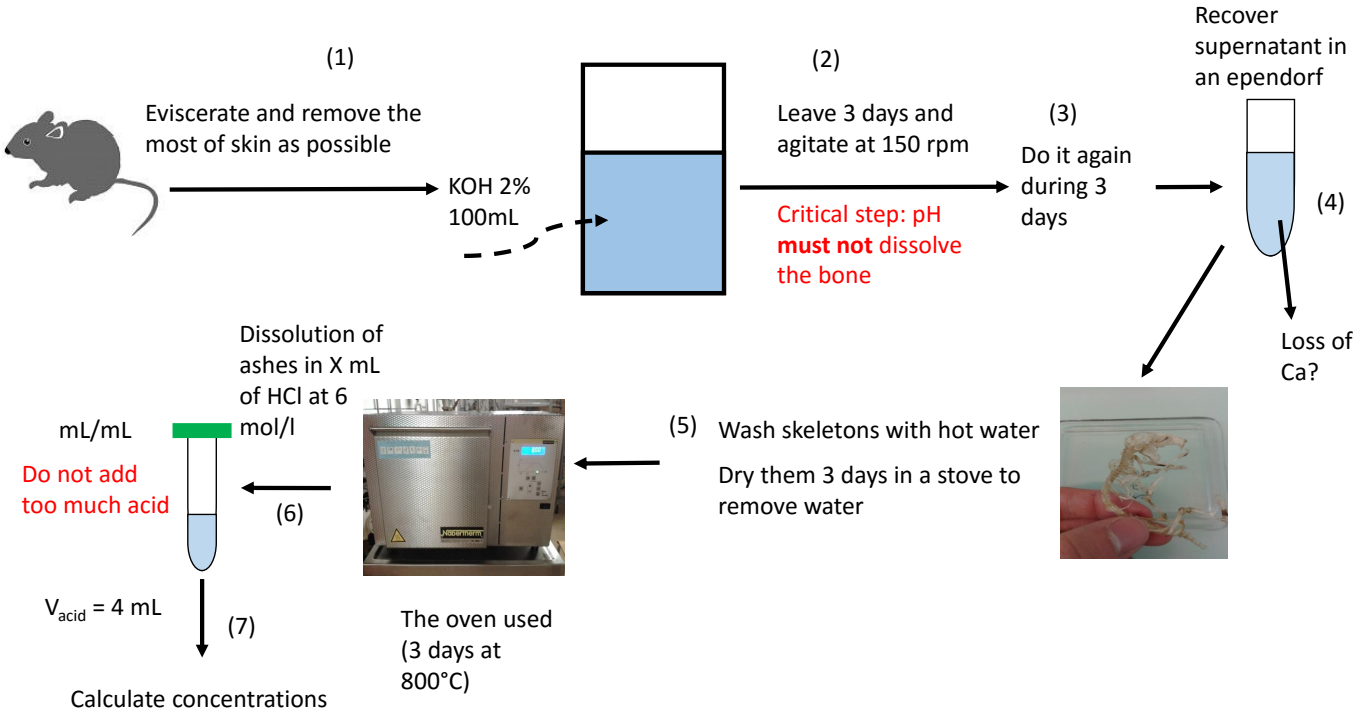


Figure 2.2: Protocol of the first experiment.

### Kinetic study of calcium exchanges between plasma and the bone compartment

We investigated the size of the rapidly exchangeable pool by injecting $^{45}$Ca intravenously and measuring the quantity of radiolabeled $^{45}$Ca appearing in plasma and bones at 2, 5, 15 and 30 minutes in mice previously treated with pamidronate, an inhibitor of bone resorption (PAM), or vehicle (total n=19 and 18 C57Bl/6J male mice aged 4 months respectively). By blocking resorption, we expected to isolate fluxes between plasma and the rapid bone pool of calcium. The dose of pamidronate approximately inhibited 70% of bone resorption [178]. For each mouse, we calculated the total quantity of $^{45}$Ca we had to inject. Based on its body weight, we injected 5$\mu$L/g BW (Figure 2.3). We also ensured that the quantity of $^{45}$Ca injected would not trigger hypercalcemia (0.03% of ionized calcemia) to avoid any hormonal effect.

Animals were put on a warm table to maintain their body temperature constant during the whole experiment. A catheter was inserted in the jugular vein and radioactivity was injected, avoiding the formation of air bubbles. Thereafter, the catheter was rinsed with a saline solution, which also allowed us to eliminate the dead volume inside it. Additionally, the health of each animal was monitored, meaning that in case of substantial hemorrhage, breathing perturbations as well as problems relative to anesthesia, mice were forthwith killed by cervical dislocation so that results were not altered. Before the end of the check point (either 2, 5, 15 or 30 minutes), blood was collected from the eye with a glass capillary. Then, the mouse was killed to harvest bones. As we did not recover the whole skeleton, we normalized the radioactivity to the mass of each skeleton, assuming the radioactivity is equally distributed along the skeleton (based on growth curves of mice available in Charles River's documentation) to take into account all the radioactivity in bone. Based upon the liquid scintillation results, we estimated the percentage of recovery of the radioactivity in plasma, urine, and bones. Since the experiments were scheduled over a duration of 3 months, we measured each time the radioactivity of the solution injected to take into account the radioactive decrease and to normalize results if required. Additionally, we checked the influence of the solution (plasma, acid, bones) in the number of counts obtained to detect possible quenching but we did not observe any quenching phenomenon.

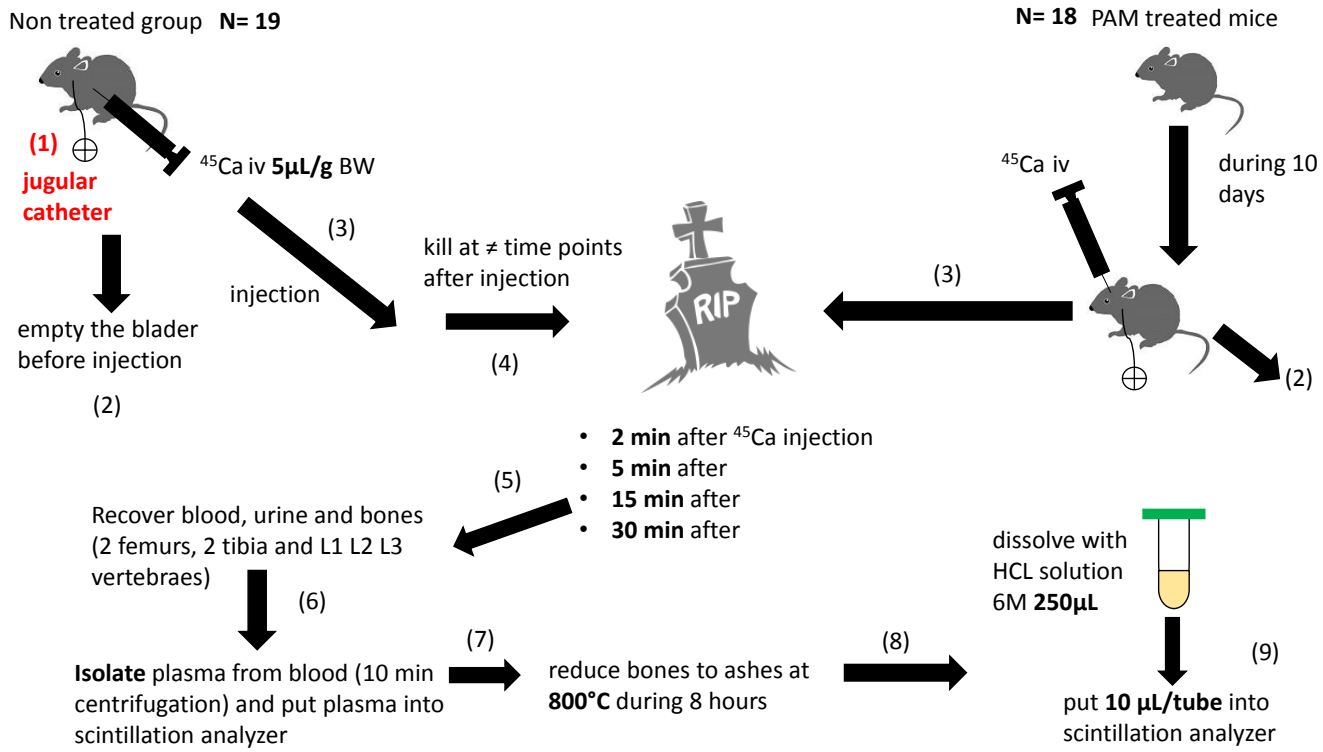


Figure 2.3: Detailed protocol of the second experiment. We compare between a control group and a pamidronate treated-group, the later designed to isolate the rapidly exchangeable bone pool compartment and the plasma compartment by blocking bone resorption, so as to determine the calcium fluxes between these two compartments.

## 2.3 Results

### 2.3.1 Calcium and phosphate content in the bone

Results for male and female mice are summarized in table 2.1. No calcium and no phosphate were lost in the supernatant during the cleaning of muscle and skin in the KOH solution. According to our measurements, there are 6.01/6.04 mmol (0.24g) calcium and 3.77/3.68 mmol (0.35g) phosphate in the skeleton of 20g male and female mice, respectively.

| | male | | female | |
|---|---|---|---|---|
| | mean | se | mean | se |
| Body weight (g) | 25.42 | 0.03 | 20.07 | 0.82 |
| Skeleton weight (g) | 0.94 | 0.04 | 1.08 | 0.02 |
| femur weight (mg) | 33 | 1.3 | 34 | 1.2 |
| tibia weight (mg) | 29 | 2 | 28 | 0.5 |
| vertebra L1/L2/L3 (mg) | 27 | 1.3 | 29 | 1.1 |
| skull (g) | 0.27 | 0.004 | $\emptyset$ | $\emptyset$ |
| $n_{Ca_b^{2+}}$ (mmol) | 6.01 | 0.38 | 6.04 | 0.19 |
| $n_{PO_{4_b}}$ (mmol) | 3.77 | 0.09 | 3.68 | 0.14 |

Table 2.1: Calcium and phosphate total bone content in 55-day old male and female mice.

### 2.3.2 Kinetic part

Results of the second experiments are shown in Figure 2.4. We used a bilateral, unpaired Student t-test for the statistical analysis. In vehicle-treated mice, there was no difference in the recovery of the amount of $^{45}$Ca in plasma 2 minutes and 5 minutes after the injection ($p = 0.35$; Figure 2.4, panel A). However, between 5 and 15 minutes, $^{45}$Ca was divided by 1.4. There was also a significant difference in plasma between the 15 min and 30 min groups ($p = 0.007$), albeit a smaller one: $^{45}$Ca was divided by 1.24 times during this interval. The pamidronate-treated mice followed the same trend. The small difference between the 15 and 30 min suggests that calcium levels in plasma reached a plateau.

In mice treated with vehicle only, calcium was progressively stored in bone over time (Figure 2.4, panel B). Indeed, except between 2 minutes and 5 minutes groups ($p = 0.07$), all results are significantly different. However, the kinetics were not the same as for plasma since at 30 min bone continued storing calcium. In the PAM-treated mice group, no significant difference was observed in bone except between 2 min and 5 minutes ($p = 0.01$). This means that saturation was quickly reached ($< 5$ minutes). Moreover, there was a large difference in bone calcium storage at 30 min between the two groups ($p = 0.002$).

Plasma counts are for 10$\mu$L of plasma but can be extended to the whole plasma volume. According to the literature, the plasma volume of a 30g mouse is about 1.8 mL (60mL/Kg of body weight; [171]). Based on this value, we estimated that 10% of the radioactivity was already in plasma 2 minutes after the $^{45}$Ca injection. Besides, radioactivity lost in the urine or stored in bone was less than 1% of the total. This strongly suggests that most of the remaining radioactivity is in the interstitium, since the intracellular pool of calcium is small in comparison.

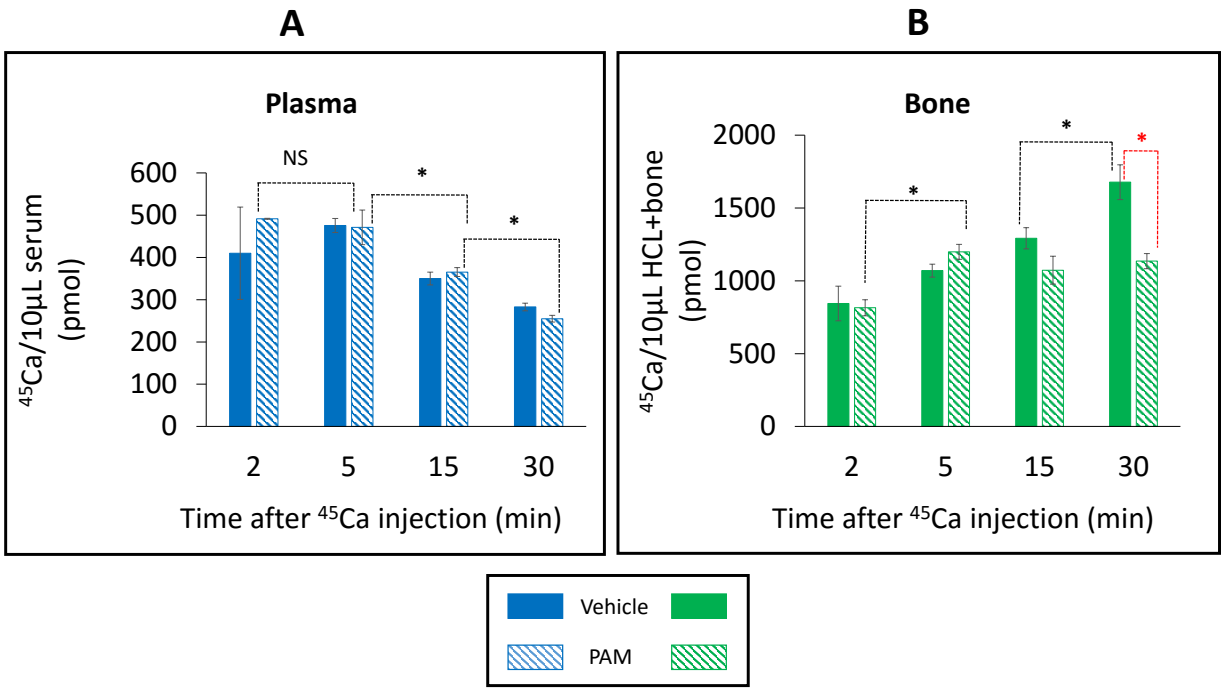


Figure 2.4: Panel A: Histogram showing radioactivity recovered in plasma 2, 5, 15, and 30 minutes after $^{45}$Ca injection. PAM-treated mice are denoted by dashed bars and vehicle-treated by plain bars. In the vehicle group N respectively equals 2, 5, 7, and 5 for each time point; in the PAM-treated goupe, N equals 2, 4, 6, and 6. Panel B: radioactivity recovered in bone 2, 5, 15, and 30 minutes after $^{45}$Ca injection.

## 2.4 Discussion

### 2.4.1 About the total pool of calcium and phosphate in bone

In a 20g mouse, we found about 6 mmol of calcium in bone, that is, 0.24g. In other words, we obtained a ratio of 0.012g Ca/g BW. For a 300g rat, using our ratio yields 3.6g (or 90 mmol) of calcium in bone.

Furthermore, Knop *et al.* [122] estimated that the rapidly exchangeable pool in bone contains 3g of calcium in a normal subject, namely 0.3 % of the total calcium bone content [122]. Extrapolating to the rat yields 0.3 mmol, which is significantly lower than the values obtained by Cohn [55] (1.3 mmol) and Blanusa *et al.* [27] (0.74 mmol). According to Peterson and Riggs [157], the calcium content of the rapid pool is between 100 and 250 mmol in humans (2.5-6.25g), that is, 0.4-1 % of the total calcium in bone. Using the latter fractions, the rapidly exchangeable pool in rats is estimated to contain 0.4-1 mmol calcium. Altogether, there remains considerable uncertainty in the calcium content of this pool in rats.

In mice, there are 0.017 g phosphate/g body weight. Using the latter ratio to estimate the

amount of phosphate in a 300 g rat yields 54 mmol phosphate. Assuming that the rapidly exchangeable pool of phosphate contains about 1% of total phosphate in bone, there is approximately 0.5 mmol phosphate in that pool.

This experiment should be improved by studying the impact of age on bone content by making at least 3 additional groups of mice of 2 weeks, 5 months and 8 months, respectively for each sex.

### 2.4.2 About the kinetic experiments

We have to acknowledge several difficulties and shortcomings in this experiment. The first issue is that urine recovery was not possible at 2 and 5 minutes after $^{45}$Ca injection. The second problem relates to the possible contamination of urine by blood vessels surrounding the bladder, which can burst during collection by catheter; this contamination was likely the source of very high counts in some urine samples, similar to those of plasma. Finally, the urinary levels of creatinine should have been counted so as to normalize results appropriately.

To estimate the quantity of radiolabeled calcium in bone, we only recovered the following bones: 2 femurs, 2 tibias, vertebrae ($L_1$, $L_2$ and $L_3$). We made an important assumption, namely that radioactivity is equally distributed in bone, so as to extrapolate the $^{45}$Ca quantity in these bones to the whole skeleton. Some experiments should be done to check whether this assumption is valid.

The results of this experiment indicate that $^{45}$Ca is quickly distributed in the plasma but the rate of incorporation into bone is very low. Indeed, 60 minutes after the injection, bones stored only 0.5% of the quantity of $^{45}$Ca injected. It would take about 200h to recover all the radioactivity in bone, assuming a constant incorporation rate. The rapidly exchangeable pool of calcium was probably saturated and we were not able to dissect its contribution.

About 10% of the radioactivity injected was found in plasma within 30 minutes. Since bone and urine stored negligible amount of calcium during this interval, it is likely that the remaining $^{45}$Ca went into the interstitial fluid. Assuming equal concentrations in plasma and interstitial fluid, we estimated the volume of the interstitial fluid as 12.5 mL. This value, however, is significantly higher than the estimate we obtained using a different approach, namely by extrapolating human results. Plasma volume is approximately 11.5 mL for a 300g rat [127] and 1.8 mL for a 30g mouse. In humans, the extracellular volume is about 15 L, 80% (12 L) of which is interstitial fluid and 20% (3L) plasma. Similar fractions yield an extracellular volume of 57.5 mL in rats and 9 mL (7.2 mL interstitial fluid) in mice.

The reduction in bone calcium storage in the PAM group can be explained by an inhibition of osteoblast activity, consecutive to the drop in osteoclast activity after the pamidronate treatment. We performed one experiment to see whether bone storage saturates in the vehicle group after 30 min. 60 min after the injection, the amount of $^{45}$Ca deposited in bone was greater than that at 30 minutes (+200 pmol/10$\mu$l HCL+ bone). However, it is not possible to draw definite conclusions since N=1. Note too that we measured the accumulation of calcium in teeth 60 min after the injection in the vehicle-treated mice: we found that the quantity stored is 15 times lower than that in the bone, so teeth are not a significant storage compartment.

To investigate the size of the rapidly exchangeable pool in bone and its exchanges with plasma an alternative solution would be to work with isolated perfused bone, which has been done by Somerville and Kaye [195]. The main idea is to study $^{45}$Ca kinetics using the tail of rats. The tail has to be washed to remove the blood and put in a warmed box. Then, $^{45}$Ca can be injected into the main artery and we measure the time needed for disappearance. Conversely, the rat can be loaded with $^{45}$Ca, then we can determine the quantity of calcium release by bone.

### 2.4.3 Conclusion

These experiments enabled us to determine the size of the total calcium and phosphate pools in bone. Yet, it was not possible to quantify the size of the rapidly exchangeable pool, so we suggest a new protocol to investigate these aspects of bone metabolism. Results in humans suggest that the rapidly exchangeable pool represents about 1% of the total bone pool.

# Chapter 3

# Model of calcium homeotasis, PTH synthesis and secretion, and vitamin $D_3$ effects

In this chapter we develop a mathematical model of PTH synthesis and secretion which will be included in a global model of calcium homeostasis. The first global model only considers PTH effects on calcium metabolism, while the second includes the contribution of both vitamin $D_3$ and PTH.

## 3.1 Mathematical model of PTH synthesis and secretion

In this part, we state all the equations that govern PTH dynamics. Then the model is scaled and analyzed to understand its behavior. Finally, we perform some simulations to compare our predictions with previous models and to adjust our parameters so that model predictions match well experimental data.

### 3.1.1 Modeling PTH synthesis

As mentioned in the introduction (1.1.3), PTH synthesis is regulated by vitamin D, through vitamin D receptors that bind to PTH promoters (Figure 1.10). Additionally, the calcium sensing receptor may affect PTH synthesis at the transcriptional level but the mechanisms are not known. Models previously developed assumed that PTH was synthesized at a constant rate (1.3.5). Denoting PTH concentration in the parathyroid gland by $PTH_g$, we consider a constant rate of PTH mRNA production, namely $k_{prod}^{PTH_g}$. Then $PTH_g$ is degraded at a rate $k_{deg}^{PTH_g}[PTH]_p$, were $[PTH]_p$ is the concentration of PTH in plasma. Moreover, it is carried out of the cell at a rate $F([Ca^{2+}]_p)[PTH]_p$, under the control of the calcium sensing receptor (Figure 3.1).

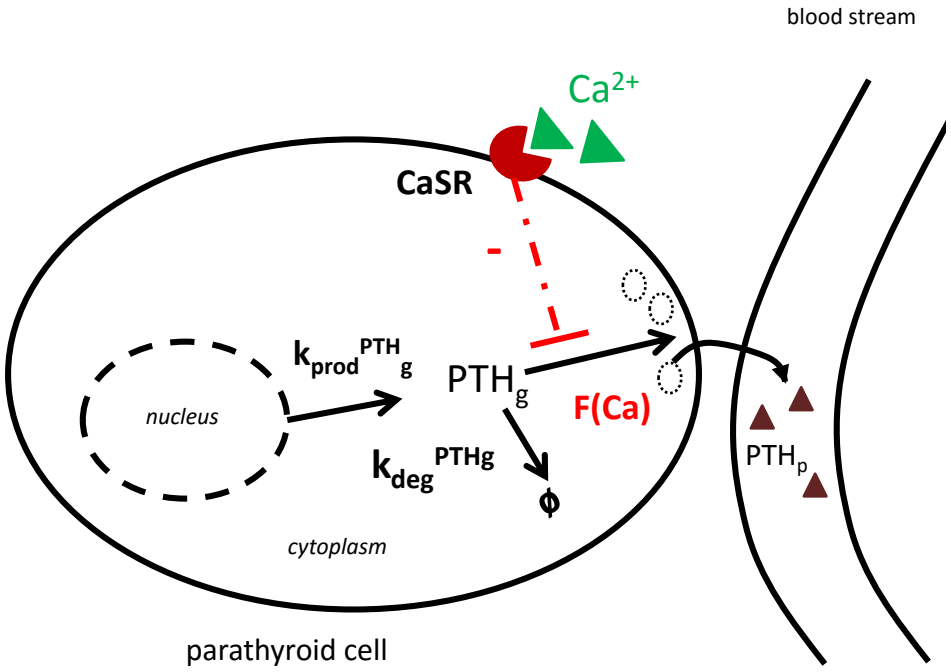


Figure 3.1: What we modeled in a parathyroid cell.

As a result, the equation describing the behaviour of $PTH_g$ is:

$$\frac{d[PTH]_g}{dt} = k_{prod}^{PTH_g} - \left(k_{deg}^{PTH_g} + F([Ca^{2+}]_p)\right)[PTH]_g. \tag{3.1}$$

### 3.1.2 PTH exocytosis from the cell

$F([Ca^{2+}]_p)$ accounts for the inhibition of PTH secretion by calcium that we describe below. We model the activity of CaSR with a Hill function, as frequently used in gene regulation. We use the following notations: $[Ca^{2+}]_p$ is the plasma calcium concentration, $[CaSR]$ is the membrane concentration of free CaSR, $[CaSR^*]$ is the membrane concentration of activated CaSR by $Ca^{2+}$ and $N_{pc}$ is the number of parathyroid cells. If we consider that there are $m$ CaSR per parathyroid cell and a total of $N_{pc}$ cells, the total number of receptors is given by (Panel 1, Figure 3.2):

$$CaSR + CaSR^* = mN_{pc} = CaSR_{tot}. \tag{3.2}$$

Furthermore, we assume that $n$ atoms of calcium bind to one CaSR to activate it (Panel 2, Figure 3.2):

$$CaSR + nCa^{2+} \rightleftharpoons CaSR^*. \tag{3.3}$$

Using the mass-action law:

$$\frac{[CaSR][Ca^{2+}]^n}{K} = [CaSR^*], \tag{3.4}$$

where $K$ is the dissociation equilibrium constant of the reaction. Moreover, we assume that the rate of secretion of PTH from the parathyroid gland is a decreasing affine function of the concentration of activated CaSR, such that:

$$F = F_0 - \frac{[CaSR^*]}{[CaSR_{tot}]}. \tag{3.5}$$

where $F_0$ is a constant. We know that:

$$[CaSR^*] = \frac{[CaSR][Ca^{2+}]_p^n}{K}. \tag{3.6}$$

As $[CaSR] + [CaSR^*] = [CaSR_{tot}]$, this yields:

$$\begin{aligned}
[CaSR^*] &= \frac{\Big([CaSR_{tot}] - [CaSR^*]\Big)[Ca^{2+}]_p^n}{K}, \\
&= \frac{[CaSR_{tot}]}{K}[Ca^{2+}]_p^n - \frac{1}{K}[CaSR^*][Ca^{2+}]_p^n, \\
\implies [CaSR^*]&\frac{K + [Ca^{2+}]_p^n}{K} = \frac{[CaSR_{tot}]}{K}[Ca^{2+}]_p^n, \\
\implies [CaSR^*] &= \frac{[CaSR_{tot}][Ca^{2+}]_p^n}{K + [Ca^{2+}]_p^n}.
\end{aligned} \tag{3.7}$$

Consequently:

$$\begin{aligned}
\frac{[CaSR^*]}{[CaSR_{tot}]} = \frac{[Ca^{2+}]_p^n}{K + [Ca^{2+}]_p^n} &= F_0 - F, \\
\implies F &= F_0 - \frac{[Ca^{2+}]_p^n}{K + [Ca^{2+}]_p^n}.
\end{aligned} \tag{3.8}$$

By defining $K_{Ca} = K^{1/n}$, the previous expression becomes:

$$F([Ca^{2+}]_p) = F_0 - \frac{[Ca^{2+}]_p^n}{K_{Ca}^n + [Ca^{2+}]_p^n}, \tag{3.9}$$

which is the expression of a Hill function. These functions, which were introduced by Archibald Vivian Hill in 1910, are widely used to analyze ligand-receptor interactions, especially in pharmacology, biochemistry together with physiology. In particular, when $F_0 = 1$, $F$ becomes:

$$F([Ca^{2+}]_p) = \frac{K_{Ca}^n}{[Ca^{2+}]_p^n + K_{Ca}^n}. \tag{3.10}$$

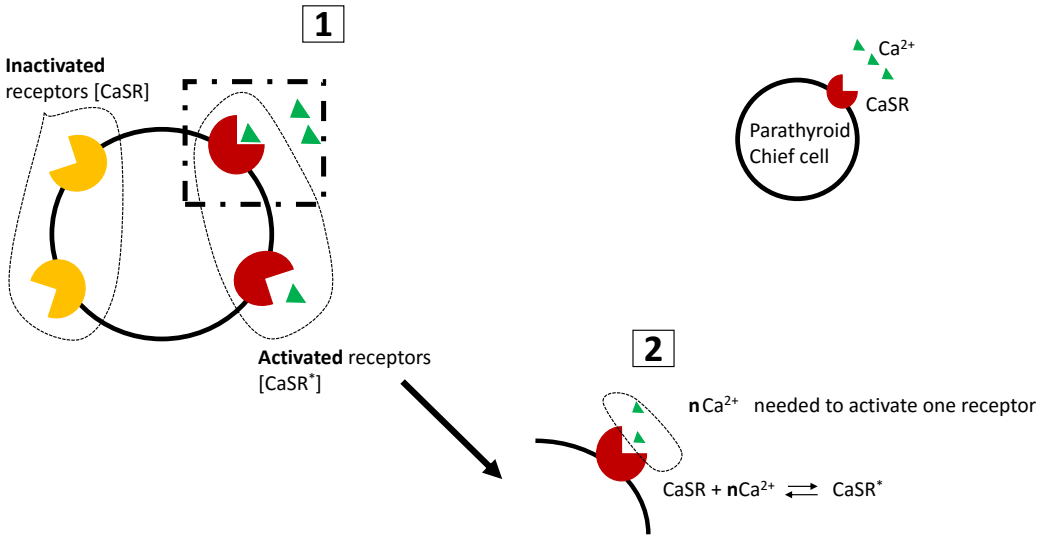


Figure 3.2: A schematic view of CaSR activation by $Ca^{2+}$ in parathyroid chief cells.

Equation (3.9) is well defined from a biological point of view when $F([Ca^{2+}]_p) > 0$. This means that $F_0 \geq 1$. In practice, the inhibition by CaSR cannot be total, thus we introduce a maximal rate of inhibition by CaSR, that is, $\gamma_{exo}^{PTH_g}$. $F_0$ is renamed $\beta_{exo}^{PTH_g}$, which is the maximal secretion of PTH without any CaSR effects. It is obvious that :

$$\beta_{exo}^{PTH_g} - \gamma_{exo}^{PTH_g} \geq 0. \tag{3.11}$$

As a result, we define:

$$F([Ca^{2+}]_p) = \beta_{exo}^{PTH_g} - \frac{\gamma_{exo}^{PTH_g}[Ca^{2+}]_p^n}{K_{Ca}^n + [Ca^{2+}]_p^n}, \quad n \geq 1. \tag{3.12}$$

It is easily shown that:

$$\lim_{[Ca^{2+}]_p \to 0} F([Ca^{2+}]_p) = \beta_{exo}^{PTH_g} \text{ and } \lim_{[Ca^{2+}]_p \to +\infty} F([Ca^{2+}]_p) = \beta_{exo}^{PTH_g} - \gamma_{exo}^{PTH_g}. \tag{3.13}$$

Moreover $F$ is a strictly decreasing function.

From a biological point of view, $PTH_g$ secretion is activated by low values of calcium, but as calcium concentration increases, $F$ decreases and $PTH_g$ secretion is slowed. Below is a quick representation of the impact of parameter variations on $F$. Panel A of Figure 3.3 represents the evolution of the exocytosis function with respect to the plasma calcium concentration when $K_{Ca}$ changes. When $K_{Ca}$ increases the curve shifts right meaning that more calcium is needed halve the rate of exocytosis (see dotted lines). Therefore $K_{Ca}$ can be interpreted as the inverse of the CaSR affinity to $Ca^{2+}$ (i.e facility to bind). If we take Equation (3.3) which accounts for the binding of

$Ca^{2+}$ and CaSR ($k_a$ is the association rate and $k_d$ is the dissociation rate):

$$[CaSR] + n[Ca^{2+}] \underset{k_d}{\overset{k_a}{\rightleftharpoons}} [CaSR^*], \tag{3.14}$$

the equilibrium constant of the reaction is:

$$K = \frac{k_d}{k_a} \Longleftrightarrow K_{Ca} = \sqrt[n]{\frac{k_d}{k_a}} = \exp\left(\frac{1}{n}\ln\left(\frac{k_d}{k_a}\right)\right). \tag{3.15}$$

Thus $K_{Ca}$ is elevated if the dissociation coefficient $k_d$ is high or if the association coefficient $k_a$ is low. Panel B of Figure 3.3 describes the rate of exocytosis process as a function of the plasma calcium concentration for varying values of $n$. The higher the value of $n$, the steeper the slope of the curve, which means that for small variations in the concentration of plasma calcium in the vicinity of $K_{Ca}$, the response has a large amplitude.

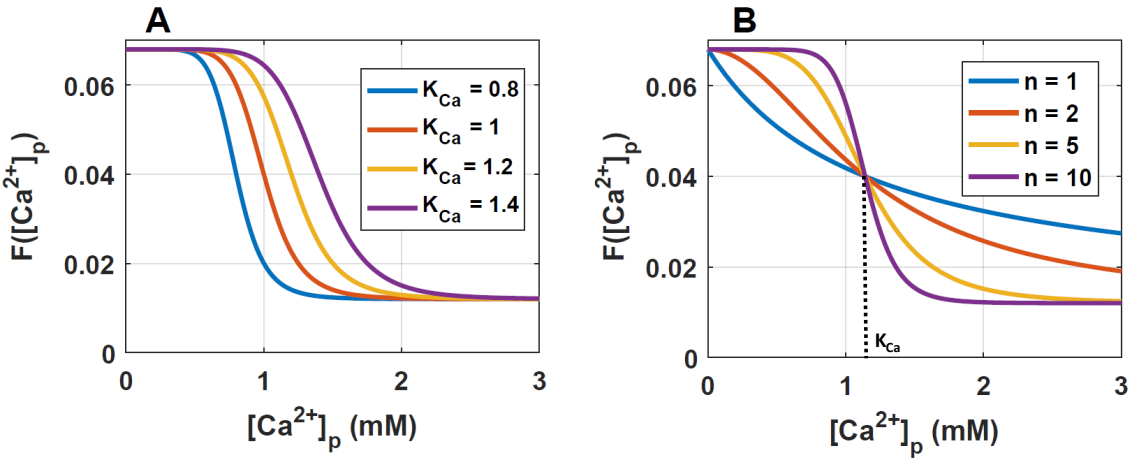


Figure 3.3: Panel A: $F$ as a function of $[Ca^{2+}]_p$ for several values of $K_{Ca}$ and parameters in Table 3.1. Panel B: $F$ as a function of $[Ca^{2+}]_p$ for several values of $n$.

Other models are available to describe the binding of $Ca^{2+}$ and CaSR, particularly cooperativity models. Cooperativity means that the binding of a molecule to a receptor affects the binding of another molecule at the surface of the previous receptor.

### 3.1.3 PTH dynamics in plasma

We assume that PTH degrades linearly with a coefficient $k_{deg}^{PTH_p}$. Thus, the equations for $PTH_p$ are:

$$\frac{d[PTH]_p}{dt} = F([Ca^{2+}]_p)\frac{V_c}{V_p}[PTH]_g - k_{deg}^{PTH_p}[PTH]_p. \tag{3.16}$$

The plasma volume $V_p$ is assumed to be constant and $V_c$ is the volume of parathyroid gland, thereby the ratio takes into account PTH dilution into plasma, which was missing from previous models (1.3.5).

### 3.1.4 Parameters

We choose a rat weighing approximately 300g as the basis for our study.

Table 3.1: PTH parameters

| Parameter | Symbol | Value | Reference |
|---|---|---|---|
| $PTH_g$ synthesis rate | $k_{prod}^{PTH_g}$ | 2.2 nmol.min$^{-1}$ | estimated |
| $PTH_g$ degradation rate constant | $k_{deg}^{PTH_g}$ | 0.035 min$^{-1}$ | [1] |
| Maximal secretion rate constant of $PTH_g$ | $\beta_{exo}^{PTH_g}$ | 0.059 min$^{-1}$ | fitted from [81] |
| Maximal inhibition of secretion by $Ca^{2+}$ | $\gamma_{exo}^{PTH_g}$ | 0.057min$^{-1}$ | fitted from [81] |
| Binding of $Ca^{2+}$ to CaSR | $K_{Ca_p^{2+}}$ | 1.14 mM | [81] |
| | $n$ | 10 | [187] |
| Equilibrium plasma calcium concentration | $[Ca^{2+}]_p^*$ | 1.2 mM | [210] |
| $PTH_p$ degradation rate constant | $k_{deg}^{PTH_p}$ | 2.2 min$^{-1}$ | [1] |

### 3.1.5 Mathematical analysis of the PTH model

This model depends on the plasma calcium concentration which we fix to a physiological observed value (1.2 mM [210]). Then we analyse the existence of steady state(s) and study its (their) stability. Afterwards, because the structure of the system allows us to find them, we compare explicit solutions performed by integration by hand to that computed by the Matlab solver. It is a way to know whether the method used in the solver is suitable or not. Then, we run simulations with 2 different initial conditions to see the evolution until steady state is reached.

We consider the system:

$$\begin{cases} \dfrac{d[PTH]_g}{dt} = k_{prod}^{PTH_g} - \Big(k_{deg}^{PTH_g} + F([Ca^{2+}]_p)\Big)[PTH]_g, \\ \dfrac{d[PTH]_p}{dt} = F([Ca^{2+}]_p)\dfrac{V_c}{V_p}[PTH]_g - k_{deg}^{PTH_p}[PTH]_p. \end{cases} \tag{3.17}$$

**Non-dimensionalization**

The plasma concentration of calcium is several orders of magnitude greater than that of $PTH_p$ and $PTH_g$. An appropriate scaling may help avoid numerical inaccuracies. We define:

$$t = \tau\tilde{t}, \qquad PTH_g = P\bar{T}H_g \times P\tilde{T}H_g \qquad \text{and} \qquad PTH_p = P\bar{T}H_p \times P\tilde{T}H_p, \tag{3.18}$$

where $\tilde{}$ indicates the non-dimensional variable, and $\bar{}$ the constant used for normalization.

As a result, the previous system 3.17 becomes:

$$\begin{cases} \dfrac{d(P\bar{T}H_g \times P\tilde{T}H_g)}{d(\tau\tilde{t})} = k_{prod}^{PTH_g} - \Big(k_{deg}^{PTH_g} + F([Ca^{2+}]_p)\Big)P\bar{T}H_g \times P\tilde{T}H_g, \\ \dfrac{d(P\bar{T}H_p \times P\tilde{T}H_p)}{d(\tau\tilde{t})} = F([Ca^{2+}]_p)\dfrac{V_c}{V_p}P\bar{T}H_g \times P\tilde{T}H_g - k_{deg}^{PTH_p}P\bar{T}H_p \times P\tilde{T}H_p. \end{cases} \tag{3.19}$$

Multiplying the two equations respectively by $\dfrac{\tau}{P\bar{T}H_g}$ and $\dfrac{\tau}{P\bar{T}H_p}$, yields the system:

$$\begin{cases} \dfrac{dP\tilde{T}H_g}{d\tilde{t}} = \dfrac{\tau k_{prod}^{PTH_g}}{P\bar{T}H_g} - \Big(k_{deg}^{PTH_g} + F([Ca^{2+}]_p)\Big)\tau P\tilde{T}H_g, \\ \dfrac{dP\tilde{T}H_p}{d\tilde{t}} = \dfrac{\tau}{P\bar{T}H_p}F([Ca^{2+}]_p)\dfrac{V_c}{V_p}P\bar{T}H_g \times P\tilde{T}H_g - \tau k_{deg}^{PTH_p}P\tilde{T}H_p. \end{cases} \tag{3.20}$$

If we set:

$$\left[\frac{\tau k_{prod}^{PTH_g}}{P\bar{T}H_g}\right] = 1, \qquad \left[\tau k_{deg}^{PTH_p}\right] = 1 \qquad and \qquad \left[\frac{P\bar{T}H_g}{P\bar{T}H_p}\frac{V_c}{V_p}\right] = 1, \tag{3.21}$$

then we have:

$$\tau = \frac{1}{k_{deg}^{PTH_p}}, \qquad P\bar{T}H_g = \frac{k_{prod}^{PTH_g}}{k_{deg}^{PTH_p}} \quad and \quad P\bar{T}H_p = \frac{k_{prod}^{PTH_g} V_c}{k_{deg}^{PTH_p} V_p}. \tag{3.22}$$

We define 2 new parameters, $\alpha$ and $\kappa$:

$$\alpha = \left[ k_{deg}^{PTH_g} \tau \right] = \frac{k_{deg}^{PTH_g}}{k_{deg}^{PTH_p}} \quad \text{and} \quad \kappa = \left[ F([Ca^{2+}]_p)\tau \right] = \frac{F([Ca^{2+}]_p)}{k_{deg}^{PTH_p}}. \tag{3.23}$$

Finally let:

$$\omega = \alpha + \kappa, \tag{3.24}$$

so that the final system is:

$$\begin{cases} \dfrac{dP\tilde{T}H_g}{d\tilde{t}} = 1 - \omega P\tilde{T}H_g, \\ \dfrac{dP\tilde{T}H_p}{d\tilde{t}} = \kappa P\tilde{T}H_g - P\tilde{T}H_p. \end{cases} \tag{3.25}$$

Parameters $\alpha$ and $\kappa$ are strictly positive.

**Existence and unicity**

The above system can be rewritten as follows:

$$X'(\tilde{t}) = P(\tilde{t})X(\tilde{t}) + Q(\tilde{t}), \tag{3.26}$$

with $X(\tilde{t}) = \begin{pmatrix} PTH_g(\tilde{t}) \\ PTH_p(\tilde{t}) \end{pmatrix}$, $P(\tilde{t}) = \begin{pmatrix} -\omega & 0 \\ \kappa & -1 \end{pmatrix}$ and $Q(\tilde{t}) = \begin{pmatrix} 1 \\ 0 \end{pmatrix}$.
All functions in the matrices $P$ and $Q$ are continuous on $\mathbb{R}$, and thus on $[0, +\infty[$. As a result, for all $\tilde{t_0}$ in $\mathbb{I}$ and for all $X_0$ in $\mathbb{R}^2$, there exists only one solution for the problem:

$$\begin{cases} X'(\tilde{t}) = P(\tilde{t})X(\tilde{t}) + Q(\tilde{t}), \\ X(\tilde{t_0}) = \begin{pmatrix} PTH_g(\tilde{t_0}) \\ PTH_p(\tilde{t_0}) \end{pmatrix}. \end{cases} \tag{3.27}$$

**Explicit solutions**

In the following sections, we omit the ˜ for non-dimensional variables. As the first equation is decoupled from the second one, we can express $PTH_g(t)$. We recall that its dynamics are governed by the following differential equation:

$$\frac{dPTH_g}{dt} = 1 - \omega PTH_g, \tag{3.28}$$

that is of the form:

$$\frac{dx}{dt} = p(t)x(t) + q(t), \tag{3.29}$$

with $x(t) = PTH_g(t)$, $p(t) = -\omega$ and $q(t) = 1$. We can see immediately that both $p(t)$ and $q(t)$ are constants, which simplifies the subsequent analysis. The general solution of the differential equation $\frac{dx}{dt} = p(t)x(t) + q(t)$ with the initial condition $x(t_0) = x_0$ is:

$$x(t) = e^{\int_{t_0}^{t} p(s)ds}\left(\int_{t_0}^{t}\Big(q(s)e^{-\int_{t_0}^{s} p(\tau)d\tau}\Big)ds + x_0\right). \tag{3.30}$$

Applying this to the normalized PTH system (3.25):

$$x(t) = x_0 e^{-\omega(t-t_0)} + \frac{1}{\omega}\Big[1 - e^{-\omega(t-t_0)}\Big]. \tag{3.31}$$

In particular, when $t_0 = 0$ it yields:

$$x(t) = e^{-\omega t}\Big[x_0 - \frac{1}{\omega}\Big] + \frac{1}{\omega}. \tag{3.32}$$

Similarly for $\text{PTH}_p$ we have:

$$\frac{dy}{dt} = \kappa x(t) - y(t), \tag{3.33}$$

the solution of which is given by Duhamel formula:

$$y(t) = e^{t_0 - t}\Big[y_0 + \frac{\kappa}{\omega(1-\omega)} - \frac{\kappa x_0}{1-\omega} - \frac{\kappa}{\omega}\Big] - \frac{\kappa}{\omega}e^{-\omega(t-t_0)} + \frac{\kappa}{\omega}, \tag{3.34}$$

When $t_0 = 0$, we have:

$$y(t) = \big[x_0 - \frac{1}{\omega}\big]\frac{\kappa}{1-\omega}e^{-\omega t} + e^{-t}\Big[y_0 + \frac{\kappa(1-x_0)}{(1-\omega)}\Big] + \frac{\kappa}{\omega} \tag{3.35}$$

A quick study of these solutions indicates that:

$$\lim_{t\to+\infty} PTH_g(t) = \frac{1}{\omega}. \tag{3.36}$$

$$\lim_{t\to+\infty} PTH_p(t) = \frac{\kappa}{\omega}. \tag{3.37}$$

that is congruent with results found by hand for steady state values in 3.1.5.

In Figure 3.4, we compare numerical results ($PTH_g^{solve}$) with exact solutions ($PTH_g^{th}$). As shown in panels C-D, the differences are very small (less than $10^{-3}$) and the two curves are indistinguishable. We define $\epsilon_g$ and $\epsilon_p$ as follows:

$$\epsilon_g = |PTH_g^{solve} - PTH_g^{th}| \text{ and } \epsilon_p = |PTH_p^{solve} - PTH_p^{th}|. \tag{3.38}$$

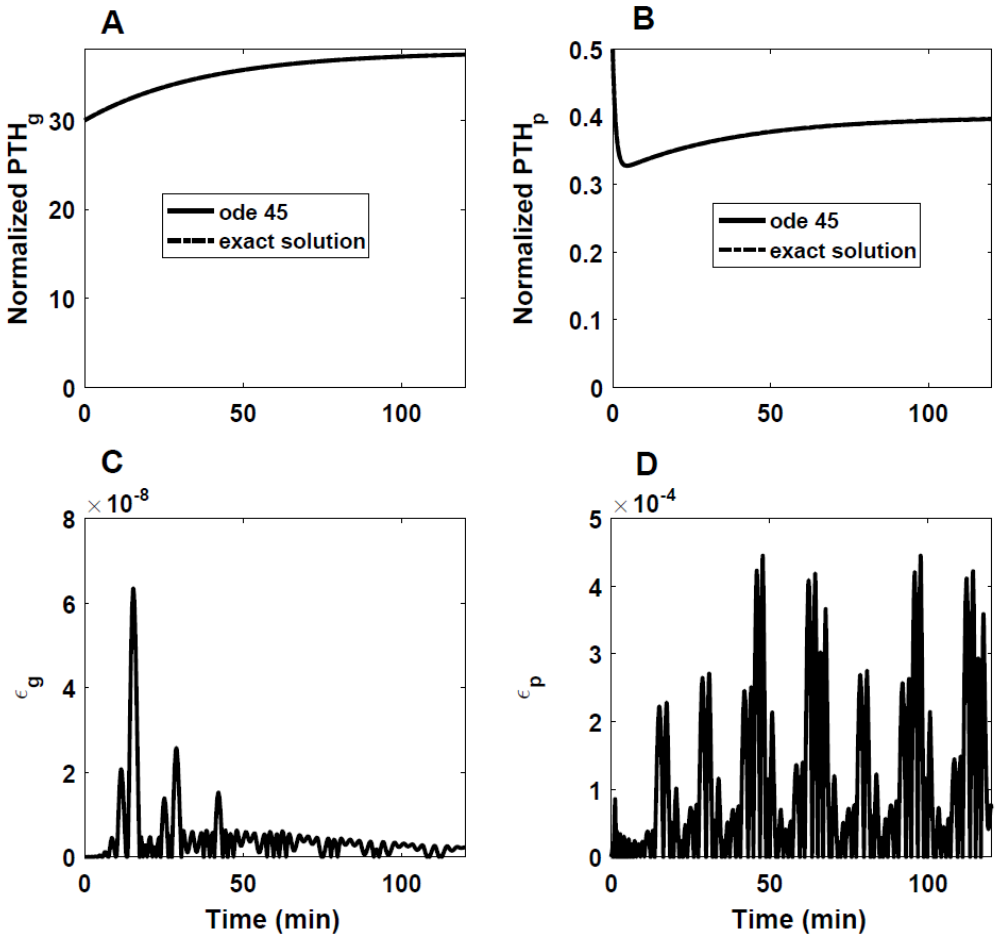


Figure 3.4: Panel A: $PTH_g$ as a function of time. Panel B: $PTH_p$ as a function of time. Panel C: difference between solver and exact solution for $PTH_g$. Panel D: difference between solver and exact solution for $PTH_p$. The initial condition is chosen as [30,0.5].

### Expected values at steady state

Steady state values are denoted by an asterisk. At steady state in system (3.25) we have:

$$\begin{cases} PTH_g^* = \dfrac{1}{\omega}, \\ PTH_p^* = \dfrac{\kappa}{\omega}. \end{cases} \tag{3.39}$$

In Figure 3.5 our results indicate that $PTH_g$ and $PTH_p$ reach the same steady state, independently of the initial conditions.

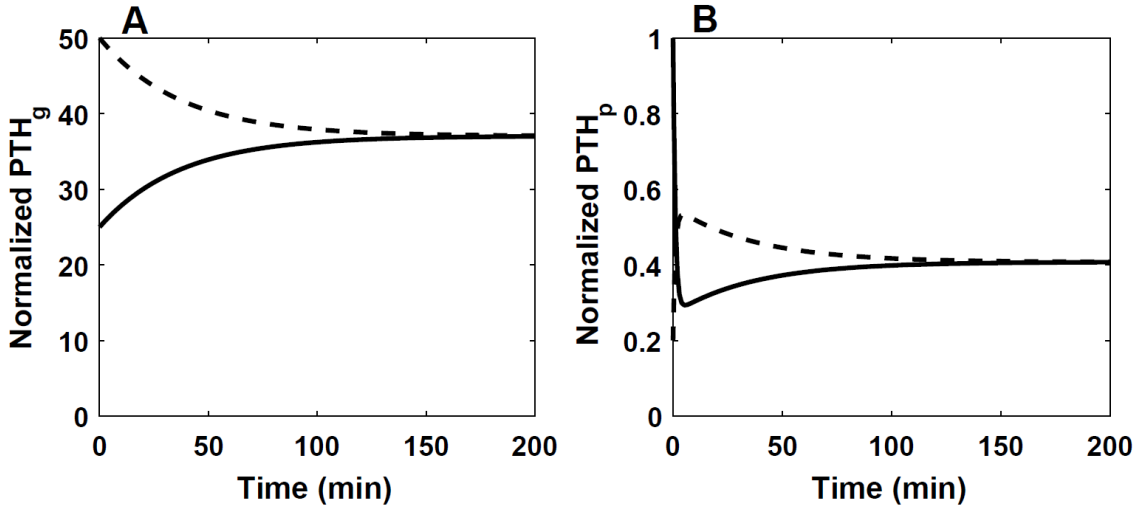


Figure 3.5: Panel A: normalized $PTH_g$ concentration as a function of time. Panel B: normalized $PTH_p$ concentration as a function of time. Initial conditions are [25,1] (solid line) and [50,0.2] (dashed line). Parameters are given in Table 3.1.

$PTH_g^*$ is a increasing function of $[Ca^{2+}]_p^*$, whereas $PTH_p^*$ decreases when $[Ca^{2+}]_p^*$ increases, as illustrated in Figure 3.6. The predicted profile of plasma PTH concentration at steady state (Panel B, Figure 3.6) is similar to the experimental profile observed by Brown (Brown, Journal of Clinical Endocrinology and Metabolism, 56, 1983).

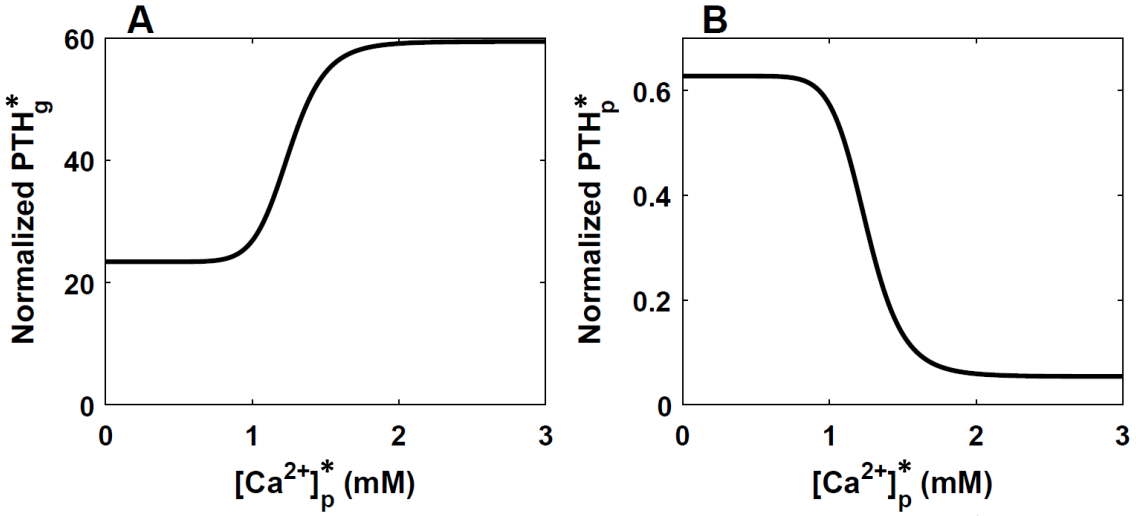


Figure 3.6: Panel A: $PTH_g^*$ (panel A) and $PTH_p^*$ (panel B( as a function of $[Ca^{2+}]_p^*$. Parameters are given in Table 3.1.

### Building of the plane phase

We build the phase plane as shown in Figure 3.7. There are 4 distincts areas in which trajectories have different behaviours. We start by determining nullclines: (1) the vertical nullcline is given by:

$$P\tilde{T}H_g = \frac{1}{\omega}, \tag{3.40}$$

which is a vertical line and the horizontal nullcline is:

$$P\tilde{T}H_p = \kappa P\tilde{T}H_g. \tag{3.41}$$

The steady state $(\frac{1}{\omega}, \frac{\kappa}{\omega})$ is located at the intersection of these two lines (green point).

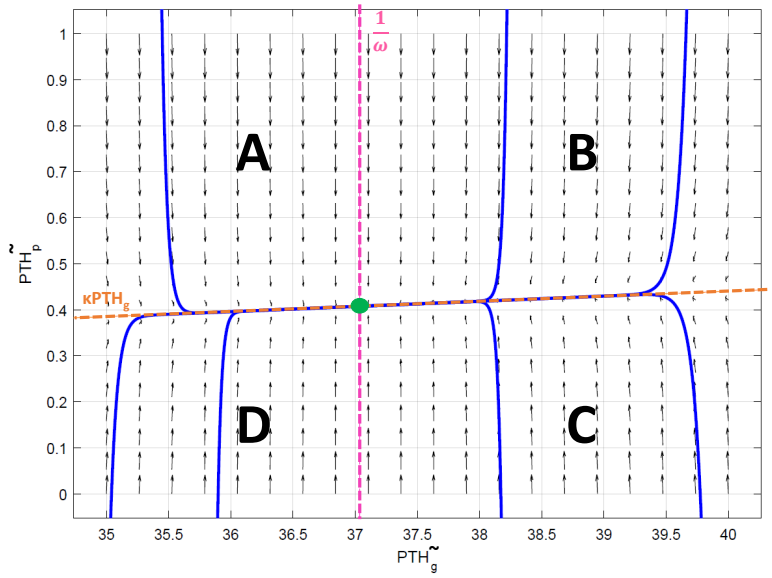


Figure 3.7: Phase plane of the normalized system with some trajectories. Parameters are given in Table 3.1.

Table 3.2: Determination of the sign of velocity vector within each area.

| | $P\tilde{T}H_g < \frac{1}{\omega}$ | $P\tilde{T}H_g > \frac{1}{\omega}$ |
|---|---|---|
| $P\tilde{T}H_p > \kappa P\tilde{T}H_g$ | A<br>$\frac{dP\tilde{T}H_g}{dt} > 0$<br>$\frac{dP\tilde{T}H_p}{dt} < 0$ | B<br>$\frac{dP\tilde{T}H_g}{dt} < 0$<br>$\frac{dP\tilde{T}H_p}{dt} < 0$ |
| $P\tilde{T}H_p < \kappa P\tilde{T}H_g$ | D<br>$\frac{dP\tilde{T}H_g}{dt} > 0$<br>$\frac{dP\tilde{T}H_p}{dt} > 0$ | C<br>$\frac{dP\tilde{T}H_g}{dt} < 0$<br>$\frac{dP\tilde{T}H_p}{dt} > 0$ |

Table 3.2 summarizes the localization of the 4 areas. By continuity, when $P\tilde{T}H_g^0 = 0$, $PTH_g$ increases. $PTH_p$ decreases until it crosses the horizontal nullcline.

By varying parameter values, it is possible to change the position of the steady state. Decreasing $\frac{1}{\omega}$ shifts this point to the right and inversely. Increasing $\kappa$ increases the slope of the horizontal nullcline, leading to a higher value of $P\tilde{T}H_p$. However, as previously demonstrated, the steady state is always asymptotically stable and no other point can appear (no bifurcation can be highlighted).

**Simulation results**

As mentioned previously in section 1.3.5, some models investigated hypocalcemic clamp situations on PTH secretion. Yet, all the available data were for humans and not for rats. We found an experimental study of the impact of acute hypocalcemia on PTH secretion in the rat [81]. In this experiment, $[Ca^{2+}]_p$ was reduced about 0.3 mM during 120 minutes. We simulated a sudden decrease in plasma calcium concentration in the system (3.25) by changing the value of $[Ca^{2+}]_p$ from 1.2 to 0.9 mM during 2 hours. Results are shown in Figure 3.8. Following an induced, acute hypocalcemia, PTH is released from parathyroid gland into plasma. The plasma concentration of PTH exhibits a peak and plateau behavior; its value at steady state is higher than its initial value, due to the induced hypocalcemia. Yet, using parameters taken in the literature does not yield a good fit (Panel A Figure 3.8). Thus, we adjusted model parameters so that predictions match the experimental data more closely, by applying the Levenberg-Marquardt algorithm on the following objective function:

$$f_{obj} = \sum_{i=1}^{n} \Big[ y_{exp} - y_{th} \Big]^2, \tag{3.42}$$

where $y_{exp}$ correspond to the experimental values of Ref. [81] and $y_{th}$ is the PTH function returned by our model. As shown in Figure 3.8, there is good agreement between model predictions and experimental observations after the parameter adjustment. Compared to previous parameters, $\beta_{exo}^{PTH_g}$ increased by 15% and $k_{deg}^{PTH_g}$ decreases by 37%; other parameters remain unchanged.

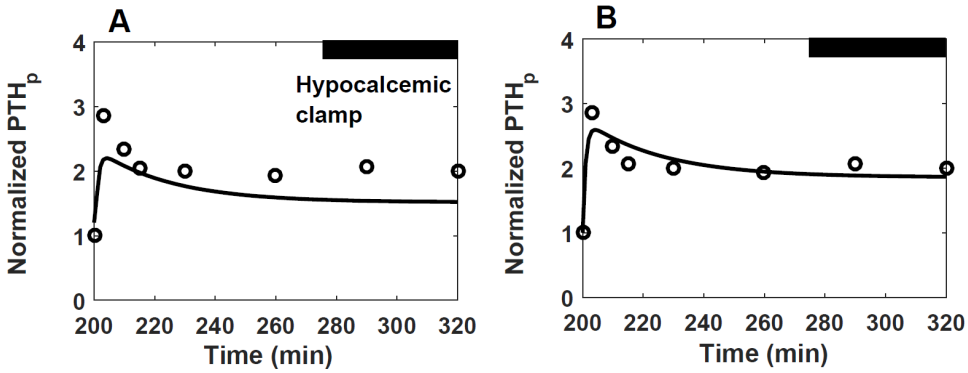


Figure 3.8: Measured and computed values of $PTH_p$ as a function of time during a hypocalcemic clamp. Open circles represent the experimental data of Fox [81], and solid lines denote model predictions. Panel A: without parameter adjustment. Panel B: with parameter adjustment using the Levenberg-Marquardt method.

We then simulated the reverse situation, namely a hypercalcemic clamp. Results are depicted in Figure 3.9. When calcium concentration is increased by 0.3 mM, $PTH_p$ drops by a factor 1.5.

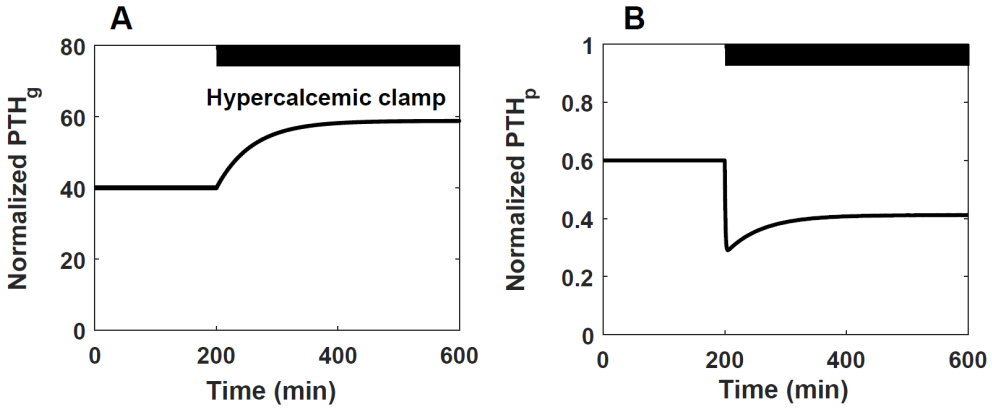


Figure 3.9: PTH profile during a hypercalcemic clamp.

### 3.1.6 Possible improvements to the PTH model

A problem that can be encountered with this model is mentioned by Shrestha *et al.* in section 1.3.5 [187]. In case of a hypercalcemic clamp, PTH secretion cannot be properly accounted for by a symmetrical sigmoidal function. Instead, it is better to replace the exponent $n$ in the PTH secretion function by an adaptive function such as:

$$n(Ca) = \frac{n_1^{exo}}{1 + e^{-\rho_{exo}(R - [Ca^{2+}]_p)}} + n_2^{exo} \tag{3.43}$$

$n_1^{exo}$ and $n_2^{exo}$ respectively characterize the sensitivity of the receptor under hypocalcemia and hypercalcemia, $R$ is the threshold between these two states, and $\rho_{exo}$ is an amplification term. When $[Ca^{2+}]_p$ is well below $R$, $n(Ca)$ tends towards an elevated value ($n_1^{exo} + n_2^{exo}$), as commonly used to fit hypocalcemia profiles [1, 165, 187]. Conversely, when $[Ca^{2+}]_p$ rises above $R$, $n(Ca)$ takes on a lower value. The outstanding features of this new function are depicted in Figure 3.10. Additionnally, as suggested by Momsen and Shwarz [144], $k_{deg}^{PTH_g}$ could be chosen as a function of plasma calcium.

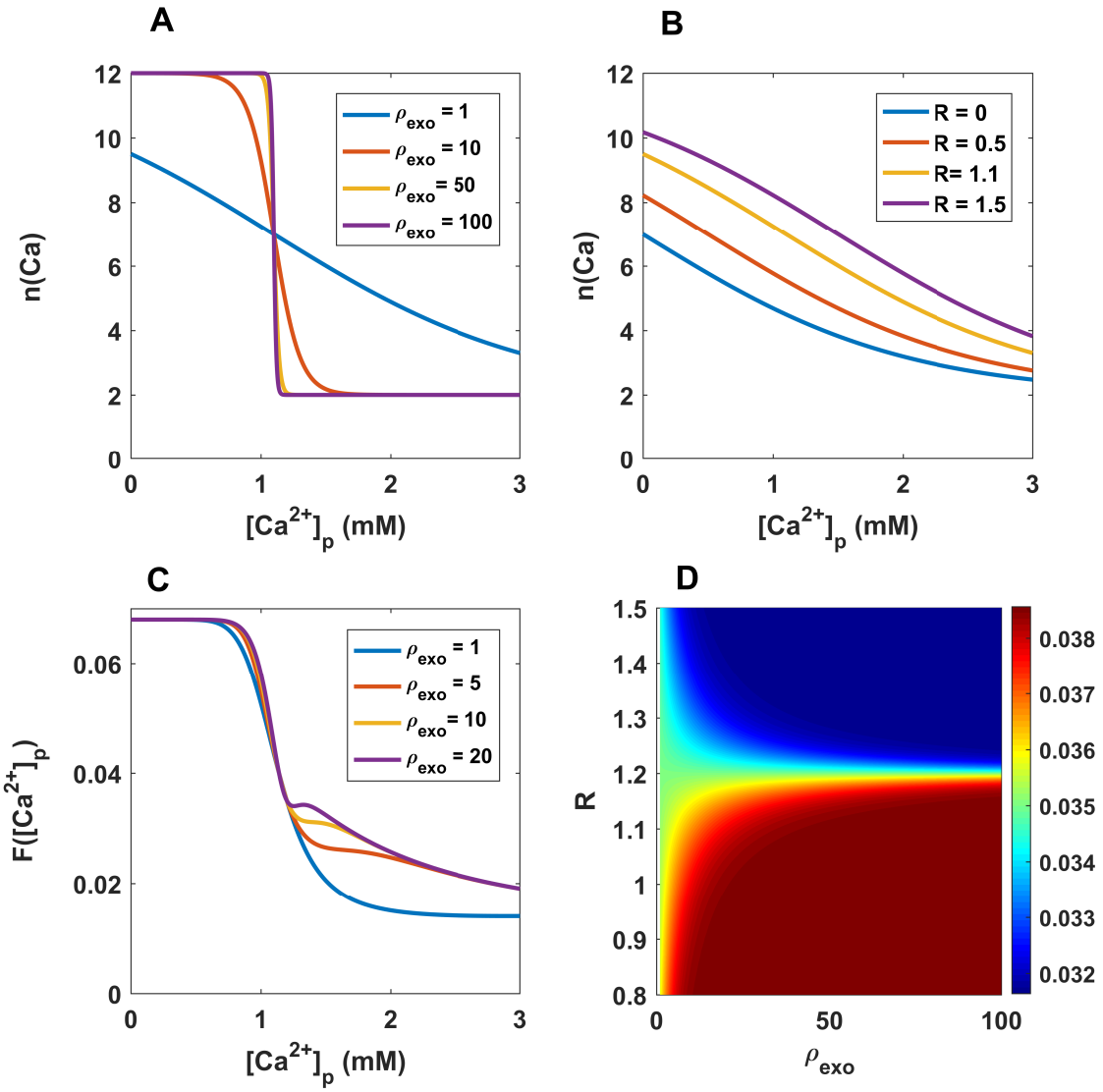


Figure 3.10: Analysis of the relationship between PTH secretion and plasma Ca2+ concentration. Panel A: $n$ as a function of $[Ca^{2+}]_p$ for varying values of $\rho_{exo}$. Panel B: $n$ as a function of $[Ca^{2+}]_p$ for varying values of $R$. Panel C: $F$ as a function of $[Ca^{2+}]_p$ some value of $\rho_{exo}$. Panel D: surface plot of $F$ as a function of $\rho_{exo}$ and $R$. When they are not varied, parameters are: $R = 1$, $n_1^{exo} = 10$, $n_2^{exo} = 2$ and $\rho_{exo} = 1.1$.

## 3.2 Mathematical model of calcium homeostasis with PTH

We present here the first version of our model of calcium homeostasis developed at the beginning of this thesis.

### 3.2.1 Calcium balance in the intestine, bone, kidney and plasma.

Letters $i$, $b$, $k$, $p$ and $g$ respectively refer to the intestinal, bone, kidney, plasma and parathyroid gland compartments. The compartments are represented as black boxes. $N_{Ca_j}$ corresponds to the quantity of calcium in compartment $j$ and $V_p$ is the total volume of plasma in rats (about 10 mL). Parameter choices and values are given in Table 3.3.

Equation (3.44) characterizes the dynamics of Ca in the intestine (Figure 3.11). It does not represent explicitly the mechanisms of calcium transport across the cells of the intestine border [117, 191, 113, 218], which could be developed in a later version of the model. The intestinal compartment has 3 fluxes of calcium: $I_{Ca}$ is the rate of calcium dietary intake, $E_{Ca}$ is the rate of net calcium fecal excretion, and $\Gamma_{abs}$ is the rate of net intestinal calcium absorption. As a first step, $\Gamma_{abs}$ is taken to be constant. The passive diffusion of calcium in the intestine is created by a gradient that can be directed either from lumen to plasma or from plasma to lumen. We have:

$$\frac{dN_{Ca_i}}{dt} = I_{Ca} - E_{Ca} - \Gamma_{abs}. \tag{3.44}$$

Furthermore, we assume that there is no net accumulation of calcium in the intestinal compartment over time, so that intestinal calcium excretion ($E_{Ca}$) is the difference between calcium intake ($I_{Ca}$) and net intestinal absorption:

$$E_{Ca} = I_{Ca} - \Gamma_{abs}. \tag{3.45}$$

Experimental findings suggest that at most, 60% of ingested calcium is absorbed into the bloodstream [46].

Equation (3.46) represents the conservation of calcium in bones. Two mechanisms are involved in bone remodeling: accretion ($\Gamma_{ac}$) and resorption (see section 1.1.2). Specific cells are involved in these processes, namely osteoblasts in accretion and osteoclasts in resorption. Our model does not take into account cellular-scale mechanisms of bone formation and removal, but they could be described in detail at a further stage.

$$\frac{dN_{Ca_b}}{dt} = \Gamma_{ac} - \Gamma^0_{res}\Big(1 + \gamma^{PTH_p}_{res}\frac{PTH_p}{K^{PTH_p}_{res} + PTH_p}\Big). \tag{3.46}$$

The resorption term is the sum of a fixed rate $\Gamma^0_{res}$ and a rate that is PTH-dependent. To ensure that the latter remains bounded, we choose a Michaelis-Menten function that represents the binding of PTH at the surface of osteoblasts to activate osteoclastogenesis (see section 1.1.2 and Figure 1.3). Neither PTH nor calcium seems to play a role in calcium accretion, although no specific study is

available. For this reason, we assume that the accretion rate ($\Gamma_{ac}$) remains constant. Since rats keep growing throughout most of the lifespan, Equation (3.46) cannot be taken to be at steady state. Instead we have:

$$\frac{dN_{Ca_b}}{dt} = \delta_b > 0. \tag{3.47}$$

where $\delta_b$ is the net difference between bone calcium accretion and resorption.

Equation (**??**) describes the overall calcium balance in the kidney compartment (see 1.1.2). Calcium is filtered non-selectively, in proportion to the glomerular filtration rate ($GFR$). A large fraction of the filtered load ($\lambda_{reab}$ is then reabsorbed, whereas a small fraction ($\lambda_u$) is excreted in urine. The rate of reabsorption includes a fixed contribution ($\lambda^0_{reab}$) as well as a PTH-dependent contribution; the latter is modeled using a function similar to that for bone resorption.

$$\begin{aligned}\frac{d[N_{Ca_k}]}{dt} &= GFR[Ca^{2+}]_p\Big[1-\lambda_{reab}-\lambda_u\Big],\\ &= GFR[Ca^{2+}]_p\Big[1-\lambda^0_{reab}\Big(1+\gamma^+_{reab}\frac{PTH_p}{K^{PTH_p}_{reab}+PTH_p}\Big)-\lambda_u\Big].\end{aligned} \tag{3.48}$$

As in the intestine, we assume that there is no accumulation of calcium in the kidney over time, so that the fractions of the filtered load that are reabsorbed and excreted in the urine sum to unity. In other words:

$$\lambda_{reab}+\lambda_u = 1 \tag{3.49}$$

Thus equation (3.48) is rewritten as:

$$\lambda_u(PTH) = 1-\lambda^0_{reab}\Big(1+\gamma^{PTH_p}_{reab}\frac{PTH_p}{K^{PTH_p}_{reab}+PTH_p}\Big). \tag{3.50}$$

Net changes in the total amount of calcium in plasma result from the combined effect of net intestinal calcium absorption, the difference between bone $Ca^{2+}$ resorption and accretion, and urinary $Ca^{2+}$ excretion, such that:

$$\begin{aligned}V_p\frac{d[Ca^{tot}]_p}{dt} = \Bigg\{&\Gamma_{abs}+\Gamma^0_{res}\Big(1+\gamma^{PTH_p}_{res}\frac{PTH_p}{K^{PTH_p}_{res}+PTH_p}\Big)\\ &-\Gamma_{ac}+GFR[Ca^{2+}]_p\Big[\lambda^0_{reab}\Big(1+\gamma^{PTH_p}_{reab}\frac{PTH_p}{K^{PTH_p}_{reab}+PTH_p}\Big)-1\Big]\Bigg\}.\end{aligned} \tag{3.51}$$

A substantial fraction of calcium ($\kappa_b$) in plasma is bound to proteins such as albumin. We assume that this fraction remains fixed at 0.5 [216, 210, 90] such that the total concentration of

calcium ($[Ca^{tot}]_p$) can be expressed as:

$$[Ca^{tot}]_p = [Ca^{2+}]_p + [Ca^{bound}]_p,\ [Ca^{bound}]_p = \kappa_b [Ca^{tot}]_p \text{ and } [Ca^{2+}]_p = (1-\kappa_b)[Ca^{tot}]_p. \quad (3.52)$$

Thus we have:

$$\begin{aligned} \frac{d[Ca^{tot}]_p}{dt} &= \frac{d[Ca^{2+}]_p}{dt} + \frac{d[Ca^{bound}]_p}{dt}, \\ &= \Big(1 + \frac{\kappa_b}{1-\kappa_b}\Big)\frac{d[Ca^{2+}]_p}{dt}, \\ &= \frac{1}{1-\kappa_b}\frac{d[Ca^{2+}]_p}{dt}. \end{aligned} \quad (3.53)$$

As a result:

$$\frac{d[Ca^{2+}]_p}{dt} = \frac{1-\kappa_b}{V_p}\Bigg\{\Gamma_{abs} + \Gamma^0_{res}\Big(1 + \gamma^{PTH_p}_{res}\frac{PTH_p}{K^{PTH_p}_{res} + PTH_p}\Big)$$

$$-\Gamma_{ac} + GFR[Ca^{2+}]_p\Bigg[\lambda^0_{reab}\Big(1 + \gamma^{PTH_p}_{reab}\frac{PTH_p}{K^{PTH_p}_{reab} + PTH_p}\Big) - 1\Bigg]\Bigg\}, \quad (3.54)$$

$$= \frac{1-\kappa_b}{V_p}\Big\{\Gamma_{abs} - \delta_b(PTH) - GFR[Ca^{2+}]_p\lambda_u(PTH)\Big\}.$$

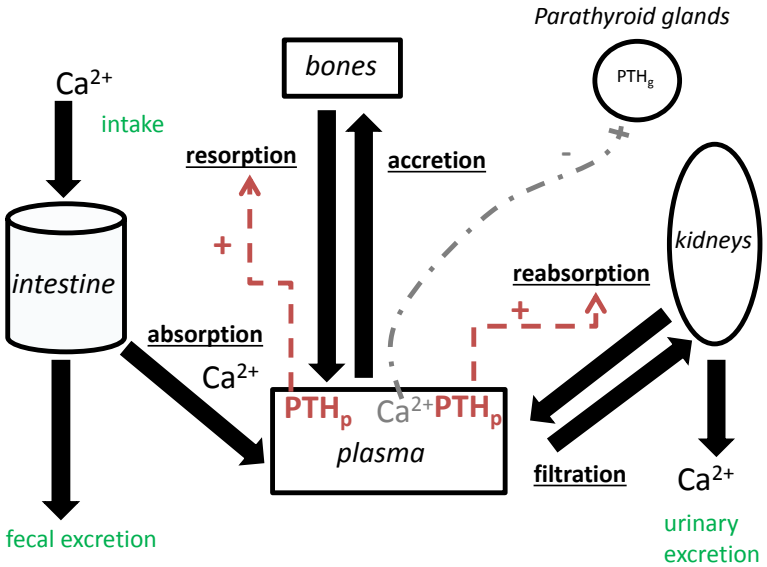


Figure 3.11: Calcium metabolism model considered in section 3.2. The regulation by calcitriol is not taken into account.

### 3.2.2 Mathematical analysis of the PTH-calcium model

In the following section, we examine the existence and numerical stability of steady state in the full calcium balance model. Our first objective is to find a coherent set of parameter values, one that yields the desired equilibrium point. To do so, we set the values of $[PTH]_p$ and $[Ca^{2+}]_p$ at their desired steady state values, namely 6 pM and 1.2 mM. The system we consider is the following:

$$\begin{cases} \dfrac{d[PTH]_g}{dt} = k_{prod}^{PTH_g} - \Big(k_{deg}^{PTH_g} + F([Ca^{2+}]_p)\Big)[PTH]_g, \\ \dfrac{d[PTH]_p}{dt} = F([Ca^{2+}]_p)\dfrac{V_c}{V_p}[PTH]_g - k_{deg}^{PTH_p}[PTH]_p, \\ \dfrac{d[Ca^{2+}]_p}{dt} = \dfrac{1-\kappa_b}{V_p}\Big\{\Gamma_{abs} - \delta_b(PTH) - GFR[Ca^{2+}]_p\lambda_u(PTH)\Big\}. \end{cases} \tag{3.55}$$

**Non-dimensionalization of the model**

We first define the parameters $\chi$, $[C\bar{a}^{2+}]_p$, $\alpha$, $\beta$, $\gamma$, $K_{\tilde{Ca}}$, $K_{res}^{\tilde{PTH}_p}$, $K_{reabs}^{\tilde{PTH}_p}$, $\Gamma_1$ and $\Gamma_2^0$ as:

$$\begin{aligned} &\chi = \frac{\tau(1-\kappa_b)}{V_p},\ [C\bar{a}^{2+}]_p = \chi\Gamma_{abs},\ \alpha = k_{deg}^{PTH_g}\tau,\ \beta = \beta_{exo}^{PTH_g}\tau,\ \gamma = \gamma_{exo}^{PTH_g}\tau,\ K_{\tilde{Ca}} = \frac{K_{Ca}}{[C\bar{a}^{2+}]_p}, \\ &K_{res}^{\tilde{PTH}_p} = \frac{K_{res}^{PTH_p}}{[P\bar{T}H]_p},\ K_{reab}^{\tilde{PTH}_p} = \frac{K_{reab}^{PTH_p}}{[P\bar{T}H]_p},\ \Gamma_1 = \frac{\Gamma_{ac}}{\Gamma_{abs}} \text{ and } \Gamma_2^0 = \frac{\Gamma_{res}^0}{\Gamma_{abs}}. \end{aligned} \tag{3.56}$$

According to the scaling made in section 3.1.5, we have the non-dimensional system:

$$\begin{cases} \dfrac{d\tilde{PTH}_g}{d\tilde{t}} = 1 - \Big[\alpha + \beta - \dfrac{\gamma}{1+\Big(\dfrac{K_{\tilde{Ca}}}{\tilde{Ca}_p^{2+}}\Big)^n}\Big]\tilde{PTH}_g, \\ \dfrac{d\tilde{PTH}_p}{d\tilde{t}} = \Big[\beta - \dfrac{\gamma}{1+\Big(\dfrac{K_{\tilde{Ca}}}{\tilde{Ca}_p^{2+}}\Big)^n}\Big]\tilde{PTH}_g - \tilde{PTH}_p, \\ \dfrac{d\tilde{Ca}_p^{2+}}{d\tilde{t}} = 1 - \Gamma_1 + \Gamma_2^0\Big[1 + \gamma_{res}^+\dfrac{\tilde{PTH}_p}{\tilde{PTH}_p + K_{res}^{\tilde{PTH}_p}}\Big] \\ \qquad\qquad -\chi GFR\tilde{Ca}_p^{2+}\Big[1 - \lambda_{reab}^0\Big(1 + \gamma_{reab}^+\dfrac{\tilde{PTH}_p}{\tilde{PTH}_p + K_{reab}^{\tilde{PTH}_p}}\Big)\Big]. \end{cases} \tag{3.57}$$

### Identification of steady state

In this section, $Ca_p^{2+}$ is denoted $Ca_p^*$ when it is at steady state. At steady state, system (3.57) yields:

$$\begin{aligned}
P\tilde{TH}_g^* &= \frac{1}{\alpha+\beta-\dfrac{\gamma}{1+\Big(\dfrac{\tilde{K_{Ca}}}{\tilde{Ca}_p^*}\Big)^n}},\\
P\tilde{TH}_p^* &= \Big[\beta-\frac{\gamma}{1+\Big(\dfrac{\tilde{K_{Ca}}}{\tilde{Ca}_p^*}\Big)^n}\Big]P\tilde{TH}_g^*,\\
\tilde{Ca}_p^* &= \frac{1-\Gamma_1+\Gamma_2^0\Big[1+\gamma_{res}^+\dfrac{P\tilde{TH}_{p*}}{P\tilde{TH}_p^*+K_{res}^{P\tilde{TH}_p}}\Big]}{\chi GFR\Big[1-\lambda_{reab}^0\Big(1+\gamma_{reab}^+\dfrac{P\tilde{TH}_{p*}}{P\tilde{TH}_{p*}+K_{reab}^{P\tilde{TH}_p}}\Big)\Big]}.
\end{aligned} \tag{3.58}$$

Since the term within brackets in the denominator, which corresponds to $\lambda_u(PTH)$, is strictly positive, for $\tilde{Ca}_p^*$ to also be positive it is necessary that:

$$\Gamma_1-\Gamma_2^0\Big[1+\gamma_{res}^+\frac{P\tilde{TH}_{p*}}{P\tilde{TH}_p^*+K_{res}^{P\tilde{TH}_p}}\Big]\leq 1, \tag{3.59}$$

meaning that the normalized intestinal absorption has to be higher than the difference between bone accretion and bone resorption.

### Numerical stability of the steady state

The calculation of the Jacobian yields a rather complex matrix, thus the Routh-Hurwitz criterion is not easy to apply. As a result, we propose to use the Lyapunov stability, introduced by Alexander Lyapunov in 1892. This concept considers a dynamical system in terms of energy. If the energy of this system decreases as time increases, it reaches an equilibrium. This energy can be defined as follows:

$$\begin{aligned}
&(i)\quad V(0,0,0)=0,\\
&(ii)\quad V(x,y,z)>0,\forall(x,y,z)\neq(0,0,0),\\
&(iii)\quad \dot{V}(x,y,z)\leq 0,\forall(x,y,z)\neq(0,0,0).
\end{aligned} \tag{3.60}$$

The two first points ensure that the energy is indeed well defined (as a positive function) while the third one corresponds to the property of energy dispersal. Furthermore, the latter implies that $V$ must be differentiable. If a function $V$ satisfies all the properties listed above in (3.60), it is a weak Lyapunov function. For a system having a weak lyapunov function, the equilibrium is locally

stable (but not asymptotically stable). Moreover, if the following condition is fulfilled:

$$\dot{V}(x,y,z) < 0, \forall (x,y,z) \neq (0,0,0), \tag{3.61}$$

then $V$ is a strong Lyapunov function, meaning that the equilibrium is asymptotically stable.

In the following, we try to show that the system (3.57) has a Lyapunov function. The system (3.57) is centered to make calculation simpler.

We let:

$$x = P\tilde{TH}_g,\ y = P\tilde{TH}_p \text{ and } z = \tilde{Ca}_p^{2+}. \tag{3.62}$$

We perform the following change of coordinates, so that (0,0,0) is the steady state:

$$u = x - x^*,\ v = y - y^* \text{ and } w = z - z^*. \tag{3.63}$$

Following several algebraic manipulations, we obtain:

$$\begin{cases} \dfrac{du}{d\tilde{t}} = -\Big[\alpha + \beta - \dfrac{\gamma}{1 + \Big(\dfrac{\tilde{K_{Ca}}}{w + z^*}\Big)^n}\Big]u, \\ \dfrac{dv}{d\tilde{t}} = \Big[\beta - \dfrac{\gamma}{1 + \Big(\dfrac{\tilde{K_{Ca}}}{w + z^*}\Big)^n}\Big]u - v, \\ \dfrac{dw}{dt} = -\chi GFR\Big[1 - \lambda^0_{reab}\Big(1 + \gamma^+_{reab}\dfrac{v + y^*}{v + y^* + K^{\tilde{PTH}_p}_{reab}}\Big)\Big]w. \end{cases} \tag{3.64}$$

We consider the function $V$ such that:

$$V(u,v,w) = \frac{1}{2}(u^2 + v^2 + w^2), \tag{3.65}$$

which satisfies the two first properties of (3.60). We have to check if the energy along the trajectories of the system dissipates. Taking the total derivative of $V$:

$$\dot{V} = -A_1u^2 - A_2v^2 - A_3w^2 + A_4uv, \tag{3.66}$$

with $A_1 = \alpha + \beta - \dfrac{\gamma}{1 + \Big(\dfrac{\tilde{K_{Ca}}}{w + z^*}\Big)^n}$, $A_2 = 1$, $A_3 = \chi GFR\Big[1 - \lambda^0_{reab}\Big(1 + \gamma^+_{reab}\dfrac{v + y^*}{v + y^* + K^{\tilde{PTH}_p}_{reab}}\Big)\Big]$ and

$A_4 = \beta - \dfrac{\gamma}{1+\Big(\dfrac{\tilde{K_{Ca}}}{w+z^*}\Big)^n}$. We search for the extremum of $\dot{V}$:

$$\nabla_{\dot{V}} = \overrightarrow{0} \Longleftrightarrow \begin{cases} -2\big[\alpha+\beta-\dfrac{\gamma}{1+\Big(\dfrac{\tilde{K_{Ca}}}{w+z^*}\Big)^n}\big]u + \big[\beta-\dfrac{\gamma}{1+\Big(\dfrac{\tilde{K_{Ca}}}{w+z^*}\Big)^n}\big]v = 0, \\ \big[\beta-\dfrac{\gamma}{1+\Big(\dfrac{\tilde{K_{Ca}}}{w+z^*}\Big)^n}\big]u - 2v + \chi GFR\lambda^0_{reab}\gamma^+_{reab}\dfrac{K^{\tilde{PTH}_p}_{reab}}{(v+y^*+K^{\tilde{PTH}_p}_{reabs})^2}w^2 = 0, \\ f(w)u^2 + g(w)uv - 2\chi GFR\Big[1-\lambda^0_{reab}\Big(1+\gamma^+_{reab}\dfrac{v+y^*}{v+y^*+K^{\tilde{PTH}_p}_{reab}}\Big)\Big]w = 0. \end{cases} \tag{3.67}$$

$f$ is the partial derivative of $A_1$ and $g$ is the partial derivative of $A_4$, with respect to $w$. If we set $w = 0$, the previous system becomes:

$$\begin{cases} u\Bigg[-\alpha-3\big(\alpha+\beta-\dfrac{\gamma}{1+\Big(\dfrac{\tilde{K_{Ca}}}{z^*}\Big)^n}\big)\Bigg] = 0, \\ \big[\beta-\dfrac{\gamma}{1+\Big(\dfrac{\tilde{K_{Ca}}}{z^*}\Big)^n}\big]u - 2v = 0, \\ f(w)u^2 + g(w)uv = 0 \end{cases} \tag{3.68}$$

In the first equation, either $u = 0$ or $-\alpha = 3\big(\alpha+\beta-\dfrac{\gamma}{1+\Big(\dfrac{\tilde{K_{Ca}}}{z^*}\Big)^n}\big)$. The second case is impossible since $\alpha > 0$ and the term on the right-hand-side is also positive. As a result, $u = 0$ and $v = 0$, as derived from the second equation. With $u = 0$, according to the third equation, either $w = 0$ or $1-\lambda^0_{reab}\Big(1+\gamma^+_{reab}\dfrac{v+y^*}{v+y^*+K^{\tilde{PTH}_p}_{reab}}\Big) = 0$. The second case is not biologically realistic since $\lambda_u > 0$, so $w = 0$, leading to $v = 0$ in the second equation. Consequently, (0,0,0) is an extremum of $\dot{V}$. Applying the Taylor formula (order 2) around (0,0,0) to $\dot{V}$ and using the Schwarz theorem, we

calculate the second order derivatives:

$$\begin{aligned}
&\frac{1}{2}\frac{\partial^2 V}{\partial u^2}\bigg|_{(0,0,0)} = -\Big[\alpha+\beta-\frac{\gamma}{1+\Big(\frac{\tilde{K_{Ca}}}{z^*}\Big)^n}\Big] < 0,\ \frac{1}{2}\frac{\partial^2 V}{\partial v^2}\bigg|_{(0,0,0)} = -1 < 0,\\
&\frac{1}{2}\frac{\partial^2 V}{\partial w^2}\bigg|_{(0,0,0)} = -\chi GFR\Big[1-\lambda^0_{reab}\Big(1+\gamma^+_{reab}\frac{y^*}{y^*+K^{\tilde{PTH}_p}_{reab}}\Big)\Big] < 0,\\
&\frac{\partial^2 V}{\partial u\partial v}\bigg|_{(0,0,0)} = \Big[\beta-\frac{\gamma}{1+\Big(\frac{\tilde{K_{Ca}}}{z^*}\Big)^n}\Big] > 0,\ \frac{\partial^2 V}{\partial u\partial w}\bigg|_{(0,0,0)} = 0,\ \frac{\partial^2 V}{\partial v\partial w}\bigg|_{(0,0,0)} = 0
\end{aligned} \tag{3.69}$$

Thus:

$$\dot{V}(u,v,w)-\dot{V}(0,0,0) = -\Big[\alpha+\beta-\frac{\gamma}{1+\Big(\frac{\tilde{K_{Ca}}}{z^*}\Big)^n}\Big]u^2 - v^2 + \Big[\beta-\frac{\gamma}{1+\Big(\frac{\tilde{K_{Ca}}}{z^*}\Big)^n}\Big]uv. \tag{3.70}$$

We cannot conclude regarding the sign of this expression.

However, we numerically investigated the sign of (3.70), based on parameter values. We conclude that $V$ is a strong Lyapunov function with our set of parameters so that the steady state is asymptotically stable.

### 3.2.3 Parameters of the PTH-calcium model

#### Determination of unknown parameters

Some parameters are well documented (Table 3.3) such as calcium intake, intestinal absorption, fecal excretion and bone turnover. The glomerular filtration rate and plasma volume can easily be estimated based upon the weight of the animal considered. Moreover, at equilibrium and under basal conditions, the urinary excretion of calcium is on the order of 1-2%. However, parameters describing the activation by PTH of bone resorption ($\gamma_{res}^{PTH_p}$ and $K_{res}^{PTH_p}$) as well as calcium reabsorption ($\gamma_{reab}^{PTH_p}$ and $K_{reab}^{PTH_p}$) are not known. Yet, they can be determined under certain conditions, and/or by making some assumptions. First, a common practice consists in setting a given affinity constant equal to the equilibrium concentration of the solute to which it is related. Since $[PTH]_p$ is about 6 pM at steady state in the rat, we set $K_{res}^{PTH_p} = K_{reab}^{PTH_p} = 6$ pM.

To satisfy the requirement that, $0 < \lambda_u$, for every large values of $PTH_p$ (i.e., even when the Michaelis-Menten function that characterizes the contribution of PTH in Eq.(3.50) tends towards unity), it is necessary that $\gamma_{reabs}^{+}$ be bounded as:

$$\gamma_{reab}^{PTH_p} < \frac{1 - \lambda_{reab}^0}{\lambda_{reab}^0}. \tag{3.71}$$

Moreover at steady state, we expect $\lambda_u^* \leq 0.02$, that is to say:

$$\gamma_{reab}^{PTH_p} \geq 2\frac{(0.98 - \lambda_{reab}^0)}{\lambda_{reab}^0}. \tag{3.72}$$

As a result, $\lambda_{reab}^0$ must satisfy these two inequalities, at any time for the first one and at least at steady state for the second. Therefore, $0.96 \leq \lambda_{reab}^0 < 0.98$ and we set its value to 0.96, which yields $\gamma_{reab}^{PTH_p} \approx 0.04$.

To determine the value of $\gamma_{res}^{PTH_p}$, we choose a parameter value which must satisfy the condition 3.59 . As a result, $\gamma_{res}^{PTH_p} \approx 0.1$ is suitable.

### Parameters of the calcium/PTH model

Table 3.3: Parameters of the PTH/calcium model.

| Parameter | Symbol | Value | Reference |
|---|---|---|---|
| $PTH_g$ synthesis rate | $k_{prod}^{PTH_g}$ | 2.2 nmol.min$^{-1}$ | estimated |
| $PTH_g$ degradation rate constant | $k_{deg}^{PTH_g}$ | 0.035 min$^{-1}$ | [1] |
| Maximal secretion rate constant of $PTH_g$ | $\beta_{exo}^{PTH_g}$ | 0.068 min$^{-1}$ | fitted from [81] |
| Maximal inhibition of secretion by $Ca^{2+}$ | $\gamma_{exo}^{PTH_g}$ | 0.057min$^{-1}$ | fitted from [81] |
| Binding of $Ca^{2+}$ to CaSR | $K_{Ca_p^{2+}}$ | 1.14 mM | [81] |
| | $n_{Ca}^{exo}$ | 10 | |
| $PTH_p$ degradation rate constant $k_{deg}^{PTH_p}$ | 2.2 min$^{-1}$ | [1] | |
| Volume of parathyroid glands | $V_c$ | 0.1 $\mu$L | [98] |
| Calcium intake | $I_{Ca}$ | 3 $\mu$mol.min$^{-1}$ | [55, 134] |
| Calcium absorption | $\Gamma_{abs}$ | 1.45 $\mu$mol.min$^{-1}$ | [55] |
| Accretion rate | $\Gamma_{ac}$ | 1.4 $\mu$mol.min$^{-1}$ | [55] |
| Minimal resorption rate | $\Gamma_{res}^0$ | 0.14 $\mu$mol.min$^{-1}$ | [55] |
| Maximal effect of PTH on resorption rate | $\gamma_{res}^{PTH_p}$ | 0.1 | estimated |
| Stimulation of resorption by PTH | $K_{res}^{PTH_p}$ | 6 pM | estimated |
| Glomerular filtration rate | $GFR$ | 2 mL.min$^{-1}$ | [231] |
| Minimal calcium reabsorption | $\lambda_{reab}^0$ | 0.96 | estimated |
| Maximal effect of PTH on calcium reabsorption | $\gamma_{reab}^{PTH_p}$ | 0.04 | estimated |
| Stimulation of $Ca^{2+}$ reabsorption in by PTH | $K_{reab}^{PTH_p}$ | 6 pM | estimated |
| Plasma volume | $V_p$ | 10 mL | [127] |
| Fraction of bound calcium | $\kappa_b$ | 0.5 | [208] |

## 3.3 Mathematical model of calcium homeostasis with PTH and vitamin $D_3$

In this part, we introduce an additional factor in calcium homeostasis, namely vitamin $D_3$. This hormone affects intestinal calcium absorption, renal calcium reabsorption, bone accretion, PTH production and its own synthesis [62].

### 3.3.1 Hormonal part of the model

#### Balance equation for vitamin $D_3$

The biosynthesis pathway of vitamin $D_3$ (also denoted $1,25(OH)_2D_3$) involves a large range of components which cannot be fully represented in our model. As illustrated in Figure 3.12, we represent the synthesis of$1,25(OH)_2D_3$ as follows.

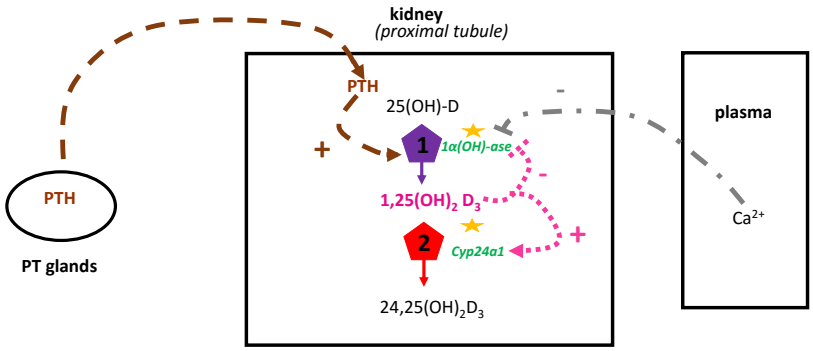


Figure 3.12: Regulation of the $1,25(OH)_2D_3$ synthesis pathway considered in our model. Step (1) characterizes the conversion of 25(OH)-vitamin D to active vitamin $D_3$ and step (2) accounts for vitamin $D_3$ degradation.

We focus on the kidney compartment where 25(OH)-vitamin D ($D_3^{inact}$) is converted into its active form, $1,25(OH)_2D_3$. This conversion is accomplished by the enzyme 1-$\alpha$-hydroxylase whose activity may be enhanced by PTH or silenced by the plasma calcium concentration. $1,25(OH)_2D_3$ negatively regulates 1-$\alpha$-hydroxylase (CYP27B1) and activates CYP24A1, which degrades $1,25(OH)_2D_3$ into $24,25(OH)_2D_3$. For simplicity, we assume that the level of $D_3^{inact}$ remains constant. Hurwitz *et al.* [106] modeled the activity of CYP27B1 with a sigmoïdal increasing function of PTH. In our model we added the contributions of vitamin $D_3$ and calcium to the conversion of $D_3^{inact}$. Finally, we make the hypothesis that inhibitors or activators of the 1-$\alpha$-hydroxylase are not in competition. Consequently, the rate of vitamin $D_3$ formation ($R_{conv}$) is expressed as:

$$R_{conv} = \left[ k_{conv}^{min} + \frac{\delta_{conv}^{max}[PTH]_p^{n_{conv}}}{([PTH]_p^{n_{conv}} + K_{conv}^{n_{conv}})(1+\gamma_{conv}^{Ca}[Ca^{2+}]_p)(1+\gamma_{conv}^{D_3}[D_3]_p)} \right] \tag{3.73}$$

It has a minimal rate $k_{conv}^{min}$ and a maximal rate $\delta_{conv}^{max}$. The parameters $\gamma_{conv}^{Ca}$ and $\gamma_{conv}^{D_3}$ respectively

account for the repression of 1-$\alpha$(OH)-ase by calcium and vitamin $D_3$.

The degradation of vitamin $D_3$ is assumed to be first order such that the dynamics of vitamin $D_3$ is:

$$\frac{d[D_3]_p}{dt} = R_{conv}([PTH]_p, [D_3]_p, [Ca^{2+}]_p)[D_3^{inact}]_p - k_{deg}^{D_3}[D_3]_p. \tag{3.74}$$

The baseline value of $D_3^{inact}$ is 25 nM [81], which appears to decrease with age. In parathyroidectomized (PTX) rats, the level of vitamin $D_3$ decreases by a factor of at least 2 [209] and our parameters are chosen to correspond to this observation. The equilibrium plasma concentration of vitamin $D_3$, namely $[D_3]_p^*$ is 200 pM in a 200-250g rat [93, 209] and decreases with aging (Negrea, Kidney Int, 44, 1993 [81, 147]. Furthermore, $k_{deg}^{D_3}$ is chosen so that the half life of vitamin $D_3$ is between 4 and 8 hours.

### Effect of vitamin $D_3$ on PTH production

Vitamin $D_3$ directly acts on the promoter of the gene that triggers PTH synthesis [189, 190], as depicted in Figure 3.13. Interestingly, Silver *et al.* [189] found an (exponential) decreasing relationship between the mRNA expression of the PTH precursor in parathyroid glands and the injected quantity of vitamin $D_3$. Thus, we model PTH synthesis by the following function:

$$PTH_{synthesis} = \frac{k_{prod}^{PTH_g}}{1 + \gamma_{prod}^{D_3}[D_3]_p}. \tag{3.75}$$

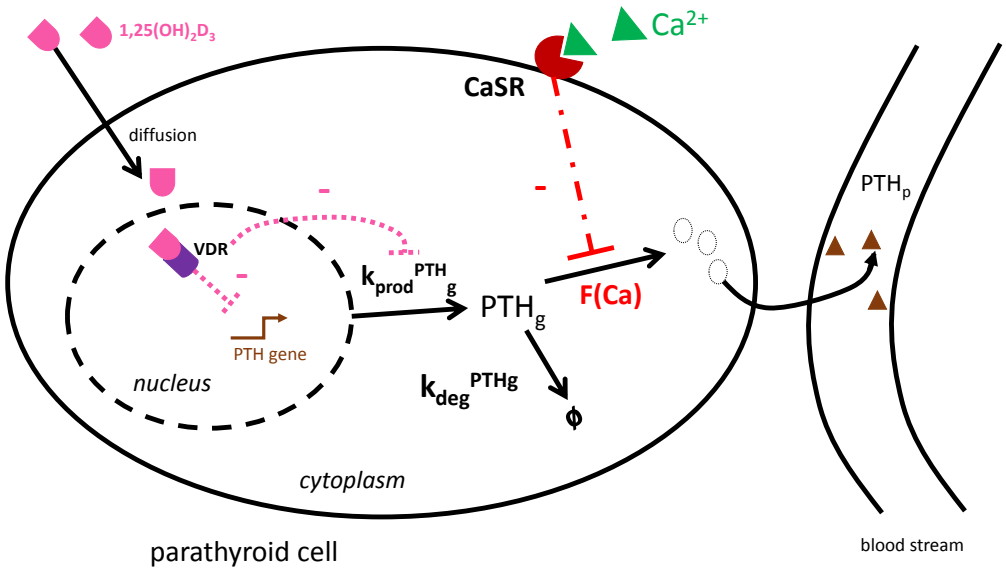


Figure 3.13: Regulation of PTH synthesis by vitamin $D_3$ in our model.

The repression factor $\gamma_{prod}^{D_3}$ is adjusted so that at steady state, the synthesis of PTH is reduced by 33 %, in agreement with [189].

### 3.3.2 Effect of vitamin $D_3$ on calcium metabolism

#### Regulation of intestinal calcium absorption

In section 3.2.1 (Equation (3.44)), the equation describing the evolution of the amount of calcium in the intestine was:

$$E_{Ca} = I_{ca} - \Gamma_{abs}, \tag{3.76}$$

with $\Gamma_{abs}$ taken to be constant. Yet, vitamin $D_3$ is known to exert several effects within intestinal cells (Figure 1.4): (1) it regulates the transcellular transport of calcium by increasing the activity of TRPV6 which is responsible for calcium entry from the lumen into the border cells (enterocytes), even if there may exist other $Ca^{2+}$ transporters yet to-be-identified in the gut [17]; (2) vitamin $D_3$ enhances the transcription of the calbindin ($CaBD_{9k}$) gene which facilitates to the calcium transport inside each cell; (3) additionally, it improves calcium extrusion at the basal pole of the cell by acting on the membrane pump PMCA1b [4, 77]; (4) finally vitamin $D_3$ modulates the paracellular transport of calcium by increasing the permeability of tight junctions such as claudin 2 and claudin 12 [84]. As a result, mutant VDR mice show a decrease in the intestinal calcium absorption. Some investigations such as that of Carlsson *et al.* [46] have found that vitamin $D_3$ increases calcium absorption up to 60% of calcium intake. As a result, we use the following function to represent the calcium absorption in the intestine:

$$\Gamma_{abs}(D_3) = I_{Ca}\Big(\Gamma^0_{abs} + \frac{(0.6 - \Gamma^0_{abs})[D_3]_p}{K^{D_3}_{abs} + [D_3]_p}\Big), \tag{3.77}$$

$\Gamma^0_{abs}$ represents the ratio of basal (i.e., in the absence of vitamin $D_3$) to total absorption (at saturating levels of vitamin $D_3$), and is taken as 0.4. With this choice of parameters, the model predicts that vitamin $D_3$ contributes to one third of calcium intestinal absorption, as observed experimentally [46]. The sensitivity of model predictions to the parameters $\Gamma^0_{abs}$ and $K^{D_3}_{abs}$ is illustrated in Figure 3.14. In order to obtain a physiological equilibrium value for $[Ca^{2+}]_p$ (about 1.2 mM), we choose $K^{D_3}_{abs} = 200$ pM and $\Gamma^0_{abs} = 0.2$, which corresponds to the yellow curve in the panel A of Figure 3.14. Thereby, when vitamin $D_3$ is at steady state (100 pM for a 300g rat), intestinal absorption of calcium is 40% of the intake, which is consistent with the literature.

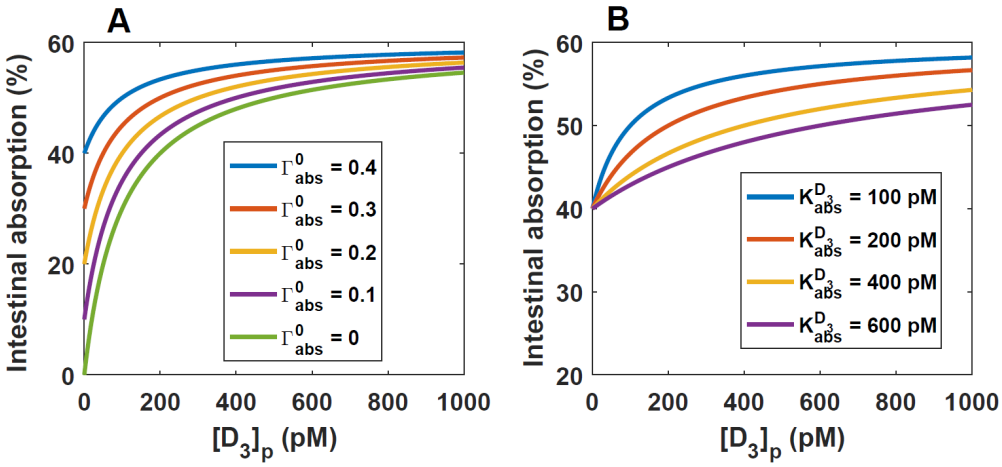


Figure 3.14: Panel A: effect of vitamin $D_3$ contribution on intestinal calcium absorption. The base case is in blue. Panel B: effect of varying $K_{abs}^{D_3}$ on intestinal calcium absorption.

### Regulation of bone remodeling

Similarly to PTH, vitamin $D_3$ is known to increase the production of RANK-L by binding to the vitamin D receptor in osteoblasts, which enhances the maturation of osteoclasts, thereby stimulating bone resorption (Figure 1.3) [200, 227]. However, few models have taken this feature into account (except that of Raposo *et al.*, [168]). As a result, we consider an equation similar to that of PTH and assume that the two pathways are independent:

$$\Gamma_{res}(PTH, D_3) = \Gamma_{res}^0 \Big[1 + \gamma_{res}^{PTH_p} \frac{[PTH]_p}{[PTH]_p + K_{res}^{PTH_p}} + \gamma_{res}^{D_3} \frac{[D_3]_p}{[D_3]_p + K_{res}^{D_3}}\Big]. \tag{3.78}$$

$K_{res}^{D_3}$ is chosen equal to the plasma equilibrium concentration of vitamin $D_3$, that is, 100 pM. The relative contribution of PTH and $D_3$ is unknown. We assume that $\gamma_{res}^{D_3} = \gamma_{res}^{PTH_p} = 0.05$ (to have a positive value of $[Ca^{2+}]_p^*$).

### Regulation of kidney reabsorption

Vitamin $D_3$ enhances calcium transport in the kidney [4, 32] by several mechanisms (Figure 1.7), even though its contribution is lower than that of PTH: (1) it positively regulates the TRPV5 channel that allows calcium to enter cells in the DCT; (2) it increases the expression of two calcium-binding proteins (calbindin-$D_{28K}$ and calbindin-$D_{9K}$), to respectively facilitate the transport of calcium at the apical side and at the basolateral side; and (3) it may indirectly regulate the activity of the renal calcium pump by acting on calbindin-$D_{9K}$ expression. Here too, we assume that $D_3$ and PTH exert independent effects on calcium reabsorption [25, 83]. The equation (3.48) that describes calcium urinary excretion is therefore rewritten as:

$$\lambda_u(PTH, D_3) = 1 - \lambda_{reabs}^0 \Big[1 + \gamma_{reab}^{PTH_p} \frac{[PTH]_p}{[PTH]_p + K_{reab}^{PTH_p}} + \gamma_{reab}^{D_3} \frac{[D_3]_p}{[D_3]_p + K_{reab}^{D_3}}\Big]. \tag{3.79}$$

It is thought that PTH has a greater impact than vitamin $D_3$ on $\lambda_u(PTH, D_3)$, yet their relative contributions are not well characterized. We assume that $\gamma_{reab}^{PTH_p} = 2\gamma_{reab}^{D_3}$. We can estimate the bounds of $\gamma_{reab}^{D_3}$ assuming that, at steady state, $0 < \lambda_u(PTH, D_3) \leq 0.02$. This condition yields:

$$\frac{0.98 - \lambda_{reab}^0}{3\lambda_{reab}^0} \leq \gamma_{reabs}^{D_3} \leq \frac{1 - \lambda_{reab}^0}{3\lambda_{reab}^0}. \tag{3.80}$$

This yields $0.046 \leq \gamma_{reab}^{D_3} \leq 0.054$. We choose $\gamma_{reab}^{D_3} = 0.05$, leading to $\gamma_{reab}^{PTH_p} = 0.1$.

### 3.3.3 Equations of the model

#### Equations of the hormonal system

To obtain non-dimensional variables, we define the parameters $\bar{D_3}$, $\gamma_{prod}^{\tilde{D_3}}$, $k_{conv}$, $\tilde{K_{conv}}$, $\gamma_{conv}^{\tilde{Ca}}$, $\gamma_{conv}^{\tilde{D_3}}$ and $\nu$ as:

$$\begin{gathered}\bar{D_3} = \delta_{conv}^{max}[D_3^{inact}]_p\tau,\ \gamma_{prod}^{\tilde{D_3}} = \gamma_{prod}^{D_3}\bar{D_3},\ k_{conv} = \frac{k_{conv}^{min}}{\delta_{conv}^{max}},\ \tilde{K_{conv}} = \frac{K_{conv}}{P\bar{T}H_p}, \\ \gamma_{conv}^{\tilde{Ca}} = \gamma_{conv}^{Ca}\bar{Ca_p^{2+}},\ \gamma_{conv}^{\tilde{D_3}} = \gamma_{conv}^{D_3}\bar{D_3} \text{ and } \nu = \tau k_{deg}^{D_3}.\end{gathered} \tag{3.81}$$

Scaling the equations as in 3.1.5 and assuming that the plasma calcium concentration is fixed at a given steady-state value, we obtain:

$$\begin{cases} \dfrac{dP\tilde{T}H_g}{d\tilde{t}} = \dfrac{1}{1 + \gamma_{prod}^{\tilde{D_3}}\tilde{D_3}} - \omega P\tilde{T}H_g, \\ \dfrac{dP\tilde{T}H_p}{d\tilde{t}} = \kappa P\tilde{T}H_g - P\tilde{T}H_p, \\ \dfrac{d\tilde{D_3}}{d\tilde{t}} = k_{conv} + \dfrac{1}{\left[1 + \left(\dfrac{\tilde{K_{conv}}}{P\tilde{T}H_p}\right)^{n_{conv}}\right]\left(1 + \gamma_{conv}^{\tilde{Ca}}\tilde{Ca_p^{2+}}\right)\left(1 + \gamma_{conv}^{\tilde{D_3}}\tilde{D_3}\right)} - \nu\tilde{D_3}. \end{cases} \tag{3.82}$$

A mathematical analysis of this model could be performed, as in section 3.1.5.

#### Equations of calcium homeostasis regulated by PTH and D3

For the global model of calcium homeostasis, we define the additional parameters $[\bar{Ca^{2+}}]_p$, $K_{abs}^{\tilde{D_3}}$, $K_{res}^{\tilde{D_3}}$, $K_{reab}^{\tilde{D_3}}$, $\Gamma_1$ and $\Gamma_2^0$:

$$\begin{gathered}[\bar{Ca^{2+}}]_p = \chi I_{Ca},\ K_{abs}^{\tilde{D_3}} = \frac{K_{abs}^{D_3}}{\bar{D_3}},\ \Gamma_1 = \frac{\Gamma_{ac}}{I_{Ca}}, \\ K_{res}^{\tilde{D_3}} = \frac{K_{res}^{D_3}}{\bar{D_3}},\ K_{reab}^{\tilde{D_3}} = \frac{K_{reab}^{D_3}}{\bar{D_3}},\ \Gamma_2^0 = \frac{\Gamma_{res}^0}{I_{Ca}}.\end{gathered} \tag{3.83}$$

Based on equations written in sections 3.2.1 and 3.3.2, we have:

$$\begin{cases} \dfrac{dP\tilde{T}H_g}{d\tilde{t}} = \dfrac{1}{1+\gamma_{prod}^{\tilde{D}_3}\tilde{D}_3} - \Big[\alpha+\beta-\dfrac{\gamma}{1+\Big(\dfrac{\tilde{K_{Ca}}}{\tilde{Ca_p^{2+}}}\Big)^n}\Big]P\tilde{T}H_g, \\ \dfrac{dP\tilde{T}H_p}{d\tilde{t}} = \Big[\beta-\dfrac{\gamma}{1+\Big(\dfrac{\tilde{K_{Ca}}}{\tilde{Ca_p^{2+}}}\Big)^n}\Big]P\tilde{T}H_g - P\tilde{T}H_p, \\ \dfrac{d\tilde{D}_3}{d\tilde{t}} = k_{conv} + \dfrac{1}{\Big[1+\Big(\dfrac{\tilde{K_{conv}}}{P\tilde{T}H_p}\Big)^{n_{conv}}\Big]\Big(1+\gamma_{conv}^{\tilde{Ca}}\tilde{Ca_p^{2+}}\Big)\Big(1+\gamma_{conv}^{\tilde{D}_3}\tilde{D}_3\Big)} - \nu\tilde{D}_3, \\ \dfrac{d\tilde{Ca_p^{2+}}}{d\tilde{t}} = \Gamma_{abs}^0 + (0.6-\Gamma_{abs}^0)\dfrac{\tilde{D}_3}{\tilde{D}_3+K_{abs}^{\tilde{D}_3}} - \Gamma_1 + \Gamma_2^0\Big[1+\gamma_{res}^{PTH_p}\dfrac{P\tilde{T}H_p}{P\tilde{T}H_p+K_{res}^{\tilde{PTH}_p}} + \gamma_{res}^{D_3}\dfrac{\tilde{D}_3}{\tilde{D}_3+K_{res}^{\tilde{D}_3}}\Big] \\ \qquad -\chi GFR\tilde{Ca_p^{2+}}\Big[1-\lambda_{reab}^0\Big(1+\gamma_{reab}^{PTH_p}\dfrac{P\tilde{T}H_p}{P\tilde{T}H_p+K_{reab}^{\tilde{PTH}_p}} + \gamma_{reab}^{D_3}\dfrac{\tilde{D}_3}{\tilde{D}_3+K_{reab}^{\tilde{D}_3}}\Big)\Big]. \end{cases} \tag{3.84}$$

The condition to obtain a positive value of $\tilde{Ca_p^{2+}}$ is:

$$\Gamma_{abs}^0 + (0.6-\Gamma_{abs}^0)\frac{\tilde{D}_3}{\tilde{D}_3+K_{abs}^{\tilde{D}_3}} - \Gamma_1 + \Gamma_2^0\Big[1+\gamma_{res}^{PTH_p}\frac{P\tilde{T}H_p}{P\tilde{T}H_p+K_{res}^{\tilde{PTH}_p}} + \gamma_{res}^{D_3}\frac{\tilde{D}_3}{\tilde{D}_3+K_{res}^{\tilde{D}_3}}\Big] \geq 0. \tag{3.85}$$

Figure 3.15 summarizes all the mechanisms taken into account in this model.

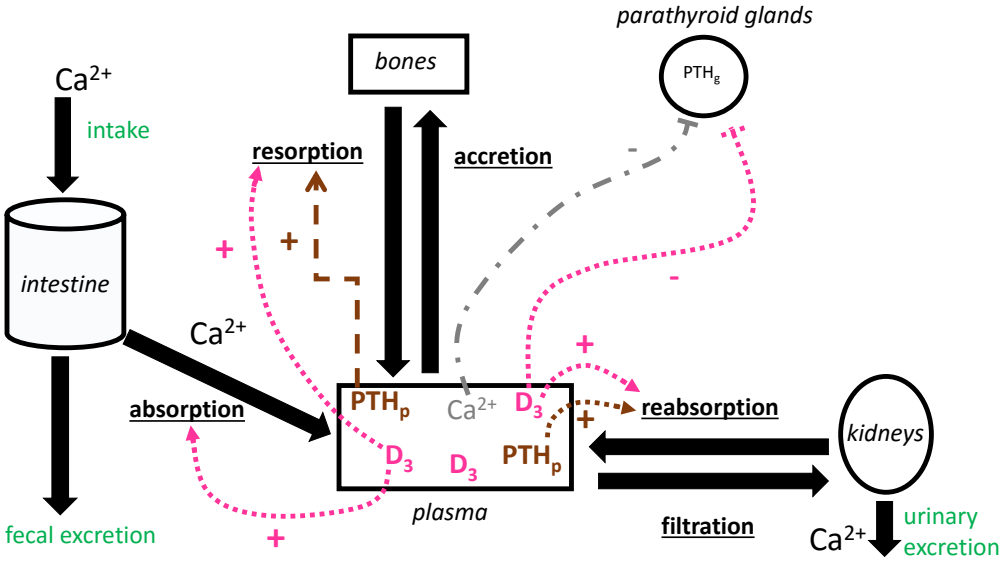


Figure 3.15: Calcium homeostasis model with PTH and vitamin $D_3$. The regulation of vitamin $D_3$ synthesis is shown in Figure 3.12.

### Parameters of the calcium homeostasis model

Table 3.4: Vitamin $D_3$ parameters

| Parameter | Symbol | Value | Reference |
|---|---|---|---|
| Minimum production rate constant of vitamin $D_3$ | $k_{conv}^{min}$ | $6.6 \times 10^{-6}$ min$^{-1}$ | [209] |
| Maximal increase in vitamin $D_3$ production rate | $\delta_{conv}^{max}$ | $9.03 \times 10^{-5}$ min$^{-1}$ | [209] |
| Plasma concentration of $D_3^{inact}$ | $[D_3^{inact}]_p$ | 25 nM | [81] |
| Activation of vitamin $D_3$ production by PTH | $K_{conv}$ | 6 pM | estimated |
| PTH sensitivity coefficient | $n_{conv}$ | 6 | estimated |
| Inhibition of $D_3$ production by $Ca^{2+}$ | $\gamma_{conv}^{Ca}$ | 0.3 mM$^{-1}$ | estimated |
| Inhibition of vitamin $D_3$ production by itself | $\gamma_{conv}^{D_3}$ | $1.2 \times 10^{-2}$ pM$^{-1}$ | estimated |
| Degradation rate constant of vitamin $D_3$ | $k_{deg}^{D_3}$ | 0.0029 min$^{-1}$ | [12, 64, 111] |

Table 3.5: Parameters of the PTH-vitamin $D_3$-calcium model.

| Parameter | Symbol | Value | Reference |
|---|---|---|---|
| $PTH_g$ synthesis rate | $k_{prod}^{PTH_g}$ | 2.2 $\mu$mol.min$^{-1}$ | estimated |
| Inhibition of $PTH_g$ synthesis by vitamin $D_3$ | $\gamma_{prod}^{D_3}$ | 5 pM$^{-1}$ | estimated |
| $PTH_g$ degradation rate constant | $k_{deg}^{PTH_g}$ | 0.022 min$^{-1}$ | [1] |
| Maximal secretion rate constant of $PTH_g$ | $\beta_{exo}^{PTH_g}$ | 0.068 min$^{-1}$ | fitted from [81] |
| Maximal inhibition of secretion by $Ca^{2+}$ | $\gamma_{exo}^{PTH_g}$ | 0.057min$^{-1}$ | fitted from [81] |
| Binding of $Ca^{2+}$ to CaSR | $K_{Ca_p^{2+}}$ | 1.14 mM | [81] |
| | $n_{Ca}^{exo}$ | 10 | |
| $PTH_p$ degradation rate constant | $k_{deg}^{PTH_p}$ | 2.2 min$^{-1}$ | [1] |
| Volume of parathyroid glands | $V_c$ | 0.1 $\mu$L | [98] |
| Calcium intake | $I_{Ca}$ | 2.1 $\mu$mol.min$^{-1}$ | [55, 134] |
| Basal absorption without $D_3$ | $\Gamma_{abs}^0$ | 0.2 | estimated |
| Stimulation of absorption by $D_3$ | $K_{abs}^{D_3}$ | 200 pM | estimated |
| Accretion rate | $\Gamma_{ac}$ | 1.4 $\mu$mol.min$^{-1}$ | [55] |
| Minimal resorption rate | $\Gamma_{res}^0$ | 0.8 $\mu$mol.min$^{-1}$ | [55] |
| Maximal effect of PTH on resorption rate | $\gamma_{res}^{PTH_p}$ | 0.1 | estimated |
| Maximal effect of $D_3$ on resorption rate | $\gamma_{res}^{D_3}$ | 0.1 | estimated |
| Stimulation of resorption by PTH | $K_{res}^{PTH_p}$ | 6 pM | estimated |
| Stimulation of resorption by $D_3$ | $K_{res}^{D_3}$ | 100 pM | estimated |
| Glomerular filtration rate | $GFR$ | 2 mL.min$^{-1}$ | [231] |
| Minimal calcium reabsorption | $\lambda_{reabs}^0$ | 0.86 | estimated |
| Maximal effect of PTH on calcium reabsorption | $\gamma_{reab}^{PTH_p}$ | 0.1 | estimated |
| Maximal effect of $D_3$ on calcium reabsorption | $\gamma_{reab}^{D_3}$ | 0.05 | estimated |
| Stimulation of $Ca^{2+}$ reabsorption in by PTH | $K_{reab}^{PTH_p}$ | 6 pM | estimated |
| Stimulation of $Ca^{2+}$ reabsorption in by $D_3$ | $K_{reab}^{D_3}$ | 100 pM | estimated |
| Plasma volume | $V_p$ | 10 mL | [127] |
| Fraction of bound calcium | $\kappa_b$ | 0.5 | [208] |

## 3.4 Summary of the mathematical properties of the model

In section 3.2.2, we show the existence of a physiological (positive) steady state in the model of calcium homeostasis with PTH under a given condition in Equation (3.59). The stability analysis is quite complex and tightly depends on parameter values. With parameters considered in Table 3.3, the steady state is stable from a numerical point of view. In the calcium homeostasis model with PTH and vitamin $D_3$, the existence condition is very similar. We did not investigate its stability from a theoretical point of view, but numerical simulations suggest that the system is indeed stable around the steady state.

## 3.5 Discussion and improvements to the model

In contrast with most of the mathematical studies introduced in 1.3, this model includes the metabolism of vitamin $D_3$ (albeit a simplified representation), as well as its actions on calcium homeostasis. As such, the model could serve to investigate the relative role of PTH and vitamin $D_3$ on calcium renal reabsorption and bone resorption.

However, it does not consider the rapidly exchangeable bone pool of bone, which is a major shortcoming. Experiments performed by Lewin and coworkers [132] have shown that after a 20 min EGTA infusion, calcium returned quickly to its physiological steady-state value, independently of PTH. The role of the rapid pool is precisely to buffer these perturbations. This might explain why our model predicts extremely low values of calcium in case of dietary calcium deprivation (results not shown), which is not realistic.

Additionally, as mentioned in section 3.1.6, the response of PTH to calcium should be asymmetric to fit acute/chronic hypocalcemic perturbations as well as acute/chronic hypercalcemic situations, which was not the case with the function we used above. Moreover, some factors in the regulation of vitamin $D_3$ synthesis and degradation are missing. First, we did not take into consideration the delay needed for PTH to activate 1-$\alpha$-(OH)-ase (CYP27B1), that is, about 4 hours. This feature has not been incorporated in models up to now. From a mathematical point of view, the main challenge is to handle delay-differential equations, which are more complex to numerically solve than classical ordinary differential equations, especially when the system is stiff. Secondly, among a lot of factors, PTH has been shown to repress the activity of CYP24A1 [232, 112].

Finally, one of the most predominant issues is the description of renal calcium reabsorption. Indeed, the model presented above does not accurately represent the role of PTH and vitamin $D_3$ in the kidney. The effects of PTH are considered to be global whereas PTH has been shown to exert opposite effects in the proximal tubule (inhibition), and in the thick ascending limb and distal convoluted tubule (activation). As a result, the model should take into account each part of the nephron, with their contribution to calcium reabsorption (65% in the proximal tubule, 25% in the thick ascending limb and 10% in the distal convoluted tubule). Furthermore, the implications of the recent finding that calcium sensing receptor inhibits calcium reabsorption in the thick ascending limb [134] should be investigated.

# Chapter 4

# A Mathematical Model of Calcium Homeostasis in the Rat

This chapter is taken from the article "accepted for publication" in the American Journal of Physiology: Granjon D, Bonny O, and Edwards A. A Model of Calcium Homeostasis in the Rat. Am J Physiol Renal Physiol, 29 June 2016. DOI: 10.1152/ajprenal.00230.2016.

It describes the full model of calcium homeostasis developed during the thesis. As illustrated in Figure 4.1, this model contains the missing features mentioned in section 3.5: (1) the effects of the calcium sensing receptor on calcium reabsorption in the thick ascending limb; (2) the delayed response of vitamin $D_3$ synthesis to PTH; (3) the contribution of PTH on calcium reabsorption in the proximal tubule; (4) the rapidly exchangeable pool in the bone; (5) and the asymmetry of the PTH response to changes in plasma calcium.

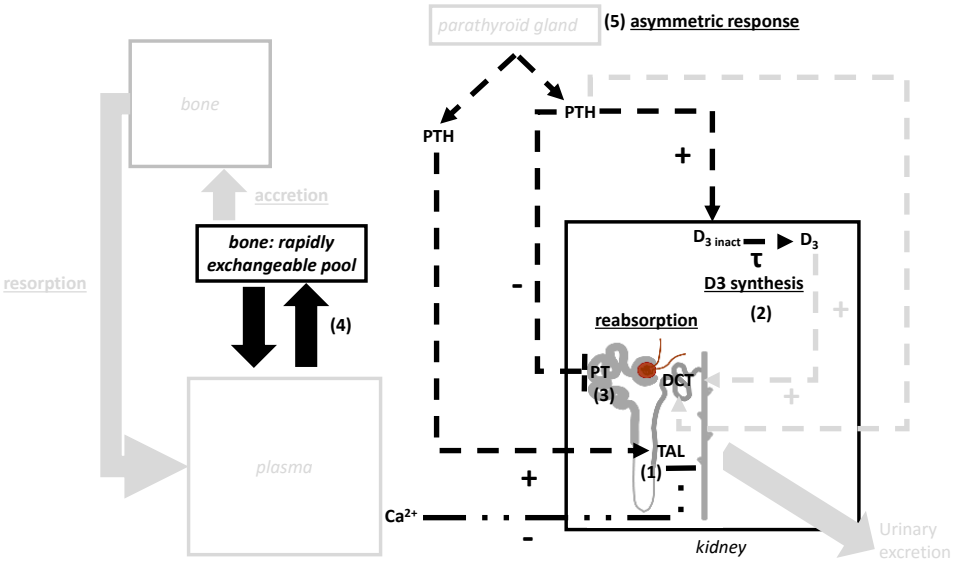


Figure 4.1: New features of the model. The reabsorption of $Ca^{2+}$ in the kidney is significantly more detailed than in the model built in section 3.3.

## 4.1 Introduction

As summarized in Figure 4.2, the mechanisms that regulate plasma $Ca^{2+}$ levels are highly coupled and can be hard to decipher. The major objective of this study was to develop a mathematical model of calcium homeostasis in the rat so as to better understand the impact of dysfunctions (such as primary hyperparathyroidism) on calcium balance and concentration. Several models in humans have been developed [51, 128, 157, 168], however they do not incorporate a number of findings that the present study seeks to account for: the role of the renal CaSR, the delayed response of vitamin $D_3$ synthesis to changes in PTH levels, and the rapidly exchangeable pool in bone (with the exception, for the latter, of the model of Peterson and Riggs [157]).

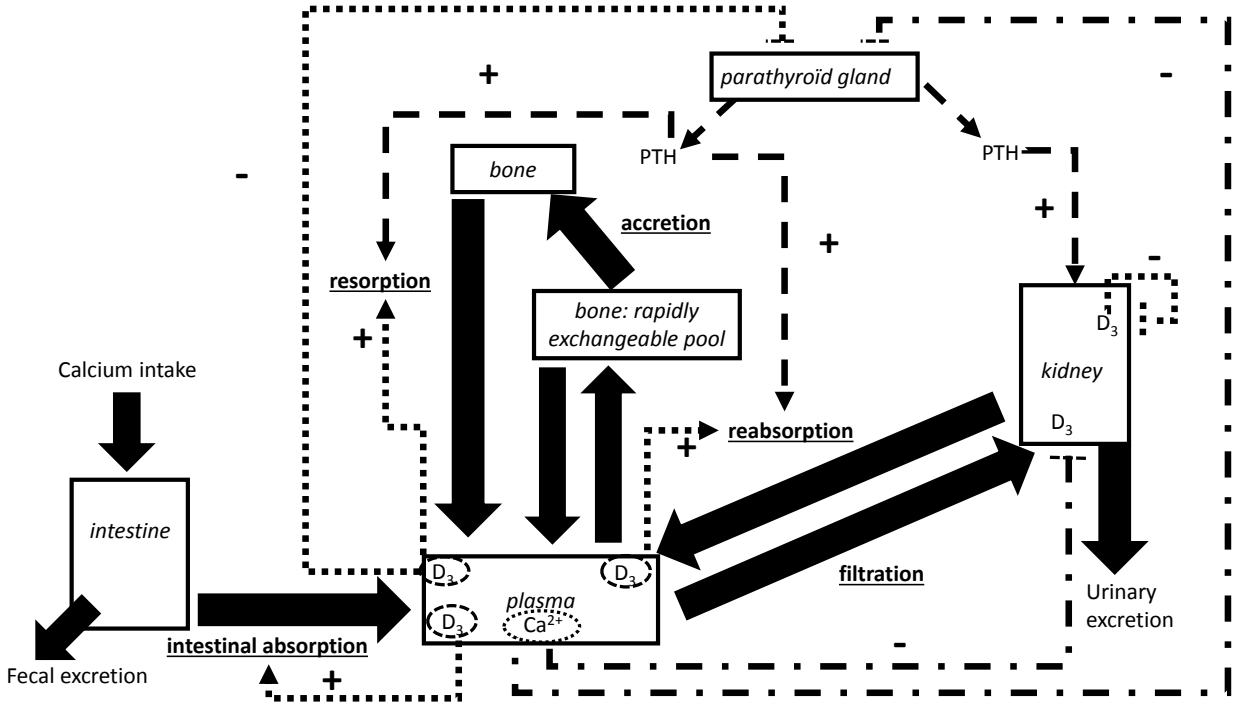


Figure 4.2: Schematic diagram of calcium exchanges between plasma, bone, intestine, and kidney. Calcium fluxes between compartments are depicted with black arrows. Regulation by parathyroid hormone (shown in dashed arrows) acts to enhance bone resorption and renal calcium reabsorption, and to stimulate the conversion of the inactive form of vitamin $D_3$ into its active form. Regulation by vitamin $D_3$ (dotted arrows) acts to increase bone resorption, intestinal calcium absorption, and renal calcium reabsorption; vitamin $D_3$ also represses its own synthesis. In addition, plasma calcium levels regulate PTH secretion via the calcium-sensing receptor (CaSR) and inhibit the synthesis of vitamin $D_3$. CaSR-mediated effects on renal calcium reabsorption are not shown in this figure.

## 4.2 Mathematical Model

Our model of calcium homeostasis is based on conservation equations that yield the plasma concentration of $Ca^{2+}$, PTH, and vitamin $D_3$ in rats, as well as $Ca^{2+}$ fluxes between plasma, bone, intestine, and kidneys. Model parameters apply to a rat weighing about 300 g (i.e.,$\sim$ 2 month old).

### 4.2.1 PTH synthesis and secretion

We recall that changes in $[PTH]_g$ with time are given by:

$$\frac{d[PTH]_g}{dt} = \frac{k_{prod}^{PTHg}}{1+\gamma_{prod}^{D_3}[D_3]_p} - \Big(k_{deg}^{PTH_g} + F([Ca^{2+}]_p)\Big)[PTH]_g \tag{4.1}$$

The first term on the right-hand-side represents the synthesis of PTH modulated by vitamin $D_3$. The exocytosis function is defined as:

$$F([Ca^{2+}]_p) = \beta_{exo}^{PTH_g} - \frac{\gamma_{exo}^{PTH_g}[Ca^{2+}]_p^{n(Ca)}}{[Ca^{2+}]_p^{n(Ca)} + K_{Ca}^{n(Ca)}} \tag{4.2}$$

As discussed in section 3.1.6, to properly account for the effects of both hypercalcemia and hypocalcemia on PTH secretion, it is necessary to use an adaptive $n$, which is calculated as:

$$n(Ca) = \frac{n_1^{exo}}{1+e^{-\rho_{exo}(R-[Ca^{2+}]_p)}} + n_2^{exo} \tag{4.3}$$

$n_1^{exo}$ and $n_2^{exo}$ respectively characterize the sensitivity of the receptor under hypocalcemia and hypercalcemia, $R$ is the threshold between these two states, and $\rho_{exo}$ is an amplification term. When $[Ca^{2+}]_p$ is well below $R$, $n(Ca)$ tends towards high values (>100), as commonly used to fit hypocalcemia profiles [1, 165, 187]. Conversely, when $[Ca^{2+}]_p$ rises above $R$, $n(Ca)$ takes on a lower value. The values of the parameters $n_1^{exo}$, $n_2^{exo}$, $R$ and $\rho_{exo}$ were chosen so as to fit the experimental data of Lewin et al. [132] (see sections 4.2.5 and 4.3.2).

### 4.2.2 Vitamin $D_3$

The dynamic evolution of the plasma concentration of vitamin $D_3$ is now determined as:

$$\frac{d[D_3]_p}{dt} = \left[k_{conv}^{min} + \frac{\delta_{conv}^{max}[PTH(t-\tau)]_p^{n_{conv}}}{\Big([PTH(t-\tau)]_p^{n_{conv}} + K_{conv}^{n_{conv}}\Big)\big(1+\gamma_{conv}^{Ca}[Ca^{2+}]_p\big)\big(1+\gamma_{conv}^{D_3}[D_3]_p\big)}\right][D_3^{inact}]_p - \frac{k_{deg}^{D_3}[D_3]_p}{1+\gamma_{deg}^{PTH_p}[PTH]_p} \tag{4.4}$$

The first term on the right-hand side represents the formation of vitamin $D_3$; it assumes that PTH activates vitamin $D_3$ synthesis with a delay $\tau$ of 4 hours. The second term represents the degradation

rate of vitamin $D_3$ in plasma, which is catalyzed by CYP24A1 and regulated by calcitriol and PTH (among other factors). $\gamma_{deg}^{PTH_g}$ accounts for PTH-induced repression of CYP24A1.

### 4.2.3 Calcium exchanges between organs

#### The intestinal compartment

Experimental findings suggest that at most, 70% of ingested calcium is absorbed into the bloodstream [46], and that two thirds of intestinal calcium transport are modulated by vitamin $D_3$ [34]. The rate of net intestinal calcium absorption is thus determined as:

$$\Gamma_{abs}(D_3) = I_{Ca}\Big(0.25 + \frac{0.45[D_3]_p^2}{[D_3]_p^2 + (K_{abs}^{D_3})^2}\Big) \tag{4.5}$$

Compared to the previous version of this equation (Equation (3.77)), we added an exponent 2 in the term that describes the regulation of absorption by vitamin $D_3$, so as to obtain a more adequate response following vitamin $D_3$ stimulation.

#### The bone compartment

The bone compartment can be divided into a rapidly exchangeable pool and a slowly exchangeable pool as mentioned in sections 1.3.3 and 3.5; the amount of $Ca^{2+}$ they respectively contain is denoted $N_{Ca_f}$ and $N_{Ca_s}$. The rapidly exchangeable (or "fast") pool is thought to mediate the short-term regulation of calcium homeostasis, but it remains poorly characterized [36, 158]. We assume that the amount of $Ca^{2+}$ in the fast pool is given by:

$$\frac{dN_{Ca_f}}{dt} = k_{p-f}^{Ca}[Ca^{2+}]_p V_p - k_{f-p}^{Ca} N_{Ca_f} - \Gamma_{ac} N_{Ca_f} \tag{4.6}$$

The first two terms on the right-hand-side represent the flow of $Ca^{2+}$ from the plasma to the rapidly exchangeable pool and vice-versa, which we assume obey first-order kinetics. Since it remains unclear whether PTH and vitamin $D_3$ act directly on the rapidly exchangeable pool, we assume no such regulation. The last term accounts for $Ca^{2+}$ accretion from the fast to the slow pool, which we also assume to be a first-order process with a rate constant $\Gamma_{ac}$.

The amount of $Ca^{2+}$ in the slow bone pool varies with time as:

$$\frac{dN_{Ca_s}}{dt} = \Gamma_{ac} N_{Ca_f} - \Gamma_{res}(PTH, D_3) \tag{4.7}$$

where the $Ca^{2+}$ resorption rate, $\Gamma_{res}(PTH, D_3)$, is determined as:

$$\Gamma_{res}(PTH, D_3) = \Gamma_{res}^{min} + \delta_{res}^{max}\left(0.2 \times \frac{[PTH]_p^2}{[PTH]_p^2 + (K_{res}^{PTH_p})^2} + 0.8 \times \frac{[D_3]_p^2}{[D_3]_p^2 + (K_{res}^{D_3})^2}\right). \tag{4.8}$$

We assume that resorption is activated by (saturating levels of) PTH and $D_3$ [90, 120], and that

resorption increases 6-fold when stimulation by PTH and vitamin $D_3$ is maximal; that is, $\Gamma_{res}^{min} + \delta_{res}^{max} = 6\Gamma_{res}^{min}$. Additionally, we assume that the relative contribution of PTH and vitamin $D_3$ differs, more specifically that vitamin $D_3$ exerts a greater impact that PTH, as this gives more accurate model predictions (see section 4.3.3).

### The kidney compartment

Our modeling approach for $Ca^{2+}$ reabsorption in the kidney is substantially revised compared to that in Chapter 3, so as to take into account the specificity of each nephron segment. The role of PTH, vitamin $D_3$, and CaSR is precisely characterized in each segment (from the proximal tubule to the distal convoluted tubule), thereby allowing us to investigate the relative contributions of each hormone on calcium reabsorption.

The fraction of calcium that is not bound to plasma proteins is filtered non-selectively in proportion to the glomerular filtration rate (GFR). Most of the filtered load (about 98 %) is then reabsorbed: roughly two thirds across the tight junctions of the proximal tubule, $\sim$ 25% via the paracellular route in the thick ascending limb (TAL), and $\sim$ 10% in distal convoluted (DCT) and connecting (CNT) tubules via transcellular pathways [82]. The contribution and mechanisms of $Ca^{2+}$ transport in the collecting duct remain poorly understood, and are not explicitly considered here.

As in the intestine, we assume that there is no accumulation of calcium in the kidney over time, so that the fractions of the filtered load that are reabsorbed ($\lambda_{reab}$) and excreted ($\lambda_u$) sum to unity. In other words:

$$\lambda_{reab} + \lambda_u = 1 \tag{4.9}$$

$Ca^{2+}$ reabsorption in the kidney (relative to its filtered load) is given by the sum of fractional $Ca^{2+}$ reabsorption in the proximal tubule ($\lambda_{PT}$), the thick ascending limb ($\lambda_{TAL}$), and the DCT-CNT ($\lambda_{DCT}$):

$$\lambda_{reab} = \lambda_{PT} + \lambda_{TAL} + \lambda_{DCT} \tag{4.10}$$

PTH inhibits $Ca^{2+}$ reabsorption in the proximal tubule indirectly: it inhibits the activity of the sodium/proton exchanger NHE3, thereby reducing the entry of $Na^+$ in cells. Since the transport of water follows that of sodium, less water is reabsorbed through cells, which reduces the lumen-to-interstitium calcium concentration gradient; as a consequence, the paracellular reabsorption of calcium is lowered [6, 153]. We assume that $\lambda_{PT}$ is given by:

$$\lambda_{PT} = \lambda_{PT}^0 + \frac{\delta_{PT}^{max}}{1 + \left(\frac{[PTH]_p}{PTH_{ref}}\right)^{n_{PT}}}. \tag{4.11}$$

where $\lambda_{PT}^0$ is taken as 0.60, $\delta_{PT}^{max}$ as 0.05, $PTH_{ref}$ as 15 pM, and $n_{PT}$ as 5. Besides, $\lambda_{TAL}$ is modulated by $Ca^{2+}$ (via CaSR) and PTH, and $\lambda_{DCT}$ by PTH and vitamin $D_3$. In the thick

ascending limb, we assume that:

$$\lambda_{TAL} = \lambda^0_{TAL} + \delta_{TAL}(Ca) + \delta_{TAL}(PTH) \tag{4.12}$$

where

$$\delta_{TAL}(Ca) = \frac{\delta^{max}_{CASR}}{1 + \Big(\frac{[Ca^{2+}]_p}{C^{ref}}\Big)^{n_{TAL}}} \tag{4.13}$$

$$\delta_{TAL}(PTH) = \frac{\delta^{max}_{PTH}[PTH]_p}{[PTH]_p + K^{PTH}_{TAL}} \tag{4.14}$$

The maximum value of $\lambda_{TAL}$ is set to 0.250; $\lambda^0_{TAL}$ is taken as 0.225, $\delta^{max}_{CASR}$ as 0.0175, and $\delta^{max}_{PTH}$ as 0.0075. We assume that $C^{ref}$ equals 1.33 mM and $n_{TAL}$ equals 4, so that the regulation by CaSR is very sensitive to small changes in $Ca^{2+}$ levels. Similarly, fractional $Ca^{2+}$ reabsorption in the DCT-CNT is calculated as:

$$\lambda_{DCT} = \lambda^0_{DCT} + \delta_{DCT}(PTH, D_3) \tag{4.15}$$

where

$$\delta_{DCT}(PTH, D_3) = \delta^{max}_{DCT}\Big(0.8 \times \frac{[PTH]_p}{[PTH]_p + K^{PTH}_{DCT}} + 0.2 \times \frac{[D_3]_p}{[D_3]_p + K^{D_3}_{DCT}}\Big) \tag{4.16}$$

The maximum value of $\lambda_{DCT}$ equals 0.10, with $\lambda^0_{DCT}$ set to 0.08 and $\delta^{max}_{DCT}$ to 0.02. Equation (4.16) assumes that the contribution of PTH is greater than that of vitamin $D_3$ [211].

**The plasma compartment**

Net changes in the total amount of calcium in plasma result from the combined effects of intestinal calcium absorption, $Ca^{2+}$ resorption from the slow bone pool, $Ca^{2+}$ exchanges with the fast pool, and urinary $Ca^{2+}$ excretion, such that:

$$\begin{aligned}\frac{d[Ca^{2+}]_p}{dt} = \frac{(1-\kappa_b)}{V_p}\Big\{&\Gamma_{abs}(D_3) + \Gamma_{res}(PTH, D_3) + k^{Ca}_{f-p}[Ca^{2+}]_f V_f - k^{Ca}_{p-f}[Ca^{2+}]_p V_p \\ &-\lambda_u GFR[Ca^{2+}]_p\Big\}\end{aligned} \tag{4.17}$$

### 4.2.4 Determination of unknown parameters

Similarly to what was done in section 3.2.3, we determine unknown parameters as follows. All affinity constants are initially set to the equilibrium value of the hormone or component they are related to. These affinities, as well as the coefficients $n$ (such as $n_{TAL}$, $n_{PT}$, ...) and the threshold parameters $PTH_{ref}$ and $C_{ref}$ are then chosen so as to fit the experimental data introduced in section 4.3.2.

Parameters in the rapidly exchangeable pool are determined based upon steady state conditions. Indeed, taking Equation 4.6 at steady state yields:

$$k_{f-p}^{Ca} = \frac{1}{N_{Ca_f}^*}\Big(k_{p-f}^{Ca} \times [Ca^{2+}]_p^* \times V_p - \Gamma_{ac} N_{Ca_f}^*\Big), \tag{4.18}$$

Knowing the content of calcium in the rapid pool $N_{Ca_f}$ and fixing $k_{p-f}^{Ca}$, we can determine $k_{f-p}^{Ca}$. Moreover, $k_{f-p}^{Ca} > 0$ so that the term in parenthesis has to be positive:

$$k_{p-f}^{Ca}[Ca^{2+}]_p^* V_p - \Gamma_{ac} N_{Ca_f}^* > 0 \Longleftrightarrow k_{p-f}^{Ca} > \Gamma_{ac} \frac{N_{Ca_f}^*}{[Ca^{2+}]_p^* V_p}, \tag{4.19}$$

This condition is used to select an appropriate value for $k_{p-f}^{Ca}$. With the parameters given in Table 4.3, Eq.(4.19) implies that $k_{p-f}^{Ca} > 0.13$. We set $k_{p-f}^{Ca} = 0.17$ min$^{-1}$, which produces a suitable fit in section 4.3.2 and leads to $k_{f-p}^{Ca} = 2.75 \times 10^{-4}$ min$^{-1}$.

Parameters related to the metabolism of PTH, vitamin $D_3$, and calcium are respectively listed in Tables 4.1, 4.2, and 4.3.

Table 4.1: PTH parameters

| Parameter | Symbol | Value | Reference |
|---|---|---|---|
| $PTH_g$ synthesis rate | $k_{prod}^{PTH_g}$ | 1.8 $\mu$mol.min$^{-1}$ | estimated |
| Inhibition of $PTH_g$ synthesis by vitamin $D_3$ | $\gamma_{prod}^{D_3}$ | $5 \times 10^{-3}$ pM$^{-1}$ | estimated |
| $PTH_g$ degradation rate constant | $k_{deg}^{PTH_g}$ | 0.035 min$^{-1}$ | [1] |
| Maximal secretion rate constant of $PTH_g$ | $\beta_{exo}^{PTH_g}$ | 0.059 min$^{-1}$ | fitted from [81] |
| Maximal inhibition of secretion by $Ca^{2+}$ | $\gamma_{exo}^{PTH_g}$ | 0.057min$^{-1}$ | fitted from [81] |
| Binding of $Ca^{2+}$ to CaSR | $K_{Ca_p^{2+}}$ | 1.16 mM | [81] |
| | $n_1^{exo}$ | 100 | [187] |
| | $n_2^{exo}$ | 15 | [187] |
| | $R$ | 1.1 mM | [187] |
| | $\rho_{exo}$ | $10^6$ mM$^{-1}$ | [187] |
| $PTH_p$ degradation rate constant | $k_{deg}^{PTH_p}$ | 2.2 min$^{-1}$ | [1] |
| Volume of parathyroid glands | $V_c$ | 0.1 $\mu$L | [98] |

$PTH_g$ and $PTH_p$ respectively denote parathyroid hormone in the parathyroid gland and in plasma.

Table 4.2: Vitamin $D_3$ parameters

| Parameter | Symbol | Value | Reference |
|---|---|---|---|
| Minimum production rate constant of vitamin $D_3$ | $k_{conv}^{min}$ | $4.4 \times 10^{-6}$ min$^{-1}$ | [209] |
| Maximal increase in vitamin $D_3$ production rate | $\delta_{conv}^{max}$ | $6.02 \times 10^{-5}$ min$^{-1}$ | [209] |
| Plasma concentration of $D_3^{inact}$ | $[D_3^{inact}]_p$ | 25 nM | [81] |
| Activation of vitamin $D_3$ production by PTH | $K_{conv}$ | 3 pM | estimated |
| PTH sensitivity coefficient | $n_{conv}$ | 6 | estimated |
| Time delay for PTH effects on $D_3^{inact}$ conversion | $\tau$ | 240 min | [125] |
| Inhibition of $D_3$ production by $Ca^{2+}$ | $\gamma_{conv}^{Ca}$ | 0.3 mM$^{-1}$ | estimated |
| Inhibition of vitamin $D_3$ production by itself | $\gamma_{conv}^{D_3}$ | $1.8 \times 10^{-2}$ pM$^{-1}$ | estimated |
| Degradation rate constant of vitamin $D_3$ | $k_{deg}^{D_3}$ | 0.0029 min$^{-1}$ | [12, 64, 111] |
| Inhibition of CYP24A1 by PTH | $\gamma_{deg}^{PTH_p}$ | 0.52 pM$^{-1}$ | estimated |

Table 4.3: $Ca^{2+}$ parameters

| Parameter | Symbol | Value | Reference |
|---|---|---|---|
| Calcium intake | $I_{Ca}$ | 2.2 $\mu$mol.min$^{-1}$ | [55, 134] |
| Stimulation of absorption by $D_3$ | $K_{abs}^{D_3}$ | 100 pM | estimated |
| Rate constant of $Ca^{2+}$ transfer from plasma to fast bone pool | $k_{pf}^{Ca}$ | 0.17 min$^{-1}$ | estimated |
| Rate constant of $Ca^{2+}$ transfer from fast bone pool to plasma | $k_{fp}^{Ca}$ | 2.75 $\times 10^{-4}$ min$^{-1}$ | estimated |
| Initial calcium content in bone | $N_{Ca_b}$ | 105 mmol | measured |
| Initial calcium content in rapidly exchangeable pool | $N_{Ca_f}$ | 1.60 mmol | measured |
| Accretion rate constant | $\Gamma_{ac}$ | 1.0 min$^{-1}$ | [55] |
| Minimal resorption rate | $\Gamma_{res}^{min}$ | 0.142 $\mu$mol.min$^{-1}$ | [55] |
| Maximal resorption rate | $\delta_{res}^{max}$ | 0.950 $\mu$mol.min$^{-1}$ | [55] |
| Stimulation of resorption by $D_3$ | $K_{res}^{D_3}$ | 100 pM | estimated |
| Stimulation of resorption by PTH | $K_{res}^{PTH_p}$ | 1.75 pM | estimated |
| Glomerular filtration rate | $GFR$ | 2 mL.min$^{-1}$ | [231] |
| Minimal fractional reabsorption of $Ca^{2+}$ in the PT | $\lambda_{PT}^{0}$ | 0.60 | [20, 154] |
| Stimulation of $Ca^{2+}$ reabsorption in PT by PTH | $\delta_{PT}^{max}$ | 0.05 | estimated |
| Sensitivity of $Ca^{2+}$ reabsorption in PT to PTH | $PTH_{ref}$ | 15 pM | estimated |
| Minimal fractional reabsorption of $Ca^{2+}$ in the TAL | $\lambda_{TAL}^{0}$ | 0.225 | [20, 154] |
| Stimulation of $Ca^{2+}$ reabsorption in TAL by PTH | $\delta_{PTH}^{max}$ | 0.0075 | estimated |
| Sensitivity of $Ca^{2+}$ reabsorption in TAL to PTH | $K_{TAL}^{PTH_p}$ | 1.2 pM | estimated |
| Stimulation of $Ca^{2+}$ reabsorption in TAL by CaSR | $\delta_{CaSR}^{max}$ | 0.0175 | estimated |
| Sensitivity of $Ca^{2+}$ reabsorption in TAL to $Ca^{2+}$ | $C^{ref}$ | 1.33 mM | estimated |
| Minimal fractional reabsorption of $Ca^{2+}$ in the DCT-CNT | $\lambda_{DCT}^{0}$ | 0.080 | [20, 154] |
| Stimulation of $Ca^{2+}$ reabsorption in the DCT-CNT by PTH and vitamin $D_3$ | $\delta_{DCT}^{max}$ | 0.020 | estimated |
| Sensitivity of $Ca^{2+}$ reabsorption in the DCT-CNT to PTH | $K_{DCT}^{PTH_p}$ | 1.8 pM | estimated |
| Sensitivity of $Ca^{2+}$ reabsorption in the DCT-CNT to vitamin $D_3$ | $K_{DCT}^{D_3}$ | 80 pM | estimated |
| Plasma volume | $V_p$ | 10 mL | [127] |
| Fraction of bound calcium | $\kappa_b$ | 0.4 | [208] |

PT: proximal tubule; TAL: thick ascending limb; DCT: distal convoluted tubule; CNT: connecting tubule. Parameters apply to a 300 g (2 month-old) male rat.

### 4.2.5 Numerical methods

The differential equations were integrated using the MATLAB solver dde23. Simulations were performed on a personal computer with an Intel-based processor. Model adjustement to experimental data was done using the Levenberg-Marquardt algorithm of the MATLAB function lsqnonlin.

## 4.3 Results

### 4.3.1 Experimental Measurements

Most of the variables used for the model were obtained from the literature. However, bone calcium content was measured directly in mice and extrapolated to a 300 g rat as described in Chapter 2. Briefly, the calcium content of the whole mouse skeleton was measured as 6.02 +/- 0.57 mmol per animal (n = 10) with a mean weight of 20 g, or 0.012g/g BW. We extrapolate these data to a 300 g rat, assuming that the ratio of bone calcium to body weight is the same in rats and mice. With this hypothesis, the total amount of calcium in the rat skeleton was estimated as 90 mmol, which is similar to the value of 105 mmol reported by Peterson and Riggs [157]. Based upon this value and

other model parameters, the amount of calcium in the rapidly exchangeable pool was estimated as 1.6 mmol, or 1.5% of the total amount in bone.

### 4.3.2 Model Validation

Predicted values of $Ca^{2+}$, PTH, and vitamin $D_3$ plasma concentrations at steady-state, summarized in Table 4.4, all fall within the experimental range. The plasma concentration of free $Ca^{2+}$ (denoted $[Ca^{2+}]_p$) is predicted as 1.21 mM. Intestinal $Ca^{2+}$ absorption is computed as 1.06 $\mu$mol/min, urinary excretion is 0.047 $\mu$mol/min, and the balance (1.02 $\mu$mol/min) is the net flux of $Ca^{2+}$ into bone (i.e., the difference between accretion and resorption). We also validated our model by comparing the predicted and measured profiles of $[Ca^{2+}]_p$ as a function of time under different scenarios.

Table 4.4: Steady-state values under normal conditions

| | Steady State | range | Source |
|---|---|---|---|
| $[Ca^{2+}]_p$ (mM) | 1.21 | 1.1-1.3 | [24, 33, 168, 211] |
| $[PTH]_p$ (pM) | 1.93 | 1.5-13 | [24, 49, 81, 211] |
| $[D_3]_p$ (pM) | 94.5 | 80-250 | [41, 50, 93] |
| Intestinal $Ca^{2+}$ absorption ($\mu$mol/min) | 1.06 | 0.55-1.22 | [78, 134] |
| Fractional intestinal absorption, $F_{intest}$ (%) | 46.2 | 40-60 | [46] |
| $Ca^{2+}$ accretion ($\mu$mol/min) | 1.50 | | |
| $Ca^{2+}$ resorption ($\mu$mol/min) | 0.48 | | |
| Net $Ca^{2+}$ flux into bone ($\mu$mol/min) | 1.02 | | |
| Urinary $Ca^{2+}$ excretion ($\mu$mol/min) | 0.047 | 0.015-0.054 | [115, 134, 180, 231] |
| Fractional excretion, $\lambda_u$ (%) | 1.95 | 0-2 | [115, 134, 180, 231] |

#### Acutely induced hypocalcemia

Lewin and coworkers infused the chelating agent EGTA into normal and parathyroidectomized rats during two hours [132]. They observed a steep decrease in $[Ca^{2+}]_p$ during the first 20 minutes, followed by a two-phase return to steady state over the next 3 hours. We simulated this experiment by accounting for the reaction between calcium and EGTA in the plasma compartment, as described in the Appendix. As shown in Figure 4.3, the dynamic behavior of $[Ca^{2+}]_p$ (normalized by its initial, pre-injection value) that our model predicts closely matches the experimental data in normal rats.

We also compared model predictions of the plasma concentration of PTH (denoted $[PTH]_p$) with measured values reported in another study. As observed by Fox [81], when EGTA was infused at a exponentially decreasing rate during 2 hours, $[PTH]_p$ exhibited a peak-and-plateau behavior: $[PTH]_p$ reached its peak value in less than 10 minutes, and its plateau value was twice as high as its steady-state value. In section 3.1.5, we were unable to investigate the effect of EGTA on $[Ca^{2+}]_p$ since this section was devoted to the study of PTH secretion, thus calcium did not explicitly appear in a differential equation; this is why we imposed the 0.3 mM drop in plasma calcium concentration

that Fox had observed [81]. In the current model, we introduce two equations to describe the reaction between calcium and EGTA (see section 4.4). As illustrated in Figure 4.3, the predicted and experimental time courses of $[PTH]_p$ are in good agreement.

### Acutely induced hypercalcemia

Finally, we simulated the experiment performed by Bronner and Stein, in which rats received an intravenous calcium gluconate bolus [36]. As shown in Figure 4.3, predicted values of $[Ca^{2+}]_p$ fit the experimental data well in the initial phase, but the model predicts too rapid a return to steady state. Part of this discrepancy may stem from the fact that the rats in these experiments weighed significantly less than our model rats (180 vs. 300 g), such that there must have existed important differences in plasma volume, $[PTH]_p$ and/or calcium bone content between the two populations.

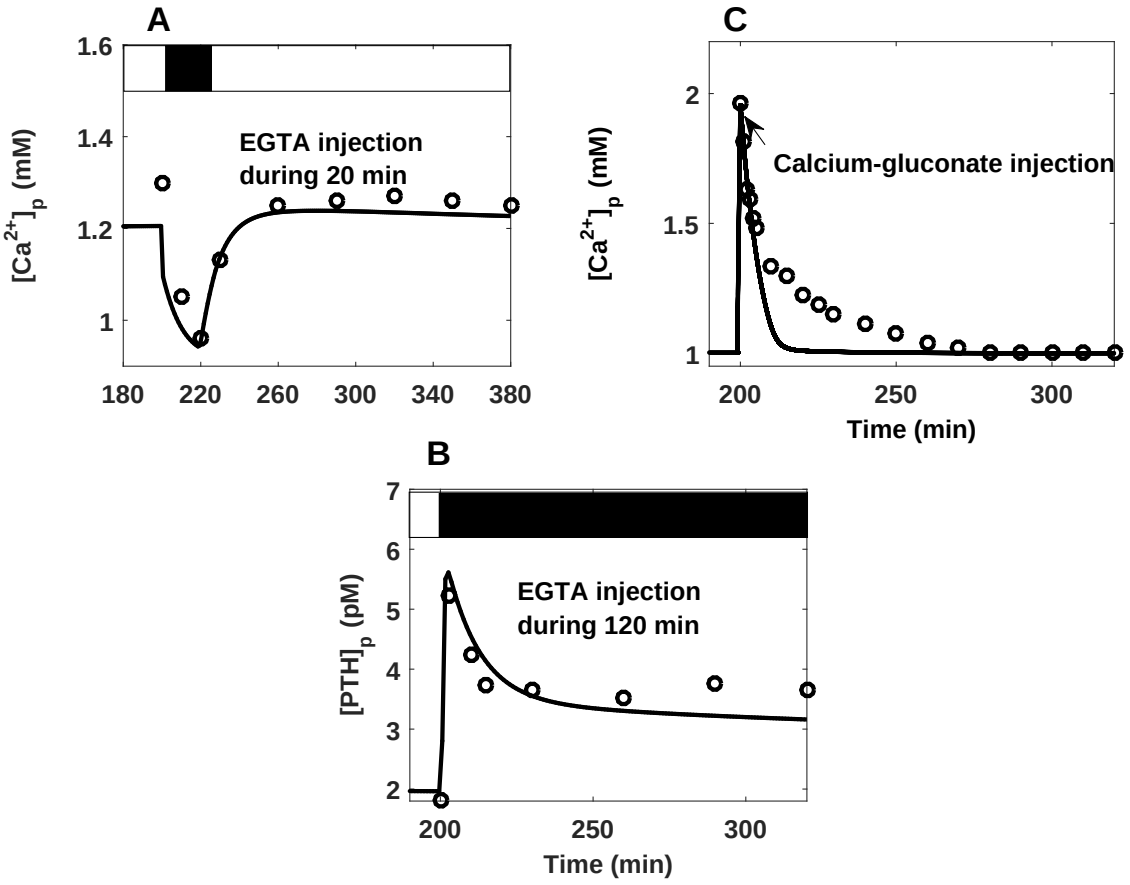


Figure 4.3: Comparison of model results (solid curves) with experimental data (circles). Panel A depicts the $[Ca^{2+}]_p$ profile obtained by Lewin et al. following a 20 minute infusion of EGTA [132]. Panel B represents the plasma concentration of PTH measured by Fox during a 2 hour administration of EGTA [81]. Panel C shows the $[Ca^{2+}]_p$ profile obtained by Bronner and Stein following the rapid intravenous injection of calcium-gluconate [36].

### 4.3.3 Model Predictions

We then used the model to better understand how the plasma concentration of $Ca^{2+}$ is regulated following various metabolic perturbations.

**Primary hyperparathyroidism**

Primary hyperparathyroidism was simulated by increasing the base-case PTH synthesis rate ($k_{prod}^{PTH_g}$) by a factor ranging from 1 to 100. Shown in Figure 4.4 are the predicted steady-state values of $[PTH]_p$, $[Ca^{2+}]_p$, and $[D_3]_p$, as well as intestinal calcium absorption, urinary excretion, resorption, and accretion, as a function of $k_{\text{prod}}^{\text{PTH}_\text{g}}$. The focus of these simulations is not on transient (dynamic) profiles, but on concentrations and fluxes once steady-state is reached.

Our model suggests that $[PTH]_p$ increases approximately linearly with $k_{\text{prod}}^{\text{PTH}_\text{g}}$. Since PTH stimulates bone $Ca^{2+}$ resorption and reabsorption, as well as the synthesis of vitamin $D_3$ (which in turn enhances intestinal calcium absorption), $[Ca^{2+}]_p$ and $[D_3]_p$ rise in parallel with $[PTH]_p$. Given that the effects of PTH on vitamin $D_3$ production and calcium exchanges between compartments are modeled as saturable processes, the rate at which $[Ca^{2+}]_p$ and $[D_3]_p$ increase with PTH synthesis diminishes as $k_{\text{prod}}^{\text{PTH}_\text{g}}$ is elevated beyond 20 times its baseline value.

Note that the rise in $[Ca^{2+}]_p$ leads to a partial, CaSR-mediated inhibition of PTH exocytosis. This, combined with the inhibitory effects of vitamin $D_3$ on PTH synthesis, explains why the rate at which $[PTH]_p$ varies with $k_{\text{prod}}^{\text{PTH}_\text{g}}$ is slow at first; the slope increases once $k_{\text{prod}}^{\text{PTH}_\text{g}}$ reaches 10 times its baseline value (Figure 4.4).

Interestingly, our results suggest that fractional urinary calcium excretion and total urinary calcium excretion ($U_{\text{Ca}}$) may not vary monotonically with $k_{\text{prod}}^{\text{PTH}_\text{g}}$. Indeed, urinary $Ca^{2+}$ excretion is regulated by counterbalancing mechanisms: whereas an increase in vitamin $D_3$ favors enhanced $Ca^{2+}$ reabsorption, increases in $[Ca^{2+}]_p$, via the renal calcium-sensing receptor (CaSR), act instead to inhibit renal calcium reabsorption; moreover, PTH inhibits and stimulates $Ca^{2+}$ transport, respectively, in the proximal tubule and in the distal nephron. Our model predicts that urinary calcium excretion first increases rapidly with increasing $k_{\text{prod}}^{\text{PTH}_\text{g}}$, because CaSR-mediated effects prevail. As $k_{\text{prod}}^{\text{PTH}_\text{g}}$ is elevated above 20 times its baseline value, $[PTH]_p$ increases at a much greater rate than $[Ca^{2+}]_p$ and PTH-mediated effects thus become dominant; given the counteracting effects of PTH along the nephron, $U_{\text{Ca}}$ is predict to decrease slightly before rising steeply (Figure 4.4). It is equal to 2.4 times its base-case value when $k_{\text{prod}}^{\text{PTH}_\text{g}}$ is multiplied by 100, and 4.7 times at its plateau level (Figure 4.5).

These results were obtained assuming a constant GFR. There is evidence that GFR decreases under hypercalcemic conditions; a large enough GFR reduction could abolish the CaSR-induced $U_{\text{Ca}}$ increase. According to our simulations, a 30 % GFR decrease, as reported in Ref. [130], lowers urinary $Ca^{2+}$ excretion below its base-case value if $k_{\text{prod}}^{\text{PTH}_\text{g}}$ is increased by a factor $< 60$ above its baseline value (and PTH levels by a factor $< 4.5$); above that, urinary $Ca^{2+}$ excretion is predicted to be higher than in the base case.

The extent to which PTH modulates $Ca^{2+}$ transport in the proximal tubule remains to be

determined. To evaluate the impact of this uncertainty on model results, we varied the PTH-dependent component of $Ca^{2+}$ reabsorption in the PT (i.e, the parameter $\delta_{PT}^{max}$ in Eq. 4.11) between 0 and 0.10; its baseline value is 0.05. In these simulations, the total percentage of $Ca^{2+}$ reabsorbed by the PT was kept fixed at 65%, and the PTH synthesis rate ($k_{prod}^{PTH_g}$) was increased by a factor ranging from 1 to 300.

In the absence of PTH effects on proximal tubule $Ca^{2+}$ transport (i.e., $\delta_{PT}^{max} = 0$), urinary calcium excretion fluctuates less as $k_{prod}^{PTH_g}$ is varied. As $k_{prod}^{PTH_g}$ is increased above 20 times its baseline value, PTH-mediated stimulation of $Ca^{2+}$ reabsorption in the TAL and DCT/CNT predominates and $U_{\mathrm{Ca}}$ decreases (Figure 4.5). Conversely, when the (inhibitory) effects of PTH in the proximal tubule are enhanced (i.e., $\delta_{PT}^{max} = 0.10$), urinary calcium excretion varies much more significantly with $k_{prod}^{PTH_g}$. Assuming a constant GFR, absolute urinary calcium excretion (which equals 0.047 $\mu$mol/min in the base case) is predicted to reach a maximal value of 0.06 $\mu$mol/min for $\delta_{PT}^{max} = 0$, 0.22 $\mu$mol/min for $\delta_{PT}^{max} = 0.05$, and 0.37 $\mu$mol/min for $\delta_{PT}^{max} = 0.10$ (Figure 4.5). In the remainder of the study, $\delta_{PT}^{max}$ is fixed at 0.05.

Experimental evidence suggests that CaSR and PTH act via independent pathways in the TAL [134]. However, their respective contributions to $Ca^{2+}$ handling in that segment also remains unclear. To probe the impact of this uncertainty, we conducted simulations in which we enhanced the contribution of CaSR relative to that of PTH in the TAL (while keeping the total contribution fixed), and vice-versa. More specifically, we first increased $\delta_{CaSR}^{max}$ from 0.0175 to 0.0200, while decreasing $\delta_{PTH}^{max}$ from 0.0075 to 0.0050 (Eq. 4.12). Conversely, we then raised $\delta_{PTH}^{max}$ from 0.0075 to 0.0200 while reducing $\delta_{CaSR}^{max}$ from 0.0175 to 0.0050.

As expected, when the maximal amplitude of CaSR-mediated inhibition is enhanced and that of PTH-mediated stimulation is reduced as described above, the model predicts that total urinary calcium excretion is higher than with base-case parameters, by about 0.006 $\mu$mol/min at a given value of $k_{prod}^{PTH_g}$ (Figure 4.6). Conversely, when the maximal amplitude of CaSR-mediated inhibition is reduced and that of PTH-mediated stimulation is augmented as described above, $\mathrm{U_{Ca}}$ is about 0.03 $\mu$mol/min lower than with base-case parameters at a given value of $k_{prod}^{PTH_g}$ (Figure 4.6).

Altogether, these results suggest that the extent to which primary hyperparathyroidism affects urinary $Ca^{2+}$ excretion is strongly dependent on the balance between PTH- and CaSR-mediated effects along the nephron. The influence of other factors, such as the hydration status and possible variations in vitamin $D_3$ levels, was not considered here.

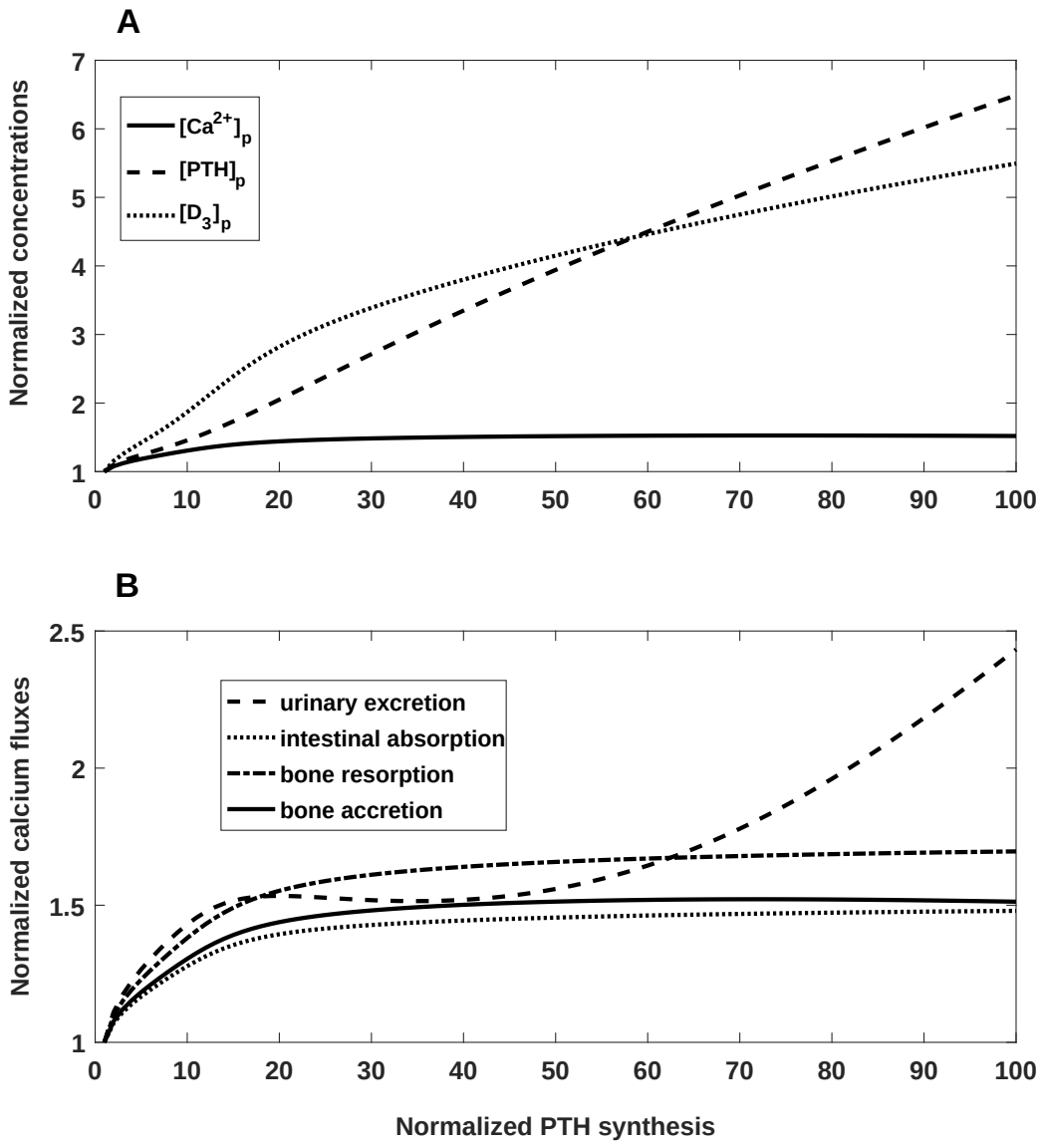


Figure 4.4: Predicted effects of primary hyperparathyroidism on concentrations and fluxes at steady state. Panel A: normalized plasma concentration (relative to base-case value) of $Ca^{2+}$ (solid curve), PTH (dashed curve), and vitamin $D_3$ (dotted curve), as a function of PTH synthesis (normalized by its base-case value). The rate of PTH synthesis ($k_{prod}^{PTH_g}$) is increased by a factor ranging from 1 to 100. Panel B: urinary $Ca^{2+}$ excretion (dashed curve), intestinal calcium absorption (dotted curve), bone accretion (solid curve), and bone resorption (dot-dashed curve), as a function of PTH synthesis (normalized by its base-case value); fluxes are normalized by their base-case value.

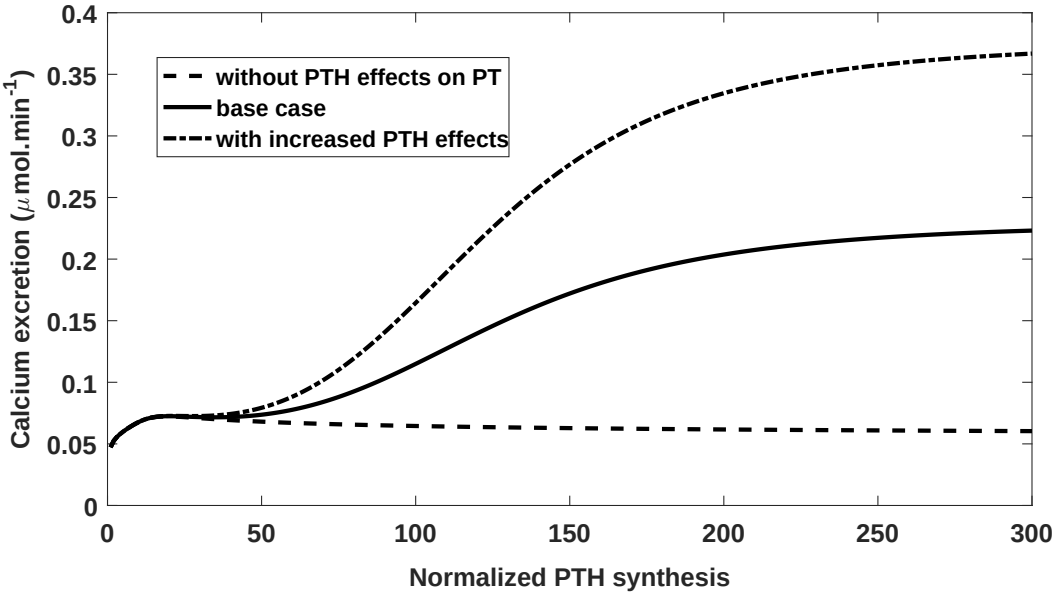


Figure 4.5: Predicted urinary $Ca^{2+}$ excretion as a function of the normalized PTH synthesis rate, depending on the relative contribution of PTH to $Ca^{2+}$ reabsorption in the proximal tubule. The rate of PTH synthesis ($k_{prod}^{PTH_g}$) is increased by a factor ranging from 1 to 300. The parameters $\lambda_{PT}^0$ and $\delta_{PT}^{max}$ are respectively taken as 0.65 and 0 (dashed curve; without PTH effects on proximal tubule reabsorption), 0.60 and 0.05 (solid curve, base-case values), and 0.55 and 0.10 (dot-dashed curve).

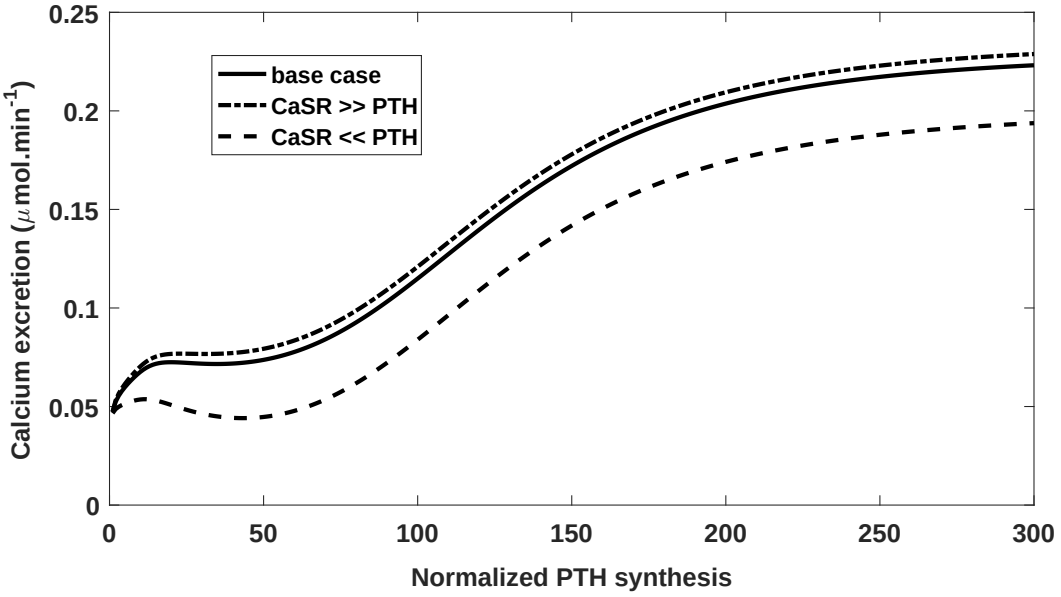


Figure 4.6: Predicted urinary $Ca^{2+}$ excretion as a function of the normalized PTH synthesis rate, depending on the relative contribution of PTH and the renal CaSR to $Ca^{2+}$ reabsorption in the thick ascending limb. The rate of PTH synthesis ($k_{prod}^{PTH_g}$) is increased by a factor ranging from 1 to 300. The parameters $\delta_{CaSR}^{max}$ and $\delta_{PTH}^{max}$ in Eq. 4.13 and Eq. 4.14 are respectively taken as 0.0175 and 0.0075 (solid curve; base-case values), 0.020 and 0.005 (dot-dashed curve), and 0.005 and 0.020 (dotted curve).

**Primary hypoparathyroidism**

We then simulated the opposite scenario, hypoparathyroidism, by decreasing $k_{prod}^{PTH_g}$ from its base-case value to zero. Depicted in Figure 4.7 are the steady-state values of $[PTH]_p$, $[Ca^{2+}]_p$, $[D_3]_p$ as well as $Ca^{2+}$ fluxes between compartments. As shown, the plasma concentration of PTH decreases slowly for small reductions in $k_{prod}^{PTH_g}$, and faster as $k_{prod}^{PTH_g}$ nears zero; indeed, the compensatory effects exerted by vitamin $D_3$ and $Ca^{2+}$ diminish as their own concentration decreases.

In the absence of PTH, $[D_3]_p$ and $[Ca^{2+}]_p$ are respectively 59 % and 41 % lower than in the base case: whereas vitamin $D_3$ synthesis isn't stimulated by PTH any more, it is also less inhibited by calcium under these hypocalcemic conditions. In the absence of PTH, calcium bone resorption is reduced by 55 % (relative to the base case) as a result of the $[PTH]_p$ and $[D_3]_p$ decrease, while calcium bone accretion is reduced by 40 % owing to the $[Ca^{2+}]_p$ decrease. Intestinal absorption is 33 % lower than in the base case.

Urinary $Ca^{2+}$ excretion was computed assuming a constant GFR, as suggested by studies in hypocalcemic dogs [176]. $U_{\mathrm{Ca}}$ is determined by the balance between counteracting effects: whereas the reduced levels of PTH and vitamin $D_3$ act to lower $Ca^{2+}$ reabsorption, lower plasma $Ca^{2+}$ levels decrease the filtered load. As shown in Figure 4.7, the latter effects predominate (i.e., $U_{\mathrm{Ca}}$ decreases) until PTH synthesis is almost fully abolished.

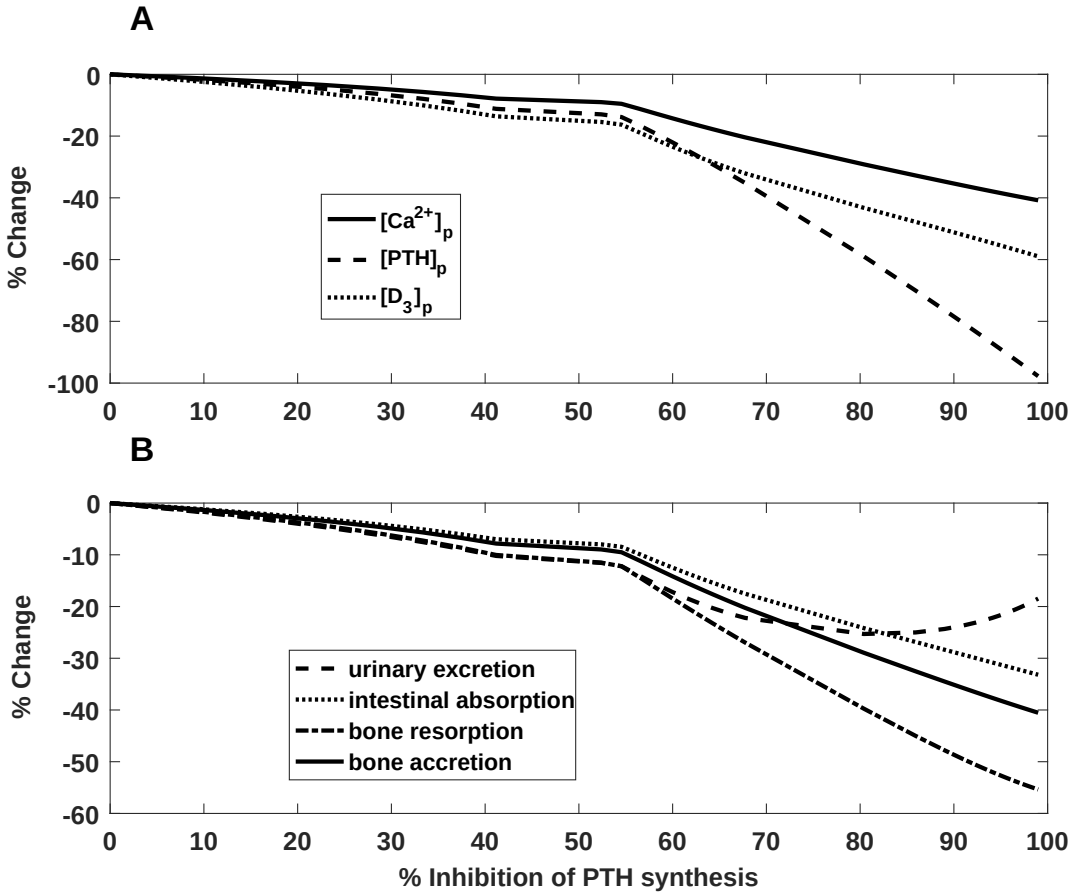


Figure 4.7: Predicted effects of primary hypoparathyroidism on concentrations and fluxes at steady state. Panel A: fractional change in the plasma concentration of $Ca^{2+}$, PTH, and vitamin $D_3$, as a function of the percentage of PTH synthesis inhibition. Panel B: fractional change in urinary $Ca^{2+}$ excretion, intestinal calcium absorption, bone accretion, and bone resorption, as a function of the percentage of PTH synthesis inhibition.

**Vitamin $D_3$ deficiency**

To investigate the effects of vitamin $D_3$ deficiency, we decreased the concentration of its precursor ($[D_3^{inact}]$) by a factor ranging from 1 to 100. In these simulations too, we focused on steady-state profiles. As shown in Figure 4.8, diminishing $[D_3^{inact}]$ reduces the rate of vitamin $D_3$ synthesis, which subsequently decreases the rate of intestinal $Ca^{2+}$ absorption and bone resorption, thereby lowering $[Ca^{2+}]_p$. In parallel, diminishing $[D_3^{inact}]$ reduces the inhibitory effects of vitamin $D_3$ on PTH production, thereby elevating $[PTH]_p$. Together, the $[Ca^{2+}]_p$ decrease and $[PTH]_p$ increase accelerate the conversion of $D_3^{inact}$ to vitamin $D_3$ (i.e., by stimulating 1-$\alpha$(OH)-ase), therefore mitigating the effects of decreasing the concentration of its precursor. Owing to these feedback mechanisms, when $[D_3^{inact}]$ is halved, $[D_3]_p$ is predicted to decrease by 10 % only. Intestinal $Ca^{2+}$ absorption concomitantly decreases from 1.06 to 1.01 $\mu$mol/min.

Relative to its base-case value, $[PTH]_p$ is 28 % higher when $[D_3^{inact}]$ is halved. The increase in PTH levels favors enhanced $Ca^{2+}$ reabsorption along the nephron, but the $[D_3]_p$ decrease acts in the opposite direction. The net result is a decrease in fractional $Ca^{2+}$ excretion (from 1.95 to 1.75 %), i.e., an increase in fractional reabsorption. Note that since the filtered load of $Ca^{2+}$ is lower, absolute $Ca^{2+}$ reabsorption is nevertheless slightly reduced (from 2.37 to 2.28 $\mu$mol/min).

Similarly, the $[PTH]_p$ increase stimulates $Ca^{2+}$ resorption whereas the $[D_3]_p$ decrease has opposite effects. There is near compensation; i.e., bone resorption diminishes slightly, from 0.48 (base case) to 0.47 $\mu$mol/min when $[D_3^{inact}]$ is halved. The overall effect of the reduction in calcium absorption, resorption, and urinary excretion is a 4 % decrease in $[Ca^{2+}]_p$ (from 1.21 to 1.16 mM).

As $[D_3^{inact}]$ is decreased by more than a factor of 10, vitamin $D_3$ concentrations are predicted to fall more rapidly: the counterbalancing effects of $Ca^{2+}$ and PTH on its conversion by 1-$\alpha$(OH)-ase (see above) are less potent at very low $[D_3^{inact}]$ values. Concomitantly, intestinal calcium absorption, bone resorption, and urinary $Ca^{2+}$ excretion decrease more rapidly, and variations in $[Ca^{2+}]_p$ and $[PTH]_p$ with $[D_3^{inact}]$ become more significant (Figure 4.8). Since bone accretion decreases at a faster rate than bone resorption, calcium retention diminishes, but it remains positive even under vitamin $D_3$ depletion.

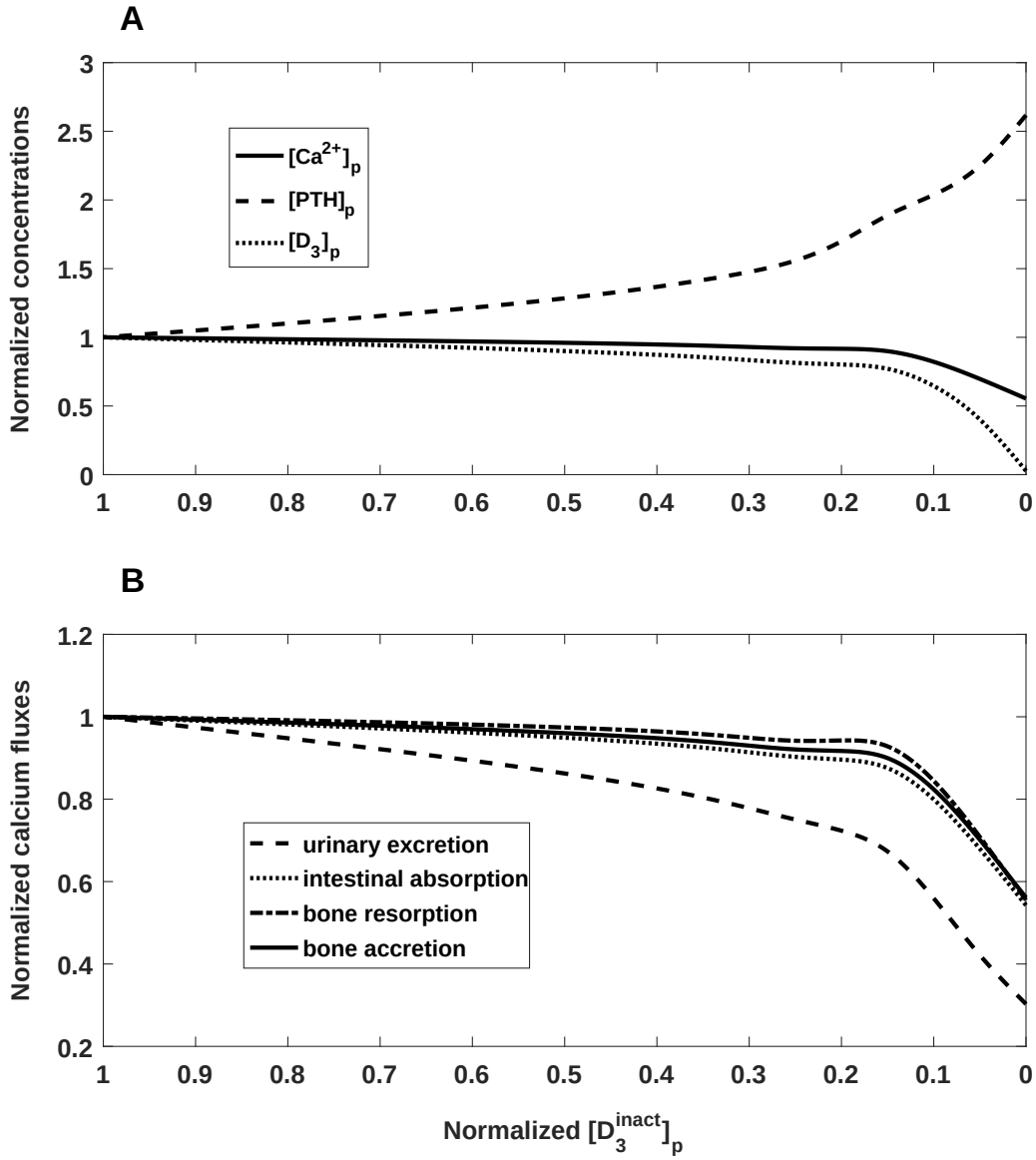


Figure 4.8: Predicted effects of vitamin $D_3$ deficiency on steady-state concentrations and fluxes. Panel A: normalized plasma concentration of $Ca^{2+}$, PTH, and vitamin $D_3$, as a function of $[D_3^{inact}]_p$ (normalized by its base-case value). Panel B: normalized urinary $Ca^{2+}$ excretion, intestinal calcium absorption, bone accretion, and bone resorption, as a function of $[D_3^{inact}]_p$ (normalized by its base-case value).

### CYP24A1 inhibition

To mimic the effects of an inactivating CYP24A1 mutation, we set the degradation rate constant $k_{deg}^{D_3}$ to zero. The model then predicts an 8-fold increase in $[D_3]_p$, a 95 % reduction in $[PTH]_p$ (since vitamin $D_3$ inhibits PTH synthesis), and a 44% increase in $[Ca^{2+}]_p$. Calcium intestinal absorption

and calcium bone resorption respectively increase by 49% and 42%. The $[PTH]_p$ reduction, in combination with the increase in the filtered load of $Ca^{2+}$, enhances total calcium excretion by a factor of 2.6. In comparison, in CYP24A1 knock-out mice, $[D_3]_p$ and $[Ca^{2+}]_p$ were respectively increased by a factor of 9 and 2 [197].

**Inhibition of resorption**

Bisphosphonates, which inhibit bone resorption, are used to treat several bone diseases, such as osteoporosis and Paget's disease. To investigate the effects of bisphosphonates on calcium metabolism, we performed simulations in which the maximal resorption rate (the sum of $\Gamma_{res}^{min}$ and $\delta_{res}^{max}$ in Eq. 4.7) was progressively reduced to zero. We first examined the dynamic effects of halving the maximal rate of resorption on the dynamic evolution of plasma $Ca^{2+}$, PTH, and vitamin $D_3$ levels. As depicted in Figure 4.9, diminishing the resorption rate leads to a sudden decrease in $[Ca^{2+}]_p$, which in turn triggers a rapid increase in PTH levels, and parallel reductions in accretion and urinary $Ca^{2+}$ excretion. Since the effects of PTH on vitamin $D_3$ production occur with a time delay (taken as 4 hours in our model), $[D_3]_p$ varies slowly over the first 4 hours. When it starts to rise significantly, intestinal calcium absorption is augmented, which in turn elevates $[Ca^{2+}]_p$ and conversely lowers $[PTH]_p$. Due to these feedback mechanisms, oscillations ensue, but they dampen rapidly. At steady-state, the predicted value of $[Ca^{2+}]_p$ is 5 % lower than its basal value, which is similar to the values reported by Fleisch [78]. The steady-state values of $[PTH]_p$ and $[D_3]_p$ are respectively 17 % and 30% higher than in the base case, which is also comparable to experimental measurements [75].

We then varied the resorption rate over a large range, from its base-case value to zero. Shown in Figure 4.10 are predicted concentrations and fluxes at steady state (i.e., once equilibrium has been reached) as a function of the resorption rate. As described above, inhibiting resorption lowers the plasma level of $Ca^{2+}$, raises that of PTH and vitamin $D_3$, enhances $Ca^{2+}$ absorption, decreases $Ca^{2+}$ accretion, and reduces both absolute and fractional urinary $Ca^{2+}$ excretion.

Our results suggest that the (steady-state) plasma concentration of PTH increases with decreasing resorption, before reaching saturation (Figure 4.10): as $[Ca^{2+}]_p$ decreases, CaSR-mediated inhibition of PTH exocytosis is reduced. Since PTH stimulates the synthesis of vitamin $D_3$ and inhibits its degradation, $[D_3]_p$ increases in parallel with PTH (Figure 4.10). In counterbalance, the increase in vitamin $D_3$ levels lowers the rate of PTH synthesis.

Intestinal calcium absorption, which is stimulated by vitamin $D_3$, increases as the resorption rate is lowered, whereas $Ca^{2+}$ accretion decreases (Figure 4.10). The model predicts that the rate of accretion falls more slowly than that of resorption, so that $Ca^{2+}$ retention increases, as observed experimentally [78, 169]. Urinary $Ca^{2+}$ excretion decreases with the resorption rate, which indicates that the reabsorption-enhancing effects of PTH and vitamin $D_3$ (as a result of PTH and vitamin $D_3$ elevation) are greater than the excretion-enhancing effects of $Ca^{2+}$ (via CaSR).

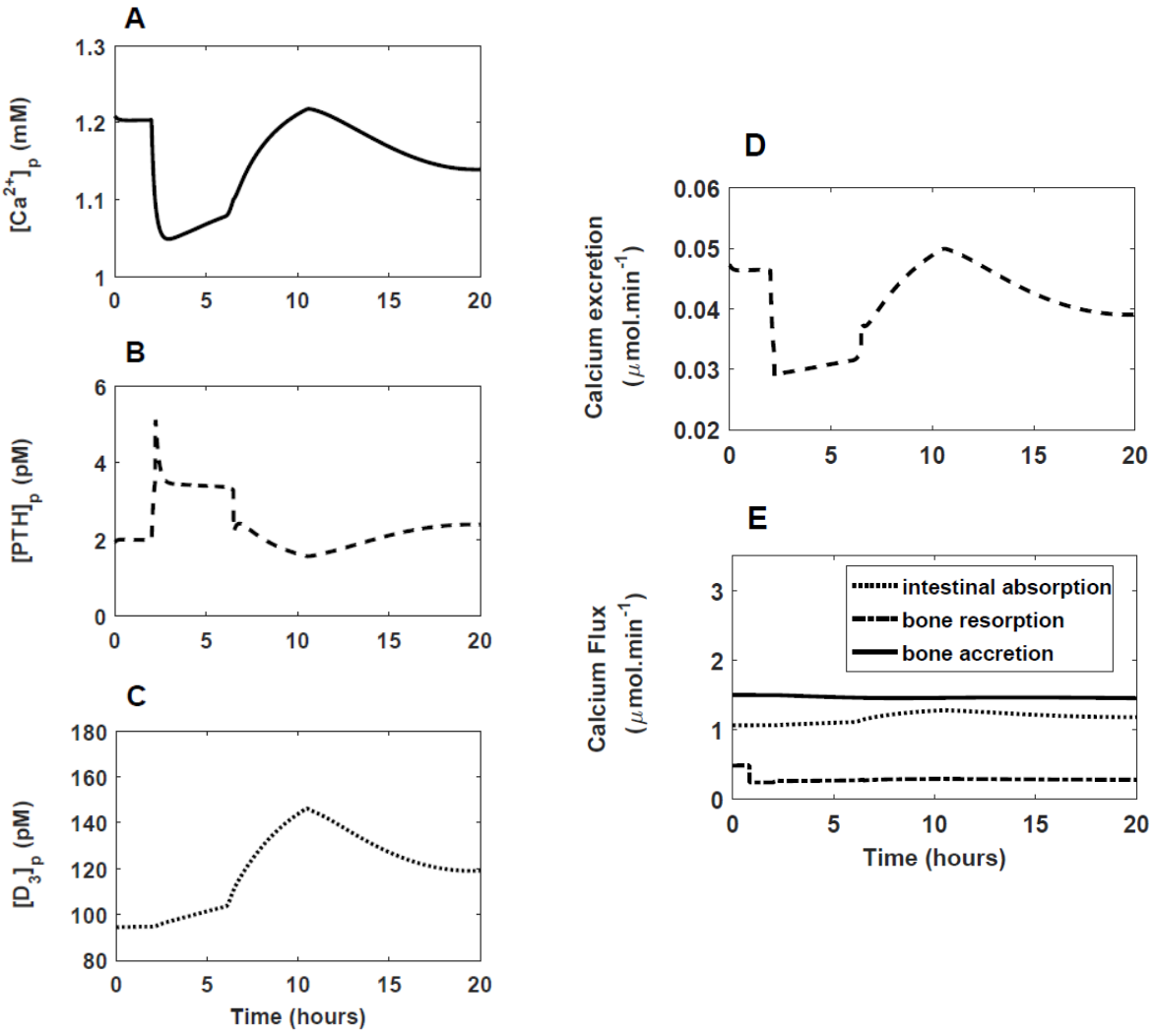


Figure 4.9: Predicted effects of inhibiting bone resorption on the evolution of concentrations and fluxes with time. In this simulation, the maximal bone resorption rate ($\delta_{res}^{max}$) is divided by 2 starting at t = 2 hours. Panels A, B, and C respectively depict the plasma concentration of $Ca^{2+}$, PTH, and vitamin $D_3$, as a function of time; panel D: urinary $Ca^{2+}$ excretion; panel E: intestinal calcium absorption, accretion, and resorption.

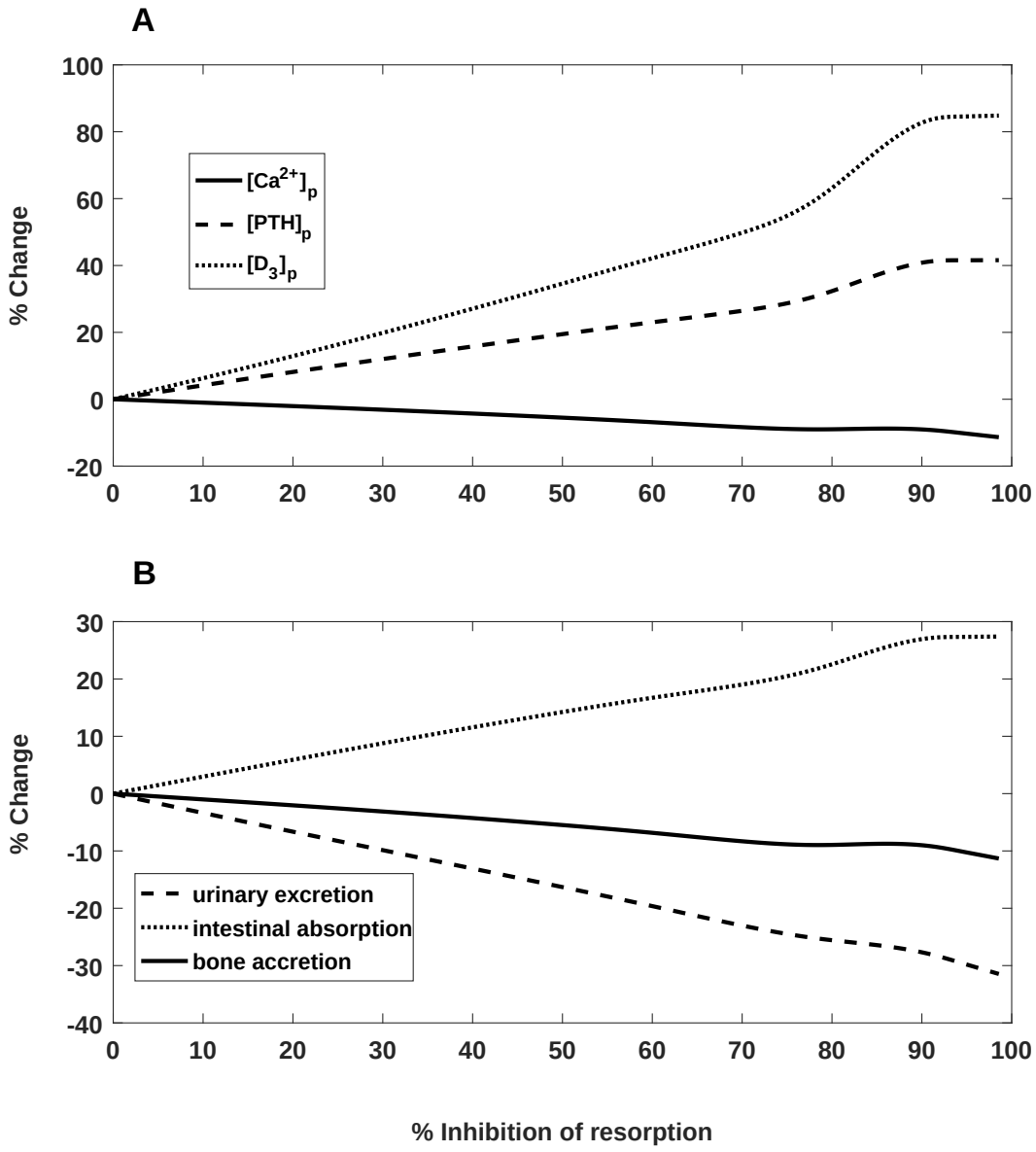


Figure 4.10: Predicted effects of inhibiting bone resorption on steady-state concentrations and fluxes. Panel A: fractional change in the plasma concentration of $Ca^{2+}$, PTH, and vitamin $D_3$, as a function of the percentage of inhibition. Panel B: fractional change in urinary $Ca^{2+}$ excretion, intestinal calcium absorption, bone accretion, and bone resorption, as a function of the percentage of inhibition.

**Cinacalcet treatment**

Cinacalcet, a calcimimetic agent that acts on the calcium sensing receptor by increasing its sensitivity to calcium, is commonly used to treat secondary hyperparathyroidism in chronic renal failure or, more rarely, primary hyperparathyroidism. Cinacalcet decreases PTH exocytosis from parathyroid glands, and decreases $Ca^{2+}$ reabsorption in the TAL [134].

To assess the theoretical impact of Cinacalcet on rats with hyperparathyroidism, we performed the following simulations. To mimic primary hyperparathyroidism, we increased the rate of PTH synthesis by a factor of 185, so that the plasma concentration of PTH is 10-fold its basal value. To mimic the effects of Cinacalcet, we fixed the rate of PTH exocytosis to its minimal value, and maximized the inhibitory effects of CaSR on $Ca^{2+}$ reabsorption in the TAL. As illustrated in Table 4.5, Cinacalcet is predicted to return both $[PTH]_p$ and $[D_3]_p$ in rats with hyperparathyroidism to their levels in control animals; the plasma calcium concentration is thus rescued, i.e., its predicted value (1.24 mM) falls within the normal range. The rates of calcium exchanges between compartments are also very close to their base-case values (i.e., without primary hyperparathyroidism).

Table 4.5: Effects of Cinacalcet administration to rats with primary hyperparathyroidism

| | Control | PHPT | PHPT with Cinacalcet |
|---|---|---|---|
| $[Ca^{2+}]_p$ (mM) | 1.21 | 1.79 | 1.24 |
| $[PTH]_p$ (pM) | 1.93 | 19.5 | 2.01 |
| $[D_3]_p$ (pM) | 94.6 | 665.5 | 100.4 |
| Intestinal $Ca^{2+}$ absorption ($\mu$mol/min) | 1.06 | 1.59 | 1.09 |
| $Ca^{2+}$ accretion ($\mu$mol/min) | 1.50 | 2.21 | 1.57 |
| $Ca^{2+}$ resorption ($\mu$mol/min) | 0.48 | 0.83 | 0.51 |
| Net $Ca^{2+}$ flux into bone ($\mu$mol/min) | 1.02 | 1.38 | 1.06 |
| Urinary $Ca^{2+}$ excretion ($\mu$mol/min) | 0.047 | 0.200 | 0.030 |

Primary hyperparathyroidism (PHPT) is simulated by increasing the rate of PTH synthesis ($k_{prod}^{PTH_g}$) by a factor of 185 (so that $[PTH]_p$ is multiplied by 10). In the presence of Cinacalcet, the rate of PTH exocytosis is set to its minimum value (0.00007 $min^{-1}$ vs. 0.0199 in the base case), and the inhibitory effects of CaSR on $Ca^{2+}$ reabsorption in the TAL are maximized ($\delta_{TAL}(Ca)$ from Eq. 4.13 is set to 0.0175, vs 0.010 in the base case).

**Effects of age and sex on calcium homeostasis**

Maintenance of the calcium balance varies between the two sexes; it also evolves with age. In particular, the plasma concentration of vitamin $D_3$ is about 50% lower in female rats than in age-matched male rats [150]. Vitamin $D_3$ levels (and intestinal calcium absorption) also decrease with age [223]. Conversely PTH levels increase with age, but do not vary significantly between age-matched female and male rats [81, 96, 150]. Bone turnover is also widely affected by aging [30, 67]. Despite these differences, plasma calcium concentration varies very little as a function of either age or sex, under physiological conditions.

We used the model to examine how $[Ca^{2+}]_p$ can remain stable given these documented variations in hormonal levels. We considered 2- and 8-month old, male and female rats, and accounted for differences in PTH and vitamin $D_3$ synthesis, as described above. We also accounted for sex- and age-based differences in plasma volume ($V_p$), glomerular filtration rate ($GFR$), calcium intake ($I_{Ca}$), the sensitivity of intestinal absorption to vitamin $D_3$ ($K_{abs}^{D_3}$), and the rate of bone resorption (i.e., the parameters $\Gamma_{res}^{min}$ and $\delta_{res}^{max}$), as summarized in Table 4.6. The model predicts that to maintain $[Ca^{2+}]_p$ around 1.2 mM in all 4 rat groups, it is also necessary to posit sex- and age-based differences in the rate of calcium exchanges between plasma and the rapidly exchangeable bone pool (i.e., $k_{fp}^{Ca}$ and $k_{pf}^{Ca}$), as also suggested by one study [27]. However, other model parameters need not change (Table 4.6).

Intestinal absorption is predicted to be halved in 2-month old female rats compared to young male rats, mainly because vitamin $D_3$ levels are 50% lower in females. Bone resorption follows the same trend. Bone accretion is decreased in females because they have less calcium in the rapidly exchangeable bone pool than males. This results in a lower bone turnover in females and a net calcium flux into the deep bone that is halved, which is observed during menopause, due to the lack of estrogens. Urinary calcium excretion is predicted to be reduced in females, as a result of the lower GFR, even though fractional calcium excretion is higher in females (owing to lower levels of vitamin $D_3$). In 8-month old animals, the intestinal absorption and bone accretion of calcium are substantially reduced ($\sim$ -50% in both sexes) [30, 67, 223]. Given that PTH levels increase with age [81, 96, 150], urinary calcium excretion is predicted to be lower (-15% and -17%, respectively, in 8-month old male and female rats).

Table 4.6: Predicted impact of age and sex on calcium homeostasis

| | 2 months old | | 8 months old | | Source |
|---|---|---|---|---|---|
| | male | female | male | female | |
| Body weight (g) | 300 | 150 | 400 | 200 | [150] |
| Plasma volume (mL) | 10 | 5 | 15 | 7.5 | [127] |
| GFR (mL.min$^{-1}$) | 2 | 1 | 2 | 1 | [127] and [76] |
| $\beta_{exo}^{PTH_g}$ (min$^{-1}$) | 0.059 | 0.018 | 0.25 | 0.063 | |
| $\gamma_{exo}^{PTH_g}$ (min$^{-1}$) | 0.057 | 0.017 | 0.057 | 0.057 | |
| $k_{conv}^{min}$ (min$^{-1}$) | 4.4× $10^{-6}$ | 2.2× $10^{-6}$ | 2.64× $10^{-7}$ | 1.10× $10^{-7}$ | |
| $\delta_{conv}^{max}$ (min$^{-1}$) | 6.02× $10^{-5}$ | 3.01× $10^{-5}$ | 3.61× $10^{-6}$ | 1.50× $10^{-6}$ | |
| $I_{Ca}$ ($\mu$mol.min$^{-1}$) | 2.3 | 1.5 | 2.0 | 1.0 | |
| $K_{abs}^{D_3}$ (pM) | 100 | 100 | 200 | 200 | [223] |
| $\Gamma_{res}^{min}$ ($\mu$mol.min$^{-1}$) | 0.142 | 0.142 | 0.043 | 0.028 | |
| $\delta_{res}^{max}$ ($\mu$mol.min$^{-1}$) | 0.70 | 0.70 | 0.21 | 0.14 | |
| $k_{pf}^{Ca}$ (min$^{-1}$) | 0.125 | 0.140 | 0.063 | 0.063 | |
| $k_{fp}^{Ca}$ (min$^{-1}$) | $10^{-5}$ | $10^{-5}$ | 8.5×$10^{-4}$ | $10^{-3}$ | |
| $[Ca^{2+}]_p$ (mM) | 1.21 | 1.20 | 1.20 | 1.20 | |
| $[PTH]_p$ (pM) | 1.93 | 1.93 | 3.88 | 4.05 | [150] |
| $[D_3]_p$ (pM) | 94.6 | 51.5 | 40.0 | 20.8 | [150] |
| Intestinal $Ca^{2+}$ absorption ($\mu$mol/min) | 1.06 | 0.52 | 0.53 | 0.25 | |
| Fractional intestinal absorption, $F_{intest}$ (%) | 46.0 | 34.6 | 26.7 | 25.5 | |
| $Ca^{2+}$ accretion ($\mu$mol/min) | 1.5 | 0.83 | 0.60 | 0.29 | |
| $Ca^{2+}$ resorption ($\mu$mol/min) | 0.48 | 0.34 | 0.13 | 0.06 | |
| Net $Ca^{2+}$ flux into bone ($\mu$mol/min) | 1.02 | 0.49 | 0.47 | 0.25 | |
| Urinary $Ca^{2+}$ excretion ($\mu$mol/min) | 0.047 | 0.024 | 0.040 | 0.020 | |
| Fractional excretion, $\lambda_u$ (%) | 1.95 | 2.00 | 1.64 | 1.68 | |

Shown in the upper part of the table are the parameters that we varied as a function of sex and age. Model predictions are given in the lower part of the table.

## 4.4 Discussion

**Scope of model**

We have developed a mathematical model that describes $Ca^{2+}$ exchanges between the intestine, plasma, slowly and rapidly exchangeable bone pools, and the kidneys, as well as their regulation by PTH and vitamin $D_3$. To our knowledge, this is the first such model of $Ca^{2+}$ homeostasis that applies to the rat, accounts for the rapidly exchangeable pool in bone, and considers the impact of the renal CaSR. As shown in Figure 4.3, the model adequately reproduces experimental findings in different scenarios.

**Model limitations**

We should nevertheless acknowledge a number of limitations. Model parameters apply to $\sim$ 300 g rats, a weight at which rats are typically used for physiological experiments but for which experimental calcium measurements are limited. We thus extrapolated measured values of calcium bone content in mice. The model also assumes fixed values for plasma volume and GFR, whereas these may vary in tandem with $Ca^{2+}$ and/or PTH under certain conditions. Taking into consideration the numerous factors that regulate plasma volume and GFR is beyond the scope of this model. Instead, we accounted for observed changes in GFR in specific simulations.

In addition, our model does not consider the interactions between calcium and phosphate, which are particularly relevant in bone. Accounting for this coupling is challenging because the regulation of phosphate homeostasis has not been fully characterized. Fibroblast growth factor 23 (FGF23), a bone-derived hormone that regulates systemic phosphate homeostasis, has recently been recognized as an important component of the bone-parathyroid-kidney axis; in particular, FGF23 inhibits the synthesis of vitamin $D_3$ and the secretion of PTH [19]. Of note, FGF23 may have also a direct effect on calcium transport in the kidney [7]. A better quantitative understanding of phosphate metabolism is needed before it can be added to the model.

Since we do not represent the metabolism of compounds other than $Ca^{2+}$, PTH, and vitamin $D_3$, we cannot account for the allosteric factors that modulate the binding affinity of CaSR to $Ca^{2+}$, such as sodium and ionic strength. Nor can we account for the effects of plasma volume, sodium reabsorption, and thiazides on the fraction of $Ca^{2+}$ that is reabsorbed in the proximal tubule ($\lambda_{PT}$). Similarly, the model does not consider other known regulators of calcium homeostasis, including klotho, calcitonin, and steroids. Sex hormones are also known to regulate calcium homeostasis by modifying calcium absorption in the intestine, calcium bone metabolism, and renal calcium reabsorption. The model does not explicitly represent the mechanisms underlying these regulations and takes into account only some aspects of sex-based differences (body size, calcium intake, as well as PTH and vitamin $D_3$ levels) [65, 105, 152].

Finally, the model is hampered by its description of organs as black boxes, meaning that transport and regulation mechanisms at the molecular and cellular scales are described instead by simplified relationships, such as first-order kinetics and Michaelis-Menten equations. There exist detailed, cellular-based models of calcium homeostasis in the kidney [69] and intestine [73, 99, 191];

these could be integrated in the present mathematical model in the future. Similarly, models of bone remodeling could be incorporated to describe more accurately the dynamics of bone resorption and formation [129, 159].

**PTH-related disorders and $Ca^{2+}$ metabolism**

Our results suggest that the effects of primary hyperparathyroidism (HPTH) on urinary $Ca^{2+}$ excretion (and thus hypercalciuria) depend in part on the degree to which PTH levels are increased. PTH favors the release of $Ca^{2+}$ from bone and therefore enhances its filtered load, but it also stimulates $Ca^{2+}$ reabsorption along the nephron. Moreover, PTH and $Ca^{2+}$ exert opposite effects on $Ca^{2+}$ fluxes in the thick ascending limb. Whereas an increase in PTH stimulates reabsorption therein, increased binding of $Ca^{2+}$ to calcium-sensing receptors expressed by that segment inhibit reabsorption. Thus, our model predicts that whether urinary $Ca^{2+}$ excretion increases or decreases varies according to the balance between PTH and $Ca^{2+}$, i.e., their respective contribution to $Ca^{2+}$ fluxes along the nephron. The inconstant presence of hypercalciuria in primary hyperparathyroidism may also be due to variations in vitamin D levels. Broadus et al. observed a strong positive correlation between plasma levels of vitamin D and calcium excretion in humans with primary hyperparathyroidism [31]. Altogether these results suggest that the high variability of hypercalciuria in primary hyperparathyroidism may be related to differences in PTH-CaSR and/or vitamin D levels.

Patients with hypoparathyroidism are treated with vitamin D supplements that restore their plasma $Ca^{2+}$ levels but promote hypercalciuria, since intestinal calcium reabsorption is stimulated while PTH-enhancing effects on renal $Ca^{2+}$ reabsorption are significantly reduced [220, 221]. It has been suggested that CaSR inhibitors may be used to treat disorders related to impaired PTH secretion [134], and a recent model of $Ca^{2+}$ transport along the nephron suggests that blocking the renal CaSR could significantly reduce urinary $Ca^{2+}$ excretion in the absence of PTH secretion [69]. In the present study, fractional $Ca^{2+}$ reabsorption along the entire nephron equals 88.2 % in parathyroidectomized rats. Inhibition of the renal CaSR would raise that fraction to 92.4 %, without a noticeable impact on $[Ca^{2+}]_p$ or on calcium exchanges between other compartments. However, given that concentration of $Ca^{2+}$ in the tubular fluid increases approximately 10-fold along the collecting duct, a small increase in reabsorption in the TAL can have a significant impact on urinary concentration [69]. The current model does not track tubular and urinary $Ca^{2+}$ concentrations, however.

**Other regulations of $Ca^{2+}$ metabolism**

According to our simulations, when PTH synthesis is raised so that $[PTH]_p$ is doubled, $[Ca^{2+}]_p$ increases by 44%. In contrast, when $[D_3^{inact}]$ is raised so that $[D_3]_p$ is doubled, $[Ca^{2+}]_p$ increases by 26%. However, we cannot conclude that plasma $Ca^{2+}$ levels are more sensitive to changes in PTH levels than in vitamin $D_3$ levels, since raising $[PTH]_p$ stimulates calcitriol production, whereas raising $[D_3]_p$ represses PTH synthesis. Given the combination of both negative and positive

feedback mechanisms, the interactions between $Ca^{2+}$, PTH, and vitamin $D_3$ are highly non-linear, as illustrated in Figures 4.4, 4.6, and 4.8.

We investigated the effects of bisphosphonates on calcium metabolism in rats by lowering the maximal resorption rate over the entire duration of the simulation. Thus our results should be compared with experimental studies in which bisphosphonates were administered to rats chronically. In accordance with these studies, our model predicts that inhibiting resorption reduces plasma $Ca^{2+}$ concentrations and increases $Ca^{2+}$ retention [169]. The model also predicts that the secondary hyperparathyroidism of bisphosphonate treatment reduces urinary $Ca^{2+}$ excretion, as observed by Bushinsky et al. [39]; other studies, however, have found that at high doses, bisphosphonates may raise $U_{\mathrm{Ca}}$, for reasons that remain unclear [169]. It has been suggested that some bisphosphonates may exert direct effects on tubular calcium transport in the kidney [169].

Overall, the effect of vitamin $D_3$ on intestinal calcium absorption is predicted to be limited. In our simulations, primary hyperparathyroidism resulted in only a 1.5-fold increase in intestinal calcium reabsorption despite a 7-fold increase in vitamin $D_3$ levels. During profound vitamin $D_3$ deficiency, however, intestinal calcium absorption decreased significantly. The proposed model for calcium homeostasis takes into account the role of the two CYP450 enzymes involved in the tight control of vitamin $D_3$ metabolism, i.e., CYP27B1 and CYP24A1. The latter enzyme has been shown to be critical for regulating calcemia, as genetic variants lead to hypersensitivity to vitamin $D_3$ supplementation and hypercalcemia. We reproduced here the phenotype induced by decreasing CYP24A1 activity and found that vitamin $D_3$ levels increased 8-fold, plasma calcium by 44%, and calciuria by a factor of 2.6. Overall, the model fits well with observations in infantile hypercalcemia [181].

The model takes into account a pool of calcium that is rapidly available from the bone. This pool was described several decades ago following radiolabeled calcium experiments in vivo [217]. Our model suggests that calcium exchanges between plasma and the rapidly exchangeable pool are 2- to 20-fold greater (depending upon $[Ca^{2+}]_p$) than those between plasma and the slowly exchangeable pool. As currently integrated in the model, the rapid exchange of calcium between plasma and bone plays an important role in both the dynamic evolution and the overall stability of plasma calcium levels.

In summary, this model of calcium homeostasis, which includes two important calcium regulators, i.e., the renal CaSR and the rapidly exchangeable bone calcium pool for which renewed interest has been evinced, shows robustness when challenged. In particular, it predicts that hypercalciuria in primary hyperparathyroidism is dependent upon the ratio of PTH vs. CaSR activity and upon vitamin $D_3$ levels. In primary hypoparathyroidism, urinary calcium excretion is partly sustained, given the absence of PTH-induced stimulation of calcium reabsorption.

# Appendix

In a subset of simulations, we considered the reaction between calcium and the chelator ethylene glycol tetraacetic acid (EGTA):

$$[Ca^{2+}] + [EGTA] \underset{k^-_{\text{EGTA}}}{\overset{k^+_{\text{EGTA}}}{\rightleftharpoons}} [Ca.EGTA] \tag{4.20}$$

The rate of reaction ($R_{\text{EGTA}}$) is given by:

$$R_{\text{EGTA}} = -k^+_{\text{EGTA}}[Ca^{2+}][EGTA] + k^-_{\text{EGTA}}[Ca.EGTA] \tag{4.21}$$

In the presence of EGTA in plasma, the conservation equation of $Ca^{2+}$ in plasma (Eq. (5.47)) is thus written as:

$$\frac{d[Ca^{2+}]_p}{dt}|_{\text{EGTA}} = \frac{(1-\kappa_b)}{V_p}\Big\{\Gamma_{abs}(D_3) + \Gamma_{res}(PTH, D_3) + k^{Ca}_{f-p}[Ca^{2+}]_f V_f \\ -k^{Ca}_{p-f}[Ca^{2+}]_p V_p - \lambda_u GFR[Ca^{2+}]_p\Big\} - R_{\text{EGTA}} \tag{4.22}$$

The kinetic rates $k^+_{\text{EGTA}}$ and $k^-_{\text{EGTA}}$ are respectively taken as $9\times10^4$ $\text{mM}^{-1}\cdot\text{min}^{-1}$ and 18 $\text{min}^{-1}$ [2, 193, 194]. To mimic the protocol used by Lewin et al. [132], we simulated a continuous intravenous injection of EGTA during 20 min using the following differential equations:

$$\frac{d[EGTA]_p}{dt} = \frac{1}{V_p}k^{EGTA}_{inject} + R_{\text{EGTA}} \tag{4.23}$$

$$\frac{d[Ca.EGTA]_p}{dt} = k^+_{\text{EGTA}}[Ca^{2+}]_p[EGTA]_p - k^-_{\text{EGTA}}[Ca.EGTA]_p \tag{4.24}$$

where $k^{EGTA}_{inject}$ is the rate of injection. During the injection, this rate is set to $3\times10^{-4}$ $\text{mmol.min}^{-1}$, as estimated from the concentration of the EGTA solution, the rate of injection, and the total volume injected. Before and after the 20 minute injection, $k^{EGTA}_{inject}$ is set to 0. In addition, immediately prior to injection, the plasma concentrations of EGTA and Ca.EGTA are zero, whereas $[Ca^{2+}]_p$ is equal to its equilibrium value (1.21 mM). To reproduce the $[Ca^{2+}]_p$ profile obtained by Fox and coworkers [81], we used the same equations, but modified the injection rate. During the first 2 minutes, $k^{EGTA}_{inject}$ was set to $1.7\times10^{-3}$ $\text{mmol.min}^{-1}$, yielding the observed 0.3 mM decrease in $[Ca^{2+}]_p$. For the next 118 minutes, during which $[Ca^{2+}]_p$ remained stable, the rate of injection was set to:

$$k^{EGTA}_{inject} = 1.6\times10^{-4}\Big[e^{0.001(t-10)} + e^{0.0025(t-30)}\Big]. \tag{4.25}$$

where time ($t$) is expressed in minutes.

# Chapter 5

# A Model of Calcium and Phosphate Homeostasis in the Rat

As mentioned in section 1.2, the homeostatic regulation of calcium is tightly coupled to that of phosphate. The calcium model we built in Chapters 3 and 4 did not account for phosphate, and the objective of the present chapter is to remedy this omission. A major challenge is that the regulation of phosphate homeostasis has not been characterized as well as that of calcium.

In this chapter, we begin by introducing a new hormone, namely FGF23. Next, we modify the equations that govern vitamin $D_3$ and PTH dynamics to account for the effects of FGF23 and those of phosphate. Additionally, we describe the chemical reactions between calcium and phosphate in both plasma and the rapid bone pool compartment. We then describe the phosphate conservation equations, and make necessary changes in the model of calcium homeostasis; those changes include incorporating explicitly the binding kinetics of calcium with proteins, which we previously did not account for (section 3.2.1). Finally, we validate the combined calcium-phosphate model and perform a set of simulations in line with those of Chapter 4.

## 5.1 Mathematical model

Our model describes calcium and phosphate homeostasis, and is based upon the conservation equations of $Ca^{2+}$, $PO_4$, PTH, vitamin $D_3$ and FGF23. It applies to a rat weighing about 300 g (male, 2 months old). As mentioned in the discussion of Chapter 4, parameters can be adapted to rats of different sex and/or age.

### 5.1.1 Hormone conservation equations

#### FGF23 dynamics

In the following equations, FGF23 is denoted FGF and its corresponding concentration in plasma is $[FGF]_p$. In light of the uncertainties described above, we assume that FGF23 synthesis is directly modulated only by vitamin $D_3$ and phosphate. The conservation of FGF23 is thus expressed as:

$$\frac{d[FGF]_p}{dt} = k_{prod}^{FGF}\Big(1 + G_1([D_3]_p) + G_2([PO_4]_p)\Big) - k_{deg}^{FGF}[FGF]_p. \tag{5.1}$$

The first term on the right-hand-side denotes the amount of FGF23 that has been generated in bone and transported into plasma; the coefficient $k_{prod}^{FGF}$ represents the basal synthesis rate. The second term represents the degradation of FGF23, with a rate constant $k_{deg}^{FGF}$ taken as 0.013 $\text{min}^{-1}$ [229], consistent with its half life of 46-58 minutes [118].

The previous equation assumes that vitamin $D_3$ and phosphate independently modulate the production of FGF23 [184, 179]. More specifically, we make the hypothesis that:

$$G_1([D_3]_p) = \frac{\delta_{prod}^{FGF}[D_3]_p^{n_{prod}^{FGF}}}{(K_{prod}^{D_3})^{n_{prod}^{FGF}} + [D_3]_p^{n_{prod}^{FGF}}}, \tag{5.2}$$

$$G_2([PO_4]_p) = \frac{[PO_4]_p}{K_{prod}^{PO_4} + [PO_4]_p}. \tag{5.3}$$

These equations assume that vitamin $D_3$ can increase the production of FGF23 by, at most, a factor of $\delta_{prod}^{FGF} = 10$, whereas phosphate can increase it by, at most, a factor of 2. Thus, in case of high stimulation by both vitamin $D_3$ and $PO_4$, the FGF23 synthesis rate is multiplied by 12 relative to its basal value. The constants $K_{prod}^{D_3}$ and $K_{prod}^{PO_4}$ are set to the equilibrium values of the plasma concentration of vitamin $D_3$ and phosphate, respectively.

Since we could not find estimates of $k_{prod}^{FGF}$ in the literature, we estimated its value based on steady-state conditions. Additionally, the basal concentration of FGF23 is taken as 15 pM [205].

**Conservation of Vitamin $D_3$**

FGF23 and phosphate both inhibit CYP27B1, whereas FGF23 also activates CYP24A1. The conservation equation for vitamin $D_3$ is therefore rewritten as:

$$\frac{d[D_3]_p}{dt} = \left[k_{conv}^{min} + \frac{\delta_{conv}^{max}[PTH(t-\tau)]_p^{n_{conv}}}{\left([PTH(t-\tau)]_p^{n_{conv}} + K_{conv}^{n_{conv}}\right)} \times \frac{1}{(1+\gamma_{conv}^{Ca}[Ca^{2+}]_p)(1+\gamma_{conv}^{D_3}[D_3]_p)} \times \frac{1}{(1+\gamma_{conv}^{FGF}[FGF]_p)(1+\gamma_{conv}^{PO_4}[PO_4]_p)}\right][D_3^{inact}]_p - \frac{k_{deg}^{D_3}(1+\gamma_{deg}^{FGF}[FGF]_p)[D_3]_p}{1+\gamma_{deg}^{PTH_p}[PTH]_p}, \tag{5.4}$$

The first term within brackets on the right-hand-side represents the basal synthesis rate of vitamin $D_3$. The next term accounts for its activation by PTH and its repression by vitamin $D_3$, $Ca^{2+}$, FGF23 and $PO_4$. We assume that FGF23 and $PO_4$ act independently, with respective sensitivity coefficients $\gamma_{conv}^{FGF}$ and $\gamma_{conv}^{PO_4}$. The last term on the right-hand-side characterizes the degradation of vitamin $D_3$, which is henceforth activated by FGF23 in proportion to $\gamma_{deg}^{FGF}$, in addition to being repressed by PTH, as already included in the model.

### 5.1.2 Conservation equation for PTH

In section 1.2.3, we highlighted the fact that the interactions between FGF23 and PTH remain to be clarified (Figure 1.12). These interactions are not included in the current model, but they could be incorporated at a later stage once more experimental data become available. We account for the effects of phosphate on PTH production as follows:

$$\frac{d[PTH]_g}{dt} = \frac{k_{prod}^{PTHg}\beta_{prod}^{PO_4}[PO_4]^{n_{prod}^{PO_4}}}{(1+\gamma_{prod}^{D_3}[D_3]_p)((K_{prod_{PTH}}^{PO_4})^{n_{prod}^{PO_4}} + [PO_4]^{n_{prod}^{PO_4}})} - \left(k_{deg}^{PTH_g} + F([Ca^{2+}]_p)\right)[PTH]_g, \tag{5.5}$$

The first term on the right-hand-side now includes the activation of PTH synthesis by phosphate. The second term characterizes PTH degradation and exocytosis. The modulation of CaSR or VDR expression by FGF23 is not taken into account as quantitative data are lacking.

Corresponding parameters are listed in Table 5.1, Table 5.2 and Table 5.3.

Table 5.1: PTH parameters

| Parameter | Symbol | Value | Reference |
|---|---|---|---|
| $PTH_g$ synthesis rate | $k_{prod}^{PTH_g}$ | 52.4 $\mu$mol.min$^{-1}$ | estimated |
| Inhibition of $PTH_g$ synthesis by vitamin $D_3$ | $\gamma_{prod}^{D_3}$ | $8.33 \times 10^{-4}$ pM$^{-1}$ | estimated |
| $PTH_g$ degradation rate constant | $k_{deg}^{PTH_g}$ | 0.035 min$^{-1}$ | [1] |
| Maximal secretion rate constant of $PTH_g$ | $\beta_{exo}^{PTH_g}$ | 0.059 min$^{-1}$ | fitted from [81] |
| Maximal inhibition of secretion by $Ca^{2+}$ | $\gamma_{exo}^{PTH_g}$ | 0.057min$^{-1}$ | fitted from [81] |
| Binding of $Ca^{2+}$ to CaSR | $K_{Ca_p^{2+}}$ | 1.16 mM | [81] |
| | $n_1^{exo}$ | 100 | [187] |
| | $n_2^{exo}$ | 15 | [187] |
| | $R$ | 1.1 mM | [187] |
| | $\rho_{exo}$ | 10 mM$^{-1}$ | [187] |
| $PTH_p$ degradation rate constant | $k_{deg}^{PTH_p}$ | 1.3 min$^{-1}$ | [1] |
| Volume of parathyroid glands | $V_c$ | 0.1 $\mu$L | [98] |
| Sensitivity of PTH production to $PO_4$ | $K_{prod}^{PO_4}$ | 2.4 mM | estimated |
| Maximal stimulation of PTH synthesis by $PO_4$ | $\beta_{prod}^{PO_4}$ | 1 | estimated |
| | $n_{prod}^{PO_4}$ | 5 | estimated |

Table 5.2: Vitamin $D_3$ parameters

| Parameter | Symbol | Value | Reference |
|---|---|---|---|
| Minimum production rate constant of vitamin $D_3$ | $k_{conv}^{min}$ | $8.8 \times 10^{-6}$ min$^{-1}$ | [209] |
| Maximal increase in vitamin $D_3$ production rate | $\delta_{conv}^{max}$ | $1.4 \times 10^{-4}$ min$^{-1}$ | [209] |
| Plasma concentration of $D_3^{inact}$ | $[D_3^{inact}]_p$ | 25 nM | [81] |
| Activation of vitamin $D_3$ production by PTH | $K_{conv}$ | 15.7 pM | estimated |
| PTH sensitivity coefficient | $n_{conv}$ | 6 | estimated |
| Time delay for PTH effects on $D_3^{inact}$ conversion | $\tau$ | 240 min | [125] |
| Inhibition of $D_3$ production by $Ca^{2+}$ | $\gamma_{conv}^{Ca}$ | 0.3 mM$^{-1}$ | estimated |
| Inhibition of vitamin $D_3$ production by itself | $\gamma_{conv}^{D_3}$ | $3 \times 10^{-3}$ pM$^{-1}$ | estimated |
| Degradation rate constant of vitamin $D_3$ | $k_{deg}^{D_3}$ | 0.001 min$^{-1}$ | [12, 64, 111] |
| Inhibition of CYP24A1 by PTH | $\gamma_{deg}^{PTH_p}$ | 1 pM$^{-1}$ | estimated |
| Inhibition of $D_3$ production by $PO_4$ | $\gamma_{conv}^{PO_4}$ | 0.2 mM$^{-1}$ | estimated |
| Inhibition of $D_3$ production by FGF23 | $\gamma_{conv}^{FGF}$ | 0.02 pM$^{-1}$ | estimated |
| Activation of CYP24A1 by FGF23 | $\gamma_{deg}^{FGF}$ | 0.13 pM$^{-1}$ | estimated |

Table 5.3: FGF23 parameters

| Parameter | Symbol | Value | Reference |
|---|---|---|---|
| FGF23 synthesis rate | $k_{prod}^{FGF}$ | 8.12 fM.min$^{-1}$ | estimated |
| Modulation of FGF23 synthesis by $D_3$ | $K_{prod}^{D_3}$ | 564 pM | [229] |
| Maximal activation of FGF23 by $D_3$ | $\delta_{prod}^{FGF}$ | 10 | estimated |
| Sensitivity of FGF23 synthesis to $D_3$ | $n_{prod}^{FGF}$ | 5 | estimated |
| Modulation of FGF23 synthesis by $PO_4$ | $K_{prod}^{PO_4}$ | 1.6 mM | [229] |
| FGF23 degradation rate constant | $k_{deg}^{FGF}$ | 0.038 min$^{-1}$ | [229, 118] |

### 5.1.3 Modeling calcium-phosphate binding in plasma and bone

Even though they were never considered previously in models (section 1.3), the mechanisms by which phosphate and calcium bind to each other are crucial to bone formation (formation of hydroxyapatite). They are tightly controlled by inhibitors of aggregation such as Fetuin-A (section 1.2.4). Dysregulations can lead to precipitation beyond the bone compartment that can ultimately generate calcium-phosphate crystals in kidneys or in other organs and widely increase the risk of mortality.

#### Formation of $CaHPO_4$ and $CaH_2PO_4^+$ salts in plasma

The reactions between $Ca^{2+}$ and the two main phosphate components in plasma, $HPO_4^{2-}$ and $H_2PO_4^-$ (see section1.2.4), are:

$$Ca^{2+} + HPO_4^{2-} \underset{k_d^{\mathrm{CaHPO_4}}}{\overset{k_f^{\mathrm{CaHPO_4}}}{\rightleftharpoons}} CaHPO_4.$$

$$Ca^{2+} + H_2PO_4^- \underset{k_d^{\mathrm{CaH_2PO_4^+}}}{\overset{k_f^{\mathrm{CaH_2PO_4^+}}}{\rightleftharpoons}} CaH_2PO_4^+,$$

The equilibrium constants of these reactions are given by:

$$K = \frac{a(CaHPO_4)}{a(Ca^{2+})a(HPO_4^{2-})} = \frac{k_f^{\mathrm{CaHPO_4}}}{k_d^{\mathrm{CaHPO_4}}}. \tag{5.6}$$

$$K = \frac{a(CaH_2PO_4^+)}{a(Ca^{2+})a(H_2PO_4^-)} = \frac{k_f^{\mathrm{CaH_2PO_4+}}}{k_d^{\mathrm{CaHPO_4+}}}. \tag{5.7}$$

where $a(i)$ denotes the activity of ion $i$, i.e., the product of the concentration and activity coefficient of $i$. The equilibrium constants of the first and second reactions (Eq. (5.6) and Eq. (5.7)) are respectively equal to 681 $\mathrm{M}^{-1}$ and 31.9 $\mathrm{M}^{-1}$ at 37°C [135, 213]. Assuming that the plasma concentrations of $\mathrm{Ca}^{2+}$, $\mathrm{H_2PO_4^-}$ and $\mathrm{HPO_4^{2-}}$ (at pH 7.4) are about 1.2, 0.32, 1.28 mM respectively, the plasma concentrations of $\mathrm{CaHPO_4}$ and $\mathrm{CaH_2PO_4^+}$ can be estimated as:

$$[CaHPO_4]_p = 0.681 \times [Ca^{2+}]_p \times f_2 \times [HPO_4^{2-}]_p \times f_2 = 0.11 \text{ mM}.$$

$$[CaH_2PO_4^+]_p = 0.032 \times [Ca^{2+}]_p \times f_2 \times [H_2PO_4^-]_p \times f_1 = 0.003 \text{ mM} = 3 \ \mu\text{M}.$$

Note that it is essential to take into account activity coefficients in the previous calculations [52]. Note too that the concentration of the complex $\mathrm{CaHPO_4}$ is about 10% that of $[Ca^2+]_p$, that is, a non-negligible fraction. In the dynamic model, we do not assume instant equilibrium between these species. Instead, we fix the value of $k_d^{\mathrm{CaHPO_4}}$ and $k_d^{\mathrm{CaH_2PO_4^+}}$ at 100 $\mathrm{s}^{-1}$ (1.7 $\mathrm{min}^{-1}$). With this assumption, we have $k_f^{\mathrm{CaHPO_4^{2-}}} = 1.16$ $\mathrm{mM}^{-1}.\mathrm{min}^{-1}$ and $k_f^{\mathrm{CaHPO_4^{2-}}} = 0.054$ $\mathrm{mM}^{-1}.\mathrm{min}^{-1}$.

### Regulation of bone mineralization by fetuin-A

We assume that the reaction between fetuin-A and either $\mathrm{CaHPO_4}$ or $\mathrm{CaH_2PO_4^+}$ is a first order, irreversible kinetic process. Thus, the dynamic evolution of the plasma concentrations of $\mathrm{CaHPO_4}$ and $\mathrm{CaH_2PO_4^+}$ is given by:

$$\begin{aligned}\frac{d[CaHPO_4]_p}{dt} &= k_f^{\mathrm{CaHPO_4}}[Ca^{2+}]_p[HPO_4^{2-}]_p f_2^2 - k_d^{\mathrm{CaHPO_4}}[CaHPO_4]_p \\ &\quad -k_f^{fetA}[CaHPO_4]_p,\end{aligned} \tag{5.8}$$

$$\begin{aligned}\frac{d[CaH_2PO_4^+]_p}{dt} &= k_f^{\mathrm{CaH_2PO_4^+}}[Ca^{2+}]_p[H_2PO_4^-]_p f_1 f_2 - k_d^{\mathrm{CaH_2PO_4^+}}[CaH_2PO_4^+]_p f_1 \\ &\quad -k_f^{fetA}[CaH_2PO_4^+]_p f_1.\end{aligned} \tag{5.9}$$

In the absence of data, we assume that the rate of reaction between fetuin-A on one hand and either $\mathrm{CaHPO_4}$ or $\mathrm{CaH_2PO_4^+}$ on the other hand is the same. To simplify notations, we define $k_{on}^{\mathrm{CaHPO_4}} = k_f^{\mathrm{CaHPO_4}} f_2^2$ , $k_{off}^{\mathrm{CaH_2PO_4^+}} = k_d^{\mathrm{CaH_2PO_4^+}} f_1$ , $k_{on}^{\mathrm{CaH_2PO_4^+}} = k_f^{\mathrm{CaH_2PO_4^+}} f_1 f_2$, and $k_{on}^{fetA} = k_f^{fetA} f_1$.

Finally, the dynamics of calciprotein particles (CPPs) is governed by the following equation:

$$\frac{d[CPP]_p}{dt} = k_f^{fetA}\Big([CaHPO_4]_p + f_1[CaH_2PO_4^+]_p\Big) - k_c^{CPP}[CPP]_p. \tag{5.10}$$

The first term on the right-hand side accounts for the binding of fetuin to calcium-phosphate complexes. The last term characterizes CPP degradation through the reticuloendothelial system [102] which occurs over several minutes. Thus, the constant $k_c^{CPP}$ is taken equal to 3 $\text{min}^{-1}$ [102].

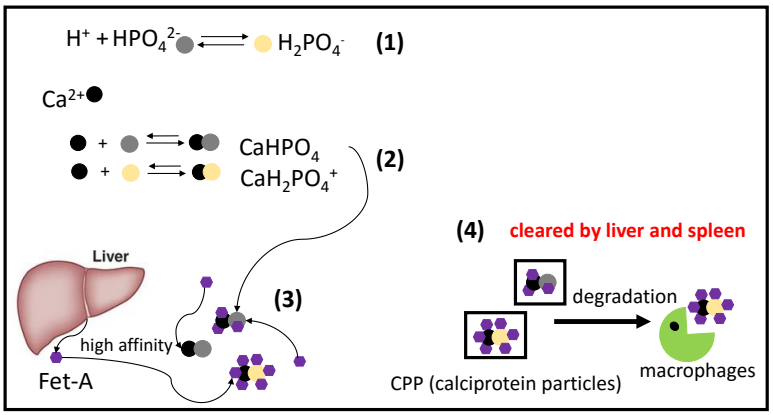


Figure 5.1: Calcium and phosphate complexation mechanisms considered in the model. (1) There are two forms of phosphate in plasma: $HPO_4^{2-}$ and $H_2PO_4^-$. (2) These species can react with calcium ($Ca^{2+}$) to form complexes. (3) Fetuin-A (Fet-A), which is synthetized by the liver, prevents these complexes from aggregating and forming calcium salt crystals. Calciprotein particles (CPP) result from the binding of Fet-A with calcium-phosphate complexes. (4) Finally, CPP are quickly cleared by macrophages.

### Calcium and phosphate in the rapid bone pool

We make the hypothesis that the rapidly exchangeable pool is composed of $Ca^{2+}$, $HPO_4^{2-}$, $H_2PO_4^-$, $CaHPO_4$, as well as $CaH_2PO_4^+$.

The total amount of calcium and phosphate in this pool varies jointly with fluxes between plasma and the rapidly exchangeable pool, the loss due to accretion in the deep bone pool, and complexation reactions, such that:

$$\begin{aligned}\frac{dN_{Ca_f^{2+}}}{dt} &= k_{p-f}^{Ca}[Ca^{2+}]_p V_p - k_{f-p}^{Ca} N_{Ca_f^{2+}} - \Gamma_{ac} N_{Ca_f^{2+}} \\ &- \frac{dN_{CaHPO4_f}}{dt} - \frac{dN_{CaH_2PO4_f^+}}{dt},\end{aligned} \tag{5.11}$$

and

$$\begin{aligned}\frac{dN_{PO_{4_f}}}{dt} &= k_{p-f}^{Pho}[PO_4]_p V_p - k_{p-f}^{Pho} N_{PO_{4_f}} - \Gamma_{ac} N_{PO_{4_f}} \\ &- \frac{dN_{CaHPO4_f}}{dt} - \frac{dN_{CaH_2PO4_f^+}}{dt}.\end{aligned} \tag{5.12}$$

As noted above in section 1.2.4, we define:

$$\begin{aligned}N_{HPO_{4_p^{2-}}} &= aN_{PO_{4_f}}, \\ N_{H_2PO_{4_p^-}} &= bN_{PO_{4_f}},\end{aligned} \tag{5.13}$$

where $a$ and $b$ are:

$$\begin{aligned}a &= \frac{10^{pH-pKa}}{1+10^{pH-pKa}}, \\ b &= \frac{a}{10^{pH-pKa}},\end{aligned} \tag{5.14}$$

which yields $a = 0.8$ and $b = 0.2$ at pH 7.4. Finally, the conservation equations for the two complexes are:

$$\frac{dN_{CaHPO4_f}}{dt} = k_{on}^{CaHPO_4} N_{Ca_f^{2+}} a N_{PO_{4_f}} - k_d N_{CaHPO4_f}, \tag{5.15}$$

and

$$\frac{dN_{CaH_2PO4_f^+}}{dt} = k_{on}^{CaH_2PO_4} N_{Ca_f^{2+}} b N_{PO_{4_f}} - k_{off} N_{CaH_2PO4_f^+}. \tag{5.16}$$

### 5.1.4 Equations for phosphate

Our phosphate homeostasis model is built following the same approach as that used to develop the calcium model. In the following, we denote $PO_4$ the sum of $HPO_4^{2-}$ and $H_2PO_4^-$.

#### Intestinal absorption of phosphate

Assuming no accumulation of phosphate in the intestinal compartment, we have:

$$E_{PO_4} = I_{PO_4} - \Gamma_{abs}^{PO_4}([D_3]_p), \tag{5.17}$$

where $I_{PO_4}$, $\Gamma_{abs}^{PO_4}$, and $E_{PO_4}$ respectively represent phosphate intake, net intestinal phosphate absorption, and fecal phosphate excretion. We assume that vitamin $D_3$ contributes to at most 3/7

$= 43\%$ of $\Gamma_{abs}^{PO_4}$, and that the remaining $4/7 = 57\%$ are unregulated; that is:

$$\Gamma_{abs}^{PO_4}([D_3]_p) = I_{PO_4}\Big(0.4 + \frac{0.3[D_3]_p^{n_{abs}}}{[D_3]^{n_{abs}} + (K_{abs}^{D_3})^{n_{abs}}}\Big). \tag{5.18}$$

Moreover, we consider that $n_{abs}$ and $K_{abs}^{D_3}$ are the same for calcium and phosphate.

### Intracellular phosphate

To our knowledge, the quantity of intracellular phosphate in rats, $N_{PO_{4_c}}$, has not been determined. This parameter is therefore estimated during the model validation phase (see section 5.3.1). Intracellular phosphate can be bound or incorporated into the phospholipids of cell membranes but most of the phosphate is in mitochondria. Besides, there exists a weak outgoing phosphate concentration gradient from the cytosol to plasma [72]. Assuming that phosphate fluxes between plasma and the intracellular compartment obey first-order dynamics, we have:

$$\frac{dN_{PO_{4c}}}{dt} = k_{p-c}[PO_4]_p V_p - k_{c-p} N_{PO_{4_c}}. \tag{5.19}$$

where $k_{p-c}$ characterizes the rate of phosphate transport from plasma to cells and $k_{c-p}$ that from cells to the plasma.

### Hormonal control of phosphate reabsorption in the kidney

The ionized and ion-bound forms of phosphate are freely filtered by the kidney, representing about 90 % of the total plasma phosphate, but this fraction can decrease in case of hypercalcemia probably because of calcium-phosphate fetuin complexes [162]. Approximately 70 to 80 % of the filtered load is reabsorbed in the proximal tubule [203], mostly via the cotransporter NaPi-IIa (or SLC34A1), which accounts for 80% of phosphate reabsorption in that segment. In the absence of phosphate accumulation in the kidney, the sum of fractional reabsorption ($\lambda_{reab}^{PO_4}$) and fractional excretion ($\lambda_u^{PO_4}$) is unity:

$$\lambda_{reab}^{PO_4} + \lambda_u^{PO_4} = 1. \tag{5.20}$$

We assume that phosphate reabsorption occurs essentially in the PT and DCT, such that:

$$\lambda_{reab}^{PO_4} = \lambda_{PT}^{PO_4} + \lambda_{DCT}^{PO_4}. \tag{5.21}$$

In the proximal tubule, phosphate reabsorption is negatively regulated by PTH, FGF23 [114, 184], and high phosphate intake. We therefore rewrite $\lambda_{PT}^{PO_4}$ as:

$$\lambda_{PT}^{PO_4}(PTH_p, FGF_p, PO_{4_p}) = \lambda_{PT}^0 + \delta_{PT}(PTH_p) + \delta_{PT}(FGF_p) + \delta_{PT}(PO_{4_p}) \tag{5.22}$$

where

$$\delta_{PT}(PTH_p) = \frac{\delta_{PTH}^{max}(K_{PT}^{PTH})^{n_{reab}^{PO_4}}}{[PTH]_p^{n_{reab}^{PO_4}} + (K_{PT}^{PTH})^{n_{reab}^{PO_4}}}, \tag{5.23}$$

$$\delta_{PT}(FGF_p) = \frac{\delta_{FGF}^{max}(K_{PT}^{FGF})^{n_{reab}^{PO_4}}}{[FGF]_p^{n_{reab}^{PO_4}} + (K_{PT}^{FGF})^{n_{reab}^{PO_4}}}, \tag{5.24}$$

$$\delta_{PT}(PO_{4_p}) = \frac{\delta_{PO_4}^{max}(K_{PT}^{PO_4})^{n_{reab}^{PO_4}}}{[PO_4]_p^{n_{reab}^{PO_4}} + (K_{PT}^{PO_4})^{n_{reab}^{PO_4}}}. \tag{5.25}$$

We make the following assumptions: $\lambda_{PT}^0$ is fixed at 55%; PTH and $PO_4$ contribute equally to the variable part of phosphate reabsorption in the PT, i.e., $\delta_{PTH}^{max^{PO_4}}$ and $\delta_{PO_4}^{max}$ are each taken as 5%; FGF23 is the main regulator of phosphate transport in the PT, and we assume that its fractional contribution is $\delta_{FGF23}^{max} = 25\%$; the constants $K_{PT}^{PTH}$, $K_{PT}^{FGF}$, and $K_{PT}^{PO_4}$ are given in Table 5.4; $n_{reab}^{PO_4}$ is taken equal to 5; lastly, fractional phosphate reabsorption in the distal tubule ($\lambda_{DCT}^{PO_4}$) is taken to be fixed (10%).

Since the role of vitamin $D_3$ in the regulation of renal phosphate reabsorption remains unclear [85], it is not considered in this model.

### Phosphate in the bone compartment

The bone compartment is divided into a rapidly exchangeable pool and a slowly exchangeable pool. We respectively denote $N_{PO_{4_f}}$ and $N_{PO_{4_b}}$ the amounts of phosphate in these pools. In section 2.4.1, we estimated $N_{PO_{4_b}}$ as about 54 mmol in a 300 g male rat and $N_{PO_{4_f}}$ as about 0.5 mmol. The dynamics of phosphate in the fast pool is described in Eq. (5.12):

$$\begin{aligned}\frac{dN_{PO_{4_f}}}{dt} &= k_{p-f}^{PO_4}[PO_4]_p V_p - k_{f-p}^{PO_4} N_{PO_{4_f}} - \Gamma_{ac}^{PO_4} N_{PO_{4_f}} \\ &\quad - \frac{dN_{CaHPO4_f}}{dt} - \frac{dN_{CaH_2PO4_f^+}}{dt}.\end{aligned} \tag{5.26}$$

The amount of phosphate in the deep bone varies with time as:

$$\frac{dN_{PO_{4_b}}}{dt} = \Gamma_{ac}^{PO_4} N_{PO_{4_f}} - \Gamma_{res}^{PO_4}(PTH, D_3). \tag{5.27}$$

The rates of phosphate accretion ($\Gamma_{ac}^{PO_4}$) and resorption ($\Gamma_{res}^{PO_4}$) are chosen to fit the experimental data of Thomas *et al.* (Thomas *et al.*, JASN, in Press, 2016)(Table 5.6).

### Phosphate binding to $Na^+$

Sodium-phosphate complexes ($NaPO_4$) account for 30% of total plasma phosphate and thus have to be taken into consideration. There are two species: $NaHPO_4^-$ and $NaH_2PO_4$, whose proportion depends on plasma pH. The corresponding reactions are as follows:

$$Na^+ + HPO_4^{2-} \underset{k_d^{NaHPO_4^-}}{\overset{k_f^{NaHPO_4^-}}{\rightleftharpoons}} NaHPO_4^-, \tag{5.28}$$

with the association constant:

$$K_{NaHPO_4^-} = \frac{[NaHPO_4^-]_p}{[Na^+]_p[HPO_4^{2-}]_p} = \frac{k_f^{NaHPO_4^-}}{k_d^{NaHPO_4^-}}.$$

The second reaction is:

$$Na^+ + H_2PO_4^{2-} \underset{k_d^{NaH_2PO_4}}{\overset{k_f^{NaH_2PO_4}}{\rightleftharpoons}} NaH_2PO_4, \tag{5.29}$$

with the association constant:

$$K_{NaH_2PO_4} = \frac{[NaH_2PO_4]_p}{[Na^+]_p[H_2PO_4^-]_p} = \frac{k_f^{NaH_2PO_4}}{k_d^{NaH_2PO_4}}.$$

The equilibrium constants $K_{NaHPO_4^-}$ and $K_{NaH_2PO_4}$ have been measured as, respectively, 4.70 $\times 10^{-3}$ $mM^{-1}$ and 2.94 $\times 10^{-3}$ $mM^{-1}$ [143]. If we assume that $k_d^{NaH_2PO_4}$ and $k_d^{NaHPO_4^-}$ are 1.7 $min^{-1}$, then $k_f^{NaHPO_4^-}$ and $k_f^{NaH_2PO_4}$ are, respectively, 8 $\times 10^{-3}$ $mM^{-1}.min^{-1}$ and 5 $\times 10^{-3}$ $mM^{-1}.min^{-1}$.

In addition, $NaH_2PO_4$ and $NaHPO_4^-$ form an acid/base pair:

$$NaHPO_4^- + H^+ \rightleftharpoons NaH_2PO_4, \tag{5.30}$$

with $pK_A$ equal to 7.2. Thus, the ratio between the two species at pH 7.4 is:

$$\frac{[NaHPO_4^-]_p}{[NaH_2PO_4]_p} = 10^{pH-pkA} \approx 1.6.$$

This means that we have the following proportions:

$$[NaHPO_4^-]_p = c[NaPO_4]_p, \tag{5.31}$$

$$[NaH_2PO_4]_p = d[NaPO_4]_p. \tag{5.32}$$

where $c$ and $d$ depend on pH (similarly to $a$ and $b$ defined in Equation (5.14)), and equal 0.68 and 0.32, respectively, at pH 7.4. The dynamics of $NaPO_4$ complexes is governed by the following equations:

$$\begin{aligned}\frac{d[NaHPO_4^-]_p}{dt} = k_f^{NaHPO_4^-}[Na^+]_p[HPO_4^{2-}]_p - k_d^{NaHPO_4^-}[NaHPO_4^-]_p \\ -k_{on}[NaHPO_4^-][H^+] + k_{off}[NaH_2PO_4],\end{aligned} \tag{5.33}$$

and

$$\begin{aligned}\frac{d[NaH_2PO_4]_p}{dt} = k_f^{NaH_2PO_4}[Na^+]_p[H_2PO_4^-]_p - k_d^{NaH_2PO_4}[NaH_2PO_4]_p \\ +k_{on}[NaHPO_4^-][H^+] - k_{off}[NaH_2PO_4].\end{aligned} \tag{5.34}$$

By summing these equations we obtain:

$$\begin{aligned}\frac{d[NaPO_4]_p}{dt} = (ak_f^{NaHPO_4^-} + bk_f^{NaH_2PO_4})[Na^+]_p[PO_4]_p \\ -(ck_d^{NaHPO_4^-} + dk_d^{NaH_2PO_4})[NaPO_4]_p.\end{aligned} \tag{5.35}$$

To simplify notations, we define $k_f^{NaPO_4} = ak_f^{NaHPO_4^-} + bk_f^{NaH_2PO_4}$ and $k_d^{NaPO_4} = ck_d^{NaHPO_4^-} +$

$dk_d^{NaH_2PO_4}$. Eq. 5.35 is rewritten as:

$$\frac{d[NaPO_4]_p}{dt} = k_f^{NaPO_4}[Na^+]_p[PO_4]_p - k_d^{NaPO_4}[NaPO_4]_p. \tag{5.36}$$

We consider that $[Na^+]_p = 142$ mM [135]. Based on the chosen parameters, the quantity of $NaPO_4$ at equilibrium is:

$$[NaPO_4]_p = \frac{k_f^{NaPO_4}}{k_d^{NaPO_4}}[Na^+]_p[PO_4]_p \approx 1 \text{ mM},$$

which is about 30% of the plasma concentration of total phosphate (see below).

### Phosphate in plasma

The plasma concentration of total phosphate ($[PO_4^{tot}]_p$) is on the order of 3 mM in the rat. As mentioned above, about half of total phosphate is ionized (and present as $HPO_4^{2-}$ and $H_2PO_4^-$); the rest is bound to proteins and other ions such as $Ca^{2+}$, $Na^+$ and $Mg^{2+}$. We assume that $MgHPO_4$ is negligible [216]. In the remainder of this chapter, the term $[Ca:PO_4]$ denotes calcium-phosphate complexes (not including CPPs). Adding Eqs. (5.8) and (5.9) yields:

$$\begin{aligned}\frac{d[Ca:PO_4]}{dt} &= \frac{d[CaHPO_4]_p}{dt} + \frac{d[CaH_2PO_4^+]_p}{dt},\\ &= k_{on}^{\mathrm{CaHPO_4}}[Ca^{2+}]_p a[PO_4]_p - k_d^{\mathrm{CaHPO_4}}[CaHPO_4]_p\\ &\quad -k_f^{fetA}[CaHPO_4]_p + k_{on}^{\mathrm{CaH_2PO_4^+}}[Ca^{2+}]_p b[PO_4]_p\\ &\quad -k_{off}^{\mathrm{CaH_2PO_4^+}}[CaH_2PO_4^+]_p - k_{on}^{fetA}[CaH_2PO_4^+]_p.\end{aligned} \tag{5.37}$$

Thus we write the conservation of total phosphate in plasma as:

$$\begin{aligned}\frac{d[PO_4^{tot}]_p}{dt} &= \frac{d[PO_4]_p}{dt} + \frac{d[Ca:PO_4]}{dt} + \frac{d[NaPO_4]_p}{dt} + \frac{d[CPP]_p}{dt}\\ \iff \frac{d[PO_4]_p}{dt} &= \frac{d[PO_4^{tot}]_p}{dt} - \frac{d[Ca:PO_4]_p}{dt} - \frac{d[NaPO_4]}{dt} - \frac{d[CPP]_p}{dt},\end{aligned} \tag{5.38}$$

The total amount of phosphate in plasma varies according to the phosphate fluxes from plasma to bone ($J_{PO_4}^{pb}$), kidney ($J_{PO_4}^{pk}$), cells ($J_{PO_4}^{pc}$), intestine ($J_{PO_4}^{pi}$) and macrophages such that:

$$\frac{d[PO_4^{tot}]_p}{dt} = \frac{1}{V_p}(-J_{PO_4}^{pi} - J_{PO_4}^{pb} - J_{PO_4}^{pk} - J_{PO_4}^{pc}) - k_c^{CPP}[CPP]_p. \tag{5.39}$$

Combining Eqs. (5.38) and (5.39), macrophages and fetuin terms can be eliminated such that we finally obtain:

$$\begin{aligned}\frac{d[PO_4]_p}{dt} = \frac{1}{V_p}\Bigg\{&\Gamma_{abs}^{Pho}(D_3) - k_{p-f}^{PO_4}[PO_4]_p + k_{f-p}^{PO_4}N_{PO_{4_f}} + \Gamma_{res}^{PO_4}(PTH, D_3)\\ &-\lambda_u^{PO_4}GFR([PO_4]_p + [CaHPO_4]_p + [CaH_2PO_4^+]_p + [NaPO4]_p)\\ &+k_{c-p}N_{PO_{4_c}} - k_{p-c}[PO_4]_pV_p\Bigg\}\\ &-k_f^{NaPO_4}[Na^+]_p[PO_4]_p + k_d^{NaPO_4}[NaPO_4]_p\\ &-k_{on}^{\mathrm{CaHPO_4}}[Ca^{2+}]_pa[PO_4]_p + k_d^{\mathrm{CaHPO_4}}[CaHPO_4]_p\\ &-k_{on}^{\mathrm{CaH_2PO_4^+}}[Ca^{2+}]_pb[PO_4]_p + k_{off}^{\mathrm{CaH_2PO_4^+}}[CaH_2PO_4^+]_p.\end{aligned} \tag{5.40}$$

### 5.1.5 Determination of unknown parameters

With the addition of phosphate, the parameters related to calcium in the rapidly exchangeable pool are re-evaluated, using the same approach as in section 4.2.4, taking Eq. (5.11) at equilibrium. We also use the same method to estimate the rapid pool phosphate parameters, based upon Eq. (5.12):

$$k_{p-f}^{PO_4} > \Gamma_{ac}^{PO_4}\frac{N_{PO_{4_f}}^*}{[PO_4]_p^*V_p}. \tag{5.41}$$

The selected values of $N_{PO_{4_f}}^*$ and $\Gamma_{ac}^{PO_4}$ are given in Table 5.4. By setting $k_{p-f}^{PO_4}$ to 11.25 min$^{-1}$, we obtain $k_{f-p}^{PO_4} = 0.36$ min$^{-1}$. Note that $k_{p-f}^{PO_4}$ is chosen both to satisfy Eq. (5.41) and to fit the experimental data in section 5.3.1.

In order to estimate parameters for the intracellular phosphate, we proceed as for the rapidly exchangeable bone pool of calcium and phosphate. At equilibrium, we have:

$$\frac{dN_{PO_{4_c}}^*}{dt} = 0 \Longleftrightarrow k_{p-c} = \frac{k_{c-p}N_{PO_{4_c}}^*}{[PO_4]_p^*V_p}. \tag{5.42}$$

Setting $k_{c-p} = 0.001$ min$^{-1}$ and $N_{PO_{4_c}}^* = 3$ mmol (which yields the best fit in section 5.3.1), we obtain $k_{p-c} = 0.19$ min$^{-1}$.

Corresponding parameters are listed in Table 5.4.

Table 5.4: Phosphate metabolism parameters

| Organ | Parameter | Symbol | Value | Reference |
|---|---|---|---|---|
| Intestine | Phosphate intake | $I_{PO_4}$ | 2.2 $\mu$mol.min$^{-1}$ | [202] |
| | | $n_{abs}$ | 2 | estimated |
| | Sensitivity of $PO_4$ absorption to $D_3$ | $K_{abs}^{D_3}$ | 640 pM | estimated |
| Kidney | Minimal fractional reabsorption of $PO_4$ in the PT | $\lambda_{PT}^0$ | 0.55 | [162] |
| | Stimulation of $PO_4$ reabsorption in PT by PTH | $\delta_{PTH}^{max}$ | 0.05 | estimated |
| | Sensitivity of $PO_4$ reabsorption in PT to PTH | $K_{PT}^{PTH}$ | 20 pM | estimated |
| | Stimulation of $PO_4$ reabsorption in PT by FGF | $\delta_{FGF}^{max}$ | 0.25 | estimated |
| | Sensitivity of $PO_4$ reabsorption in PT to FGF | $K_{PT}^{FGF}$ | 20 pM | estimated |
| | Stimulation of $PO_4$ reabsorption in PT by $PO_4$ | $\delta_{PO_4}^{max}$ | 0.05 | estimated |
| | Sensitivity of $PO_4$ reabsorption in PT to $PO_4$ | $K_{PT}^{PO_4}$ | 1.6 mM | [229] |
| | Fractional reabsorption of $PO_4$ in the DCT | $\lambda_{DCT}^{PO_4}$ | 0.1 | [162] |
| | | $n_{reab}^{PO_4}$ | 5 | estimated |
| Slow Bone | $PO_4$ accretion rate | $\Gamma_{ac}^{PO_4}$ | 1.2 $\mu$mol.min$^{-1}$ | [157] |
| | Pho resorption rate | $\Gamma_{res}^{PO_4}$ | 0.7 $\Gamma_{res}^{Ca}$ | [157] |
| | Stimulation of resorption by $D_3$ | $K_{res}^{D_3}$ | 600 pM | estimated |
| | Stimulation of resorption by PTH | $K_{res}^{PTH_p}$ | 6.12 pM | estimated |
| Fast Bone | Rate constant of $PO_4$ transfert from plasma to fast bone pool | $k_{p-f}^{PO_4}$ | 11.25 min$^{-1}$ | estimated |
| | Rate constant of $PO_4$ transfert from fast bone pool to plasma | $k_{p-f}^{PO_4}$ | 0.29 min$^{-1}$ | estimated |
| Intracellular Phosphate | Total quantity of $PO_4$ in cells | $N_{PO_{4_c}}$ | 3 mmol | estimated |
| | Rate constant of $PO_4$ transfert from plasma to intracellular pool | $k_{p-c}$ | 0.19 min$^{-1}$ | estimated |
| | Rate constant of $PO_4$ transfert from intracellular pool to plasma | $k_{c-p}$ | 0.001 min$^{-1}$ | estimated |

### 5.1.6 Improvement to the calcium homeostasis model

We previously assumed (see section 3.2.1) that the fraction $\kappa_b$ of calcium bound to proteins such as albumin remained constant. However, this is not accurate since the concentration of both calcium and plasma proteins may vary at any time. Therefore, we refine our model by taking into account the binding of calcium to albumin.

#### Calcium binding to proteins

In plasma, about 50% of calcium is bound to proteins, with albumin being the dominant ligand (46%) [22]. Let $Alb^{2-}$ denote the free calcium binding sites on the albumin molecules and CaAlb the number of bound sites. The binding of calcium to albumin binding can be represented as

follows:

$$Ca^{2+} + Alb^{2-} \underset{k_d^{CaAlb}}{\overset{k_f^{CaAlb}}{\rightleftharpoons}} CaAlb, \tag{5.43}$$

with the association constant:

$$K_A = \frac{[CaAlb]_p}{[Ca^{2+}]_p[Alb^{2-}]_p}.$$

At pH 7.4, $K_A = 0.1$ mM$^{-1}$ and the number of available binding sites $N_{Alb}$ per albumin molecule is equal to 20 [79]; note that $N_{Alb}$ is not very sensitive to small pH variations. We thus have:

$$N_{Alb} \times [Alb^{tot}]_p = [Alb^{2-}]_p + [CaAlb]_p \Longleftrightarrow [Alb^{2-}]_p = N_{Alb} \times [Alb^{tot}]_p - [CaAlb]_p.$$

Assuming that $k_d^{CaAlb} = 1.7$ min$^{-1}$, we have $k_f^{CaAlb} = 0.19$ mM$^{-1}$.min$^{-1}$. The conservation equation for the calcium-albumin complex is:

$$\begin{aligned} \frac{d[CaAlb]_p}{dt} &= k_f^{CaAlb}[Ca^{2+}]_p[Alb^{2-}]_p - k_d^{CaAlb}[CaAlb]_p, \\ &= k_f^{CaAlb}[Ca^{2+}]_p(N_{Alb}[Alb^{tot}]_p - [CaAlb]_p) - k_d^{CaAlb}[CaAlb]_p. \end{aligned} \tag{5.44}$$

We assume that $[Alb^{tot}]_p$ is constant and equal to 0.6 mM. Thus, at equilibrium the concentration of bound sites on albumin molecules is estimated as:

$$[CaAlb]_p \approx K_A[Ca^{2+}]_p[Alb^{tot}]_p N_{Alb} = 1.44 \text{ mM}.$$

### Conservation equation for plasma calcium

As in section 5.1.4, the term $[Ca : PO_4]_p$ denotes calcium-phosphate complexes (not including CPPs), and its derivative is given by Eq. (5.37). Assuming that albumin is the main protein ligand of calcium, the conservation equation for calcium in plasma can be written as:

$$\begin{aligned} \frac{d[Ca^{tot}]_p}{dt} &= \frac{d[Ca^{2+}]_p}{dt} + \frac{d[CaAlb]_p}{dt} + \frac{d[Ca:PO_4]_p}{dt} + \frac{d[CPP]_p}{dt} \\ \Longleftrightarrow \frac{d[Ca^{2+}]_p}{dt} &= \frac{d[Ca^{tot}]_p}{dt} - \frac{d[CaAlb]_p}{dt} - \frac{d[Ca:PO_4]_p}{dt} - \frac{d[CPP]_p}{dt}. \end{aligned} \tag{5.45}$$

As described previously, the total amount of calcium in plasma varies according to the calcium fluxes from plasma to bone ($J_{Ca}^{pb}$), kidney ($J_{Ca}^{pk}$), intestine ($J_{Ca}^{pi}$), and the macrophage compartment

for CPP degradation, such that:

$$\frac{d[Ca^{tot}]_p}{dt} = \frac{1}{V_p}(-J_{Ca}^{pi} - J_{Ca}^{pb} - J_{Ca}^{pk}) - k_c^{CPP}[CPP]_p. \tag{5.46}$$

$J_{Ca}^{pb}$ corresponds to bone resorption and the exchanges between the rapidly exchangeable pool and plasma.

Combining Eqs. (5.45) and (5.46), the terms related to fetuin complexation and macrophage-induced degradation can be eliminated such that we finally obtain:

$$\begin{aligned}\frac{d[Ca^{2+}]_p}{dt} = \frac{1}{V_p}\Bigg\{&\Gamma_{abs}(D_3) + \Gamma_{res}(PTH, D_3) - k_{p-f}^{Ca}[Ca^{2+}]_p V_p + k_{f-p}^{Ca} N_{Ca_f^{2+}} \\ &-\lambda_u GFR([Ca^{2+}]_p + [CaHPO_4]_p + [CaH_2PO_4^+]_p)\Bigg\} \\ &-k_f^{CaAlb}[Ca^{2+}]_p N_{Alb}[Alb^{tot}]_p + k_d^{CaAlb}[CaAlb]_p \\ &-k_{on}^{\mathrm{CaHPO_4}}[Ca^{2+}]_p a[PO_4]_p + k_d^{\mathrm{CaHPO_4}}[CaHPO_4]_p \\ &-k_{on}^{\mathrm{CaH_2PO_4^+}}[Ca^{2+}]_p b[PO_4]_p + k_{off}^{\mathrm{CaH_2PO_4^+}}[CaH_2PO_4^+]_p.\end{aligned} \tag{5.47}$$

The terms weighted by $\frac{1}{V_p}$ refer to external fluxes while the others are associated with reactions within plasma. All new parameters are listed in Table 5.5.

Table 5.5: Calcium metabolism parameters

| Organ | Parameter | Symbol | Value | Reference |
|---|---|---|---|---|
| Intestine | Calcium intake | $I_{Ca}$ | 2.2 $\mu$mol.min$^{-1}$ | [55, 134] |
| | Stimulation of absorption by $D_3$ | $K_{abs}^{D_3}$ | 640 pM | estimated |
| Kidney | Glomerular filtration rate | $GFR$ | 2 mL.min$^{-1}$ | [231] |
| | Minimal fractional reabsorption of $Ca^{2+}$ in the PT | $\lambda_{PT}^{0}$ | 0.64 | [20, 154] |
| | Stimulation of $Ca^{2+}$ reabsorption in PT by PTH | $\delta_{PT}^{max}$ | 0.01 | estimated |
| | Sensitivity of $Ca^{2+}$ reabsorption in PT to PTH | $PTH_{ref}$ | 15 pM | estimated |
| | Minimal fractional reabsorption of $Ca^{2+}$ in the TAL | $\lambda_{TAL}^{0}$ | 0.225 | [20, 154] |
| | Stimulation of $Ca^{2+}$ reabsorption in TAL by PTH | $\delta_{PTH}^{max}$ | 0.0075 | estimated |
| | Sensitivity of $Ca^{2+}$ reabsorption in TAL to PTH | $K_{TAL}^{PTH_p}$ | 4.2 pM | estimated |
| | Stimulation of $Ca^{2+}$ reabsorption in TAL by CaSR | $\delta_{CaSR}^{max}$ | 0.0175 | estimated |
| | Sensitivity of $Ca^{2+}$ reabsorption in TAL to $Ca^{2+}$ | $C^{ref}$ | 1.33 mM | estimated |
| | Minimal fractional reabsorption of $Ca^{2+}$ in the DCT-CNT | $\lambda_{DCT}^{0}$ | 0.090 | [20, 154] |
| | Stimulation of $Ca^{2+}$ reabsorption in the DCT-CNT by PTH and vitamin $D_3$ | $\delta_{DCT}^{max}$ | 0.010 | estimated |
| | Sensitivity of $Ca^{2+}$ reabsorption in the DCT-CNT to PTH | $K_{DCT}^{PTH_p}$ | 6.3 pM | estimated |
| | Sensitivity of $Ca^{2+}$ reabsorption in the DCT-CNT to vitamin $D_3$ | $K_{DCT}^{D_3}$ | 480 pM | estimated |
| Slow Bone | Initial calcium content in bone | $N_{Ca_b}$ | 105 mmol | measured |
| | Accretion rate constant | $\Gamma_{ac}$ | 0.5 min$^{-1}$ | [55] |
| | Minimal resorption rate | $\Gamma_{res}^{min}$ | 0.10 $\mu$mol.min$^{-1}$ | [55] |
| | Maximal resorption rate | $\delta_{res}^{max}$ | 0.30 $\mu$mol.min$^{-1}$ | [55] |
| | Stimulation of resorption by $D_3$ | $K_{res}^{D_3}$ | 600 pM | estimated |
| | Stimulation of resorption by PTH | $K_{res}^{PTH_p}$ | 16.12 pM | estimated |
| Fast Bone | Initial calcium content in rapidly exchangeable pool | $N_{Ca_f}$ | 1.60 mmol | measured |
| | Rate constant of $Ca^{2+}$ transfer from plasma to fast bone pool | $k_{pf}^{Ca}$ | 0.41 min$^{-1}$ | estimated |
| | Rate constant of $Ca^{2+}$ transfer from fast bone pool to plasma | $k_{fp}^{Ca}$ | 2.30 $\times 10^{-3}$ min$^{-1}$ | estimated |
| Other parameters | Plasma volume | $V_p$ | 10 mL | [127] |

Table 5.6: Complexation parameters

| Reaction | Parameter | Symbol | Value | Reference |
|---|---|---|---|---|
| Calcium-albumin | CaAlb formation rate constant | $k_f^{CaAlb}$ | 0.19 $mM^{-1}.min^{-1}$ | [79] |
| | CaAlb dissociation rate constant | $k_d^{CaAlb}$ | 1.7 $min^{-1}$ | estimated |
| | Concentration of albumine in plasma | $[Alb^{tot}]_p$ | 0.6 mM | ? |
| Sodium-phosphate | $NaHPO_4^-$ formation rate constant | $k_f^{NaHPO_4^-}$ | 8× $10^{-3}$ $mM^{-1}.min^{-1}$ | [143] |
| | $NaHPO_4^-$ dissociation rate constant | $k_d^{NaHPO_4^-}$ | 1.7 $min^{-1}$ | estimated |
| | $NaH_2PO_4$ formation rate constant | $k_f^{NaH_2PO_4}$ | 5× $10^{-3}$ $mM^{-1}.min^{-1}$ | [143] |
| | $NaH_2PO_4$ dissociation rate constant | $k_d^{NaH_2PO_4}$ | 1.7 $min^{-1}$ | estimated |
| | Sodium plasma concentration | $[Na^+]_p$ | 142 mM | [135] |
| Calcium-Phosphate precipitation | $CaHPO_4$ formation rate constant | $k_f^{CaHPO_4}$ | 1.16 $mM^{-1}.min^{-1}$ | [213] |
| | $CaHPO_4$ dissociation rate constant | $k_d^{CaHPO_4}$ | 1.7 $min^{-1}$ | estimated |
| | $CaH_2PO_4^+$ formation rate constant | $k_f^{CaH_2PO_4^+}$ | 0.054 $mM^{-1}.min^{-1}$ | [213] |
| | $CaH_2PO_4^+$ dissociation rate constant | $k_d^{CaH_2PO_4^+}$ | 1.7 $min^{-1}$ | estimated |
| | Fetuin-A binding to $CaHPO_4$ and $CaH_2PO_4^+$ | $k_{fetA}$ | 0.3 $min^{-1}$ | estimated |
| | CPP degradation | $k_{deg}^{CPP}$ | 3 $min^{-1}$ | [102] |

## 5.2 Summary of the main equations

In this part, we summarize the main equations developed in the previous sections. The hormonal part of the model is composed of the following equations:

$$\frac{d[PTH]_g}{dt} = \frac{k_{prod}^{PTHg}\beta_{prod}^{PO_4}[PO_4]^{n_{prod}^{PO_4}}}{(1+\gamma_{prod}^{D_3}[D_3]_p)((K_{prod_{PTH}}^{PO_4})^{n_{prod}^{PO_4}}+[PO_4]^{n_{prod}^{PO_4}})} - \Big(k_{deg}^{PTH_g}+F([Ca^{2+}]_p)\Big)[PTH]_g, \tag{5.48}$$

$$\frac{d[PTH]_p}{dt} = F([Ca^{2+}]_p)\frac{V_c}{V_p}[PTH]_g - k_{deg}^{PTH_p}[PTH]_p, \tag{5.49}$$

$$\begin{aligned}\frac{d[D_3]_p}{dt} = \Bigg[k_{conv}^{min} + \frac{\delta_{conv}^{max}[PTH(t-\tau)]_p^{n_{conv}}}{\Big([PTH(t-\tau)]_p^{n_{conv}}+K_{conv}^{n_{conv}}\Big)} \times \frac{1}{(1+\gamma_{conv}^{Ca}[Ca^{2+}]_p)(1+\gamma_{conv}^{D_3}[D_3]_p)} \\ \times\frac{1}{(1+\gamma_{conv}^{FGF}[FGF]_p)(1+\gamma_{conv}^{PO_4}[PO_4]_p)}\Bigg][D_3^{inact}]_p \\ -\frac{k_{deg}^{D_3}(1+\gamma_{deg}^{FGF}[FGF]_p)[D_3]_p}{1+\gamma_{deg}^{PTH_p}[PTH]_p},\end{aligned} \tag{5.50}$$

$$\frac{d[FGF]_p}{dt} = k_{prod}^{FGF}\Big(1+G_1([D_3]_p)+G_2([PO_4]_p)\Big) - k_{deg}^{FGF}[FGF]_p, \tag{5.51}$$

respectively describing the dynamics of $PTH_g$, $PTH_p$, $D_3$ and $FGF_p$.

The equations corresponding to the dynamics of $CaHPO_4$, $CaH_2PO_4^+$ complexes and calciprotein particles in plasma are:

$$\begin{aligned}\frac{d[CaHPO_4]_p}{dt} = k_f^{\mathrm{CaHPO_4}}[Ca^{2+}]_p[HPO_4^{2-}]_p f_2^2 - k_d^{\mathrm{CaHPO_4}}[CaHPO_4]_p \\ -k_f^{fetA}[CaHPO_4]_p,\end{aligned} \tag{5.52}$$

$$\begin{aligned}\frac{d[CaH_2PO_4^+]_p}{dt} = k_f^{\mathrm{CaH_2PO_4^+}}[Ca^{2+}]_p[H_2PO_4^-]_p f_1 f_2 - k_d^{\mathrm{CaH_2PO_4^+}}[CaH_2PO_4^+]_p f_1 \\ -k_f^{fetA}[CaH_2PO_4^+]_p f_1.\end{aligned} \tag{5.53}$$

$$\frac{d[CPP]_p}{dt} = k_f^{fetA}\Big([CaHPO_4]_p + f_1[CaH_2PO_4^+]_p\Big) - k_c^{CPP}[CPP]_p. \tag{5.54}$$

In the rapidly exchangeable pool, there are two differential equations which account for the dynamics of $CaHPO_4$ as well as $CaH_2PO_4^+$:

$$\frac{dN_{CaHPO4_f}}{dt} = k_{on}^{CaHPO_4} N_{Ca_f^{2+}} a N_{PO_{4_f}} - k_d N_{CaHPO4_f}, \tag{5.55}$$

and

$$\frac{dN_{CaH_2PO4_f^+}}{dt} = k_{on}^{CaH_2PO_4} N_{Ca_f^{2+}} b N_{PO_{4_f}} - k_{off} N_{CaH_2PO4_f^+}. \tag{5.56}$$

Equations describing the dynamics of binding between calcium and albumin and between phosphate ($HPO_4^{2-}$ and $H_2PO_4^-$) and sodium are:

$$\frac{d[CaAlb]_p}{dt} = k_f^{CaAlb}[Ca^{2+}]_p N_{Alb}[Alb^{tot}]_p - k_d^{CaAlb}[CaAlb]_p. \tag{5.57}$$

and

$$\frac{d[NaPO_4]_p}{dt} = k_f^{NaPO_4}[Na^+]_p[PO_4]_p - k_d^{NaPO_4}[NaPO_4]_p. \tag{5.58}$$

Then, the equations characterizing the dynamics of calcium in plasma, in the rapidly exchange-

able pool in bone and in the deep bone pool are:

$$\begin{aligned}\frac{d[Ca^{2+}]_p}{dt} = \frac{1}{V_p}\Big\{&\Gamma_{abs}(D_3) + \Gamma_{res}(PTH, D_3) - k^{Ca}_{p-f}[Ca^{2+}]_p V_p + k^{Ca}_{f-p} N_{Ca^{2+}_f} \\ &-\lambda_u GFR([Ca^{2+}]_p + [CaHPO_4]_p + [CaH_2PO_4^+]_p)\Big\} \\ &-k^{CaAlb}_f [Ca^{2+}]_p N_{Alb}[Alb^{tot}]_p + k^{CaAlb}_d [CaAlb]_p \\ &-k^{\mathrm{CaHPO_4}}_{on}[Ca^{2+}]_p a[PO_4]_p + k^{\mathrm{CaHPO_4}}_d [CaHPO_4]_p \\ &-k^{\mathrm{CaH_2PO_4^+}}_{on}[Ca^{2+}]_p b[PO_4]_p + k^{\mathrm{CaH_2PO_4^+}}_{off}[CaH_2PO_4^+]_p,\end{aligned} \tag{5.59}$$

$$\begin{aligned}\frac{dN_{Ca^{2+}_f}}{dt} = &k^{Ca}_{p-f}[Ca^{2+}]_p V_p - k^{Ca}_{f-p} N_{Ca^{2+}_f} - \Gamma_{ac} N_{Ca^{2+}_f} \\ &-\frac{dN_{CaHPO4_f}}{dt} - \frac{dN_{CaH_2PO4^+_f}}{dt},\end{aligned} \tag{5.60}$$

$$\frac{dN_{Ca_s}}{dt} = \Gamma_{ac} N_{Ca_f} - \Gamma_{res}(PTH, D_3). \tag{5.61}$$

Finally, the equations describing the dynamics of phosphate in plasma, the rapidly exchangeable pool of phosphate in bone, the deep bone pool of phosphate and the cellular pool of phosphate are:

$$\begin{aligned}\frac{d[PO_4]_p}{dt} = \frac{1}{V_p}\Big\{&\Gamma^{Pho}_{abs}(D_3) - k^{PO_4}_{p-f}[PO_4]_p + k^{PO_4}_{f-p} N_{PO_4{}_f} + \Gamma^{PO_4}_{res}(PTH, D_3) \\ &-\lambda^{PO_4}_u GFR([PO_4]_p + [CaHPO_4]_p + [CaH_2PO_4^+]_p + [NaPO4]_p) \\ &+k_{c-p} N_{PO_4{}_c} - k_{p-c}[PO_4]_p V_p\Big\} \\ &-k^{NaPO_4}_f [Na^+]_p [PO_4]_p + k^{NaPO_4}_d [NaPO_4]_p \\ &-k^{\mathrm{CaHPO_4}}_{on}[Ca^{2+}]_p a[PO_4]_p + k^{\mathrm{CaHPO_4}}_d [CaHPO_4]_p \\ &-k^{\mathrm{CaH_2PO_4^+}}_{on}[Ca^{2+}]_p b[PO_4]_p + k^{\mathrm{CaH_2PO_4^+}}_{off}[CaH_2PO_4^+]_p,\end{aligned} \tag{5.62}$$

$$\frac{dN_{PO_{4_f}}}{dt} = k_{p-f}^{Pho}[PO_4]_p V_p - k_{p-f}^{Pho} N_{PO_{4_f}} - \Gamma_{ac} N_{PO_{4_f}} - \frac{dN_{CaHPO4_f}}{dt} - \frac{dN_{CaH_2PO4_f^+}}{dt}, \tag{5.63}$$

$$\frac{dN_{PO_{4_b}}}{dt} = \Gamma_{ac}^{PO_4} N_{PO_{4_f}} - \Gamma_{res}^{PO_4}(PTH, D_3), \tag{5.64}$$

$$\frac{dN_{PO_{4c}}}{dt} = k_{p-c}[PO_4]_p V_p - k_{p-c} N_{PO_{4_c}}. \tag{5.65}$$

## 5.3 Results

### 5.3.1 Model validation

As for the model of calcium homeostasis, we compared the steady-state values predicted by the combined model to those in the literature, as summarized in Table 5.7. The model was further validated by simulating different scenarios.

Table 5.7: Steady-state values under normal conditions.

| | Model Prediction | Experimental Range |
|---|---|---|
| $[Ca^{2+}]_p$ (mM) | 1.21 | 1.1-1.3 |
| $[P_i]_p$ (mM) | 1.50 | 0.8-1.6 |
| $[PTH]_p$ (pM) | 5.94 | 1.5-15 |
| $[D_3]_p$ (pM) | 536 | 80-700 |
| $[FGF23]_p$ (pM) | 14.80 | 11.7-21.1 |
| Calcium intestinal absorption (%) | 43.5 | 40-60 |
| Phosphate intestinal absorption (%) | 52.4 | 50-80 |
| Fractional calcium excretion (%) | 1.65 | 0-2 |
| Fractional phosphate excretion (%) | 11.2 | 0-15 |

#### Calcium and Phosphate in Primary Hyperparathyroidim

Jaeger and coworkers [108] developed an experimental model of primary hyperparathyroidism in the rat. Sprague-Dawley PTX and thyroparathyroidectomized (TPTX) rats weighing 215-295g were infused with $PTH_{1-34}$ via mini-pumps at varying doses. The highest dose yielded a 3.5-fold increase in plasma PTH concentration. They observed a 50% increase in $[Ca^{2+}]_p$, whereas $[PO_4]_p$ was reduced by 35%. Additionally, vitamin $D_3$ levels were multiplied by 3 compared to the base case. We simulated this experiment by increasing the coefficient of PTH production ($k_{prod}^{PTH_g}$) until $[PTH]_p$ reached 3.5 times its basal value, in agreement with the experimental value [108], and computed the corresponding steady-state concentrations. Results are summarized in Table 5.8 and

shown in Figure 5.2. Overall, our model predicts that calcium concentration increases by 55%, while phosphate decreases by 30%. Vitamin $D_3$ concentration is 3.3 times higher than its basal value. In other words, there is a good agreement between our model predictions and observations in the primary hyperparathyroidism study of Jaeger and coworkers [108].

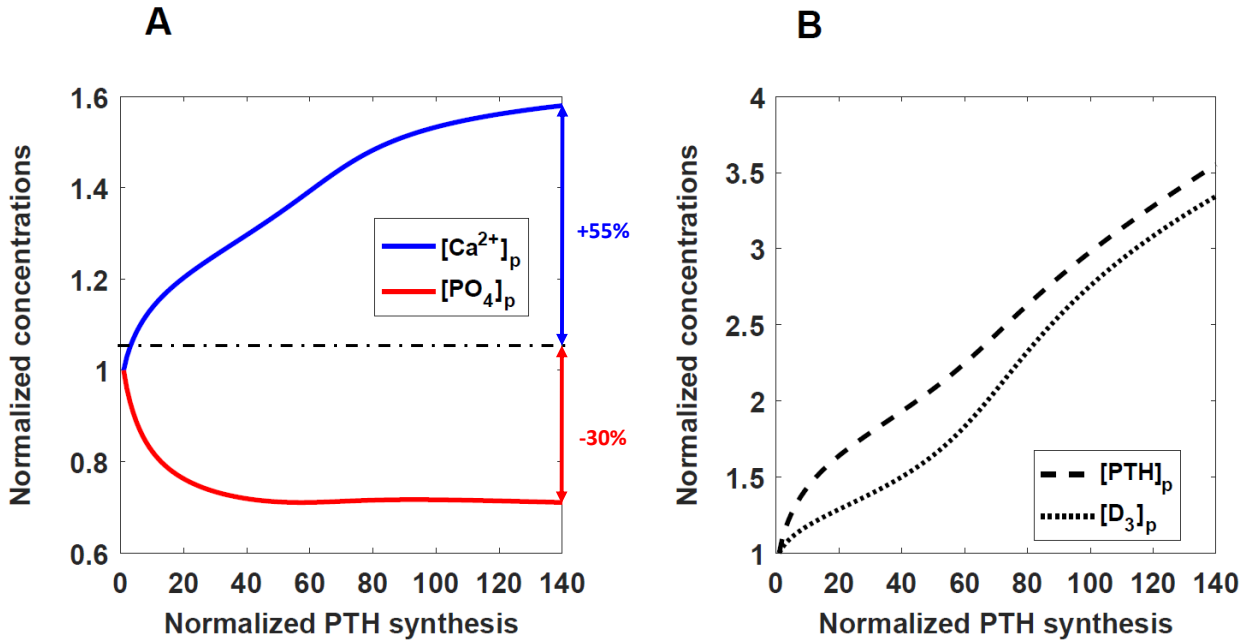


Figure 5.2: A simulation of primary hyperparathyroidism in rats. Panel A: normalized plasma concentrations of calcium and phosphate as a function of the normalized PTH synthesis rate ($k_{prod}^{PTH_g}$). Panel B: normalized plasma concentration of PTH and vitamin $D_3$ as a function of the normalized PTH synthesis rate. See Table 5.8 for comparison with the data of Jaeger *et al.* [108].

### FGF23 deficiency

Shimada *et al.* investigated the suppresion of FGF23 in mice [185]. They observed that $PO_4$ concentration was increased by 30%, $Ca^{2+}$ concentration was not significantly different from the base case, and vitamin $D_3$ was not increased (however, there was a large uncertainty in the measurements). We simulated the full inhibition of FGF23 (denoted FGF23 KO below) by setting the coefficient of FGF23 production, $k_{prod}^{FGF}$, to 0, and the initial plasma FGF23 concentration to 0.

Table 5.8: Comparison of model prediction with experimental data in rats with primary hyperparathyroidism (PHP1) rats [108] and in FGF23 KO mice [185].

| Simulation | Variable | Model of Chapter 4 | Model Predictions | Experimental Values |
|---|---|---|---|---|
| PHP1 | $[Ca^{2+}]_p$ | +60% | +55 % | +50% |
| | $[P_i]_p$ | $\emptyset$ | -30% | -35% |
| | $[D_3]_p$ | 4 fold higher | 3.3 fold higher | 3 fold higher |
| FGF23 KO | $[Ca^{2+}]_p$ | $\emptyset$ | NS | NS |
| | $[P_i]_p$ | $\emptyset$ | +14% | +30% |
| | $[D_3]_p$ | $\emptyset$ | +40% | NS (large standard error) |

### Intravenous injection of Phosphate

We also validated our model against the experimental data of Thomas *et al.* [205], who infused rats with 0.5 mmol $Na_2HPO_4/NaH_2PO_4$ over 2-3 minutes. To simulate an intravenous injection of phosphate with our model, we increased the concentration of $PO_4$ concentration by a factor 2 in 10 minutes. The glomerular filtration rate was varied as in the experimental study. Numerical results are compared to experimental data, as illustrated in Figure 5.3. Overall, our model fit the experimental data well. As shown in panel A, the slope of the phosphate curve is in agreement with the experimental values. The amount of calcium that is not bound to phosphate drops at once by 20% after the infusion and does not return to its initial value after 250 minutes (panel B). This is due to the precipitation of calcium and phosphate which cannot be measured. Finally, PTH concentration rises substantially in response to $PO_4$, but it is not maintained at the end of the simulation contrary to experimental observations, which show $[PTH]_p$ remaining stable at 10 times its basal value (Panel C). The reason for this discrepancy is unclear; there may be a delay in the feedback mechanism between changes in plasma phosphate and PTH synthesis that the model does not capture.

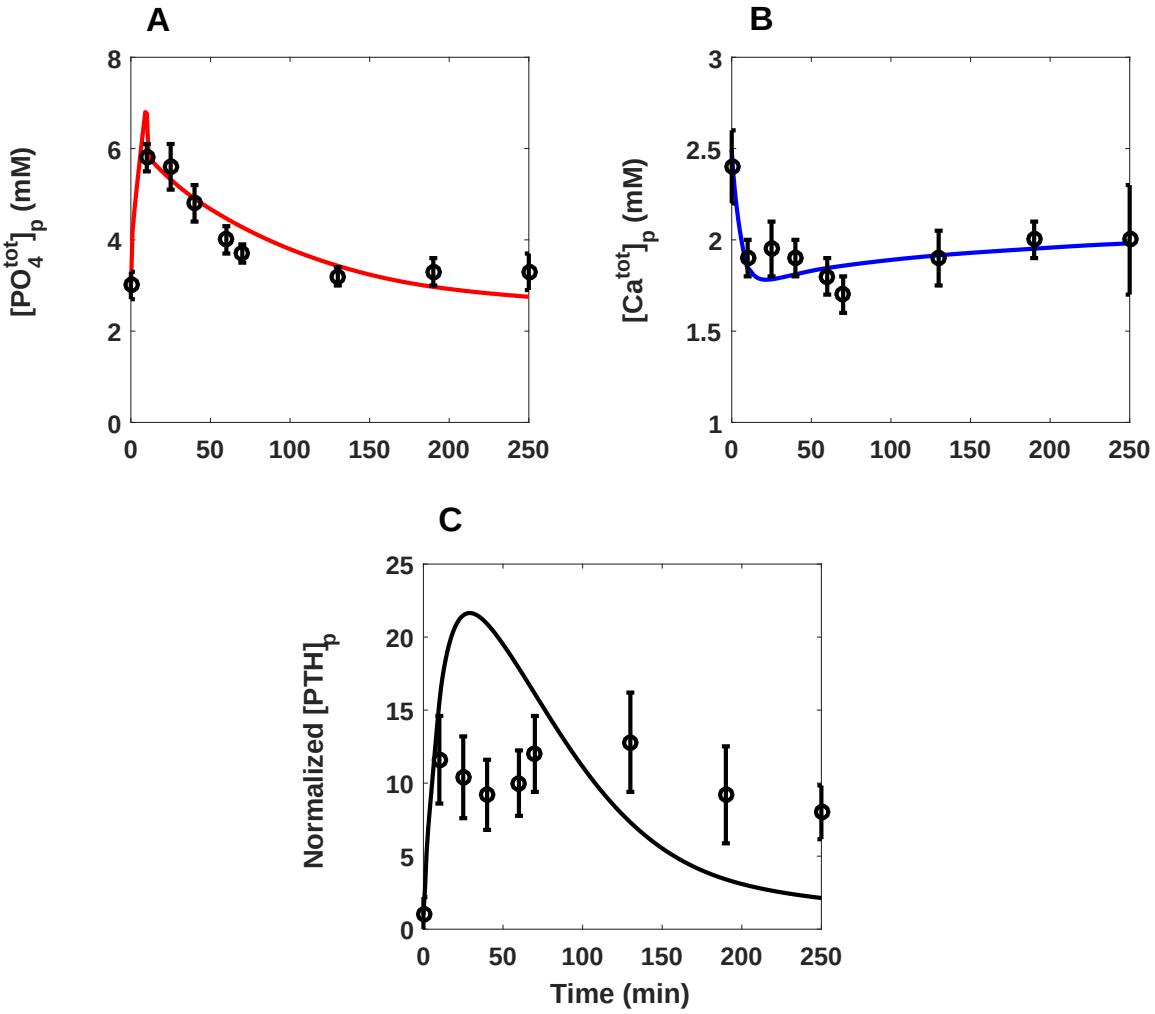


Figure 5.3: A simulation of phosphate intravenous infusion. Experimental values are represented by open circles. Panel A: $PO_4$ total concentration as a function of time. Panel B: total Ca concentration (without calcium/phosphate complexes) as a function of time. Panel C: normalized plasma PTH concentration.

### Phosphate gavage

In the same study, another set of rats received the same amount (500 $\mu$mol) of $Na_2HPO_4/NaH_2PO_4$ by intestinal gavage. Experimental results are presented in Figure 5.4. Our model adequatly reproduces experimental data. The standard errors are quite large for calcium (Panel B), so there is not necessarily a discrepancy between model predictions and experimental observations. The authors did not observe any significant difference in calcium concentration and our model agrees with this fact. Phosphate is slightly increased 25 minutes after the gavage, while PTH is doubled. As previously, the predicted value of plasma PTH returns to its base case value faster than observed experimentally.

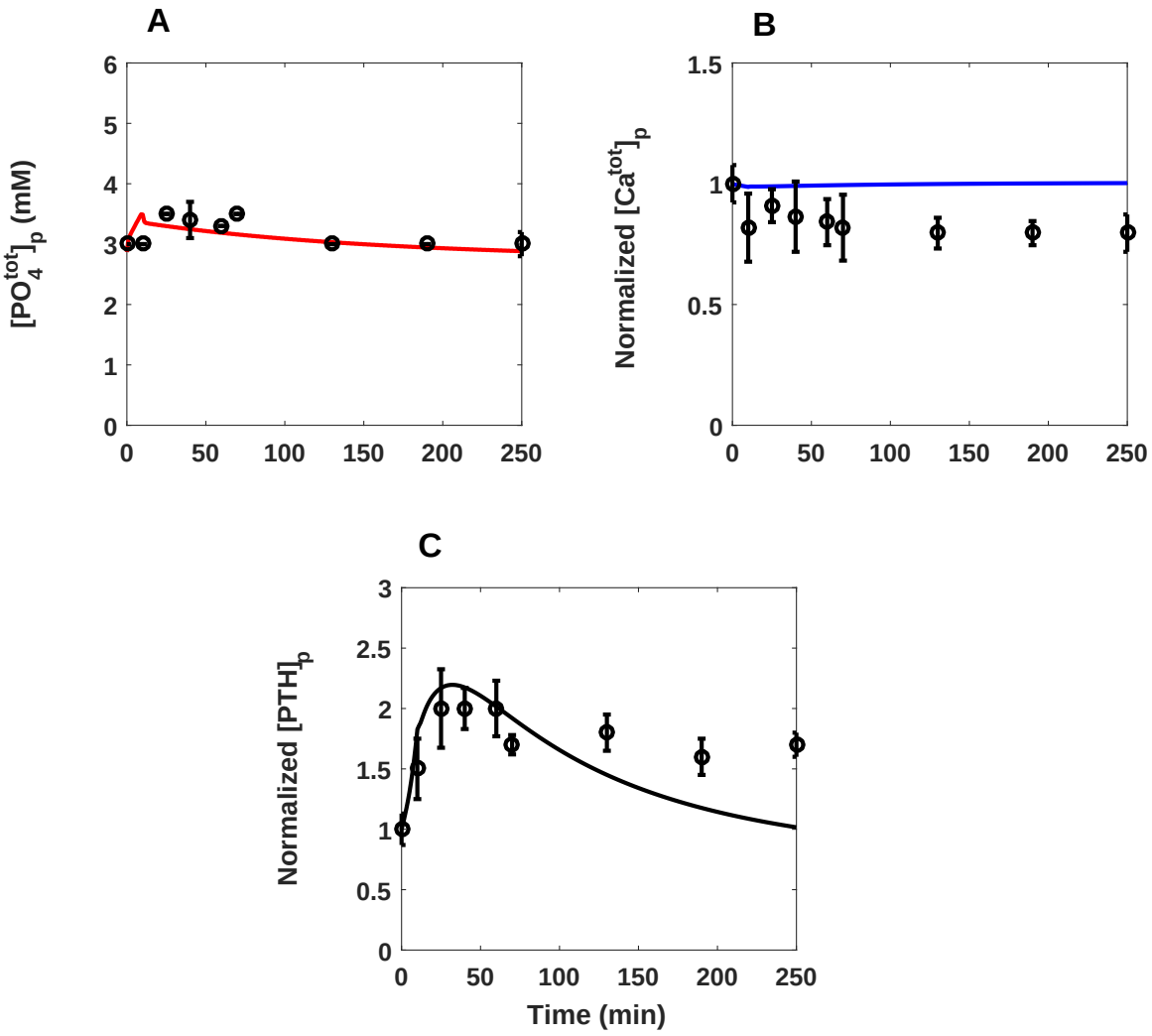


Figure 5.4: A simulation of phosphate gavage. Experimental values are represented by open circles. Panel A: $PO_4$ total concentration as a function of time. Panel B: normalized total Ca concentration (without calcium/phosphate complexes). Panel C: normalized plasma PTH concentration.

### 5.3.2 Model Predictions

The predictions of the combined model are then compared to those obtained with the calcium homeostasis model developed in Chapter 4.

#### Primary hyperparathyroidism

Primary hyperparathyroidism was simulated by increasing the base-case PTH synthesis rate ($k_{prod}^{PTHg}$) by a factor ranging from 1 to 300 as in Chapter 4. Shown in Figure 5.5 are the predicted steady-state values of urinary excretion, intestinal absorption, bone accretion and bone resorption for calcium (Panel C) and phosphate (Panel D), as a function of the normalized PTH synthesis rate, namely $k_{prod}^{PTH_g}$.

Vitamin $D_3$ increases as a direct consequence of the PTH elevation. This increase is counterbalanced by the inhibiting effects of FGF23 which increases as well as calcium, but to a lesser extent than PTH. During primary hyperparathyroidism, our model predicts that $[FGF23]_p$ increases owing to vitamin $D_3$, despite the reduction in phosphate levels which has a lesser impact than the increase in vitamin D3 levels. Moreover, $[FGF23]_p$ reaches a saturation value that is 2-fold it baseline value, as soon as the rate of PTH synthesis is increased by a factor 50. This can be explained by the drop in phosphate concentration, which blunts the activating effect of vitamin $D_3$ on FGF23.

Calcium urinary excretion is predicted to increase monotonically with the rate of PTH synthesis, but at a rate that diminishes with increasing $k_{prod}^{PTHg}$. Our model suggests that for small elevations of $k_{prod}^{PTHg}$ (<100), the effects of CaSR predominate over those of PTH and vitamin $D_3$, which explains the rapid increase in $Ca^{2+}$ urinary excretion. Conversely, for higher degrees of hyperparathyroidism (>100), the contributions of PTH and vitamin $D_3$ rise because of elevated levels of PTH and vitamin $D_3$, while that of CaSR decreases as a result of a saturation in $[Ca^{2+}]_p$. This explains why $U_{Ca}$ reaches a plateau.

Both calcium bone accretion and resorption are predicted to increase and saturate at about 1.6 times their basal value. Moreover, the difference between these two fluxes does not vary, which implies that the net calcium bone flux remains constant. Finally, the intestinal absorption of calcium is enhanced by a factor 1.5 and saturates as well.

Phosphate urinary excretion also increases with $k_{prod}^{PTHg}$ (Panel D), in part as a direct effect of higher PTH levels, but more importantly as a result of the rise in FGF23 concentration (Panel D). It reaches saturation (at a value that is 2.25 times higher than its base-case value) mainly because of saturating levels of FGF23.

As in the case for calcium, phosphate bone storage is predicted to remain constant. The intestinal absorption of phosphate also increases with $k_{prod}^{PTHg}$, albeit less than that of calcium (that of $PO_4$ increases by a factor of 1.3 at saturating levels). This is because vitamin $D_3$ is assumed to have a lower effect on the intestinal absorption of phosphate than on that of calcium (section 5.1.4, Equation 5.18).

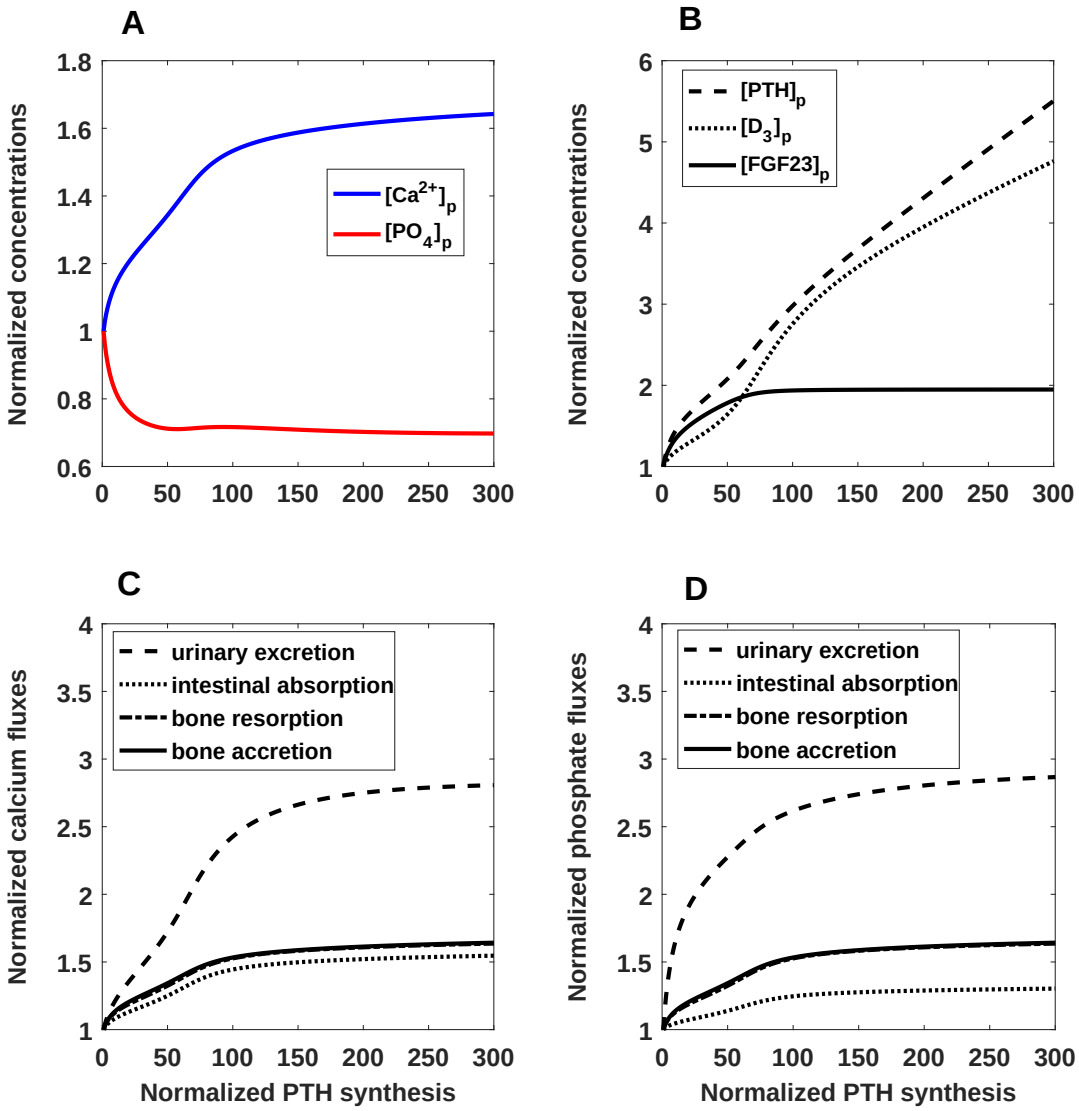


Figure 5.5: A simulation of primary hyperparathyroidism in rats. Panel A: normalized $Ca^{2+}$ and $PO_4$ concentrations as a function of the normalized PTH synthesis rate ($k_{prod}^{PTH_g}$). Panel B: normalized PTH, D3 and FGF23 concentrations. Panel C: normalized $Ca^{2+}$ fluxes. Panel D: normalized $PO_4$ fluxes.

In the combined calcium-phosphate model, $[PTH]_p$ is predicted to be significantly lower than in the model built in Chapter 4 (Figure 5.6, panels A and B). When $k_{prod}^{PTH_g}$ is increased, $[PTH]_p$ increases, which triggers an increase in of the urinary excretion of phosphate (since PTH inhibits phosphate reabsorption). Besides, the elevation of $[FGF]_p$ also increases phosphate excretion. As a result, this lowers $[PO_4]_p$. Since phosphate is an activator of PTH synthesis, the drop in plasma $PO_4$ levels (Figure 5.5, panel A) explains why [PTH]p doesn't rise as much as in the absence of phosphate effects. As a direct consequence, the plasma concentration of vitamin $D_3$ is also predicted

to increase significantly less with increasing $k_{prod}^{PTH_g}$. Besides, $[Ca^{2+}]_p$ saturates for higher levels of PTH synthesis than in the previous model. Panels C and D show that the bone resorption, bone accretion, and intestinal absorption of calcium do not saturate as rapidly as in the Chapter 4 model; however they reach the same value when $k_{prod}^{PTH_g}$ is multiplied by 100. Finally, the profile of the urinary excretion of calcium differs between the two models: while it was non monotonic in the calcium homeostasis model, it is continuously increasing in the present model. This is due to the change in the relative contribution of PTH and $Ca^{2+}$ to the renal reabsorption of calcium. Indeed, in the present model, $\lambda_{DCT}^0$ (the basal fractional reabsorption of calcium in the DCT) is increased by 12%, meaning that in the DCT, hormones have less influence (the total fractional reabsorption in the DCT is kept fixed). In particular, the effects of PTH are blunted, thereby increasing urinary calcium excretion. Finally, the sensitivity coefficients to PTH in the TAL and DCT are increased compared to the previous model, meaning that for the same variation in $[PTH]_p$, the response is reduced and calcium urinary excretion is enhanced.

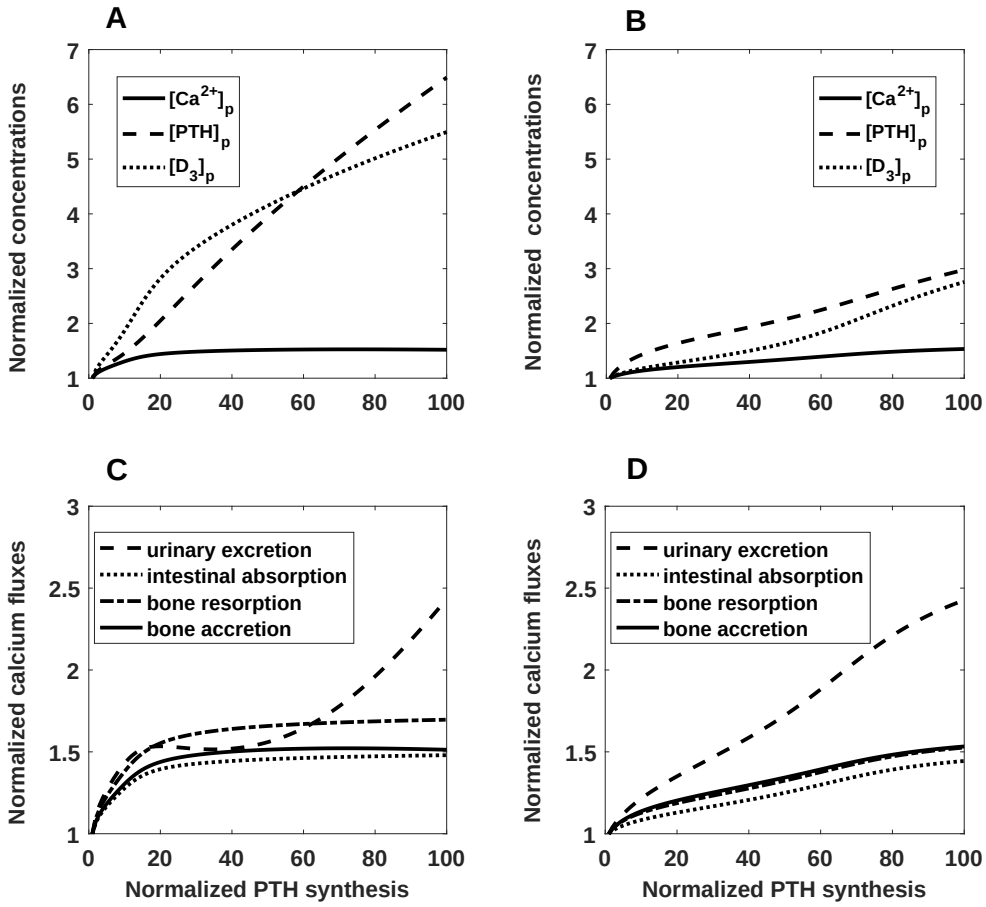


Figure 5.6: Comparison between the predictions of the Chapter 4 model and the combined calcium-phosphate model, in the case of primary hyperparathyroidism. Panels A-B: normalized $Ca^{2+}$, PTH and vitamin $D_3$ plasma concentrations as a function of the normalized PTH synthesis rate ($k_{prod}^{PTH_g}$), using the Chapter 4 model (panel A) and the combined calcium-phosphate model (panel B). Panels C and D: normalized $Ca^{2+}$ fluxes, using the Chapter 4 model (panel C) and the combined calcium-phosphate model (panel D).

### Primary hypoparathyroidism

To simulate primary hypoparathyroidism, we conversely decreased $k_{prod}^{PTH_g}$ from its base-case value to zero. Results are depicted in Figure 5.7.

In the absence of PTH, vitamin $D_3$ and FGF23 levels are both predicted to fall by 70 % (Panel B), which is expected since PTH enhances the synthesis of vitamin $D_3$, and the latter in turn activates FGF23 production. The drop in vitamin $D_3$ triggers a decrease in both calcium and phosphate intestinal absorption (respectively -35% and -20% in the absence of PTH, Panel C and D). Additionally, predicted bone resorption is drastically reduced due to the PTH and vitamin $D_3$ decline (-45% for calcium and phosphate, in the absence of PTH), together with bone accretion. Moreover, the predicted difference between accretion and resorption appears to grow with the degree of hypoparathyroidism.

Calcium urinary excretion is predicted to fall by about 20% in the absence of PTH, mainly due to the diminished filtered load of calcium, even though the stimulating effects of vitamin $D_3$ and PTH on $Ca^{2+}$ reabsorption are blunted. Interestingly, predicted phosphate urinary excretion decreases even more, because of the $[\text{FGF23}]_p$ reduction; it is reduced by 50% in the absence of PTH.

The decrease in calcium bone resorption as well as intestinal absorption explains why $[Ca^{2+}]_p$ drops by 35%. The slight increase in $[PO_4]_p$ for small decreases in $k_{prod}^{PTH_g}$ can be explained by the rapid drop of phosphate urinary excretion compared to other fluxes. For larger decreases in $k_{prod}^{PTH_g}$, resorption and absorption are sufficiently reduced so that $[PO_4]_p$ decreases as well.

The predictions of the Chapter 4 model and the present model are compared side by side on Figure 5.8. As illustrated, the predicted curves are significantly smoother using the combined calcium-phosphate model. Indeed, in the calcium-phosphate homeostasis model, all sensitivity coefficients to hormones such as PTH and vitamin $D_3$ were changed to correctly reproduce the experimental observations of Thomas *et al.* [205] (Table 5.9). In particular, $[PTH]_p$ decreases approximately linearly with $k_{prod}^{PTH_g}$ in the present model (panel B), in contrast with previous results (panel A). In total absence of PTH, the present model predicts a 35% decrease in the plasma concentration of calcium, versus 40% using the previous model; conversely, the plasma concentration of vitamin $D_3$ decreases more (70% vs 60% before). In addition, the urinary excretion of calcium is now predicted to decrease in a monotonic manner (panel D), which was not the case using the previous model (panel C). This is likely due to the fact that in the combined calcium-phosphate model, the contribution of PTH to calcium reabsorption in the PT is significantly reduced ($\delta_{PT}^{max} = 0.05$ in the previous model, vs $\delta_{PT}^{max} = 0.01$ in the present model, Table 5.9). Lastly, when $[PTH]_p$ is reduced to 0, bone resorption is decreased by 45% in the present model, vs 55% using the previous model.

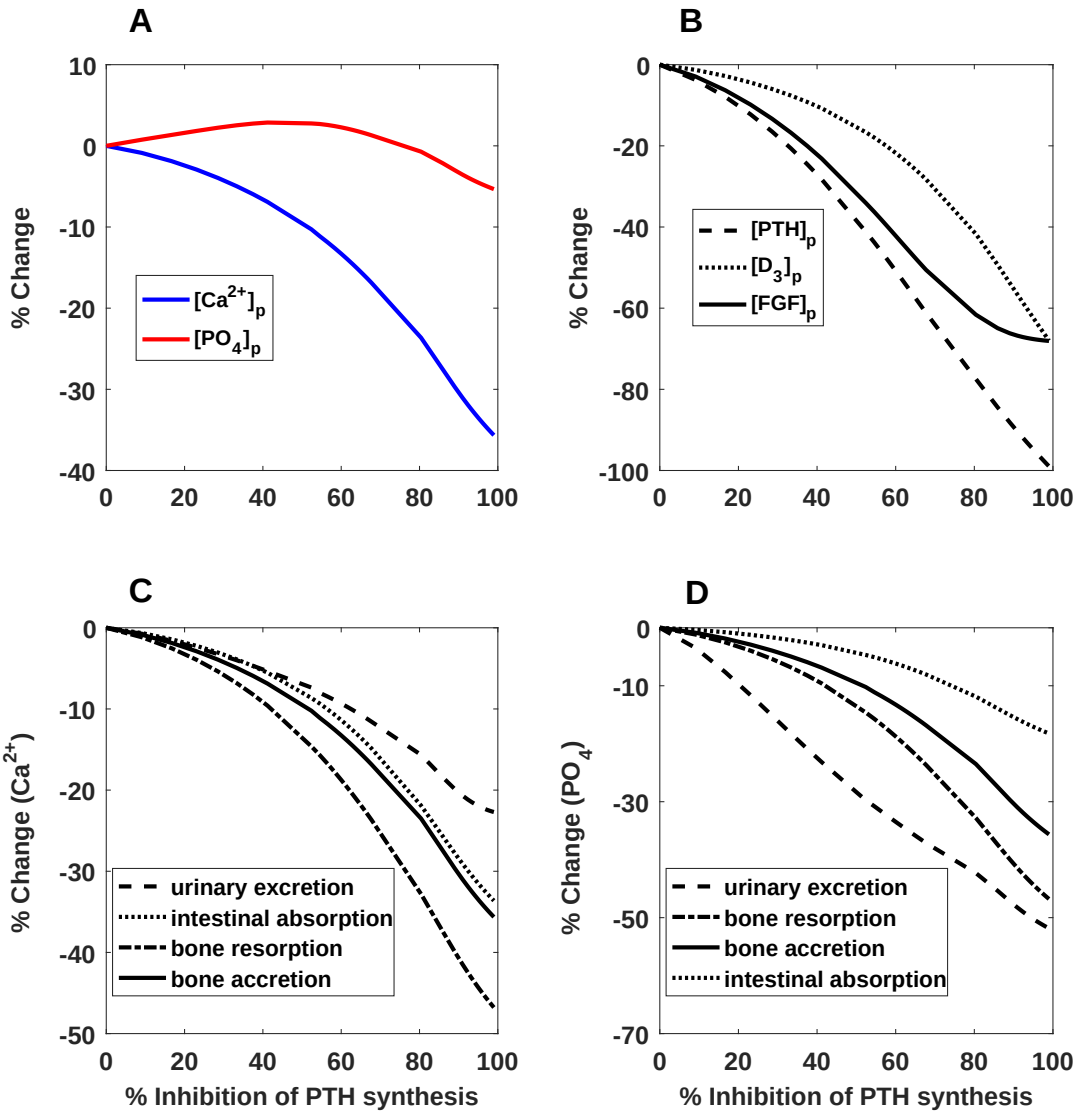


Figure 5.7: A simulation of primary hypoparathyroidism in rats. Panel A: fractional change in the plasma concentration of $Ca^{2+}$ and $PO_4$ as a function of the percentage of PTH synthesis inhibition. Panel B: fractional change in the plasma concentration of PTH, vitamin $D_3$ and FGF23. Panel C: fractional change in calcium fluxes. Panel D: fractional change in phosphate fluxes.

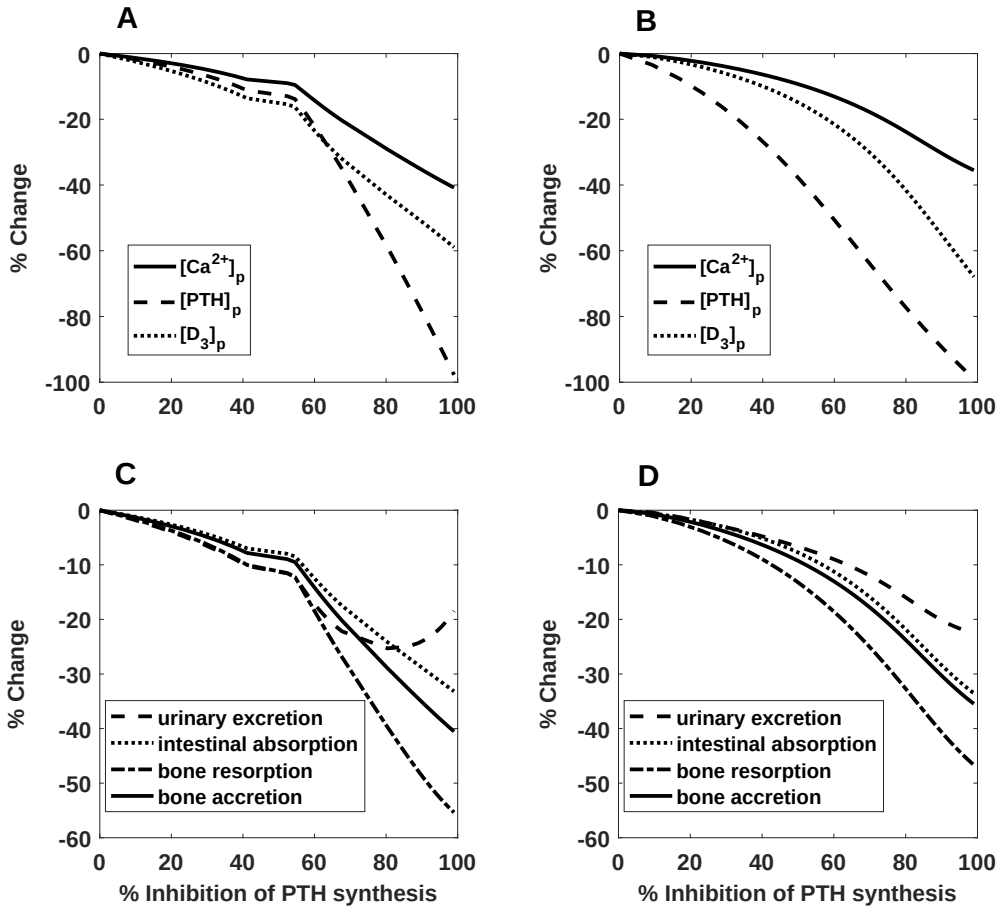


Figure 5.8: Comparison between the predictions of the Chapter 4 model and the combined calcium-phosphate model, in the case of primary hypoparathyroidism. Panels A-B: fractional change in the plasma concentration of $Ca^{2+}$, PTH and vitamin $D_3$ as a function of the percentage of PTH synthesis inhibition, using the Chapter 4 model (panel A) and the combined calcium-phosphate model (panel B). Panels C and D: normalized $Ca^{2+}$ fluxes, using the Chapter 4 model (panel C) and the combined calcium-phosphate model (panel D).

### Vitamin $D_3$ deficiency

To simulate the effects of vitamin $D_3$ deficiency, we decreased the concentration of its precursor, namely $[D_3^{inact}]_p$,by a factor ranging from 1 to 100. Results are shown in Figure 5.9.

The plasma concentration of calcium is predicted to remain stable until $[D_3^{inact}]_p$ is divided by 10, when it drops by 40 % (panel A). That of phosphate slightly increases for small variations in $[D_3^{inact}]_p$, because FGF23 slightly diminishes (panel B), thereby increasing $PO_4$ reabsorption in the proximal tubule. Besides, the inhibitory effects of PTH (panel B) and $PO_4$ itself are not enough to reduce phosphate levels. When $[D_3^{inact}]_p$ is divided by a factor of 10 or more, $[PO_4]_p$ starts decreasing, owing to a significantly reduced intestinal absorption (-50%), caused by the decrease in $[D_3]_p$ (panels B and D).

The profile of calcium urinary excretion is noteworthy (panel C). First, it decreases until $[D_3^{inact}]_p$ is halved, then it rises until $[D_3^{inact}]_p$ is divided by 10 and finally it substantially drops. The initial decrease can be explained by the enhancing effects of PTH on $Ca^{2+}$ reabsorption in the thick ascending limb, which predominate over the inhibitory effects of PTH on $Ca^{2+}$ reabsorption in the proximal tubule; moreover, the contribution of CaSR is small due to the $[Ca^{2+}]_p$ reduction. Then, as PTH keeps increasing (panel B), its inhibitory effects in the proximal tubule prevail over its stimulating effects in the TAL. Indeed, the sensitivity of $Ca^{2+}$ reabsorption to PTH differs between the two segments (Equation 4.11 and Equation 4.14). The final drop is directly related to the filtered load which decreases in parallel with $[Ca^{2+}]_p$ (panel A), thus counteracting the hormonal effects.

Interestingly, the bone storage of calcium and phosphate is affected by vitamin $D_3$ deficiency. Bone resorption is regulated predominantly by vitamin $D_3$, and to a lesser extent by PTH. Up to the point where $[D_3^{inact}]_p$ is divided by 10, bone resorption increases (in parallel with $[PTH]_p$) whereas bone accretion decreases, meaning that the bone balance is negative. Note that this effect is more significant for calcium than for phosphate. When $[D_3]_p$ starts decreasing markedly, bone resorption diminishes as well.

The predictions of the Chapter 4 model and the present model are compared side by side on Figure 5.10. As illustrated, the $[Ca^{2+}]_p$ profiles are similar, but there are differences in the $[PTH]_p$ profiles. When the concentration of the vitamin $D_3$ precursor is divided by 10, the combined calcium-phosphate model predicts that phosphate bone release decreases substantially, which lowers $[PO_4]_p$, and therefore also slightly reduces $[PTH]_p$ (since phosphate is an activator of PTH synthesis). In the complete absence of the vitamin $D_3$ precursor, $[PTH]_p$ is 3-fold higher than its basal value based upon the present model, vs. 2.75-fold higher based upon the Chapter 4 model. Note too that the calcium urinary excretion profile is different from that obtained previously (panels C-D), owing to our adjustment of PTH-related parameters in the proximal tubule (Table 5.9). In the complete absence of the vitamin $D_3$ precursor, urinary $Ca^{2+}$ excretion is reduced by 45% compared to base case using the present model, vs. 70% using the previous model.

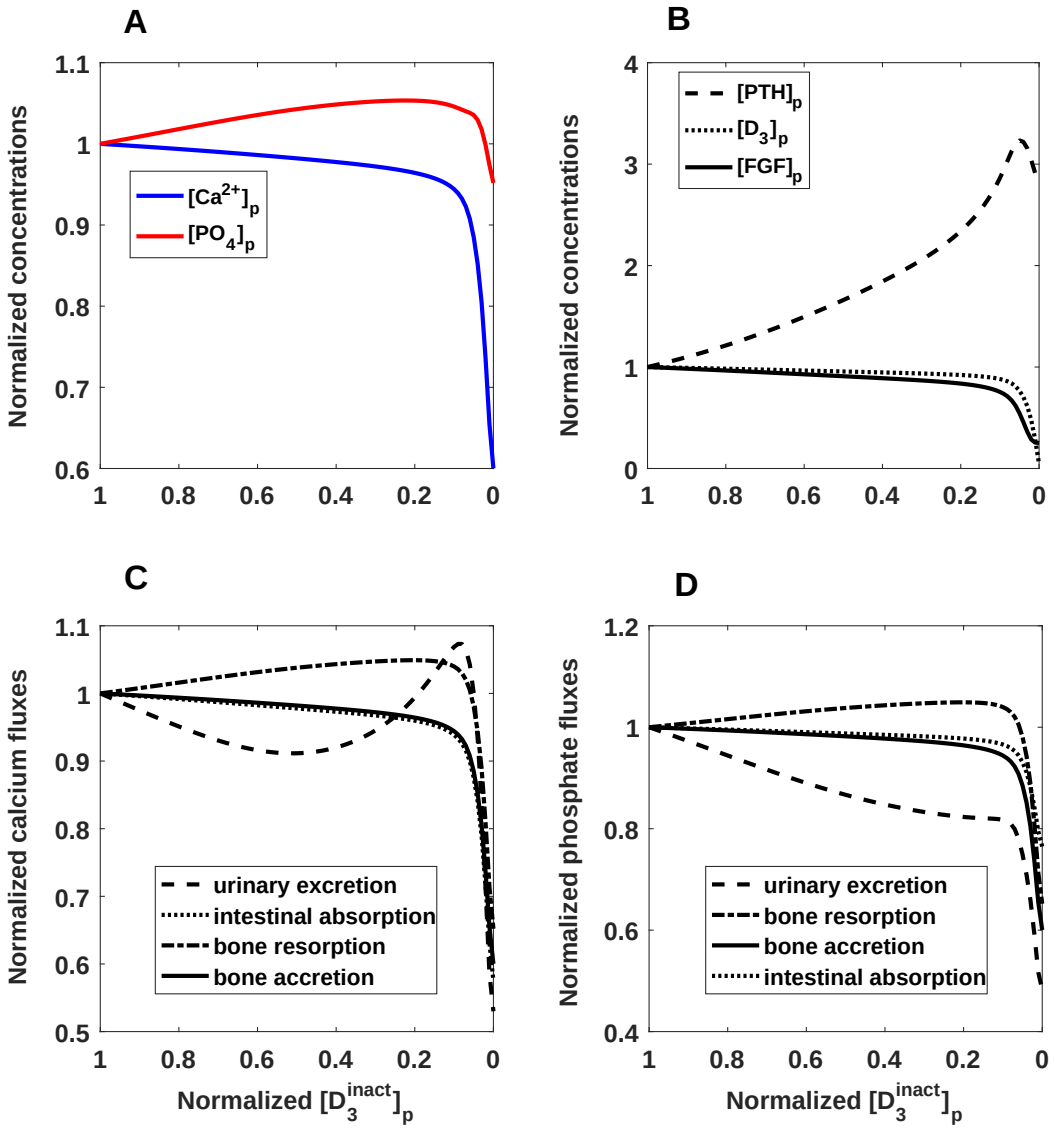


Figure 5.9: A simulation of vitamin $D_3$ deficiency in rats. Panel A: normalized $Ca^{2+}$ and $PO_4$ concentrations as a function of the normalized $[D_3^{inact}]_p$. Panel B: PTH, vitamin $D_3$ and FGF23 concentrations. Panel C: normalized calcium fluxes. Panel D: normalized phosphate fluxes.

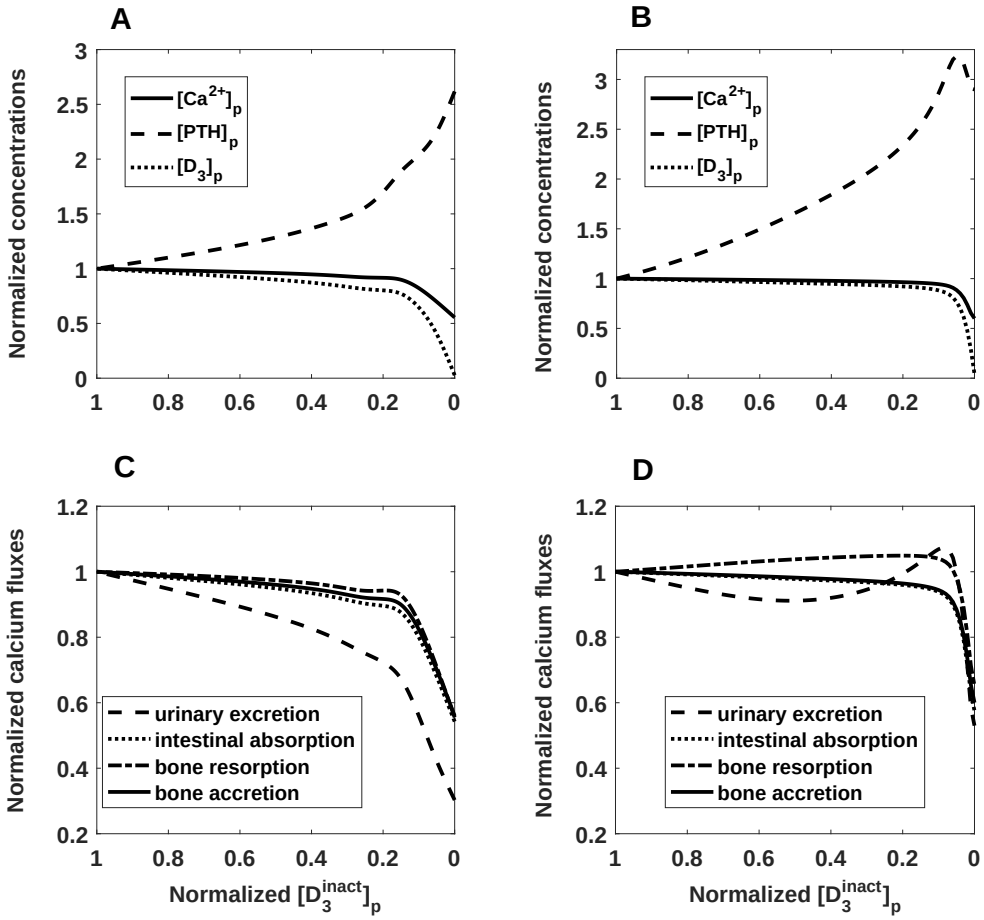


Figure 5.10: Comparison between the predictions of the Chapter 4 model and the combined calcium-phosphate model, in the case of vitamin $D_3$ deficiency. Panels A-B: normalized $Ca^{2+}$, PTH and vitamin $D_3$ plasma concentrations as a function of the normalized $[D_3^{inact}]_p$, using the Chapter 4 model (panel A) and the combined calcium-phosphate model (panel B). Panels C and D: normalized $Ca^{2+}$ fluxes, using the Chapter 4 model (panel C) and the combined calcium-phosphate model (panel D).

## 5.4 Discussion

### 5.4.1 Scope of the model

Our model of calcium and phosphate homeostasis describes $Ca^{2+}$ and $PO_4$ exchanges between the intestine, plasma, the kidneys and the two bone pools. It accounts for the regulation by PTH, vitamin $D_3$ as well as FGF23; the recent discovery of the latter means that FGF23 was ignored in all but the latest homeostasis models. This model is validated against several scenarios such as primary hyperparathyroidism [108] and phosphate infusion or gavage, which are correctly reproduced (Figures 5.5, 5.3 and 5.4).

### 5.4.2 Model limitations

Our model is hampered by the lack of data, meaning that some parameter values are uncertain. For instance, the amount of phosphate in the intracellular compartment is not known, to our knowledge, nor are the rates of exchange between $PO_4$ in plasma and cells (and inversely, between cells and plasma). The intracellular amount of $PO_4$ in rats could be measured using a similar method as the one we used to determine the quantity of calcium and phosphate in bone. It should be possible to harvest some muscles, reduce them to ashes, measure the amount of phosphate, and extrapolate these data to the whole body. This would yield at the very least an order-of-magnitude estimate of the total quantity of intracellular phosphate.

This model also involves kinetic constants related to sodium-phosphate binding, calcium-phosphate-fetuin binding and calcium-albumin reactions. Whereas the equilibrium constants of these reactions can easily be found in chemical handbooks, we were not able to obtain separate estimates of the formation and dissociation rates. Moreover, a lot of external factors are known to affect these rates, such as pH, concentration of the reactants, temperature [213, 135].

Regarding the binding of calcium and albumin, we assume a constant concentration of albumin in our model. Yet, several factors affect plasma albumin levels and ultimately plasma calcium concentration. In diabetic patients, albumin is decreased because of the reduction of insulin; besides, fasting, nephrotic syndrome, liver disease or cardiac insufficiency are other factors that affect albumin levels [148]. Nevertheless, taking all these factors into consideration is beyond the scope of this model. Nevertheless, they can be incorporated in specific situations, by modifying albumin levels in certain scenarios.

In the current state, the model does not consider the effects of insulin on phosphate metabolism [63, 149]; insulin is known to decrease urinary phosphate excretion. Nowicki and coworkers [149] also observed a reduction in PTH levels in case of hyperinsulinemia. Recent findings suggest that the reduction in plasma phosphate is responsible for the decrease of PTH [119, 188], which is already included in our model.

### 5.4.3 Calcium and phosphate metabolism

According to our simulations, when PTH synthesis is raised so that $[PTH]_p$ is doubled, calcium increases by 30% (vs 44% in the model of calcium homeostasis), while phosphate is reduced by 30%. Besides, when $[D_3^{inact}]_p$ is raised so that $[D_3]_p$ is doubled, $[Ca^{2+}]_p$ increases by 36% (vs 26% previously) whereas $[PO_4]_p$ is decreased by 27%, as a consequence of the 2-fold rise in $[FGF]_p$.

Our model does not fully support the PTH dynamics observed by Thomas *et al.* (Thomas *et al.*, JASN, in Press, 2016) following an intravenous infusion of phosphate. The discrepancy suggests that there may be a delay in the regulation of PTH synthesis by phosphate, meaning that a decrease in phosphate would not immediately lower PTH synthesis. This would explain why the observed plasma concentration of PTH stays high even after phosphate levels return to normal in the experiments of Thomas *et al.* [205]. Note that $[Ca^{2+}]_p$ is reduced by 0.5 mM (Figure 5.3, Panel C), which is not sufficient to maintain $[PTH]_p$ about 10 times above its basal value [81].

### 5.4.4 Calcium and phosphate metabolism dysfunctions

Compared to the model of calcium homeostasis in Chapter 4, less PTH is produced during primary hyperparathyroidism when phosphate is present. This is explained by the reduction in plasma phosphate levels, as a consequence of the inhibitory effects of PTH on phosphate reabsorption; since phosphate is an activator of PTH synthesis, any decrease in $[PO_4]_p$ lowers $[PTH]_p$ (Figure 1.12). The model predicts that vitamin $D_3$ plasma levels are also lower as a direct consequence of the reduction in $[PTH]_p$. Calcium urinary excretion is predicted to increase continuously as a function of the PTH production rate, whereas it did not change in monotonic manner in the previous model.

During vitamin $D_3$ deficiency, the combined calcium-phosphate model predicts that $[Ca^{2+}]_p$, $[PTH]_p$ and all calcium fluxes decrease more slowly than in the previous model. This change is a consequence of parameter adjustments we made; as described above, we modified the sensitivity of receptors to PTH and vitamin $D_3$ in bone and kidney (Table 5.9), so that the present model could correctly fit the experimental data presented in section 5.3.1.

In case of FGF23 deficiency, Shimada *et al.* found that $[D_3]_p$ is not affected immediately. However, the standard errors in their measurements are large so that they cannot detect any statistical difference. Our model predicts that vitamin $D_3$ increases by at least 40%, which is expected since one of the roles of FGF23 is to prevent vitamin $D_3$ toxicity.

In summary, the addition of phosphate to our previous model of calcium homeostasis does not radically change the behaviour of the calcium homeostasis model and improves its physiological relevance. Indeed, the present model better describes the case of primary hyperparathyroidism than the model developed in Chapter 4 (Figure 5.2). It predicts that calcium-phosphate complexation mechanisms underlie important fluctuations in the plasma concentration of calcium when phosphate is infused intravenously.

Table 5.9: Differences in the parameters of calcium metabolism between the two models.

| Organ | Parameter | Symbol | Value in Chapter 4 | Value in Chapter 5 |
|---|---|---|---|---|
| Intestine | Stimulation of absorption by vitamin $D_3$ | $K_{abs}^{D_3}$ | 100 pM | 640 pM |
| Kidney | Minimal fractional reabsorption of $Ca^{2+}$ in the PT | $\lambda_{PT}^{0}$ | 0.60 | 0.64 |
| | Stimulation of $Ca^{2+}$ reabsorption in PT by PTH | $\delta_{PT}^{max}$ | 0.05 | 0.01 |
| | Sensitivity of $Ca^{2+}$ reabsorption in TAL to PTH | $K_{TAL}^{PTH_p}$ | 1.2 pM | 4.2 pM |
| | Minimal fractional reabsorption of $Ca^{2+}$ in the DCT-CNT | $\lambda_{DCT}^{0}$ | 0.080 | 0.090 |
| | Stimulation of $Ca^{2+}$ reabsorption in the DCT-CNT by PTH and vitamin $D_3$ | $\delta_{DCT}^{max}$ | 0.020 | 0.010 |
| | Sensitivity of $Ca^{2+}$ reabsorption in the DCT-CNT to PTH | $K_{DCT}^{PTH_p}$ | 1.8 pM | 6.3 pM |
| | Sensitivity of $Ca^{2+}$ reabsorption in the DCT-CNT to vitamin $D_3$ | $K_{DCT}^{D_3}$ | 80 pM | 480 pM |
| Slow Bone | Accretion rate constant | $\Gamma_{ac}$ | 1 $min^{-1}$ | 0.5 $min^{-1}$ |
| | Minimal resorption rate | $\Gamma_{res}^{min}$ | 0.142 $\mu$mol.$min^{-1}$ | 0.10 $\mu$mol.$min^{-1}$ |
| | Maximal resorption rate | $\delta_{res}^{max}$ | 0.95 $\mu$mol.$min^{-1}$ | 0.30 $\mu$mol.$min^{-1}$ |
| | Stimulation of resorption by vitamin $D_3$ | $K_{res}^{D_3}$ | 100 pM | 600 pM |
| | Stimulation of resorption by PTH | $K_{res}^{PTH_p}$ | 1.75 pM | 16.12 pM |
| Fast Bone | Rate constant of $Ca^{2+}$ transfer from plasma to fast bone pool | $k_{pf}^{Ca}$ | 0.17 $min^{-1}$ | 0.41 $min^{-1}$ |
| | Rate constant of $Ca^{2+}$ transfer from fast bone pool to plasma | $k_{fp}^{Ca}$ | 2.75 $\times 10^{-4}$ $min^{-1}$ | 2.30 $\times 10^{-3}$ $min^{-1}$ |

# Chapter 6

# Discussion and General Conclusion

The main goal of this thesis was to build a mathematical model of calcium homeostasis based on the literature described in the Introduction. In spite of some shortcomings, the models developed from 1950 until now were very useful in building our own model. This thesis work allowed us to answer 3 of the 5 questions that were raised in Chapter 1 in section 1.4: our model yielded specific insight into the mechanisms underlying hypercalciuria during primary hyperparathyroidism, the effects of bone resorption inhibition on calcium metabolism, and the impact of an intravenous infusion of phosphate on calcium and phosphate homeostasis. The two other questions cannot be investigated with our current approach, as explained below (section 6.2).

## 6.1 What does our model bring to the understanding of calcium homeostasis?

Whereas most calcium homeostasis models developed up to now represent the kidney as a homogeneous black box compartment, our approach to represent renal $Ca^{2+}$ reabsorption is novel. Indeed, we distinguish between reabsorption along the different segments of the nephron, and we consider the effects of PTH, calcitriol, and the CaSR, in specific segments. In particular, the counteracting effects of PTH and CaSR in the thick ascending limb (TAL) may partly explain the variable behaviour of calciuria during primary hyperparathyroidism. Our model suggests that the dynamics of calciuria is strongly dependent upon the relative contribution of calcium and PTH. For example, increasing the impact of CaSR relative to that of PTH would result in enhanced $Ca^{2+}$ excretion and conversely.

Our model also takes into consideration the inhibition by PTH of $Ca^{2+}$ reabsorption in the proximal tubule, which was missing from previous studies, mainly because the underlying mechanisms are still not clear. Our predictions indicate that when the contribution of PTH is twice its basal value, urinary $Ca^{2+}$ excretion may increase by as much as a factor of 10 during primary hyperparathyroidism. Inversely, assuming no PTH effects in the proximal tubule, urinary $Ca^{2+}$ excretion remains approximately constant as the rate of PTH synthesis is increased. Altogether,

these results highlight the need to conduct experimental studies to assess the relative importance of the contribution of PTH and CaSR to renal $Ca^{2+}$ reabsorption.

In both vitamin $D_3$ deficiency and primary hypoparathyroidism, our model suggests that the calcium homeostatic system is robust enough to handle small perturbations in $[D_3^{inact}]$ and PTH synthesis, respectively. Yet, when the magnitude of perturbation increases, calcium concentration can be affected to a significant extent ($[Ca^{2+}]_p$ decreases by 50% when $[D_3^{inact}]$ is zero and -40% when PTH synthesis is zero).

Our model also accounts for all the known effects of vitamin $D_3$ on calcium metabolism, some of which were absent in previous models [157, 168]. We show that perturbations affecting vitamin $D_3$ metabolism may have noteworthy effects. For example, inactivating CYP24A1 is predicted to raise calcium intestinal absorption and bone resorption by about 50%. The subsequent reduction in PTH levels, in addition to the higher filtered load, generates significant hypercalciuria. This leads to a doubled calcemia, with the resulting consequences, which is observed experimentally [197].

Bisphosphonates are used to treat several bone diseases such as osteoporosis. Our model allows us to predict the effects of bisphosphonates on calcium metabolism. More precisely, we examined the change in plasma concentrations at steady state as a function of the degree of inhibition of bone resorption. Overall, our results suggest that complex feedback mechanisms act to compensate for the loss of calcium from bone, by increasing intestinal absorption as well as lowering calcium excretion. Consequently, this prevents plasma calcium levels from falling (only 10% of loss at maximal inhibition of resorption).

We also discuss the effects of age and sex on calcium metabolism, which were first mentioned by Hurwitz in 1987 [107] but absent in later models. Overall, our model predicts that even though calcium concentration remains stable in rats regardless of their sex and age, intestinal absorption is significantly reduced in old animals (-50% compared to young rats in both males and females) [223]. Besides, bone turnover is also halved in aging animals. Finally, urinary excretion is predicted to be lower in females due to a reduced GFR (related to weight).

Previous models such as that of Peterson and Riggs [157] already took into consideration phosphate, in addition to calcium. However, they did not consider the mechanisms of calcium and phosphate binding in plasma and bone, or the interactions between calcium and albumin. In contrast, our model accounts for all these kinetic processes. This allows us to include plasma pH as a parameter, and will make it possible to examine the impact of acidosis or alkalosis; note that the distribution of phosphate species is highly dependent on pH. Our model is also the only one, to our knowledge, that is adapted to investigate the effects of precipitation inhibitors such as Fetuin-A, so as to examine the consequences of a deficiency in this protection against calcification.

To conclude, this model is adapted to study global dysregulations in calcium and phosphate homeostasis, such as primary hyperparathyroidism, vitamin $D_3$ deficiency, as well as treatments

such as bisphosphonate or cinacalcet. Primary-hyperparathyroidism was investigated by simply increasing the synthesis of PTH, which allows the modeler to focus on the evolution of all calcium and phosphate fluxes. The simulation of treatments is more arbitrary, as discussed below.

## 6.2 What is still missing?

We must acknowledge several limitations in our current approach. Firstly, the main organs involved in calcium and phosphate metabolism are considered to be 'black boxes', which could be improved upon in the future by including the detailed organ models cited in Chapter 4, at least in the kidney. For the moment, our model cannot be used to predict urinary calcification, mainly because the kidney is modeled as a blackbox. Similarly, the current model is not suited to investigate the impact of mutations in specific transporters. Bonny and Edwards [29] developed a detailed model of calcium reabsorption across each cell of the distal convoluted and connecting tubules, which represents the specific apical and basolateral ionic transporters. They examined the effects of aldosterone, amiloride, furosemide and pH on calcium transport. In comparison, our model cannot predict the effects of inhibiting transporters such as TRPV5 or NCX1 as they do not appear explicitly in the model. More recently, Edwards published a detailed, cell-based, model of calcium reabsorption along the distal nephron, from the thick ascending limb to the inner medullary collecting duct [69]. Integrating this detailed model into our global model of calcium homeostasis would be a logical next step.

The modeling approach chosen for the bone compartment could also be improved. Indeed, in the current version of the model, the resorption rate does not depend on the quantity of bone calcium and phosphate. Until now, it was not a problem since we were not interested in the evolution of bone mass, but were focusing instead on the rapidly exchangeable pool. Yet, if we want to simulate bone mass diseases such as osteoporosis as well as osteopetrosis, we should take this into consideration. Additionally, the formation/dissociation of calcium and phosphate complexes in the deep bone is not modeled and should be considered in the future. Moreover, in section 5.1.3, we assumed that there is no exchange of calcium-phosphate complexes between plasma and bone. The reason for this assumption is the absence of parameters for these fluxes. These exchanges should be included in a further version of the model when experimental data are available.

Our model takes into account many regulatory feedback loops, as depicted in Figure 1.12. Yet, the PTH-FGF23 axis should be refined since we do not take the inhibitory effect of FGF23 on PTH synthesis, mainly because experimental data are missing.

The present model cannot be used for pharmacokinetic and pharmacodynamic simulations, unless we add specific compartments, as we did to describe the infusion of EGTA. However, this is not the main goal of the model and should be considered on an individual basis if needed. For these reasons, the remaining questions raised in 1.4, namely, the injections of vitamin $D_3$ to treat secondary hyperparathyroidism and the intestinal hyper-absorption of calcium, cannot be answered without adapting the model.

## 6.3 Further extensions?

Below we discuss a possible extension to the model, based on new experimental measurements obtained in the host laboratory in Paris.

Magnesium is an element that interacts with calcium homeostasis, especially in the kidney. Briefly, 96% of filtered magnesium is reabsorbed, of which 40 to 70% is achieved in the thick ascending limb [26, 225]. Magnesium transport occurs along with calcium through tight junctions. Moreover, it is modulated by the calcium sensing receptor, similarly as calcium, as well as by claudins (14, 16 and 19). Importantly, the CaSR can be activated by calcium and magnesium. Recent unpublished data (Tokonami and Houillier, personal communication) show that PTH-clamped rats fed with a high calcium diet have a higher urinary excretion of magnesium. Additionally, following a high magnesium diet, urinary calcium excretion rises.

Conversely, there is no evidence of coupled mechanisms between calcium and magnesium in the intestine [196], except precipitation that can occur and reduce the absorption of these ions [97].

Besides, some studies in rat parathyroid glands show that magnesium can affect parathyroid hormone secretion only under moderate hypocalcemia [174, 201, 214]. Otherwise its effects are negligible or require extremely high magnesium concentrations. Rodriguez-Ortiz and coworkers [174] observed that increasing magnesium concentration shifts the calcium-PTH curve to the left (Figure 1.19 in section 1.3.5), resulting in a decrease of the set point. Furthermore, when magnesium is increased 4-fold, the mRNA levels of CaSR and VDR are about doubled.

To include magnesium in our model is a real challenge since it has been far less studied than other ions. To our knowledge, there are no mathematical models of magnesium homeostasis. However, some balance studies are available in the rat [58], and they could serve as a basis for building a basic model of magnesium homeostasis, which could then be coupled to that of calcium and phosphate [61, 175]. It would also be fairly easy to modify the function used to model calcium reabsorption in the thick ascending limb to include the effects of magnesium on CaSR. The coupling between magnesium and phosphate is already discussed in Chapter 5 and is negligible (3% of total phosphate).

In conclusion, in addition to shedding light on complex aspects of calcium and phosphate metabolism, we hope that this model will serve as a basis for future work in the field.

# Bibliography


[1] Abraham AK, Mager DE, Gao Mi, Xand Li, Healy DR, and Maurer TS. Mechanism-based pharmacokinetic/pharmacodynamic model of parathyroid hormone-calcium homeostasis in rats and humans. *Journal of Pharmacology and Experimental Therapeutics* 330(1): 169–178, 2009.

[2] Adler EM, Augustine GJ, Duffy SN, and Charlton MP. Alien intracellular calcium chelators attenuate neurotransmitter release at the squid giant synapse. *The Journal of Neuroscience* 11(6): 1496–1507, 1991.

[3] Agus ZS, Chiu PJ, and Goldberg M. Regulation of urinary calcium excretion in the rat. *American Journal of Physiology-Renal Physiology* 232(6): F545–F549, 1977.

[4] Ajibade D, Benn BS, and Christakos S. Mechanism of action of 1,25-dihydroxyvitamin $D_3$ on intestinal calcium absorption and renal calcium transport. In: *Vitamin D: Physiology, Molecular Biology, and Clinical Applications*, edited by F. Michael Holick. Totowa, NJ: Humana Press, 2010, p. 175–187.

[5] Al-Sadi R, Boivin M, and Ma T. Mechanism of cytokine modulation of epithelial tight junction barrier. *Frontiers in bioscience: a journal and virtual library* 14: 2765–2778, 2009.

[6] Alexander RT, Dimke H, and Cordat E. Proximal tubular NHEs: sodium, protons and calcium? *American Journal of Physiology-Renal Physiology* 305(3): F229–F236, 2013.

[7] Andrukhova O, Smorodchenko A, Egerbacher M, Streicher C, Zeitz U, Goetz R, Shalhoub V, Mohammadi M, Pohl EE, Lanske B, and others . FGF23 promotes renal calcium reabsorption through the TRPV5 channel. *The EMBO Journal* 33(3): 229–246, 2014.

[8] Atkins GJ and Findlay DM. Osteocyte regulation of bone mineral: a little give and take. *Osteoporosis international* 23(8): 2067–2079, 2012.

[9] Aubert J-P, Bronner F, and Richelle LJ. Quantitation of calcium metabolism. theory. *Journal of Clinical Investigation* 42(6): 885–897, 1963.

[10] Aubert JP and Bronner F. A symbolic model for the regulation by bone metabolism of the blood calcium level in rats. *Biophysical journal* 5(3): 349–358, 1965.

[11] Aubert JP and Milhaud G. Méthode de mesure des principales voies du métabolisme calcique chez l'homme. *Biochimica et Biophysica acta* 39(1): 122–139, 1960.

[12] Barnes MS, Bonham MP, Robson PJ, Strain JJ, Lowe-Strong AS, Eaton-Evans J, Ginty F, and Wallace JMW. Assessment of 25-hydroxyvitamin D and 1,25-dihydroxyvitamin $D_3$ concentrations in male and female multiple sclerosis patients and control volunteers. *Multiple Sclerosis* 13(5): 670–672, 2007.

[13] Barnicot NA. The local action of the parathyroid and other tissues on bone in intracerebral grafts. *Journal of anatomy* 82(4): 233–248, 1948.

[14] Bellido T, Ali AA, Plotkin LI, Fu Q, Gubrij I, Roberson PK, Weinstein RS, O'Brien CA, Manolagas SC, and Jilka RL. Proteasomal degradation of Runx2 shortens parathyroid hormone-induced anti-apoptotic signaling in osteoblasts a putative explanation for why intermittent administration is needed for bone anabolism. *Journal of Biological Chemistry* 278(50): 50259–50272, 2003.

[15] Ben-Dov IZ, Galitzer H, Lavi-Moshayoff V, Goetz R, Kuro-o M, Mohammadi M, Sirkis R, Naveh-Many T, and Silver J. The parathyroid is a target organ for FGF23 in rats. *The Journal of clinical investigation* 117(12): 4003–4008, 2007.

[16] Bengele HH, Alexander EA, and Lechene CP. Calcium and magnesium transport along the inner medullary collecting duct of the rat. *American Journal of Physiology-Renal Physiology* 239(1): F24–F29, 1980.

[17] Benn BS, Ajibade D, Porta A, Dhawan P, Hediger M, Peng JB, Jiang Y, Oh GT, Jeung EB, Lieben L, and others . Active intestinal calcium transport in the absence of transient receptor potential vanilloid type 6 and calbindin-$D_{9k}$. *Endocrinology* 149(6): 3196–3205, 2008.

[18] Bergwitz C and Jüppner H. Regulation of phosphate homeostasis by PTH, vitamin D, and FGF23. *Annual review of medicine* 61: 91–104, 2010.

[19] Bergwitz C and Jüppner H. Regulation of phosphate homeostasis by PTH, vitamin D, and FGF23. *Annual Review of Medicine* 61: 91–104, 2010.

[20] Bernardo JF and Friedman PA. Renal calcium metabolism. In: *Seldin and Giebisch's The Kidney* (Fifth ed.), edited by Alpern RJ, Caplan MJ, and Moe OW. Massachusetts, Cambridge: Academic Press, 2013, p. 2225–2247.

[21] Besançon P, Guéguen L, Colette K, and Gauthier J. Les principales voies du métabolisme calcique chez le porc en croissance. *Annales de Biologie Animale Biochimie Biophysique* 9(4): 537–553, 1969.

[22] Besarab A, DeGuzman A, and Swanson JW. Effect of albumin and free calcium concentrations on calcium binding in vitro. *Journal of clinical pathology* 34(12): 1361–1367, 1981.

[23] Biber J, Hernando N, Forster I, and Murer H. Regulation of phosphate transport in proximal tubules. *Pflügers Archiv-European Journal of Physiology* 458(1): 39–52, 2009.

[24] Bichara M, Mercier O, Borensztein P, and Paillard M. Acute metabolic acidosis enhances circulating parathyroid hormone, which contributes to the renal response against acidosis in the rat. *Journal of Clinical Investigation* 86(2): 430–443, 1990.

[25] Bindels RJ, Hartog A, Timmermans J, and Van Os CH. Active $Ca^{2+}$ transport in primary cultures of rabbit kidney CCD: stimulation by 1, 25-dihydroxyvitamin $D_3$ and PTH. *American Journal of Physiology-Renal Physiology* 261(5): F799–F807, 1991.

[26] Blaine J, Chonchol M, and Levi M. Renal control of calcium, phosphate, and magnesium homeostasis. *Clinical Journal of the American Society of Nephrology* p. CJN–09750913, 2014.

[27] Blanuša M, Bogunović M, and Matković V. Kinetic parameters of calcium metabolism and femur morphometry in rats. i. influence of sex and age. *Pflügers Archiv* 375(3): 233–238, 1978.

[28] Bonewald LF and Wacker MJ. FGF23 production by osteocytes. *Pediatric nephrology* 28(4): 563–568, 2013.

[29] Bonny O and Edwards A. Calcium reabsorption in the distal tubule: regulation by sodium, ph, and flow. *American Journal of Physiology-Renal Physiology* 304(5): F585–F600, 2013.

[30] Boskey AL and Coleman R. Aging and bone. *Journal of dental research* 89(12): 1333–1348, 2010.

[31] Broadus AE, Horst RL, Lang R, Littledike ET, and Rasmussen H. The importance of circulating 1, 25-dihydroxyvitamin D in the pathogenesis of hypercalciuria and renal-stone formation in primary hyperparathyroidism. *New England Journal of Medicine* 302(8): 421–426, 1980.

[32] Bronner F. Renal calcium transport: mechanisms and regulation–an overview. *American Journal of Physiology-Renal Physiology* 257(5): F707–F711, 1989.

[33] Bronner F. Extracellular and intracellular regulation of calcium homeostasis. *The Scientific World Journal* 1: 919–925, 2001.

[34] Bronner F. Mechanisms and functional aspects of intestinal calcium absorption. *Journal of Experimental Zoology* 300(1): 47–52, 2003.

[35] Bronner F, Pansu D, and Stein WD. An analysis of intestinal calcium transport across the rat intestine. *American Journal of Physiology-Gastrointestinal and Liver Physiology* 250(5): G561–G569, 1986.

[36] Bronner F and Stein D. Calcium homeostasis: an old problem revisited. *Kinetic Models of Trace Element and Mineral Metabolism During Development* 125(7): 1987–1995, 1995.

[37] Brown EM. Four-parameter model of the sigmoidal relationship between parathyroid hormone release and extracellular calcium concentration in normal and abnormal parathyroid tissue. *The Journal of Clinical Endocrinology & Metabolism* 56(3): 572–581, 1983.

[38] Brown EM. Role of the calcium-sensing receptor in extracellular calcium homeostasis. *Best Practice & Research Clinical Endocrinology & Metabolism* 27(3): 333–343, 2013.

[39] Bushinsky DA, Neumann KJ, Asplin J, and Krieger NS. Alendronate decreases urine calcium and supersaturation in genetic hypercalciuric rats. *Kidney International* 55(1): 234–243, 1999.

[40] Bushinsky DA, Parker WR, and Asplin JR. Calcium phosphate supersaturation regulates stone formation in genetic hypercalciuric stone-forming rats. *Kidney international* 57(2): 550–560, 2000.

[41] Bushinsky DA, Riera GS, Favus MJ, and Coe FL. Evidence that blood ionized calcium can regulate serum $1,25(OH)_2D_3$ independently of parathyroid hormone and phosphorus in the rat. *Journal of Clinical Investigation* 76(4): 15991604, 1985.

[42] Canalejo R, Canalejo A, Martinez-Moreno JM, Rodriguez-Ortiz ME, Estepa JC, Mendoza FJ, Munoz-Castaneda JR, Shalhoub V, Almaden Y, and Rodriguez M. FGF23 fails to inhibit uremic parathyroid glands. *Journal of the American Society of Nephrology* 21(7): 1125–1135, 2010.

[43] Cannon WB. In: *À Charles Richet. Ses amis, ses collègues, ses élèves. 23 mai 1926*, edited by Auguste Rettit. . impr. des éditions médicales, 1926, p. 91–93.

[44] Capasso G, Geibel PJ, Damiano S, Jaeger P, Richards WG, and Geibel JP. The calcium sensing receptor modulates fluid reabsorption and acid secretion in the proximal tubule. *Kidney international* 84(2): 277–284, 2013.

[45] Capuano P, Radanovic T, Wagner CA, Bacic D, Kato S, Uchiyama Y, Arnoud RSt, and Murer J, Hand Biber. Intestinal and renal adaptation to a low-Pi diet of type ii naPi cotransporters in vitamin D receptor-and 1$\alpha$OHase-deficient mice. *American Journal of Physiology-Cell Physiology* 288(2): C429–C434, 2005.

[46] Carlsson A and Lindquist B. Comparison of intestinal and skeletal effects of vitamin D in relation to dosage. *Acta Physiologica Scandinavica* 35(1): 53–55, 1955.

[47] Carney SL and Dirks JH. Effect of parathyroid and antidiuretic hormone on water and calcium permeability in the rat collecting duct. *Mineral and electrolyte metabolism* 14(2-3): 142–145, 1987.

[48] Chanakul A, Zhang M, Louw A, Armbrecht HJ, Miller WL, Portale AA, and Perwad F. FGF-23 regulates CYP27B1 transcription in the kidney and in extra-renal tissues. *PloS one* 8(9): 1–11, 2013.

[49] Chen H, Hayakawa D, Emura S, Ozawa Y, Okumura T, and Shoumura S. Effect of low or high dietary calcium on the morphology of the rat femur. *Histology and Histopathology* 17(4): 1129–1136, 2002.

[50] Cheng Z, Liang N, Chen TH, Li A, Santa Maria C, You Ml, Ho H, Song F, Bikle D, Tu C, and others . Sex and age modify biochemical and skeletal manifestations of chronic hyperparathyroidism by altering target organ responses to $Ca^{2+}$ and parathyroid hormone in mice. *Journal of Bone and Mineral Research* 28(5): 1087–1100, 2013.

[51] Christie CR, Achenie LEK, and Ogunnaike BA. A control engineering model of calcium regulation. *The Journal of Clinical Endocrinology & Metabolism* 99(8): 2844–2853, 2014.

[52] Chughtai AR, Marshall R, and Nancollas GH. Complexes in calcium phosphate solutions. *The Journal of physical chemistry* 72(1): 208–211, 1968.

[53] Chung J, Granja I, Taylor MG, Mpourmpakis G, Asplin JR, and Rimer JD. Molecular modifiers reveal a mechanism of pathological crystal growth inhibition. *Nature* p. 1–5, 2016.

[54] Ciarelli TE, Fyhrie DP, and Parfitt AM. Effects of vertebral bone fragility and bone formation rate on the mineralization levels of cancellous bone from white females. *Bone* 32(3): 311–315, 2003.

[55] Cohn SH, Teree TM, and Gusmano EA. Effect of varying calcium intake on the parameters of calcium metabolism in the rat. *The Journal of Nutrition* 94(2): 261–267, 1968.

[56] Collazo R, Fan L, Hu MC, Zhao H, Wiederkehr MR, and Moe OW. Acute regulation of $na^+/h^+$ exchanger NHE3 by parathyroid hormone via NHE3 phosphorylation and dynamin-dependent endocytosis. *Journal of Biological Chemistry* 275(41): 31601–31608, 2000.

[57] Collip JB. The extraction of a parathyroid hormone which will prevent or control parathyroid tetany and which regulates the level of blood calcium. *Journal of Biological Chemistry* 63(2): 395–438, 1925.

[58] Cook DA. Availability of magnesium: balance studies in rats with various inorganic magnesium salts. *The Journal of nutrition* 103(9): 1365–1370, 1973.

[59] Copp DH, Cheney B, and others . Calcitonin-a hormone from the parathyroid which lowers the calcium-level of the blood. *Nature* 193: 381–382, 1962.

[60] Courbebaisse M and Souberbielle JC. Equilibre phosphocalcique: régulation et explorations. *Néphrologie & Thérapeutique* 7(2): 118–138, 2011.

[61] De Baaij JHF, Hoenderop JGJ, and Bindels RJM. Regulation of magnesium balance: lessons learned from human genetic disease. *Clinical kidney journal* 5(Suppl 1): i15–i24, 2012.

[62] Deeb KK, Trump DL, and Johnson CS. Vitamin D signalling pathways in cancer: potential for anticancer therapeutics. *Nature Reviews Cancer* 7(9): 684–700, 2007.

[63] DeFronzo RA, Cooke CR, Andres R, Faloona GR, and Davis PJ. The effect of insulin on renal handling of sodium, potassium, calcium, and phosphate in man. *Journal of Clinical Investigation* 55(4): 845–855, 1975.

[64] Del Valle HB, Yaktine AL, Taylor CL, and Ross AC. Overview of vitamin D. In: *Dietary Reference Intakes: Calcium-Vitamin D*, edited by Ross AC, Taylor CL, Yaktine AL, and Del Valle HB. D.C, Washington: National Academies Press, 2011, p. 75–125.

[65] Dick IM and Prince RL. Estrogen effects on the renal handling of calcium in the ovariectomized perfused rat. *Kidney international* 51(6): 1719–1728, 1997.

[66] Dimke H, Desai P, Borovac J, Lau A, Pan W, and Alexander RT. Activation of the $Ca^{2+}$-sensing receptor increases renal claudin-14 expression and urinary $Ca^{2+}$ excretion. *American Journal of Physiology-Renal Physiology* 304(6): F761–F769, 2013.

[67] Duque G, Daniel Rivas D, Li W, Li A, Henderson JE, Ferland G, and Gaudreau P. Age-related bone loss in the LOU/c rat model of healthy ageing. *Experimental Gerontology* 44(3): 183 – 189, 2009.

[68] Dusso AS, Brown AJ, and Slatopolsky E. Vitamin D. *American Journal of Physiology - Renal Physiology* 289(1): F8–F28, 2005.

[69] Edwards A. Regulation of calcium reabsorption along the rat nephron: A modeling study. *American Journal of Physiology-Renal Physiology* 308(6): F553–F566, 2015.

[70] Egbuna O, Quinn S, Kantham L, Butters R, Pang J, Pollak M, Goltzman D, and Brown E. The full-length calcium-sensing receptor dampens the calcemic response to $1\alpha$, 25 $(OH)_2$ vitamin $D_3$ in vivo independently of parathyroid hormone. *American Journal of Physiology-Renal Physiology* 297(3): F720–F728, 2009.

[71] Faivre-Defrance F, Marcelli-Tourvieille S, Odou M-F, Porchet N, Wemeau J-L, and Vantyghem M-C. Le récepteur sensible au calcium: physiologie et pathologie. *Annales d' Endocrinologie* 67(1): 45–53, 2006.

[72] Favus MJ, Bushinsky DA, and Lemann J. Regulation of calcium, magnesium, and phosphate metabolism. In: *Primer on the metabolic bone diseases and disorders of mineral metabolism* (Sixth ed.). Ann Harbor: American Society for Bone and Mineral Research, 2006, p. 76–83.

[73] Feher JJ, Fullmer CS, and Wasserman RH. Role of facilitated diffusion of calcium by calbindin in intestinal calcium absorption. *American Journal of Physiology-Cell Physiology* 262(2): C517–C526, 1992.

[74] Feldman RS, Krieger NS, and Tashjian Jr AH. Effects of parathyroid hormone and calcitonin on osteoclast formation in vitro. *Endocrinology* 107(4): 1137–1143, 1980.

[75] Felsenfeld AJ, Jara A, Avedian G, and Kleeman CR. Effects of fasting, feeding, and bisphosphonate administration on serum calcitriol levels in phosphate-deprived rats. *Kidney International* 58(3): 1016–1022, 2000.

[76] Fleck C. Determination of the glomerular filtration rate (GFR) methodological problems, age-dependence, consequences of various surgical interventions, and the influence of different drugs and toxic substances. *Physiological research Academia Scientiarum Bohemoslovaca* 48(4): 267–279, 1998.

[77] Fleet JC and Schoch RD. Molecular mechanisms for regulation of intestinal calcium absorption by vitamin D and other factors. *Critical Reviews in Clinical Laboratory Sciences* 47(4): 181–195, 2010.

[78] Fleisch H. The bisphosphonate ibandronate, given daily as well as discontinuously, decreases bone resorption and increases calcium retention as assessed by $^{45}$Ca kinetics in the intact rat. *Osteoporosis International* 6(2): 166–170, 1996.

[79] Fogh-Andersen N. Albumin/calcium association at different ph, as determined by potentiometry. *Clinical chemistry* 23(11): 2122–2126, 1977.

[80] Forsen S and Kordel J. Calcium in biological systems. In: *Bioinorganic Chemistry*, edited by I Bertini, HB Gray, SJ Lippard, and JS Valentine. Mill Valey, California: University Science Books: Mill Valley, CA, 1994, p. 107–166.

[81] Fox J. Regulation of parathyroid hormone secretion by plasma calcium in aging rats. *American Journal of Physiology-Endocrinology and Metabolism* 260(2): E220–E225, 1991.

[82] Friedman PA. Mechanisms of renal calcium transport. *Nephron Experimental Nephrology* 8(6): 343–350, 2000.

[83] Friedman PA and Gesek FA. Cellular calcium transport in renal epithelia: measurement, mechanisms, and regulation. *Physiological Reviews* 75(3): 429–471, 1995.

[84] Fujita H, Sugimoto K, Inatomi S, Maeda T, Osanai M, Uchiyama Y, Yamamoto Y, Wada T, Kojima T, Yokozaki H, and others . Tight junction proteins claudin-2 and-12 are critical for vitamin D-dependent $Ca^{2+}$ absorption between enterocytes. *Molecular Biology of the Cell* 19(5): 1912–1921, 2008.

[85] Fukumoto S. Phosphate metabolism and vitamin D. *BoneKEy reports* 3: 1–5, 2014.

[86] Gama L, Baxendale-Cox LM, and Breitwieser GE. $Ca^{2+}$-sensing receptors in intestinal epithelium. *American Journal of Physiology-Cell Physiology* 273(4): C1168–C1175, 1997.

[87] Gardella TJ and Jüppner H. Molecular properties of the PTH/PTHrP receptor. *Trends in Endocrinology & Metabolism* 12(5): 210–217, 2001.

[88] Garg MK and Mahalle N. Calcium homeostasis, and clinical or subclinical vitamin D deficiency–can a hypothesis of intestinal calcistat explain it all? *Medical hypotheses* 81(2): 253–258, 2013.

[89] Geibel JP and Hebert SC. The functions and roles of the extracellular $Ca^{2+}$-sensing receptor along the gastrointestinal tract. *Annual Review of Physiology* 71: 205–217, 2009.

[90] Gennero I, Moulin P, Edouard T, Conte-Auriol F, Tauber MT, and Salles JP. Métabolisme minéral osseux: données récentes et perspectives relatives à l'ostéogenèse. *Archives de Pédiatrie* 11(12): 1473–1483, 2004.

[91] Grases F, Söhnel O, Vilacampa AI, and March JG. Phosphates precipitating from artificial urine and fine structure of phosphate renal calculi. *Clinica chimica acta* 244(1): 45–67, 1996.

[92] Gray RW. Control of plasma 1, 25-$(OH)_2$-vitamin D concentrations by calcium and phosphorus in the rat: effects of hypophysectomy. *Calcified tissue international* 33(1): 485–488, 1981.

[93] Gray RW. Control of plasma 1,25-$(OH)_2$-vitamin D concentrations by calcium and phosphorus in the rat: effects of hypophysectomy. *Calcified Tissue International* 33(1): 485–488, 1981.

[94] Greger R, Lang F, Oberleithner H, and Deetjen P. Handling of oxalate by the rat kidney. *Pflügers Archiv* 374(3): 243–248, 1978.

[95] H Juppner and Portale AA. Endocrine regulation of phosphate homeostasis. In: *Textbook of Nephro-Endocrinology* (First ed.), edited by AK Singh and GH Williams. San Diego: Academic Press, 2009, p. 105 –126.

[96] Haden ST, Brown EM, Hurwitz S, Scott J, and Fuleihan G. The effects of age and gender on parathyroid hormone dynamics. *Clinical Endocrinology* 52(3): 329–338, 2000.

[97] Haderslev KV, Jeppesen PB, Mortensen PB, and Staun M. Absorption of calcium and magnesium in patients with intestinal resections treated with medium chain fatty acids. *Gut* 46(6): 819–823, 2000.

[98] Halloran B, Uden P, Duh QY, Kikuchi S, Wieder T, Cao J, and Clark O. Parathyroid gland volume increases with postmaturational aging in the rat. *American Journal of Physiology-Endocrinology and Metabolism* 282(3): E557–E563, 2002.

[99] Heideger WJ and Ferguson ME. A theoretical model for calcium absorption from the intestinal lumen. *Journal of Theoretical Biology* 114(4): 657–664, 1985.

[100] Heiss A, Pipich V, Jahnen-Dechent W, and Schwahn D. Fetuin-A is a mineral carrier protein: small angle neutron scattering provides new insight on fetuin-A controlled calcification inhibition. *Biophysical journal* 99(12): 3986–3995, 2010.

[101] Herbert FK, Miller HG, and Richardson GO. Chronic renal disease, secondary parathyroid hyperplasia, decalcification of bone and metastatic calcification. *The Journal of Pathology and Bacteriology* 53(2): 161–182, 1941.

[102] Herrmann M, Schäfer C, Heiss A, Gräber S, Kinkeldey A, Büscher A, Schmitt MMN, Bornemann J, Nimmerjahn F, Herrmann M, and others . Clearance of fetuin-A–containing calciprotein particles is mediated by scavenger receptor-A. *Circulation research* 111(5): 575–584, 2012.

[103] Hoenderop JGJ, Müller D, Kemp Van der AWCM, Hartog A, Suzuki M, Ishibashi K, Imai Mi, Sweep F, Willems PHGM, Van Os CH, and others . Calcitriol controls the epithelial calcium channel in kidney. *Journal of the American Society of Nephrology* 12(7): 1342–1349, 2001.

[104] Hoenderop JGJ, Nilius B, and Bindels RJM. Calcium absorption across epithelia. *Physiological reviews* 85(1): 373–422, 2005.

[105] Hsu YJ, Dimke H, Schoeber JPH, Hsu SC, Lin SH, Chu P, Hoenderop JGJ, and Bindels RJM. Testosterone increases urinary calcium excretion and inhibits expression of renal calcium transport proteins. *Kidney international* 77(7): 601–608, 2010.

[106] Hurwitz S, Fishman S, Bar A, Pines M, Riesenfeld G, and Talpaz H. Simulation of calcium homeostasis: modeling and parameter estimation. *American Journal of Physiology-Regulatory, Integrative and Comparative Physiology* 245(5): R664–R672, 1983.

[107] Hurwitz S, Fishman S, and Talpaz H. Model of plasma calcium regulation: system oscillations induced by growth. *American Journal of Physiology-Regulatory, Integrative and Comparative Physiology* 252(6): R1173–R1181, 1987.

[108] Jaeger P, Jones W, Kashgarian M, Baron R, Clemens TL, Segre GV, and Hayslett JP. Animal model of primary hyperparathyroidism. *American Journal of Physiology-Endocrinology And Metabolism* 252(6): E790–E798, 1987.

[109] Jahan I and Pitts RF. Effect of parathyroid on renal tubular reabsorption of phosphate and calcium. *American Journal of Physiology–Legacy Content* 155(1): 42–49, 1948.

[110] Jahnen-Dechent W, Heiss A, Schäfer C, and Ketteler M. Fetuin-A regulation of calcified matrix metabolism. *Circulation research* 108(12): 1494–1509, 2011.

[111] Jin SE, Park JS, and Kim CK. Pharmacokinetics of oral calcitriol in healthy human based on the analysis with an enzyme immunoassay. *Pharmacological Research* 60(1): 57–60, 2009.

[112] Jones G, Prosser DE, and Kaufmann M. 25-hydroxyvitamin D-24-hydroxylase (CYP24A1): its important role in the degradation of vitamin D. *Archives of biochemistry and biophysics* 523(1): 9–18, 2012.

[113] Karbach U. Paracellular calcium transport across the small intestine. *The Journal of nutrition* 122(3S): 672–677, 1992.

[114] Kempson SA, Lotscher M, Kaissling B, Biber J, Murer H, and Levi M. Parathyroid hormone action on phosphate transporter mRNA and protein in rat renal proximal tubules. *American Journal of Physiology-Renal Physiology* 268(4): F784–F791, 1995.

[115] Kenny AD. Urinary calcium response to chronic parathyroidectomy in rats. *Endocrinology* 79(1): 77–80, 1966.

[116] Khan RS and Hackett RL. Pathological crystallization of calcium oxalate and calcium phosphate. In: *Hydroxyapatite and related materials*, edited by PW Brown and B Constantz. Boca Raton, Florida: CRC press, 1994, p. 83–92.

[117] Khanal RC and Nemere I. Regulation of intestinal calcium transport. *Annual Review of Nutrition* 28: 179–196, 2008.

[118] Khosravi A, Cutler CM, Kelly MH, Chang R, Royal RE, Sherry RM, Wodajo FM, Fedarko NS, and Collins MT. Determination of the elimination half-life of fibroblast growth factor-23. *The Journal of Clinical Endocrinology & Metabolism* 92(6): 2374–2377, 2007.

[119] Kilav R, Silver J, and Naveh-Many T. Parathyroid hormone gene expression in hypophosphatemic rats. *Journal of Clinical Investigation* 96(1): 327–333, 1995.

[120] Kini U and Nandeesh BN. Physiology of bone formation, remodeling, and metabolism. In: *Radionuclide and Hybrid Bone Imaging*, edited by Fogelman I, Gnanasegaran G, and van der Wall H. Berlin: Springer, 2012, p. 29–57.

[121] Klein L. Steady-state relationship of calcium-$^{45}$ between bone and blood: differences in growing dogs, chicks, and rats. *Science* 214(4517): 190–193, 1981.

[122] Knop J, Reichstein K-H, and Montz R. A $^{47}$Calcium kinetic model with two bone compartments. *European Journal of Nuclear Medicine* 2(1): 35–41, 1977.

[123] Komaba H and Fukagawa M. FGF23–parathyroid interaction: implications in chronic kidney disease. *Kidney international* 77(4): 292–298, 2010.

[124] Krajisnik T, Björklund P, Marsell R, Ljunggren Ö, Åkerström G, Jonsson KB, Westin G, and Larsson TE. Fibroblast growth factor-23 regulates parathyroid hormone and 1$\alpha$-hydroxylase expression in cultured bovine parathyroid cells. *Journal of Endocrinology* 195(1): 125–131, 2007.

[125] Kurbel S, Radic R, Kotromanovic Z, Puseljic Z, and Kratofil B. A calcium homeostasis model: orchestration of fast acting PTH and calcitonin with slow calcitriol. *Medical Hypotheses* 61(3): 346 – 350, 2003.

[126] Kuro-o M. Calciprotein particle (CPP): a true culprit of phosphorus woes? *Nefrologia* 34(1): 1–4, 2014.

[127] Lee HB and Blaufox MD. Blood volume in the rat. *Journal of Nuclear Medicine* 26(1): 72–76, 1985.

[128] Lee WH, Cho BK, and Okos MR. A theoretical modeling for suggesting unique mechanism of adolescent calcium metabolism. *Journal of Biosystems Engineering* 38(2): 1–9, 2013.

[129] Lemaire V, Tobin FL, Greller LD, Cho CR, and Suva LJ. Modeling the interactions between osteoblast and osteoclast activities in bone remodeling. *Journal of Theoretical Biology* 229(3): 293–309, 2004.

[130] Levi M, Ellis MA, and Berl T. Control of renal hemodynamics and glomerular filtration rate in chronic hypercalcemia: role of prostaglandins, renin-angiotensin system, and calcium. *Journal of Clinical Investigation* 71(6): 1624, 1983.

[131] Levi M and Popovtzer M. Disorders of phosphate balance. In: *Atlases of Diseases of the Kidney* (First ed.), edited by Tomas Berl. Philadelphia: Current Medicine, 1999, p. 1–14.

[132] Lewin E, Wang W, and Olgaard K. Rapid recovery of plasma ionized calcium after acute induction of hypocalcaemia in parathyroidectomized and nephrectomized rats. *Nephrology Dialysis Transplantation* 14(3): 604–609, 1999.

[133] Liu S and Quarles LD. How fibroblast growth factor 23 works. *Journal of the American Society of Nephrology* 18(6): 1637–1647, 2007.

[134] Loupy A, Ramakrishnan SK, Wootla B, Chambrey R, De La Faille R, Bourgeois S, Bruneval P, Mandet C, Christensen EI, Faure H, and others . PTH-independent regulation of blood calcium concentration by the calcium-sensing receptor. *The Journal of Clinical Investigation* 122(9): 3355–3367, 2012.

[135] Lu X and Leng Y. Theoretical analysis of calcium phosphate precipitation in simulated body fluid. *Biomaterials* 26(10): 1097–1108, 2005.

[136] Magaldi AJ, Baak van AA, and Rocha AS. Calcium transport across rat inner medullary collecting duct perfused in vitro. *American Journal of Physiology-Renal Physiology* 257(5): F738–F745, 1989.

[137] Marenzana M, Shipley AM, Squitiero P, Kunkel JG, and Rubinacci A. Bone as an ion exchange organ: evidence for instantaneous cell-dependent calcium efflux from bone not due to resorption. *Bone* 37(4): 545–554, 2005.

[138] Marks J, Srai SK, Biber J, Murer H, Unwin RJ, and Debnam ES. Intestinal phosphate absorption and the effect of vitamin D: a comparison of rats with mice. *Experimental physiology* 91(3): 531–537, 2006.

[139] Martin A, David V, and Quarles LD. Regulation and function of the FGF23/klotho endocrine pathways. *Physiological Reviews* 92(1): 131–155, 2012.

[140] Martin DR, Ritter CS, Slatopolsky E, and Brown AJ. Acute regulation of parathyroid hormone by dietary phosphate. *American Journal of Physiology-Endocrinology and Metabolism* 289(4): E729–E734, 2005.

[141] Meir T, Durlacher K, Pan Z, Amir G, Richards WG, Silver J, and Naveh-Many T. Parathyroid hormone activates the orphan nuclear receptor Nurr1 to induce FGF23 transcription. *Kidney international* 86(6): 1106–1115, 2014.

[142] Meyer MB, Watanuki M, Kim S, Shevde NK, and Pike JW. The human transient receptor potential vanilloid type 6 distal promoter contains multiple vitamin D receptor binding sites that mediate activation by 1, 25-dihydroxyvitamin $D_3$ in intestinal cells. *Molecular endocrinology* 20(6): 1447–1461, 2006.

[143] Migneault DR and Forcé RK. Dissociation constants of phosphoric acid at 25 c and the ion pairing of sodium with orthophosphate ligands at 25 c. *Journal of solution chemistry* 17(10): 987–997, 1988.

[144] Momsen G and Schwarz P. A mathematical/physiological model of parathyroid hormone secretion in response to blood-ionized calcium lowering in vivo. *Scandinavian journal of clinical and laboratory investigation* 57(5): 381–394, 1997.

[145] Murayama A, Takeyama Ki, Kitanaka S, Kodera Y, Kawaguchi Y, Hosoya T, and Kato S. Positive and negative regulations of the renal 25-hydroxyvitamin $D_3$ 1$\alpha$-hydroxylase gene by parathyroid hormone, calcitonin, and 1$\alpha$,25$(OH)_2D_3$ in intact animals. *Endocrinology* 140(5): 2224–2231, 1999.

[146] Naveh-Many T, Rahamimov R, Livni N, and Silver J. Parathyroid cell proliferation in normal and chronic renal failure rats. the effects of calcium, phosphate, and vitamin D. *Journal of Clinical Investigation* 96(4): 1786–1793, 1995.

[147] Negrea L, Slatopolsky E, and Dusso A. Lower affinity for substrate for extrarenal synthesis of calcitriol in chronic uremia. *Kidney International* 44(1): 134–134, 1993.

[148] Nicholson JP, Wolmarans MR, and Park GR. The role of albumin in critical illness. *British journal of anaesthesia* 85(4): 599–610, 2000.

[149] Nowicki M, Kokot F, and Surdacki A. The influence of hyperinsulinaemia on calcium-phosphate metabolism in renal failure. *Nephrology Dialysis Transplantation* 13(10): 2566–2571, 1998.

[150] Okano T, Kimura T, Tsugawa N, Okamura Y, and Kobayashi T. Roles of parathyroid hormone and 1$\alpha$, 25-dihydroxyvitamin $D_3$ in bone growth of growing male and female rats. *Journal of Bone and Mineral Metabolism* 12(1): S23–S26, 1994.

[151] Orimo H. The mechanism of mineralization and the role of alkaline phosphatase in health and disease. *Journal of Nippon Medical School* 77(1): 4–12, 2010.

[152] Öz OK, Hajibeigi A, Howard K, Cummins CL, Van Abel M, Bindels RJM, Word R, Kuro-o M, Pak CYC, and Zerwekh JE. Aromatase deficiency causes altered expression of molecules critical for calcium reabsorption in the kidneys of female mice. *Journal of Bone and Mineral Research* 22(12): 1893–1902, 2007.

[153] Pan W, Borovac J, Spicer Z, Hoenderop JG, Bindels RJ, Shull GE, Doschak MR, Cordat E, and Alexander RT. The epithelial sodium/proton exchanger, NHE3, is necessary for renal and intestinal calcium (re) absorption. *American Journal of Physiology-Renal Physiology* 302(8): F943–F956, 2012.

[154] Parfitt AM. Calcium homeostasis. In: *Physiology and Pharmacology of Bone*, edited by Mundy GR and Martin TJ. Heidelberg: Springer Berlin Heidelberg, 1993, p. 1–65.

[155] Pasch A, Farese S, Gräber S, Wald J, Richtering W, Floege J, and Jahnen-Dechent W. Nanoparticle-based test measures overall propensity for calcification in serum. *Journal of the American Society of Nephrology* 23: 17441752„ 2012.

[156] Penido MG and Alon US. Phosphate homeostasis and its role in bone health. *Pediatric Nephrology* 27(11): 2039–2048, 2012.

[157] Peterson MC and Riggs MM. A physiologically based mathematical model of integrated calcium homeostasis and bone remodeling. *Bone* 46(1): 49–63, 2010.

[158] Pirklbauer M and Mayer G. The exchangeable calcium pool: physiology and pathophysiology in chronic kidney disease. *Nephrology Dialysis Transplantation* 26(8): 2438–2444, 2011.

[159] Pivonka P, Zimak J, Smith DW, Gardiner BS, Dunstan CR, Sims NA, Martin TJ, and Mundy GR. Model structure and control of bone remodeling: a theoretical study. *Bone* 43(2): 249–263, 2008.

[160] Powell T. A mathematical model for calcium homeostasis. *The Bulletin of mathematical biophysics* 34(4): 483–502, 1972.

[161] Pramod KL, Vaswani VR, and others . Museum preservation of skeleton of fetus & small vertebrates. *Recent Research in Science and Technology* 3(2): 54–58, 2011.

[162] Prasad N, Bhadauria D, and others . Renal phosphate handling: Physiology. *Indian journal of endocrinology and metabolism* 17(4): 620–627, 2013.

[163] Price PA and Lim JE. The inhibition of calcium phosphate precipitation by fetuin is accompanied by the formation of a fetuin-mineral complex. *Journal of Biological Chemistry* 278(24): 22144–22152, 2003.

[164] Price PA, Thomas GR, Pardini AW, Figueira WF, Caputo JM, and Williamson MK. Discovery of a high molecular weight complex of calcium, phosphate, fetuin, and matrix $\gamma$-carboxyglutamic acid protein in the serum of etidronate-treated rats. *Journal of Biological Chemistry* 277(6): 3926–3934, 2002.

[165] Pruett WA and Hester RL. Parathyroid hormone secretion by multiple distinct cell populations, a time dynamic mathematical model. *Physiological Reports* 2(2): 1–10, 2014.

[166] Qing H and Bonewald LF. Osteocyte remodeling of the perilacunar and pericanalicular matrix. *International journal of oral science* 1(2): 59–65, 2009.

[167] Ramakrishnan V, Yang QJ, Quach HP, Cao Y, Chow ECY, Mager DE, and Pang KS. Physiologically-based pharmacokinetic-pharmacodynamic modeling of $1\alpha$, 25-dihydroxyvitamin $D_3$ in mice. *Drug Metabolism and Disposition* 44(2): 189–208, 2016.

[168] Raposo JF, Sobrinho LG, and Ferreira HG. A minimal mathematical model of calcium homeostasis. *The Journal of Clinical Endocrinology & Metabolism* 87(9): 4330–4340, 2002.

[169] Reitsma PH, Bijvoet OLM, Verlinden-Ooms H, and Wee-Pals van der LJA. Kinetic studies of bone and mineral metabolism during treatment with (3-amino-1-hydroxypropylidene)-1, 1-bisphosphonate (APD) in rats. *Calcified Tissue International* 32(1): 145–157, 1980.

[170] Riccardi D, Hall AE, Chattopadhyay N, Xu JZ, Brown EM, and Hebert SC. Localization of the extracellular $Ca^{2+}$/polyvalent cation-sensing protein in rat kidney. *American Journal of Physiology-Renal Physiology* 274(3): F611–F622, 1998.

[171] Riches AC, Sharp JG, Thomas DB, and Smith SV. Blood volume determination in the mouse. *The Journal of physiology* 228(2): 279–284, 1973.

[172] Rizzoli R, Fleisch H, and Bonjour J-Ph. Role of 1, 25-dihydroxyvitamin $D_3$ on intestinal phosphate absorption in rats with a normal vitamin D supply. *Journal of Clinical Investigation* 60(3): 639–647, 1977.

[173] Robertson WG. Methods for diagnosing the risk factors of stone formation. *Arab journal of urology* 10(3): 250–257, 2012.

[174] Rodríguez-Ortiz ME, Canalejo A, Herencia C, MM Julio M, Peralta-Ramírez A, Perez-Martinez P, Navarro-González JF, Rodríguez M, Peter M, Gundlach K, and others . Magnesium modulates parathyroid hormone secretion and upregulates parathyroid receptor expression at moderately low calcium concentration. *Nephrology Dialysis Transplantation* 29(2): 282–289, 2014.

[175] Romani A. Regulation of magnesium homeostasis and transport in mammalian cells. *Archives of Biochemistry and Biophysics* 458(1): 90–102, 2007.

[176] Rouse D, Sessoms S, Stinebaugh BJ, and Suki WN. The effect of hypocalcemia on renal bicarbonate absorption. *Mineral and Electrolyte Metabolism* 10(1): 31–35, 1983.

[177] Sabbagh Yv, Giral H, Caldas Y, Levi M, and Schiavi SC. Intestinal phosphate transport. *Advances in chronic kidney disease* 18(2): 85–90, 2011.

[178] Sahni M, Guenther HL, Fleisch H, Collin P, and Martin TJ. Bisphosphonates act on rat bone resorption through the mediation of osteoblasts. *Journal of Clinical Investigation* 91(5): 2004–2011, 1993.

[179] Saito H, Maeda A, Ohtomo SI, Hirata M, Kusano K, Kato S, Ogata E, Segawa H, Miyamoto KI, and Fukushima N. Circulating FGF-23 is regulated by $1\alpha$, 25-dihydroxyvitamin D3*andphosphorusinvivo*. *JournalofBiologicalChemistry*280(4) : 2543 − −2549, 2005.

[180] Sammon PJ, Stacey RE, Bronner F, and others . Role of parathyroid hormone in calcium homeostasis and metabolism. *American Journal of Physiology* 218(2): 479–485, 1970.

[181] Schlingmann KP, Kaufmann M, Weber S, Irwin A, Goos C, John U, Misselwitz J, Klaus G, Kuwertz-Bröking E, Fehrenbach H, and others . Mutations in CYP24A1 and idiopathic infantile hypercalcemia. *New England Journal of Medicine* 365(5): 410–421, 2011.

[182] Schwarz P, Madsen JC, Rasmussen AQ, Transbøl Lb, and Brown EM. Evidence for a role of intracellular stored parathyroid hormone in producing hysteresis of the PTH–calcium relationship in normal humans. *Clinical endocrinology* 48(6): 725–732, 1998.

[183] Sharma A, Ebling WF, and Jusko WJ. Precursor-dependent indirect pharmacodynamic response model for tolerance and rebound phenomena. *Journal of pharmaceutical sciences* 87(12): 1577–1584, 1998.

[184] Shimada T, Hasegawa H, Yamazaki Y, Muto T, Hino R, Takeuchi Y, Fujita T, Nakahara K, Fukumoto S, and Yamashita T. FGF-23 is a potent regulator of vitamin D metabolism and phosphate homeostasis. *Journal of Bone and Mineral Research* 19(3): 429–435, 2004.

[185] Shimada T, Kakitani M, Yamazaki Y, Hasegawa H, Takeuchi Y, Fujita T, Fukumoto S, Tomizuka K, and Yamashita T. Targeted ablation of fgf23 demonstrates an essential physiological role of FGF23 in phosphate and vitamin D metabolism. *The Journal of clinical investigation* 113(4): 561–568, 2004.

[186] Shimada T, Yamazaki Y, Takahashi M, Hasegawa H, Urakawa I, Oshima T, Ono K, Kakitani M, Tomizuka K, Fujita T, and others . Vitamin D receptor-independent FGF23 actions in

regulating phosphate and vitamin D metabolism. *American Journal of Physiology-Renal Physiology* 289(5): F1088–F1095, 2005.

[187] Shrestha RP, Hollot CV, Chipkin SR, Schmitt CP, and Chait Y. A mathematical model of parathyroid hormone response to acute changes in plasma ionized calcium concentration in humans. *Mathematical Biosciences* 226(1): 46–57, 2010.

[188] Silver J and Naveh-Many T. Phosphate and the parathyroid. *Kidney international* 75(9): 898–905, 2009.

[189] Silver J, Naveh-Many T, Mayer H, Schmelzer HJ, and Popovtzer MM. Regulation by vitamin D metabolites of parathyroid hormone gene transcription in vivo in the rat. *Journal of Clinical Investigation* 78(5): 1296–1301, 1986.

[190] Silver J, Yalcindag C, Sela-Brown A, Kilav R, and Naveh-Many T. Regulation of the parathyroid hormone gene by vitamin D, calcium and phosphate. *Kidney International* 56: S2–S7, 1999.

[191] Slepchenko BM and Bronner F. Modeling of transcellular Ca transport in rat duodenum points to coexistence of two mechanisms of apical entry. *American Journal of Physiology-Cell Physiology* 281(1): C270–C281, 2001.

[192] Smith ER, Cai MM, McMahon LP, Pedagogos E, Toussaint ND, Brumby C, and Holt SG. Serum fetuin-A concentration and fetuin-A-containing calciprotein particles in patients with chronic inflammatory disease and renal failure. *Nephrology* 18(3): 215–221, 2013.

[193] Smith PD, Liesegang GW, Berger RL, Czerlinski G, and Podolsky RJ. A stopped-flow investigation of calcium ion binding by ethylene glycol bis ($\beta$-aminoethyl ether)-n, n'-tetraacetic acid. *Analytical Biochemistry* 143(1): 188–195, 1984.

[194] Solovey G, Fraiman D, Pando B, and Ponce Dawson S. Simplified model of cytosolic $Ca^{2+}$ dynamics in the presence of one or several clusters of $Ca^{2+}$-release channels. *Physical Review E* 78(4): 1–15, 2008.

[195] Somerville PJ and Kaye M. Action of phosphorus on calcium release in isolated perfused rat tails. *Kidney international* 22(4): 348–354, 1982.

[196] Spencer H, Fuller H, Norris C, and Williams D. Effect of magnesium on the intestinal absorption of calcium in man. *Journal of the American College of Nutrition* 13(5): 485–492, 1994.

[197] St-Arnaud R, Arabian A, Travers R, Barletta F, Raval-Pandya M, Chapin K, Depovere J, Mathieu C, Christakos S, Demay MB, and others . Deficient mineralization of intramembranous bone in vitamin D-24-hydroxylase-ablated mice is due to elevated 1, 25-dihydroxyvitamin D and not to the absence of 24, 25-dihydroxyvitamin D1. *Endocrinology* 141(7): 2658–2666, 2000.

[198] Stenvinkel P, Wang K, Qureshi AR, Axelsson J, Pecoits-Filho R, Gao P, Barany P, Lindholm B, Jogestrand T, Heimberger O, and others . Low fetuin-A levels are associated with cardiovascular death: impact of variations in the gene encoding fetuin. *Kidney international* 67(6): 2383–2392, 2005.

[199] Sun F, Ritchie CK, Hassager C, Maercklein P, and Fitzpatrick LA. Heterogeneous response to calcium by individual parathyroid cells. *Journal of Clinical Investigation* 91(2): 595–601, 1993.

[200] Takahashi N, Udagawa N, and Suda T. Vitamin D endocrine system and osteoclasts. *BoneKEy Reports* 3: 1–9, 2014.

[201] Takatsuki K, Hanley DA, and Sherwood LM. Effects of magnesium ion on parathyroid hormone secretion in vitro. *Calcified tissue international* 32(1): 201–206, 1980.

[202] Tani Y, Sato T, Yamanaka-Okumura H, Yamamoto H, Arai H, Sawada N, Genjida K, Taketani Y, and Takeda E. Effects of prolonged high phosphorus diet on phosphorus and calcium balance in rats. *Journal of clinical biochemistry and nutrition* 40(3): 221–228, 2007.

[203] Tenenhouse HS and Portale AA. Phosphate homeostasis. In: *Vitamin D* (Second ed.), edited by DAVID FELDMAN. Burlington: Academic Press, 2005, p. 453 – 475.

[204] Tepel M, Armbruster FP, Grön HJ, Scholze A, Reichetzeder C, Roth HJ, and Hocher B. Nonoxidized, biologically active parathyroid hormone determines mortality in hemodialysis patients. *The Journal of Clinical Endocrinology & Metabolism* 98(12): 4744–4751, 2013.

[205] Thomas L, Bettoni C, Knpfel T, Hernando N, Biber J, and Wagner CA. Parathyroid hormone is critical for the acute adaption to oral or intravenous phosphate loading. *Journal of the American Society of Nephrology* In Press, 2016.

[206] Tiselius HG. Measurement of the risk of calcium phosphate crystallization in urine. *Urological research* 15(2): 79–81, 1987.

[207] Tiselius HG, Ferraz RRN, and Heilberg IP. Simplified estimates of ion-activity products of calcium oxalate and calcium phosphate in mouse urine. *Urological research* 40(4): 285–291, 2012.

[208] Toffaletti J and Abrams B. Effects of in vivo and in vitro production of lactic acid on ionized, protein-bound, and complex-bound calcium in blood. *Clinical Chemistry* 35(6): 935–938, 1989.

[209] Urena P, Mannstadt M, Hruby M, Ferriera A, Schmitt F, Silve C, Ardaillou R, Lacour B, Abou-Samra AB, Segre GV, and others . Parathyroidectomy does not prevent the renal PTH/PTHrP receptor down-regulation in uremic rats. *Kidney International* 47(6): 1797–1805, 1995.

[210] Vallet M and Tack I. Physiologie du calcium et des phosphates. *Revue du Rhumatisme Monographies* 79(4): 203–209, 2012.

[211] Van Abel M, Hoenderop JGJ, Kemp Van der AWCM, Friedlaender MM, Van Leeuwen JPTM, and Bindels RJM. Coordinated control of renal $Ca^{2+}$ transport proteins by parathyroid hormone. *Kidney International* 68(4): 1708–1721, 2005.

[212] Van Cromphaut SJ, Dewerchin M, Hoenderop JGJ, Stockmans I, Van Herck E, Kato S, Bindels RJM, Collen D, Carmeliet P, Bouillon R, and others . Duodenal calcium absorption in vitamin D receptor–knockout mice: functional and molecular aspects. *Proceedings of the National Academy of Sciences* 98(23): 13324–13329, 2001.

[213] Van Kemenade MJJM and De Bruyn PL. A kinetic study of precipitation from supersaturated calcium phosphate solutions. *Journal of Colloid and Interface Science* 118(2): 564–585, 1987.

[214] Vetter T and Lohse MJ. Magnesium and the parathyroid. *Current opinion in nephrology and hypertension* 11(4): 403–410, 2002.

[215] Wald J, Wiese S, Eckert T, Jahnen-Dechent W, Richtering W, and Heiss A. Formation and stability kinetics of calcium phosphate–fetuin-A colloidal particles probed by time-resolved dynamic light scattering. *Soft Matter* 7(6): 2869–2874, 2011.

[216] Walser M. Ion association. vi. interactions between calcium, magnesium, inorganic phosphate, citrate and protein in normal human plasma. *Journal of Clinical Investigation* 40(4): 723–730, 1961.

[217] Waron M and Rich C. Rate of recovery from acute hypocalcemia as a measure of calcium homeostatic efficiency in the dog. *Endocrinology* 85(6): 1018–1027, 1969.

[218] Wasserman RH, Chandler JS, Meyer SA, Smith CA, Brindak ME, Fullmer CS, Penniston JT, and Kumar R. Intestinal calcium transport and calcium extrusion processes at the basolateral membrane. *The Journal of nutrition* 122(3S): 662–671, 1992.

[219] Wilz DR, Gray RW, Dominguez JH, and Lemann J. Plasma 1, 25-$(OH)_2$-vitamin D concentrations and net intestinal calcium, phosphate, and magnesium absorption in humans. *The American journal of clinical nutrition* 32(10): 2052–2060, 1979.

[220] Winer KK, Yanovski JA, and Cutler GB. Synthetic human parathyroid hormone 1-34 vs calcitriol and calcium in the treatment of hypoparathyroidism: Results of a short-term randomized crossover trial. *Journal of The American Medical Association* 276(8): 631–636, 1996.

[221] Winer KK, Zhang B, Shrader JA, Peterson D, Smith M, Albert PS, and Cutler Jr GB. Synthetic human parathyroid hormone 1-34 replacement therapy: a randomized crossover trial comparing pump versus injections in the treatment of chronic hypoparathyroidism. *The Journal of Clinical Endocrinology & Metabolism* 97(2): 391–399, 2011.

[222] Wong KM and Klein L. Circadian variations in contributions of bone and intestine to plasma calcium in dogs. *American Journal of Physiology-Regulatory, Integrative and Comparative Physiology* 246(5): R688–R692, 1984.

[223] Wood RJ, Fleet JC, Cashman K, Bruns ME, and Deluca HF. Intestinal calcium absorption in the aged rat: Evidence of intestinal resistance to 1,25$(OH)_2$ vitamin $D_1$. *Endocrinology* 139(9): 3843–3848, 1998.

[224] Worcester EM and Coe FL. New insights into the pathogenesis of idiopathic hypercalciuria. *Seminars in nephrology* 28(2): 120–132, 2008.

[225] Worthley LI, Baker SB, and others . The essentials of calcium, magnesium and phosphate metabolism: part i. physiology. *Critical Care and Resuscitation* 4(4): 301–306, 2002.

[226] Xu H, Bai L, Collins JF, and Ghishan FK. Age-dependent regulation of rat intestinal type iib sodium-phosphate cotransporter by 1, 25-$(OH)_2$ vitamin $D_3$. *American Journal of Physiology-Cell Physiology* 282(3): C487–C493, 2002.

[227] Yamamoto Y, Yoshizawa T, Fukuda T, Shirode-Fukuda Y, Yu T, Sekine K, Sato T, Kawano H, Aihara K, Nakamichi Y, and others . Vitamin D receptor in osteoblasts is a negative regulator of bone mass control. *Endocrinology* 154(3): 1008–1020, 2013.

[228] Yamashita T, Yoshioka M, and Itoh N. Identification of a novel fibroblast growth factor, FGF-23, preferentially expressed in the ventrolateral thalamic nucleus of the brain. *Biochemical and biophysical research communications* 277(2): 494–498, 2000.

[229] Yokota H, Raposo JF, Chen A, Jiang C, and Ferreira HG. Evaluation of the role of FGF23 in mineral metabolism. *Gene regulation and systems biology* 3: 131–142, 2009.

[230] Zaidi M, Blair HC, Moonga BS, Abe E, and Huang CLH. Osteoclastogenesis, bone resorption, and osteoclast-based therapeutics. *Journal of Bone and Mineral Research* 18(4): 599–609, 2003.

[231] Zaladek GF, Nascimento GG, Cavanal MF, Cesar KR, and Magaldi AJ. Influence of parathyroidectomy and calcium on rat renal function. *Nephron* 83(1): 59–65, 1999.

[232] Zierold C, Mings JA, and DeLuca HF. Regulation of 25-hydroxyvitamin $D_3$-24-hydroxylase mRNA by 1, 25-dihydroxyvitamin $D_3$ and parathyroid hormone. *Journal of cellular biochemistry* 88(2): 234–237, 2003.